

Cover Page



Universiteit Leiden



The handle <http://hdl.handle.net/1887/37231> holds various files of this Leiden University dissertation

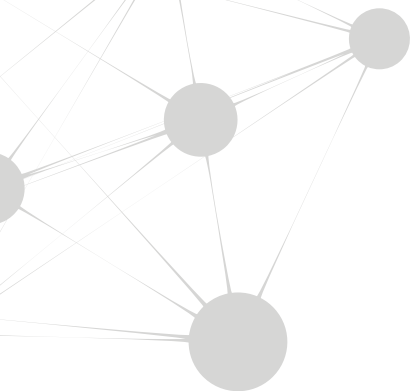
Author: Shyti, Reinald

Title: Modulating factors for and consequences of cortical spreading depression

Issue Date: 2016-01-21

**Modulating factors
for and consequences of
cortical spreading depression**

Reinald Shyti



Reinald Shyti

PhD Thesis, Leiden University, January 2016

ISBN: 978-90-9029361-5

Copyright © Reinald Shyti

Except the following chapters:

Chapter 4 and 5: Elsevier B.V.

Chapter 6: Springer International Publishing AG

Chapter 7: Royal Society of Chemistry

No part of this book may be reproduced, stored in a retrieval system, or transmitted in any form or by any means, without prior permission of the author.

Cover design and layout: Chryssanthi Tsiatsiani

Printed by: Off Page

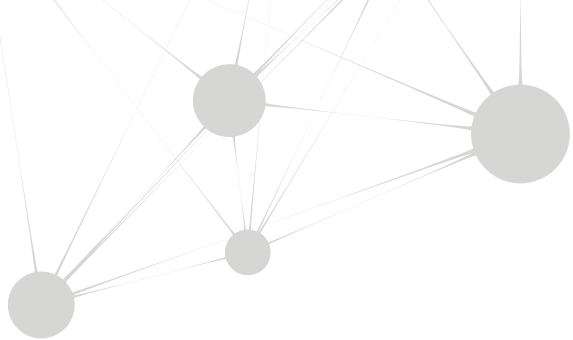


Modulating factors for and consequences of cortical spreading depression

Proefschrift

ter verkrijging van de graad van Doctor aan de Universiteit Leiden,
op gezag van Rector Magnificus prof. mr. C.J.J.M. Stolker
volgens besluit van het College voor Promoties
te verdedigen op donderdag 21 januari 2016
klokke 13.45 uur

door
Reinald Shyti
geboren te Berat (Albanië)
in 1981



Promotoren:

Prof. dr. A.M.J.M. van den Maagdenberg
Prof. dr. M.D. Ferrari

Co-promoter:

Dr. E.A. Tolner

Leden promotiecommissie:

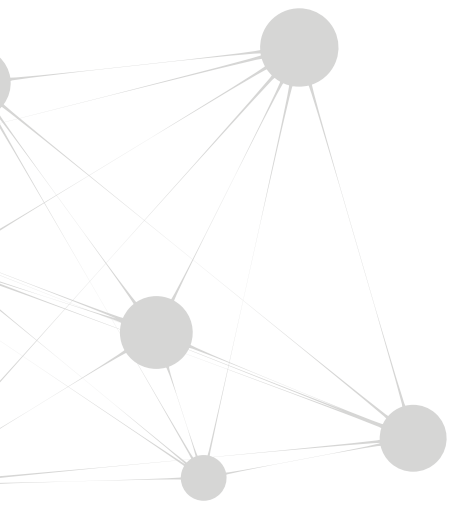
Prof. dr. J.H. Meijer
Prof. dr. M. Joëls (UMC Utrecht)
Dr. F.E. Hoebeek (Erasmus MC, Rotterdam)

The majority of the studies presented in this thesis were performed at the department of Human Genetics of the Leiden University Medical Center (LUMC). The work was supported by grants of the Dutch Organization for Scientific Research NWO (Spinoza 2009; Vici 918.56.602), the EU “EUROHEAD” grant (LSHM-CT-2004-504837), the EU Marie Curie IAPP Program “BRAINPATH” (no. 612360), the EU “EUROHEADPAIN” grant (no. 602633), LUMC Fellowship, the Marie Curie Career Integration grant (no. 294233) and the Center of Medical System Biology (CMSB) established by the Netherlands Genomics Initiative (NGI)/NWO.



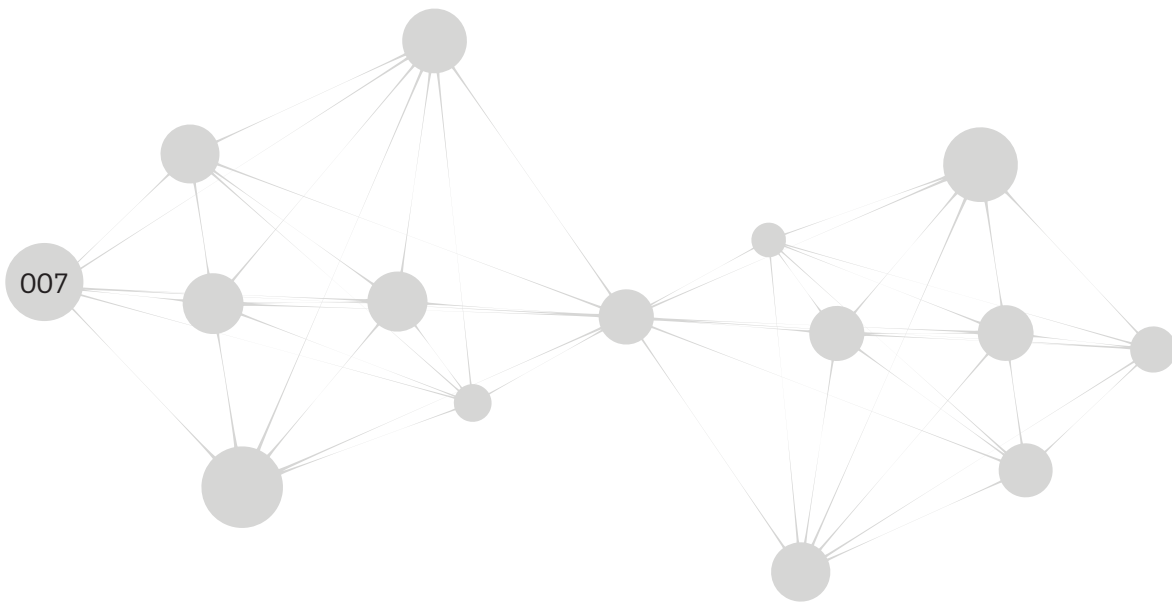
Table of contents

Chapter 1	General introduction	007
Chapter 2	Methodology driven differences in physiological parameters influence characteristics of cortical spreading depression in wild-type and familial hemiplegic migraine type 1 mice <i>In preparation</i>	029
Chapter 3	Increased EEG gamma band power and spontaneous cortical spreading depression events in Ca _v 2.1 R192Q mutant hemiplegic migraine mice <i>In preparation</i>	053
Chapter 4	Stress hormone corticosterone enhances susceptibility to cortical spreading depression in familial hemiplegic migraine type 1 mutant mice <i>Experimental Neurology 2015;263:214-20</i>	081
Chapter 5	Imaging mass spectrometry to visualize biomolecule distributions in mouse brain tissue following hemispheric cortical spreading depression <i>Journal of Proteomics 2012;75:5027-35</i>	099
Chapter 6	Large-scale mass spectrometry imaging investigation of consequences of cortical spreading depression in a transgenic mouse model of migraine <i>Journal of the American Society for Mass Spectrometry 2015;26:853-61</i>	115
Chapter 7	Plasma metabolic profiling after cortical spreading depression in a transgenic mouse model of hemiplegic migraine by capillary electrophoresis-mass spectrometry <i>Molecular Biosystems 2015;11:1462-71</i>	137
Chapter 8	General discussion	157
Summary		182
Nederlandse Samenvatting		185
Acknowledgements		188
List of publications		189
Curriculum Vitae		190



Chapter 1

General introduction



1.1 Migraine as a disease

Migraine is a common brain disorder characterized by episodic attacks of severe throbbing unilateral headache that is accompanied by nausea, vomiting, photophobia and phonophobia. Attacks can last from 4 to 72 hr (ICHD 2004). Migraine is clinically divided into two main types, migraine with aura (MA) and migraine without aura (MO); one-third of patients suffer from MA. The aura that can accompany the migraine headache in patients with MA consists of focal disturbances that almost always include visual symptoms but may also include sensory, aphasic, and motor symptoms. In western countries migraine affects about 15% of the general population (Lipton & Stewart 1998, Goadsby et al 2002). Migraine is most prevalent in the age range 25 to 55 and is three times more common in women than men (Lipton et al 2001). Attack frequency varies widely from a few attacks per year to several attacks per month; at least 10% of patients report weekly attacks (Goadsby et al 2002). Because of its severity and high prevalence the World Health Organization has rated migraine among the most common chronic disabling disorders of central nervous system (Vos et al 2013). Understanding the pathophysiology of migraine is important to identify new drug targets, which is dearly needed as many patients receive inadequate treatment despite the effectiveness of standard pain killers and serotonin agonists (so-called triptans) (Goadsby et al 2002).

1.2 Migraine pathophysiology

1.2.1 Migraine aura

Visual auras present as flashing jagged lights with fortification figures that spread from the center of the visual field to the periphery. In the beginning of the aura there is a short transient period of hyperemia with an increase in neuronal activity and cerebral blood flow (CBF) that is followed by oligemia or hypoperfusion that lasts much longer and is probably due to silencing of neuronal activity, which extends into the headache phase (Olesen et al 1981). Already early on, it was proposed that the aura was caused by cortical spreading depression (CSD) (Lauritzen 1994). The CSD phenomenon was initially discovered by Aristides Leão in 1944 (Leao 1944). While trying to record pin prick-induced seizures in the cortex of rabbits, Leão noticed that instead of inducing seizure activity he observed a temporary silencing of cortical electrical activity (presented as a flattening of the electrocorticogram trace) that propagated over the cortex. We now know that CSD is a wave of depolarization of neurons and glia cells, followed by suppression of neuronal activity, that spreads at a rate of 3-5 mm/min through the cortex via grey matter continuity and is associated with a massive disruption of ionic balance (Somjen 2001).

Evidence that CSD is relevant to migraine pathophysiology mainly comes from studies in animals. Regardless, using imaging techniques it was convincingly demonstrated that the observed temporal and spatial characteristics of cortical blood flow changes as they occur during CSD nicely correlated with patients descriptions of the spread of their aura symptoms (Hadjikhani et al 2001). Observations like these led to the now widely accepted notion that CSD is the electrophysiological correlate of

migraine aura. There is an active debate though whether CSD events also occur in migraine without aura attacks, in so-called “silent” brain areas (i.e., other than visual cortex), whereby CSD events would remain unidentifiable to the patient. Except for an isolated case with characteristic spreading blood flow changes reminiscent of a CSD in a patient with migraine without aura attacks (Woods et al 1994), it is mere speculation whether CSD indeed occurs in MO. Nonetheless, unraveling the neurobiological mechanisms underlying CSD is important for understanding not only the diseased brain but also normal brain functioning (Somjen 2004).

1.2.2 Migraine headache

How migraine pain is generated is not fully understood. The current view is that the headache is generated by activation of the trigeminovascular system (TGVS). The TGVS consists of meningeal and superficial cortical blood vessels that are innervated by the trigeminal nerve. Release of vasoactive peptides from perivascular afferents are able to trigger a series of events during which sensory (i.e., nociceptive) input is transmitted to trigeminal ganglion (TG) neurons and further to neurons in the brainstem trigeminal nucleus caudalis (TNC). Sensory signals from these nuclei are sent rostrally to thalamus and from there to higher brain centers to produce the sensation of pain (Goadsby et al 2002).

1.2.3. Can CSD/aura initiate headache mechanisms?

What the initial triggers are for activation of the TGVS remains to be determined. It is debated whether CSD events can trigger migraine headaches (Ayata 2010, Charles 2010). Although there is quite compelling evidence from studies in experimental animals suggesting that this is the case, evidence in humans is lacking. Already in 1993 it was shown by Moskowitz and colleagues (Moskowitz et al 1993) that experimentally induced CSD in rat brain can activate neurons in the ipsilateral TNC, as shown by increased expression of neuronal activation marker *c-fos*. The fact that the increased *c-fos* signal could be blocked by transection of trigeminal meningeal afferents innervating the dura, as well as by administration of 5-HT_{1B/1D} receptor agonist sumatriptan, an effective migraine drug, suggested that CSD is important in generating migraine headache. Second, it was shown that CSD induction, in addition to increasing *c-fos* immunoreactivity in TNC, also caused an increase in middle meningeal artery diameter and protein extravasation from trigeminal meningeal afferents (Bolay et al 2002). Third, CSD can activate both peripheral and central components of the trigeminovascular pathway as CSD induction has been shown to cause increased firing of (i) peripheral meningeal nociceptors that in some trials showed a time-delay reminiscent of aura-headache events seen in patients (Zhang et al 2010) and (ii) central trigeminovascular neurons in the C1-2 spinal trigeminal nucleus (Zhang et al 2011a). Sensitization of first-order neurons that project from trigeminal ganglia and innervate the meninges are believed to be responsible for the throbbing nature of migraine headache (Strassman et al 1996). Sensitization of higher-order trigeminovascular neurons of the medullary dorsal horn, which project to thalamus and receive convergent sensory information from the dura and extracranially from the skin of face and limbs, is thought to control the development of cutaneous allodynia, the perceived painful response to non-noxious stimuli such as combing one’s hair that many patients experience

during attacks (Burstein et al 2000). Figure 1 summarizes the role of pain pathway activation, and the possible relationship with CSD, in migraine headache.

1.3 Genetics of migraine

Migraine has a strong genetic component, which is already exemplified by the fact that migraine runs in families. Family- and population-based epidemiological studies revealed an increased risk for migraine in first-degree relatives of individuals with migraine (Russell & Olesen 1995, Stewart et al 1997). In addition, twin studies showed that the concordance rate was significantly higher in monozygotic than in dizygotic twins (Gervil et al 1999, Ulrich et al 1999), which is also regarded as a proof that migraine has a genetic component. The heritability (i.e., the proportion of the phenotypic variance explained by genetic factors) is approximately 50%; the other half is explained by environmental factors (Mulder et al 2003).

1.3.1 Genetic findings in common forms of migraine

The identification of genes that confer migraine risk for common forms of migraine has been challenging for a long time. Multiple gene variants, each with only a small contribution to disease risk, together with environmental factors, are expected to render an individual susceptible to common forms of migraine (de Vries et al 2009). The advent of unbiased genome-wide association studies (GWAS) in recent years has made it possible to identify migraine susceptibility genes. So-called “associated variants” show a difference in allele frequency between cases and controls for a specific single-nucleotide polymorphism (SNP) with a level of significance that survives correction for the many performed statistical tests. GWAS produce statistically robust findings, but the associated variants almost without exception have a small effect size indicating that an individual genetic factor increases disease risk by only a little. The genes that were assigned to associated loci seem to affect neurons (i.e., glutamatergic neurotransmission and the development of neurons and synapses), brain vasculature, and pain sensation (Anttila et al 2010, Chasman et al 2011, Freilinger et al 2012, Anttila et al 2013). Future research will hopefully give insight in how these genes contribute to causing migraine.

1.3.2 Genetic findings in monogenic familial hemiplegic migraine

Initial success in gene identification in migraine came from investigating familial hemiplegic migraine (FHM), a rare monogenic subtype of migraine with aura (ICHD 2004). FHM is characterized by at least some degree of body weakness (hemiparesis) during the aura that may last from min to several hr or days. Apart from the hemiparesis, the headache and aura features of an FHM attack are identical to those of attacks of common forms of migraine; the majority of FHM patients also experience attacks of “normal” migraine with or without aura that are not associated with hemiparesis (Thomsen et al 2002). Thus, from a clinical point of view, FHM seems part of the migraine spectrum, and a valid model to study the common forms of migraine. Genetic research in FHM led to the discovery of three genes (van den Maagdenberg et al 2007). FHM1 is caused by mutations in the *CACNA1A* gene, which encodes the α_1 pore-forming subunit of $\text{Ca}_v2.1$ calcium channels (Ophoff et al 1996). These channels

are involved in presynaptic release of neurotransmitters (Mintz et al 1995, Wu et al 1999). *CACNA1A* mutations are associated with various clinical phenotypes, e.g., FHM and episodic ataxia type 2 (van den Maagdenberg et al 2007). Clinical presentations with FHM1 mutations can range from pure FHM (e.g., with missense mutation R192Q) (Ophoff et al 1996) to a complex severe phenotype of FHM with cerebellar ataxia, susceptibility to seizures and sometimes lethal cerebral edema after trivial head trauma (with missense mutation S218L) (Kors et al 2001, Stam et al 2009).

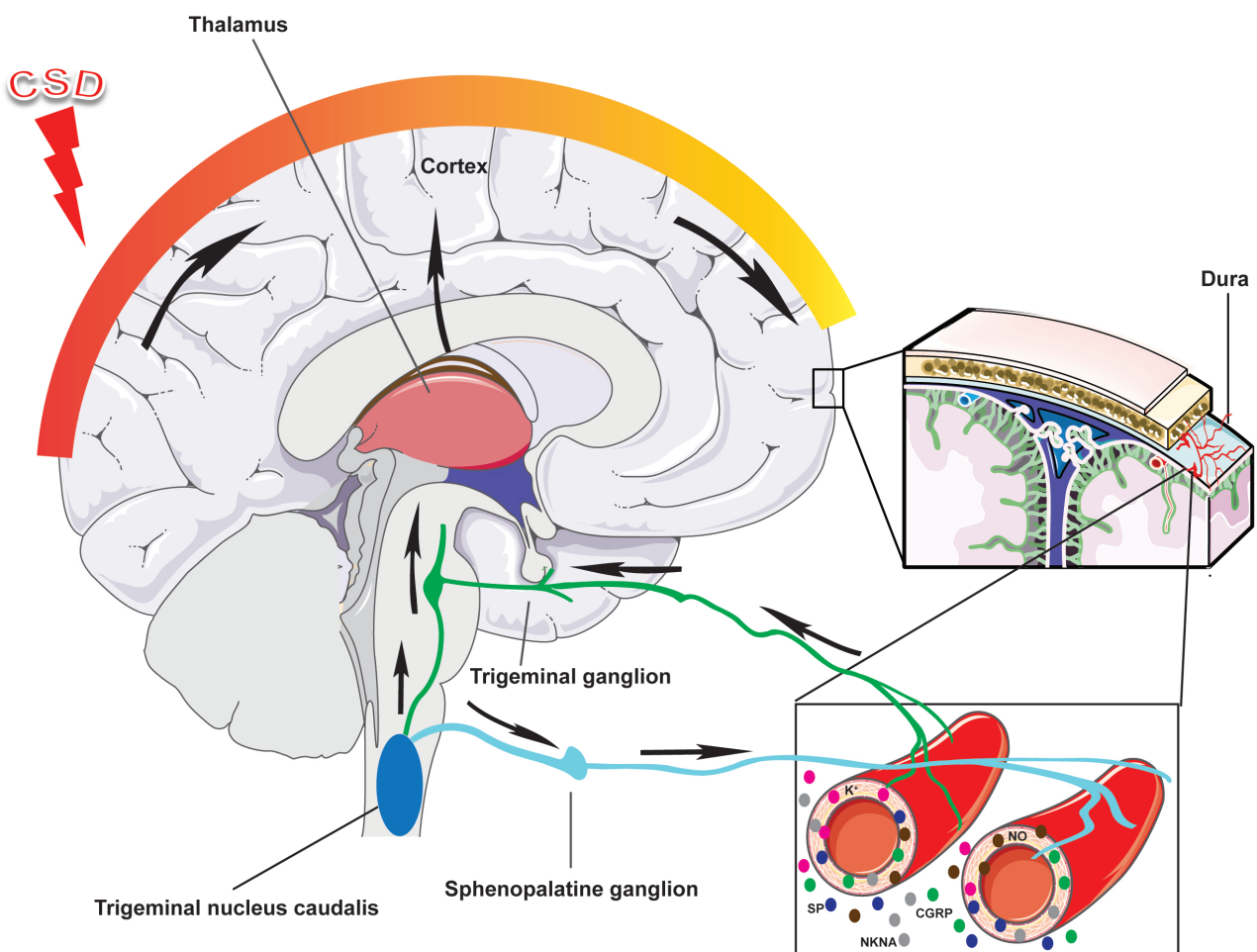


Figure 1. Schematic overview of brain anatomy and mechanisms involved in migraine aura and headache.

Cortical spreading depression (CSD) is a slowly propagating wave of neuronal and glial depolarization that starts in the visual cortex and is accompanied by the release of neurotransmitters, ions and vasoactive neuropeptides such as SP, CGRP and NKA (indicated by colored circles around dural vessels) into the extracellular space. These molecules may reach pial, arachnoid (not shown) and dural surfaces and activate the perivascular trigeminovascular sensory afferents from the trigeminal ganglion (TG) neurons. Signals of activated meningeal nociceptors are relayed via the TG to trigeminal nucleus caudalis (TNC) neurons and from there, further to thalamic and cortical areas involved in the processing of pain. From the trigeminal nucleus caudalis, collaterals are also sent to dural vessels via the sphenopalatine ganglion (SPG). Adapted from Goadsby et al 2002.

The FHM2 gene, *ATPIA2*, encodes the α_2 subunit of the Na⁺/K⁺-ATPase (De Fusco et al 2003) that in adulthood is expressed in glial cells (McGrail et al 1991). This catalytic subunit binds Na⁺, K⁺, and ATP, and utilizes ATP hydrolysis to exchange Na⁺ ions out of the cell for K⁺ ions into the cell. Thus, the ATPase is able to modulate the re-uptake of K⁺ and glutamate from the synaptic cleft into the glial cell. FHM2 mutations have been associated with pure FHM (De Fusco et al 2003, Riant et al 2005, Vanmolkot et al 2006), FHM with cerebellar ataxia (Spadaro et al 2004), and also permanent mental retardation (Jurkat-Rott et al 2004, Vanmolkot et al 2006). Finally, the FHM3, *SCN1A*, gene encodes the α_1 subunit of Na_v1.1 sodium channels (Dichgans et al 2005). These channels are mainly expressed in inhibitory interneurons (Ogiwara et al 2007) where they play a crucial role in the generation and propagation of action potentials (Catterall et al 2005).

Cellular studies of FHM mutations have suggested a single common consequence, i.e., increased excitatory neurotransmission (Figure 2); either by gain-of-function effects on Ca_v2.1 channels by FHM1 mutations in excitatory neurons, loss-of-function effects on ATPases by FHM2 mutations in glial cells, or loss-of-function effects by FHM3 mutations on inhibitory interneurons.

1.4 Modulators of migraine

1.4.1 Gender

The idea that gender is an important modulator of migraine comes from the observation that migraine is three times more common in women compared to men (Lipton et al 2001). Female hormones estrogen and progesterone have been implicated in the initiation and worsening of migraine attacks (Brandes 2006). Estrogen increases cortical excitability in humans (Smith et al 2002) and sudden changes in estrogen levels, such as estrogen withdrawal (Somerville 1972) may bring about migraine attacks. Notably, acute exposure of rat neocortical slices to estrogen and progesterone increases CSD frequency in a dose-dependent manner (Sachs et al 2007). Testosterone seems to counteract effects of estrogen as it was shown that testosterone down-regulates the expression of estrogen receptors in mouse cortex (Thakur & Sharma 2007); although it was not shown that testosterone directly inhibits neuronal excitability. Of note, danazol, a synthetic testosterone derivative, was shown effective in reducing migraine attack frequency and severity of headache in migraineurs (Lichten et al 1991).

1.4.2. Circadian rhythm

Acute shifts in daily sleeping patterns (i.e., sleeping too much or too little) have been reported to precipitate migraine attacks suggesting that circadian factors can influence attack onset (Solomon 1992). Attack occurrence has been reported to have a circadian component: migraine attacks occur more often between 4 am to 9 am, probably as a consequence of the changes that occur to prepare the body for the upcoming active period (Fox and Davis 1998). However, a prospective study in female patients pointed to a peak in attacks around the middle of the day (Alstadhaug et al 2008). The release of important hormones such as cortisol, melatonin and adenosine varies according to circadian rhythm. Presumably, particular hormonal and related neuronal activity changes occur during the transition

from the light to the dark period. It can be envisaged that the inability of an organism to adequately adapt to these abrupt changes might turn on a modulator of migraine attack onset.

1.4.3 Stress

The experience of stress and especially the recovery after a stressful period has been reported by patients as precipitating factor of their migraine attacks (Robbins 1994, Fanciullacci et al 1998, Hauge et al 2011). However, it is not known how stress would bring about migraine attacks. Of note, no significant link was observed between objective (i.e., saliva cortisol, heart rate and heart rate variability) and subjective (e.g., perception of stress) stress-related parameters and the onset of a migraine attack (Schoonman et al 2007). A recent study proposed a relationship between changes in perceived stress and migraine attacks (Lipton et al 2014) which could involve changes in perception rather than actual changes in stress levels (Goadsby 2014). Studies in rodents indicate that stress and in particular stress hormone corticosterone (i.e., the equivalent of cortisol in human) can increase neuronal excitability (Yuen et al 2009, Popoli et al 2011), which would link to migraine via the concept that cortical hyperexcitability is believed to underlie the sensitivity to migraine attacks (Aurora & Wilkinson 2007). Perhaps stress, with its associated changes in stress hormones, can act as a modulatory (i.e., additive) factor adding to the already heightened brain excitability in migraine sufferers, thus increasing the propensity for a migraine attack.

1.4.4 Migraine triggers and migraine?

Migraine is a heterogeneous disease. Not surprisingly most patients report more than one triggering factor as modulator of their migraine attacks (Hauge et al 2011, Pavlovic et al 2014). In addition to the modulators already mentioned, alcohol consumption (especially red wine), consuming certain food items, intense physical exercise, and smoking, are also often reported as migraine triggers (Hauge et al 2011). Still there is no solid scientific evidence that, and if proven, in which combination and how, the different modulatory factors, may bring about migraine attacks.

1.5 Pathways associated with cortical spreading depression

CSD, the mechanism underlying aura, can be triggered in the brain experimentally by a variety of stimuli such as pinprick, application of electrical current, application of K^+ or glutamate, and compounds such as endothelin (Somjen 2001, Dreier et al 2002). CSD can be more readily triggered in “smooth” non-convoluted brains of rodents than in convoluted brains of cats, monkeys and humans (Bures et al 1974). CSD events are associated with neuronal, glial and vascular changes in the brain, as well as inflammatory and biomolecular changes that are briefly discussed below.

1.5.1 Neuronal and glial changes associated with CSD

CSD consists of a large negative shift of extracellular potential due to a massive depolarization of neurons and glial cells which is associated with a massive redistribution of ions (Somjen 2001). The massive efflux of K^+ from neurons during CSD is accompanied by a concomitant neuronal release of

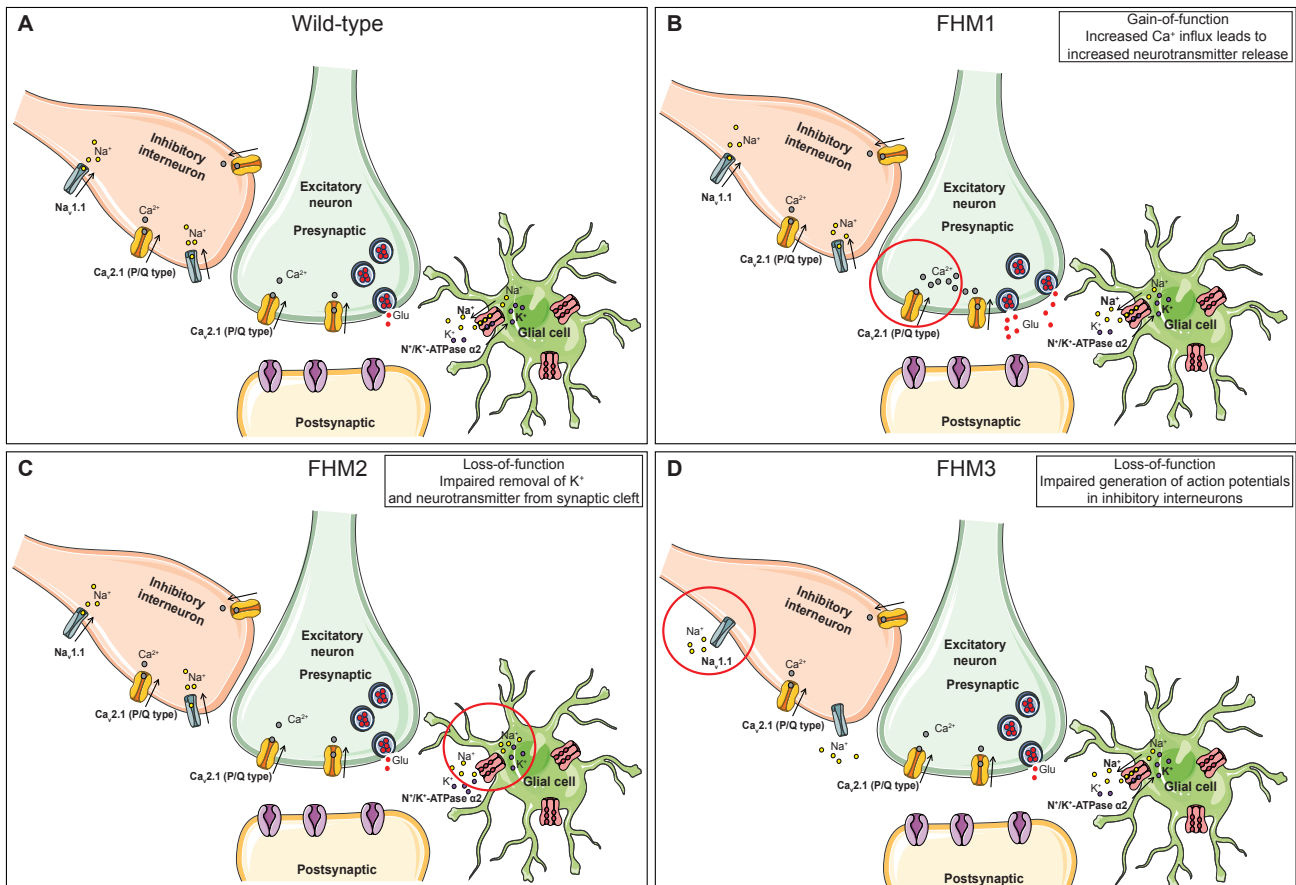


Figure 2. Functional effects of FHM mutations on neuronal excitability.

The illustration shows a glutamatergic tripartite synapse of the brain of a WT mouse (A) compared to a situation with an FHM1 (B), FHM2 (C) or FHM3 (D) mutation, respectively (red circles). (B) FHM1 mutations in the *CACNA1A* gene which encodes the pore-forming α_1 subunit of $\text{Ca}_v2.1$ calcium channels. Due to the gain-of-function effect of FHM1 mutations the influx of calcium through voltage-gated $\text{Ca}_v2.1$ channels in the presynaptic neuron terminal is enhanced causing neurotransmitter vesicles to fuse and release the neurotransmitter glutamate. Note that the gain-of-function effect is found only in the excitatory glutamatergic neurons and not in inhibitory GABAergic interneurons. (C) FHM2 mutations in the *ATPIA2* gene which encodes the α_2 isoform of the Na^+/K^+ -ATPase. FHM2 mutations lead to loss-of-function effects which abate the ability of glial cells to remove K^+ and glutamate from the synaptic cleft and terminate the action of the excitatory neuron. (D) FHM3 mutations in the *SCN1A* gene which encodes the $\text{Na}_v1.1$ voltage-gated sodium channels. FHM3 mutations lead also to loss-of-function effects inhibiting the generation and propagation of action potentials in inhibitory interneuron which regulate the activity of excitatory neurons. The net effect of each gene mutations will lead to an increase in neuronal excitability.

glutamate and organic anions (Szerb 1991, Fabricius et al 1993). At the same time there is an influx of Na^+ , Cl^- and Ca^{2+} into neurons (Hansen & Zeuthen 1981, Somjen & Aitken 1984). The excess of extracellular K^+ is taken up by glial cells mainly via passive flow through ohmic conductances and by activation of the Na^+/K^+ ATPase (Somjen 2004). On the other hand, the excess of glutamate in the synaptic cleft is removed by the excitatory-amino acids transporters (EAATs) of both neurons and glial

cells, e.g., EAAT1 and 2 (Danbolt 2001). Of the large voltage changes in neurons that occur during CSD, most notable are changes in inward and outward currents in dendrites and somata, respectively. Other notable changes are an increase in extraneuronal electrical impedance following CSD, and the increase in neuronal membrane potential that reaches almost zero during CSD (Collewijn & Harreveld 1966, Ferreira-Filho & Martins-Ferreira 1982). The glial cells follow the action of neurons during CSD. Glial cells also depolarize, mainly because of the neuronally-induced rise in extracellular K^+ that enters glial cells via their K^+ -permeable membrane (Muller & Somjen 2000), while the input resistance of glial cells drops slightly. The observation that CSD is preceded by an increase in neuronal excitability, which is a phase-locked activity of groups of neurons, led to the idea that CSD is an all-or-non phenomenon that, once started, becomes independent of the triggering stimulus (Rosenblueth & Garcia Ramos 1966, Herreras & Somjen 1993).

1.5.2 Vascular changes associated with CSD

As mentioned above, CSD is associated with a marked CBF response. The response is typically triphasic in character with an initial hypoperfusion that is followed by transient hyperemia and subsequently a pronounced oligemia that can last for an hr (Piper et al 1991, Eikermann-Haerter & Ayata 2010). Whereas the vascular response to CSD is comparable among most species, mice present a unique variability. Mice differ from for instance rats, in the sense that in mice the CSD-induced initial hypoperfusion is much more pronounced and the following hyperemia is reduced, suggesting species-specific differences in vascular sensitivity to elevated extracellular K^+ (Ayata et al 2004). Brennan and colleagues (Brennan et al 2007) studied arterial diameter in mice during CSD and reported an initial dilation which is followed by a profound constriction and subsequently an even larger dilation.

1.5.3 Neuroinflammation associated with CSD

Recently, experimental evidence emerged that provided a convincing link between CSD, inflammation and headache. Karatas and colleagues (Karatas et al 2013) provided evidence how CSD may lead to sustained activation/sensitization of trigeminovascular afferents in mice. They showed that CSD induction causes the opening of Pannexin 1 megachannels (Panx1) in neurons. Opening of Pannexin channels activates Caspase-1, which initiates a parenchymal inflammatory cascade by releasing high-mobility group box 1 (HMGB1) and interleukin- 1β (IL- 1β). In glial cells the increased levels of HMGB1 and IL- 1β can trigger the translocation to the nucleus of astrocytes of nuclear factor κ B (NF- κ B) and induction of cyclooxygenase-2 (COX2) and iNOS. The activation of this inflammatory cascade provides the necessary sustained activation for the sensitization of trigeminal afferents and initiation of headache as shown by headache-like behavior in mice. As second piece of evidence that inflammation is important in migraine comes from the fact that administration of tumor necrosis factor- α (TNF- α) in rat trigeminal ganglia induced mechanical sensitization of meningeal nociceptors via a COX-dependent mechanism, as shown by an increased firing rate of the trigeminal neurons (Zhang et al 2011b).

1.5.4 Biochemical changes associated with CSD

CSD is associated with profound changes in concentrations of various neurotransmitters, (neuro) peptides and metabolites. Elevated extracellular levels of glutamate have been detected during a CSD wave in animals (Fabricius et al 1993; Iijima et al 1998). In agreement with changes during CSD, Martinez and colleagues (Martinez et al 1993) found increased levels of glutamate in cerebrospinal fluid (CSF) in both MA and MO patients during an attack compared to controls, while glutamate levels in plasma were lower in both MA and MO compared to controls. Other studies though found increased levels of glutamate in the plasma for both MA and MO patients during migraine attacks compared to controls (Ferrari et al 1990).

During CSD in experimental animals there are also increased levels of neuropeptides such as calcitonin gene related peptide (CGRP), neurokinin- α (NKA) and substance P (SP) (Colonna et al 1994, Tozzi et al 2012). Changes in these compounds have also been observed in patients during migraine attacks. For example, during migraine attacks but not in headache-free periods, CGRP levels in plasma were higher in MA compared to MO young patients whereas the NKA levels were similarly increased in MA and MO compared to controls (Gallai et al 1995). In another study, MA and MO patients interictally had similarly elevated plasma levels of CGRP and SP (Fusayasu et al 2007).

In addition to neurotransmitters and neuropeptides, CSD induction causes changes in the levels also of metabolites in animals. CSD induction triggers an increase in levels of cyclic guanosine monophosphate (cGMP) in rats and nitric oxide (NO) in cats (Read et al 2001, Wahl et al 1994). Similar to experiments in animals, levels of cGMP and NO are increased in MA and MO patients during migraine attacks (Shimomura et al 1999, Stepien and Chalimoniuk 1998). Not surprisingly, levels of adenosine triphosphate (ATP) decrease during CSD in rats (Selman et al 2004) due to the high energy demand required to restore homeostasis following CSD. In addition, CSD triggers the release of arachidonic acid (Lauritzen et al 1990) and lactate in rats and human patients with acute brain injury (Cruz et al 1999, Feuerstein et al 2010).

From the above it is clear that CSD causes major changes in brain biochemical status which can be of relevance to migraine. Studying those changes in transgenic mice with migraine relevant mutations will potentially provide insights on the role of CSD in migraine pathophysiology.

1.6 Transgenic mouse models of migraine

1.6.1 Transgenic knock-in mice that harbor FHM1 mutations

The use of disease mouse models offers great opportunities for understanding disease pathophysiology and developing novel therapeutics. To this end knock-in (KI) mouse models were generated that carry *CACNA1A* missense mutations R192Q or S218L that both cause gain-of-function effects on Ca_v2.1 channels that were previously identified in FHM patients. The mutations were introduced in the mouse orthologous *Cacna1a* gene by homologous recombination (van den Maagdenberg et al 2004, van den Maagdenberg et al 2010). Whereas homozygous mice of the R192Q strain did

not show an overt phenotype, S218L mice showed cerebellar ataxia, a greater tendency for seizures and brain edema after a mild head trauma (van den Maagdenberg et al 2004, van den Maagdenberg et al 2010). Electrophysiological studies revealed that the mechanism underlying these phenotypes was an increased neuronal calcium influx through $Ca_v2.1$ channels with concomitant increased neurotransmitter release at peripheral and central synapses of mutant mice that was more pronounced in the severer S218L strain (van den Maagdenberg et al 2004, Eikermann-Haerter et al 2009, Tottene et al 2009, van den Maagdenberg et al 2010). Both strains of KI mice showed a marked increased propensity for CSD with a gene-dosage effect and a more pronounced phenotype in S218L mice. Furthermore, female mutant mice showed a greater CSD susceptibility compared to male mice.

1.6.2 Other transgenic mouse models of migraine

Three additional transgenic mouse models of migraine have been generated. First of all, a transgenic KI mouse FHM2 model with the W887R missense mutation in the α_2 -subunit of Na^+ , K^+ -ATPase was generated (Leo et al 2011). Heterozygous KI mice had a reduced threshold for CSD and an increased CSD propagation rate similar to effects observed with the FHM1 KI mice. Second, a “CGRP transgenic mouse model” was generated to investigate the *in vivo* role of increased CGRP levels by overexpressing the wild-type receptor activity-modifying protein-1 (RAMP1) protein under control of the *Nestin* promoter gene (Zhang et al 2007). *RAMP1* codes for a transmembrane protein that is necessary for the functioning of CGRP receptor (McLatchie et al 1998). Overexpression of human RAMP1 sensitizes the mice to the action of CGRP as a result of which mutant mice have increased CGRP-induced plasma extravasation in trigeminal ganglia which was interpreted as evidence for increased central sensitization after induction of mechanical allodynia (Marquez de Prado et al 2009). *Nestin/hRAMP1* mice showed a migraine-relevant phenotype of increased light-aversive behavior that was worsened by administration of CGRP and abrogated by a CGRP blocker (Recober et al 2009, Recober et al 2010). Third, transgenic overexpressor mice were generated that carry a mutation in casein kinase I δ (*CKI δ*), a protein kinase that plays a role in circadian rhythm, which was identified in patients with familial advanced sleep phase syndrome (FASP) and migraine with aura (Brennan et al 2013). Patients with FASP go to sleep unusually early in the evening and get-up very early in the morning. Transgenic *CKI δ* mice exhibited various migraine-relevant features including a reduced threshold for CSD and hyperalgesia after nitroglycerine administration (Brennan et al 2013).

1.7 Scope and outline of the thesis

The aim of the studies performed for this thesis was to investigate and delineate modulatory factors for and consequences of CSD in transgenic mice with the human pathogenic R192Q missense mutation in the α_1 subunit of voltage-gated $Ca_v2.1$ calcium channels that causes familial hemiplegic migraine in patients.

The physiological condition of an organism, especially blood pressure and levels of blood gases, influences the outcome of experiments that aim to determine CSD susceptibility. In **Chapter 2** we

investigated to what extent controlling and maintaining critical physiological parameters within a range, or allowing these parameters to vary freely during a course of an experiment, affects CSD frequency and threshold measurements in male and female FHM1 R192Q and WT mice.

Chapter 3 addressed the question whether the enhanced CSD susceptibility in FHM1 R192Q mice is related to changes in cortical excitability as measured by EEG and multi-unit recordings in freely behaving mice. Observed alterations in EEG activity and occurrence of CSD events in the visual and motor cortex from the long-term recordings in freely behaving mice were paralleled by studies in anesthetized and physiologically-controlled FHM1 R192Q mice in which CSD frequency and CSD threshold were compared for different times of the day and different regions of the cortex.

In **Chapter 4** the role of stress and its main hormone corticosterone on CSD susceptibility were investigated in FHM1 R192Q and WT mice. Restraint stress was used as a physiological stressor whereas corticosterone administration was used to selectively mimic the rise in stress hormone in the experiments.

In **Chapters 5** and **6** we tested the applicability of matrix-assisted laser desorption/ionization mass spectrometry (MALDI - MS) imaging to reveal changes in biomolecular distribution of proteins, peptides and metabolites in different brain regions. In **Chapter 5** we addressed the question whether CSD causes changes in composition of these compound classes after CSD in the brains of WT mice. In **Chapter 6** we assessed which molecular changes occur following CSD events in the mouse brain, but with high spatial resolution. To this end, we subjected mice to a fixed number of CSD events (or a sham procedure) after which changes in metabolite, peptide and protein distribution in the brain were measured and compared between FHM1 R192Q and WT mice.

In **Chapter 7** we addressed the question whether changes in metabolite profiles, assessed by capillary electrophoresis mass spectrometry (CE-MS) technology, could also be captured in blood after inducing CSD events in the brains of FHM1 R192Q and WT mice.

A general discussion on the experimental findings from this thesis is presented in **Chapter 8** along with suggestions for future research.

REFERENCES

- Alstadhaug K, Salvesen R, Bekkelund S. 2008. 24-hour distribution of migraine attacks. *Headache* 48:95-100
- Anttila V, Stefansson H, Kallela M, Todt U, Terwindt GM, et al. 2010. Genome-wide association study of migraine implicates a common susceptibility variant on 8q22.1. *Nat. Genet.* 42:869-73
- Anttila V, Winsvold BS, Gormley P, Kurth T, Bettella F, et al. 2013. Genome-wide meta-analysis identifies new susceptibility loci for migraine. *Nat. Genet.* 45:912-7
- Aurora SK, Wilkinson F. 2007. The brain is hyperexcitable in migraine. *Cephalalgia* 27:1442-53
- Ayata C. 2010. Cortical spreading depression triggers migraine attack: pro. *Headache* 50:725-30
- Ayata C, Shin HK, Salomone S, Ozdemir-Gursoy Y, Boas DA, et al. 2004. Pronounced hypoperfusion during spreading depression in mouse cortex. *J. Cereb. Blood Flow Metab.* 24:1172-82
- Bolay H, Reuter U, Dunn AK, Huang Z, Boas DA, Moskowitz MA. 2002. Intrinsic brain activity triggers trigeminal meningeal afferents in a migraine model. *Nat. Med.* 8:136-42
- Brandes JL. 2006. The influence of estrogen on migraine: a systematic review. *Jama* 295:1824-30
- Brennan KC, Bates EA, Shapiro RE, Zyuzin J, Hallows WC, et al. 2013. Casein kinase idelta mutations in familial migraine and advanced sleep phase. *Sci. Transl. Med.* 5:1-11
- Brennan KC, Beltran-Parrazal L, Lopez-Valdes HE, Theriot J, Toga AW, Charles AC. 2007. Distinct vascular conduction with cortical spreading depression. *J. Neurophysiol.* 97:4143-51
- Bures J, Buresova O, Krivanek J. 1974. *The Mechanism and Applications of Leao's Spreading Depression of Electroencephalographic Activity*, pp. 30-34. Prague: Academia New York: Academic Press.
- Burstein R, Yarnitsky D, Goor-Aryeh I, Ransil BJ, Bajwa ZH. 2000. An association between migraine and cutaneous allodynia. *Ann. Neurol.* 47:614-24
- Catterall WA, Goldin AL, Waxman SG. 2005. International Union of Pharmacology. XLVII. Nomenclature and structure-function relationships of voltage-gated sodium channels. *Pharmacol. Rev.* 57:397-409
- Charles A. 2010. Does cortical spreading depression initiate a migraine attack? Maybe not. *Headache* 50:731-3
- Chasman DI, Schurks M, Anttila V, de Vries B, Schminke U, et al. 2011. Genome-wide association study reveals three susceptibility loci for common migraine in the general population. *Nat. Genet.* 43:695-8
- Chesler M. 1990. The regulation and modulation of pH in the nervous system. *Prog. Neurobiol.* 34:401-27
- Collewijn H, Harreveld AV. 1966. Membrane potential of cerebral cortical cells during reading

- depression and asyxia. *Exp. Neurol.* 15: 425-36
- Colonna DM, Meng W, Deal DD, Busija DW. 1994. Calcitonin gene-related peptide promotes cerebrovascular dilation during cortical spreading depression in rabbits. *Am. J. Physiol.* 266:H1095-102
- Cruz NF, Adachi K, Dienel GA. 1999. Rapid efflux of lactate from cerebral cortex during K⁺-induced spreading cortical depression. *J. Cereb. Blood Flow Metab.* 19:380-92
- Danbolt NC. 2001. Glutamate uptake. *Prog. Neurobiol.* 65:100-105
- De Fusco M, Marconi R, Silvestri L, Atorino L, Rampoldi L, et al. 2003. Haploinsufficiency of ATP1A2 encoding the Na⁺/K⁺ pump alpha2 subunit associated with familial hemiplegic migraine type 2. *Nat. Genet.* 33:192-6
- De Vries B, Frants RR, Ferrari MD, van den Maagdenberg AM. 2009. Molecular genetics of migraine. *Hum. Genet.* 126:115-32
- Dichgans M, Freilinger T, Eckstein G, Babini E, Lorenz-Depiereux B, et al. 2005. Mutation in the neuronal voltage-gated sodium channel SCN1A in familial hemiplegic migraine. *Lancet* 366:371-7
- Dreier JP, Kleeberg J, Petzold G, Priller J, Windmuller O, et al. 2002. Endothelin-1 potently induces Leao's cortical spreading depression in vivo in the rat: a model for an endothelial trigger of migrainous aura? *Brain* 125:102-12
- Eikermann-Haerter K, Ayata C. 2010. Cortical spreading depression and migraine. *Curr. Neurol. Neurosci. Rep.* 10:167-73
- Eikermann-Haerter K, Dilekoz E, Kudo C, Savitz SI, Waeber C, et al. 2009. Genetic and hormonal factors modulate spreading depression and transient hemiparesis in mouse models of familial hemiplegic migraine type 1. *J. Clin. Invest.* 119:99-109
- Fabricius M, Jensen LH, Lauritzen M. 1993. Microdialysis of interstitial amino acids during spreading depression and anoxic depolarization in rat neocortex. *Brain Res.* 612:61-9
- Fabricius M, Lauritzen M. 1993. Transient hyperemia succeeds oligemia in the wake of cortical spreading depression. *Brain Res.* 602:350-3
- Fanciullacci C, Alessandri M, Fanciullacci M. 1998. The relationship between stress and migraine. *Funct. Neurol.* 13:215-23
- Ferrari MD, Odink J, Bos KD, Malessy MJ, Bruyn GW. 1990. Neuroexcitatory plasma amino acids are elevated in migraine. *Neurology* 40:1582-6
- Ferreira-Filho CR, Martins-Ferreira H. 1982. Electrical impedance of isolated retina and its changes during spreading depression. *Neuroscience* 7:3231-9
- Feuerstein D, Manning A, Hashemi P, Bhatia R, Fabricius M, et al. 2010. Dynamic metabolic response to multiple spreading depolarizations in patients with acute brain injury: an online microdialysis study. *J. Cereb. Blood Flow Metab.* 30:1343-55

- Fox AW, Davis RL. 1998. Migraine chronobiology. *Headache* 38:436-41
- Freilinger T, Anttila V, de Vries B, Malik R, Kallela M, et al. 2012. Genome-wide association analysis identifies susceptibility loci for migraine without aura. *Nat. Genet.* 44:777-82
- Fusayasu E, Kowa H, Takeshima T, Nakaso K, Nakashima K. 2007. Increased plasma substance P and CGRP levels, and high ACE activity in migraineurs during headache-free periods. *Pain* 128:209-14
- Gallai V, Sarchielli P, Floridi A, Franceschini M, Codini M, et al. 1995. Vasoactive peptide levels in the plasma of young migraine patients with and without aura assessed both interictally and ictally. *Cephalalgia* 15:384-90
- Gervil M, Ulrich V, Kyvik KO, Olesen J, Russell MB. 1999. Migraine without aura: a population-based twin study. *Ann. Neurol.* 46:606-11
- Goadsby PJ. 2014. Stress and migraine: something expected, something unexpected. *Neurology* 82:1388-9
- Goadsby PJ, Lipton RB, Ferrari MD. 2002. Migraine--current understanding and treatment. *N. Engl. J. Med.* 346:257-70
- Hadjikhani N, Sanchez Del Rio M, Wu O, Schwartz D, Bakker D, et al. 2001. Mechanisms of migraine aura revealed by functional MRI in human visual cortex. *Proc. Natl. Acad. Sci. USA* 98:4687-92
- Hansen AJ, Zeuthen T. 1981. Extracellular ion concentrations during spreading depression and ischemia in the rat brain cortex. *Acta Physiol. Scand.* 113:437-45
- Hauge AW, Kirchmann M, Olesen J. 2011. Characterization of consistent triggers of migraine with aura. *Cephalalgia* 31:416-38
- Herreras O, Somjen GG. 1993. Analysis of potential shifts associated with recurrent spreading depression and prolonged unstable spreading depression induced by microdialysis of elevated K⁺ in hippocampus of anesthetized rats. *Brain Res.* 610:283-94
- ICHD. 2004. The International Classification of Headache Disorders: 2nd edition. *Cephalalgia* 24 Suppl 1:9-160
- Iijima T, Shimase C, Iwao Y, Sankawa H. 1998. Relationships between glutamate release, blood flow and spreading depression: real-time monitoring using an electroenzymatic dialysis electrode. *Neurosci. Res* 32:201-7
- Jurkat-Rott K, Freilinger T, Dreier JP, Herzog J, Gobel H, et al. 2004. Variability of familial hemiplegic migraine with novel A1A2 Na⁺/K⁺-ATPase variants. *Neurology* 62:1857-61
- Karatas H, Erdener SE, Gursoy-Ozdemir Y, Lule S, Eren-Kocak E, et al. 2013. Spreading depression triggers headache by activating neuronal Panx1 channels. *Science* 339:1092-5
- Kors EE, Terwindt GM, Vermeulen FL, Fitzsimons RB, Jardine PE, et al. 2001. Delayed cerebral edema and fatal coma after minor head trauma: role of the CACNA1A calcium channel subunit

- gene and relationship with familial hemiplegic migraine. *Ann. Neurol.* 49:753-60
- Kraig RP, Ferreira-Filho CR, Nicholson C. 1983. Alkaline and acid transients in cerebellar microenvironment. *J. Neurophysiol.* 49:831-50
- Lauritzen M. 1994. Pathophysiology of the migraine aura. The spreading depression theory. *Brain* 117 (Pt 1):199-210
- Lauritzen M. 2001. Cortical spreading depression in migraine. *Cephalalgia* 21:757-60
- Lauritzen M, Hansen AJ, Kronborg D, Wieloch T. 1990. Cortical spreading depression is associated with arachidonic acid accumulation and preservation of energy charge. *J. Cereb. Blood Flow Metab.* 10:115-22
- Leao A. 1944. Spreading depression of activity in cerebral cortex. *J. Neurophysiol.* 7:359-90
- Leo L, Gherardini L, Barone V, De Fusco M, Pietrobon D, et al. 2011. Increased susceptibility to cortical spreading depression in the mouse model of familial hemiplegic migraine type 2. *PLoS Genet.* 7:e1002129
- Lichten EM, Bennett RS, Whitty AJ, Daoud Y. 1991. Efficacy of danazol in the control of hormonal migraine. *J. Reprod. Med.* 36:419-24
- Lipton RB, Buse DC, Hall CB, Tennen H, Defreitas TA, et al. 2014. Reduction in perceived stress as a migraine trigger: testing the “let-down headache” hypothesis. *Neurology* 82:1395-401
- Lipton RB, Stewart WF. 1998. Migraine headaches: epidemiology and comorbidity. *Clin. Neurosci.* 5:2-9
- Lipton RB, Stewart WF, Diamond S, Diamond ML, Reed M. 2001. Prevalence and burden of migraine in the United States: data from the American Migraine Study II. *Headache* 41:646-57
- Marquez de Prado B, Hammond DL, Russo AF. 2009. Genetic enhancement of calcitonin gene-related Peptide-induced central sensitization to mechanical stimuli in mice. *J. Pain* 10:992-1000
- Martinez F, Castillo J, Rodriguez JR, Leira R, Noya M. 1993. Neuroexcitatory amino acid levels in plasma and cerebrospinal fluid during migraine attacks. *Cephalalgia* 13:89-93
- McGrail KM, Phillips JM, Sweadner KJ. 1991. Immunofluorescent localization of three Na,K-ATPase isozymes in the rat central nervous system: both neurons and glia can express more than one Na,K-ATPase. *J. Neurosci.* 11:381-91
- McLatchie LM, Fraser NJ, Main MJ, Wise A, Brown J, et al. 1998. RAMPs regulate the transport and ligand specificity of the calcitonin-receptor-like receptor. *Nature* 393:333-9
- Mintz IM, Sabatini BL, Regehr WG. 1995. Calcium control of transmitter release at a cerebellar synapse. *Neuron* 15:675-88
- Moskowitz MA, Nozaki K, Kraig RP. 1993. Neocortical spreading depression provokes the expression of c-fos protein-like immunoreactivity within trigeminal nucleus caudalis via trigeminovascular mechanisms. *J. Neurosci.* 13:1167-77

- Mulder EJ, Van Baal C, Gaist D, Kallela M, Kaprio J, et al. 2003. Genetic and environmental influences on migraine: a twin study across six countries. *Twin Res.* 6:422-31
- Muller M, Somjen GG. 2000. Na(+) and K(+) concentrations, extra- and intracellular voltages, and the effect of TTX in hypoxic rat hippocampal slices. *J. Neurophysiol.* 83:735-45
- Ogiwara I, Miyamoto H, Morita N, Atapour N, Mazaki E, et al. 2007. Nav1.1 localizes to axons of parvalbumin-positive inhibitory interneurons: a circuit basis for epileptic seizures in mice carrying an Scn1a gene mutation. *J. Neurosci.* 27:5903-14
- Olesen J, Larsen B, Lauritzen M. 1981. Focal hyperemia followed by spreading oligemia and impaired activation of rCBF in classic migraine. *Ann. Neurol.* 9:344-52
- Ophoff RA, Terwindt GM, Vergouwe MN, van Eijk R, Oefner PJ, et al. 1996. Familial hemiplegic migraine and episodic ataxia type-2 are caused by mutations in the Ca²⁺ channel gene CACNL1A4. *Cell* 87:543-52
- Pavlovic JM, Buse DC, Sollars CM, Haut S, Lipton RB. 2014. Trigger factors and premonitory features of migraine attacks: summary of studies. *Headache* 54:1670-9
- Piper RD, Lambert GA, Duckworth JW. 1991. Cortical blood flow changes during spreading depression in cats. *Am. J. Physiol.* 261:H96-102
- Popoli M, Yan Z, McEwen BS, Sanacora G. 2011. The stressed synapse: the impact of stress and glucocorticoids on glutamate transmission. *Nat. Rev. Neurosci.* 13:22-37
- Read SJ, Hirst WD, Upton N, Parsons AA. 2001. Cortical spreading depression produces increased cGMP levels in cortex and brain stem that is inhibited by tonabersat (SB-220453) but not sumatriptan. *Brain Res.* 891:69-77
- Recober A, Kaiser EA, Kuburas A, Russo AF. 2010. Induction of multiple photophobic behaviors in a transgenic mouse sensitized to CGRP. *Neuropharmacology* 58:156-65
- Recober A, Kuburas A, Zhang Z, Wemmie JA, Anderson MG, Russo AF. 2009. Role of calcitonin gene-related peptide in light-aversive behavior: implications for migraine. *J. Neurosci.* 29:8798-804
- Riant F, De Fusco M, Aridon P, Ducros A, Ploton C, et al. 2005. ATP1A2 mutations in 11 families with familial hemiplegic migraine. *Hum. Mutat.* 26:281
- Robbins L. 1994. Precipitating factors in migraine: a retrospective review of 494 patients. *Headache* 34:214-6
- Rosenblueth A, Garcia Ramos J. 1966. Some phenomena usually associated with spreading depression. *Acta Physiol. Lat. Am.* 16:141-79
- Russell MB, Olesen J. 1995. Increased familial risk and evidence of genetic factor in migraine. *BMJ* 311:541-4
- Sachs M, Pape HC, Speckmann EJ, Gorji A. 2007. The effect of estrogen and progesterone on spreading depression in rat neocortical tissues. *Neurobiol. Dis.* 25:27-34

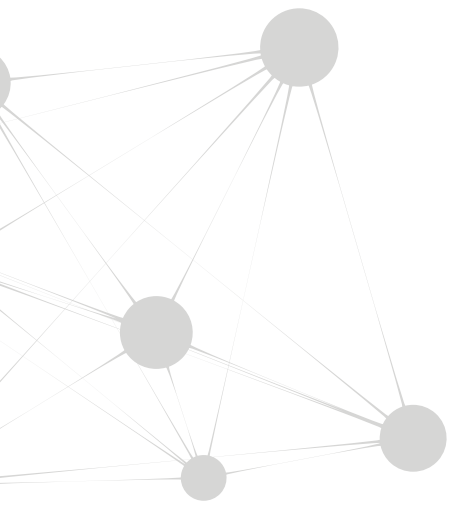
- Schoonman GG, Evers DJ, Ballieux BE, de Geus EJ, de Kloet ER, et al. 2007. Is stress a trigger factor for migraine? *Psychoneuroendocrinology* 32:532-8
- Selman WR, Lust WD, Pundik S, Zhou Y, Ratcheson RA. 2004. Compromised metabolic recovery following spontaneous spreading depression in the penumbra. *Brain Res.* 999:167-74
- Shimomura T, Murakami F, Kotani K, Ikawa S, Kono S. 1999. Platelet nitric oxide metabolites in migraine. *Cephalalgia* 19:218-22
- Smith MJ, Adams LF, Schmidt PJ, Rubinow DR, Wassermann EM. 2002. Effects of ovarian hormones on human cortical excitability. *Ann. Neurol.* 51:599-603
- Solomon GD. 1992. Circadian rhythms and migraine. *Cleve. Clin. J. Med.* 59:326-9
- Somerville BW. 1972. The role of estradiol withdrawal in the etiology of menstrual migraine. *Neurology* 22:355-65
- Somjen GG. 1984. Acidification of interstitial fluid in hippocampal formation caused by seizures and by spreading depression. *Brain Res.* 311:186-8
- Somjen GG. 2001. Mechanisms of spreading depression and hypoxic spreading depression-like depolarization. *Physiol. Rev.* 81:1065-96
- Somjen GG. 2004. *Ions in the brain*. New York: Oxford University Press
- Somjen GG, Aitken PG. 1984. The ionic and metabolic responses associated with neuronal depression of Leao's type in cerebral cortex and in hippocampal formation. *An. Acad. Bras. Cienc.* 56:495-504
- Spadaro M, Ursu S, Lehmann-Horn F, Veneziano L, Antonini G, et al. 2004. A G301R Na⁺/K⁺-ATPase mutation causes familial hemiplegic migraine type 2 with cerebellar signs. *Neurogenetics* 5:177-85
- Stam AH, Luijckx GJ, Poll-The BT, Ginjaar IB, Frants RR, et al. 2009. Early seizures and cerebral oedema after trivial head trauma associated with the CACNA1A S218L mutation. *J. Neurol. Neurosurg. Psychiatry* 80:1125-9
- Stepien A, Chalimoniuk M. 1998. Level of nitric oxide-dependent cGMP in patients with migraine. *Cephalalgia* 18:631-4
- Stewart WF, Staffa J, Lipton RB, Ottman R. 1997. Familial risk of migraine: a population-based study. *Ann. Neurol.* 41:166-72
- Strassman AM, Raymond SA, Burstein R. 1996. Sensitization of meningeal sensory neurons and the origin of headaches. *Nature* 384: 560-4
- Szerb JC. 1991. Glutamate release and spreading depression in the fascia dentata in response to microdialysis with high K⁺: role of glia. *Brain Res.* 542:259-65
- Takano T, Tian GF, Peng W, Lou N, Lovatt D, et al. 2007. Cortical spreading depression causes and coincides with tissue hypoxia. *Nat. Neurosci.* 10:754-62
- Thakur MK, Sharma PK. 2007. Transcription of estrogen receptor alpha and beta in mouse cerebral

- cortex: effect of age, sex, 17beta-estradiol and testosterone. *Neurochem. Int.* 50:314-21
- Thomsen LL, Eriksen MK, Roemer SF, Andersen I, Olesen J, Russell MB. 2002. A population-based study of familial hemiplegic migraine suggests revised diagnostic criteria. *Brain* 125:1379-91
- Tozzi A, de Iure A, Di Filippo M, Costa C, Caproni S, et al. 2012. Critical role of calcitonin gene-related peptide receptors in cortical spreading depression. *Proc. Natl Acad. Sci. USA* 109:18985-90
- Ulrich V, Gervil M, Fenger K, Olesen J, Russell MB. 1999. The prevalence and characteristics of migraine in twins from the general population. *Headache* 39:173-80
- van den Maagdenberg AM, Haan J, Terwindt GM, Ferrari MD. 2007. Migraine: gene mutations and functional consequences. *Curr. Opin. Neurol.* 20:299-305
- van den Maagdenberg AM, Pietrobon D, Pizzorusso T, Kaja S, Broos LA, et al. 2004. A *Cacna1a* knockin migraine mouse model with increased susceptibility to cortical spreading depression. *Neuron* 41:701-10
- van den Maagdenberg AM, Pizzorusso T, Kaja S, Terpolilli N, Shapovalova M, et al. 2010. High cortical spreading depression susceptibility and migraine-associated symptoms in *Ca(v)2.1* S218L mice. *Ann. Neurol.* 67:85-98
- Vanmolkot KR, Kors EE, Turk U, Turkdogan D, Keyser A, et al. 2006. Two de novo mutations in the Na,K-ATPase gene *ATP1A2* associated with pure familial hemiplegic migraine. *Eur. J. Hum. Genet.* 14:555-60
- Vos T, Flaxman AD, Naghavi M, Lozano R, Michaud C, et al. 2012. Years lived with disability (YLDs) for 1160 sequelae of 289 diseases and injuries 1990-2010: a systematic analysis for the Global Burden of Disease Study 2010. *Lancet* 380:2163-96
- Wahl M, Schilling L, Parsons AA, Kaumann A. 1994. Involvement of calcitonin gene-related peptide (CGRP) and nitric oxide (NO) in the pial artery dilatation elicited by cortical spreading depression. *Brain Res.* 637:204-10
- Woods RP, Iacoboni M, Mazziotta JC. 1994. Brief report: bilateral spreading cerebral hypoperfusion during spontaneous migraine headache. *N. Engl. J. Med.* 331:1689-92
- Wu LG, Westenbroek RE, Borst JG, Catterall WA, Sakmann B. 1999. Calcium channel types with distinct presynaptic localization couple differentially to transmitter release in single calyx-type synapses. *J. Neurosci.* 19:726-36
- Yuen EY, Liu W, Karatsoreos IN, Feng J, McEwen BS, Yan Z. 2009. Acute stress enhances glutamatergic transmission in prefrontal cortex and facilitates working memory. *Proc. Natl Acad. Sci. USA* 106:14075-9
- Zhang X, Levy D, Kainz V, Nosedà R, Jakubowski M, Burstein R. 2011a. Activation of central trigeminovascular neurons by cortical spreading depression. *Ann. Neurol.* 69:855-65
- Zhang X, Levy D, Nosedà R, Kainz V, Jakubowski M, Burstein R. 2010. Activation of meningeal

nociceptors by cortical spreading depression: implications for migraine with aura. *J. Neurosci.* 30:8807-14

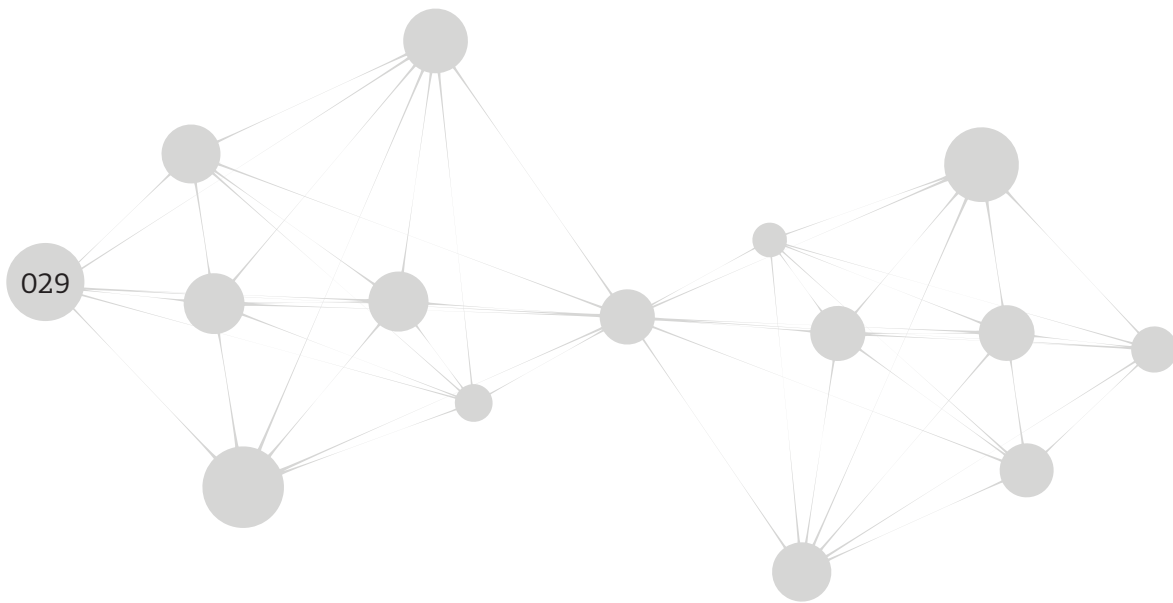
Zhang XC, Kainz V, Burstein R, Levy D. 2011b. Tumor necrosis factor-alpha induces sensitization of meningeal nociceptors mediated via local COX and p38 MAP kinase actions. *Pain* 152:140-9

Zhang Z, Winborn CS, Marquez de Prado B, Russo AF. 2007. Sensitization of calcitonin gene-related peptide receptors by receptor activity-modifying protein-1 in the trigeminal ganglion. *J. Neurosci.* 27:2693-703



Chapter 2

Methodology driven differences in physiological parameters influence characteristics of cortical spreading depression in wild-type and familial hemiplegic migraine type 1 mice



**Reinald Shyti¹, Sandra H. van Heiningen¹, Ludo A. M. Broos¹,
Michel D. Ferrari², Arn M.J.M van den Maagdenberg^{1,2*}, Else A. Tolner^{2*}**

Departments of ¹Human Genetics and ²Neurology,
Leiden University Medical Center, Leiden, The Netherlands

*equal contributions

In preparation

ABSTRACT

Changes in physiology and anesthesia modulate susceptibility to cortical spreading depression (CSD), the neurobiological correlate of migraine aura. Here we investigated to what extent CSD susceptibility parameters (frequency and threshold) depend on whether physiological parameters (pO_2 , pCO_2 , pH and blood pressure) were: i) not monitored at all, ii) only monitored (i.e., measured in blood from a femoral artery catheter; *physiological monitoring*), or iii) monitored and controlled (i.e., adjusted during the experiment by subtle changes in mechanical ventilation using tracheotomy; *physiological control*). In addition, we investigated to what extent the anesthesia gas mixture affects these CSD parameters. We studied effects of the methodologies in both wild-type (WT) mice and familial hemiplegic migraine type 1 (FHM1) transgenic mice that express the human pathogenic R192Q missense mutation in voltage-gated $Ca_v2.1$ Ca^{2+} channels (R192Q mice). A previous study revealed an enhanced CSD frequency in the visual cortex of mutant mice, an effect that was most pronounced in females, when experiments were performed with isoflurane- N_2O/O_2 anesthesia and physiological control. In the present study, however, using isoflurane-air anesthesia without physiological monitoring and without physiological control, we observed that visual cortex CSD frequency was equally enhanced in mutant mice of both genders. In contrast, a gender difference was observed for CSD threshold which was decreased in R192Q mice compared to WT to a larger extent in males than in females. The absence of a gender effect on CSD frequency in mutant mice was not related to the use of air instead of N_2O/O_2 , but to the presence of mechanical ventilation and possible subtle changes in pH, pCO_2 or blood pressure when physiological parameters were not controlled. Genotypic effects of enhanced CSD susceptibility in R192Q compared to WT mice were identified irrespective of the tested methodologies. Comparison of CSD susceptibility in visual cortex vs motor cortex revealed a regional difference in CSD susceptibility that was influenced by gender in the absence of physiological control. Physiological control can either unmask or mask a gender effect on specific CSD parameters. This sensitivity of CSD susceptibility to methodology has important implications when comparing data from different studies. Moreover, it suggests that there is a drawback of controlling physiological status of an animal as one may miss specific characteristics of CSD susceptibility when these depend on differences in physiological parameters between R192Q mutant and WT mice.

INTRODUCTION

One-third of migraine patients experience auras in addition to headaches, characterized by neurological sensory dysfunctions that in most cases consist of visual symptoms (Goadsby et al 2002, ICHD 2004). Cortical spreading depression (CSD) is the likely cause of the migraine aura, and it is characterized by a slowly propagating wave of neuronal and glial depolarization followed by a transient suppression of neuronal activity (Lauritzen 1994).

Changes in physiological parameters such as pH, pO₂, pCO₂ and blood pressure have been shown to influence CSD susceptibility measurements in animals under anesthesia as they can change neuronal excitability and vascular function (Holland et al 2012, Kudo et al 2008, Pietrobon & Moskowitz 2014, Ruusuvuori & Kaila 2014, Sukhotinsky et al 2010). For this reason, physiological parameters are in most studies monitored via femoral artery catheterization (*physiological monitoring*) and controlled using mechanical ventilation by changing the ventilation settings to adjust physiological parameters as needed (*physiological control*). In addition to the presence or absence of physiological monitoring and control, CSD experiments also vary with respect to choice of anesthesia gas mixture, which can also affect the outcome of CSD susceptibility measurements. For instance, N₂O (instead of pressurized air) in the anesthesia gas mixture has a suppressive effect on CSD parameters (Kudo et al 2008). Consequently, the experimental design of CSD experiments under anesthesia that may include physiological monitoring or physiological control, or neither, is expected to result in different outcomes of CSD frequency and threshold.

The importance of understanding the consequences of methodologies for assessing CSD parameters is especially relevant when comparing results from different studies. Here we show the relevance of different methodologies for CSD assessment with respect to the investigation of transgenic knock-in mice that carry the R192Q missense mutation in the α_1 subunit of Ca_v2.1 Ca²⁺ channels (van den Maagdenberg et al 2004). In humans, this mutation causes familial hemiplegic migraine 1 (FHM1; (Ophoff et al 1996). FHM1 R192Q mice have been used in different laboratories to unravel migraine-relevant mechanisms (Ferrari et al 2015).

Different methodologies and read-out measures have been used in different laboratories to assess the susceptibility of CSD in R192Q mice. A decreased threshold for the induction of CSD, assessed with increasing electrical stimulus intensity, was reported for the visual cortex of mutant mice that were kept under urethane anesthesia (van den Maagdenberg et al 2004, van den Maagdenberg et al 2010). Physiological parameters were not monitored during these experiments, and a gender difference was not reported. In another study, an increased frequency of CSD, assessed with a 30-min application of a cotton ball soaked in 300 mM KCl, was reported for the visual cortex of mutant mice in experiments performed with isoflurane-N₂O/O₂ (70%/30%) anesthesia and physiological monitoring and control (Eikermann-Haerter et al 2009a, Eikermann-Haerter et al 2009b). In those studies, female mutant mice showed a higher CSD frequency than male mutants; ovariectomy normalized CSD frequency in

mutant females to males levels. WT mice showed no gender difference and no effect of ovariectomy in females. Notably, a gender difference had been observed when CSD threshold was studied in the cortex of C57BL/6 WT mice that were kept under isoflurane-air anesthesia and physiologically monitored (Brennan et al 2007). Apparently, a gender difference is revealed when using one methodology but not another methodology. This leads to the question whether certain aspects of CSD susceptibility may only be observed when a specific combination of methodology and anesthetics is used, and whether results between laboratories can be compared.

We here assessed cortical CSD frequency in male and female R192Q and WT mice using various methodologies. Namely, i) without monitoring and control using isoflurane-air anesthesia, ii) monitoring without control using isoflurane-air anesthesia, iii) monitoring without control using isoflurane-N₂O/O₂ anesthesia, and iv) monitoring and control using isoflurane-N₂O/O₂ anesthesia. In addition, we compared CSD frequency and threshold in visual and motor cortex, in both male and female mice, in the absence of physiological monitoring and physiological control.

MATERIALS AND METHODS

Animals

Male and female homozygous *Cacna1a* FHM1 R192Q knock-in (“R192Q”) and wild-type (“WT”) mice of 2-4 months were used. The R192Q mice were generated by introduction of the human FHM1 pathogenic R192Q missense mutation in the mouse *Cacna1a* gene using a gene targeting approach (van den Maagdenberg et al 2004). All experiments were approved by the Animal Experiment Ethics Committee of Leiden University Medical Center.

CSD threshold and frequency recordings without physiological monitoring or physiological control

All experiments were performed during daytime between 10.00 am–13.00 pm. Mice were anesthetized using 1.5% isoflurane in pressurized air (80% N₂ and 20% O₂) and were breathing spontaneously. Core body temperature was maintained at 37 °C using a heating pad (Stoelting, Wood Dale, IL, USA). Mice were mounted into a stereotaxic frame (David Kopf Instruments, Tujunga, CA, USA). Subsequently, a midline incision of ~2.5 cm was made over the top of the head, the skin was retracted to expose the skull, and the periosteum was removed with cotton-tipped applicator sticks. Two craniotomy windows were drilled at the following coordinates in the right hemisphere (in mm with respect to Bregma): 3.5 posterior/2.0 lateral (visual cortex) and 1.5 anterior/2.0 lateral (motor cortex) (Figure 1A). Care was taken to keep the dura intact to minimize trauma to the underlying brain tissue. At the recording site a sharp glass capillary electrode (FHC Inc., Bowdoin, ME, USA) filled with 150 mM NaCl was advanced through the dura to a depth of 300 μm. After insertion of the electrode, a drop of mineral oil (~5 μL) was applied to the recording site to prevent drying of cortical tissue. The surgical procedure was completed within 20 min after the start of the anesthesia. DC-potential signals were measured

with respect to an Ag/AgCl reference electrode placed subcutaneously at the neck and amplified 10x (Molecular Devices, Sunnyvale, CA, USA). The DC signal was low-pass filtered at 4 Hz and digitized at 100–200 Hz using PowerLab 16/30 hardware (AD Instruments, Inc., Colorado Springs, CO, USA). Data were recorded and analyzed off-line using LabChart Pro (AD Instruments). In each mouse, first the CSD threshold was measured either in the visual or motor cortical window. To this end a cotton pellet (Interguide Dental Supply, Burlingame, CA, USA) soaked in a solution of KCl with a specific concentration (initially 5 mM) was placed on the dura overlaying either the visual or motor cortex for 3 min. In case no CSD was induced during this time window, the cotton pellet was replaced with another pellet that contained a higher K^+ concentration. Solutions contained increasing K^+ concentrations with 7.5-mM increments (with total osmolality kept at 300 mOsmol by addition of NaCl to the solution). The measurements continued until a CSD event was observed, so the CSD threshold could be determined. After the CSD threshold measurement, the induction site was rinsed with 150 mM NaCl. Subsequently, CSD frequency was determined at the same location. The location used (visual vs motor cortex) is mentioned for the respective CSD frequency result in the legend. For CSD frequency measurements, CSD events were induced by placement of a cotton pellet soaked in 1 M KCl on the dura overlaying the visual or motor cortex for 30 min, with refreshment of the pellet after 15 min. The total number of CSD events that occurred within 30 min was used to calculate the frequency per hr. For both the CSD threshold and frequency measurements, only reversible DC deflections with amplitudes larger than 5 mV were considered CSD events and included for further analysis.

CSD frequency recordings with physiological monitoring

Mice were maintained under 1.5% isoflurane anesthesia in 80% N_2O /20% O_2 and allowed to breathe spontaneously. Blood gas and mean arterial blood pressure values were monitored by placing a catheter in the left femoral artery. The surgical procedures were completed within 30 min after the start of the anesthesia. Blood pressure was measured continuously via a blood pressure transducer (AD instruments) connected to the femoral artery lead. To obtain information on physiological parameters (pH, pO_2 , pCO_2 ; Table 2), 40- μ L blood samples were collected before the start and at the end of the 30 min CSD frequency measurement and used for blood-gas analysis. Accepted ranges for physiological parameters were: pH=7.35-7.45; pO_2 =80-140 mmHg; pCO_2 =30-40 mmHg; and blood pressure=70-110 mmHg. Visual cortex CSD frequency measurements were performed upon induction of CSD by 1 M KCl application on the dura overlaying the visual cortex, as described above. In a subset of the experiments, isoflurane-air was used instead of isoflurane- N_2O / O_2 anesthesia.

CSD frequency recordings with physiological control

In contrast to experiments with physiological monitoring, described in the previous section, mice were now mechanically ventilated and physiological parameters adjusted when necessary. Measurement of CSD frequency with physiological control was performed as described in (Eikermann-Haerter et al 2009b), with slight modifications. In brief, mice were maintained under 1.5% isoflurane anesthesia in a gas mixture of 70-80% N_2O and 20-30% O_2 . Blood gas and mean arterial blood pressure values

were monitored via a catheter in the left femoral artery, as described above. After insertion of the catheter in the femoral artery, an endotracheal tube was inserted in the trachea that allowed artificial ventilation of the mouse. The mouse received an i.p injection of 0.04 mg/kg pancuronium for muscle paralysis to suppress spontaneous breathing and was connected to a mouse ventilator (SAR-830, CWE Inc, Ardmore, PA, USA). The surgical procedures were completed within 45 min after the start of the anesthesia. Visual cortex CSD frequency was measured upon induction of CSD by 1 M KCl application on the dura overlaying the visual cortex (Figure 1A), as described in the previous section, except that physiological parameters (i.e., pH, pO₂, pCO₂ and blood pressure) were now monitored (Table 2) and, if necessary, controlled by adjustments in ventilation. Blood pressure was measured continuously, as described above. For the other parameters, 40 µL blood samples were collected before the start and at the end of the 30 min CSD frequency measurement and used for blood-gas analysis; accepted ranges for physiological parameters were: pH=7.35-7.45; pO₂=80-140 mmHg; pCO₂=30-40 mmHg; and blood pressure=70-110 mmHg. When pH and pCO₂ values were outside the accepted ranges, breathing rate and time were adjusted. When pO₂ values were outside the accepted ranges, adjustments were made to the administered O₂ concentration. In this way physiological parameters were controlled during the experiment. The effect of the ventilator adjustments on physiological parameters was determined by taking a blood sample, immediately after the adjustment.

Ovariectomy

For removal of the ovaries, female mice were anesthetized using 1.5% isoflurane in pressurized air (80% N₂ and 20% O₂). A 1 cm incision was made in the skin of the flank followed by an incision in the muscle wall. Ovaries were separated from the surrounding tissue with ligatures, and carefully removed, after which the skin was closed with sutures. The mouse was given a subcutaneous injection of 1 mL 0.9% NaCl to maintain physiological hydration. The mouse also received an intramuscular injection of 0.1 mg/kg temgesic for post-operative analgesia. After a 2-week recovery period, CSD threshold and frequency recordings were performed using isoflurane-air anesthesia in the absence of physiological monitoring or control, as described above.

Statistical analysis

For statistical analysis of CSD threshold, which is skewed, the Mann-Whitney U-test was used. For CSD frequency values, one-way ANOVA followed by Bonferroni correction or Student's t-test was used. Statistical significance was set at 0.05.

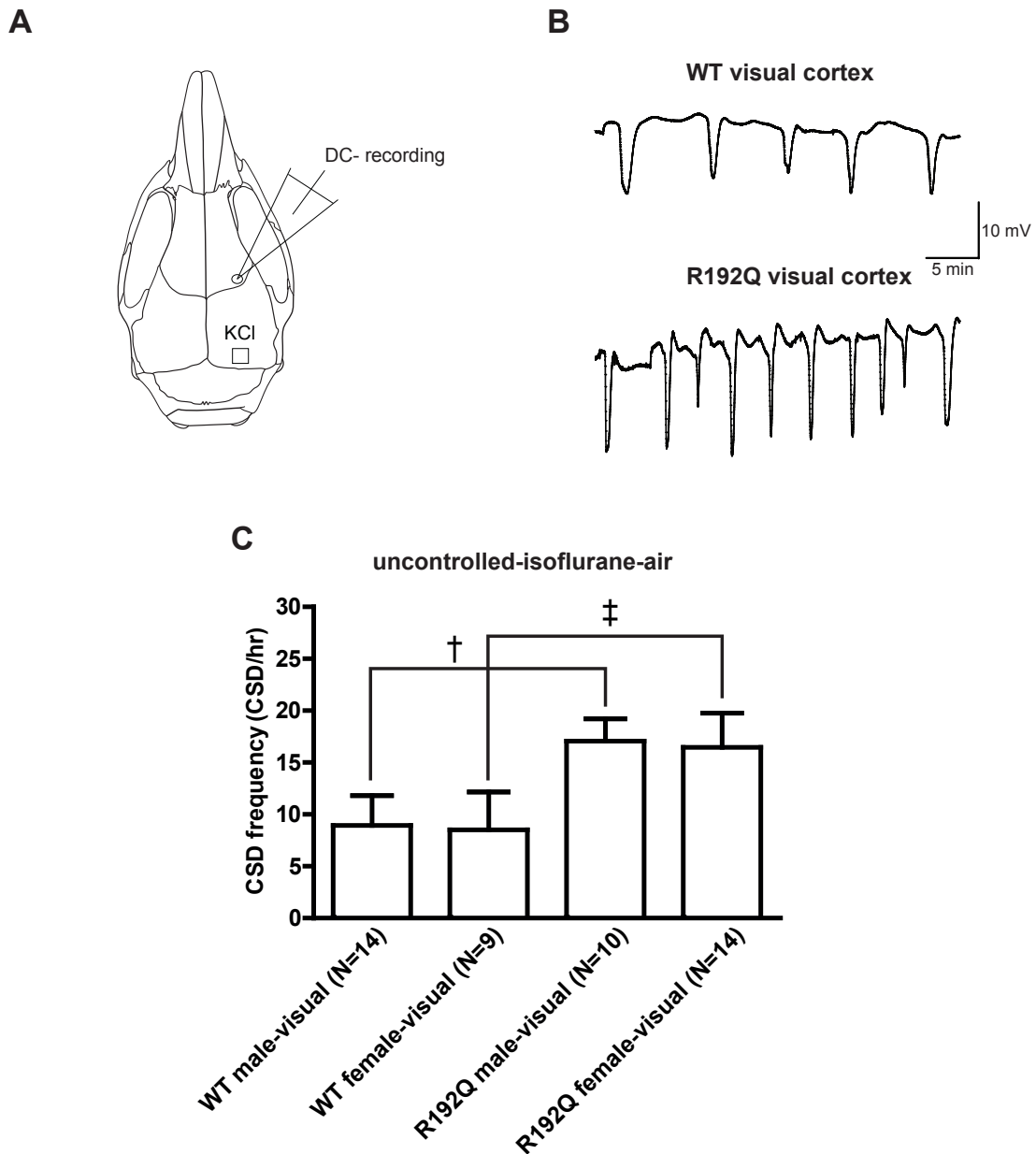


Figure 1. In the absence of physiological monitoring and control under isoflurane-air anesthesia, visual cortex CSD frequency is enhanced in R192Q mice compared with WT, with no difference between genders.

(A) Schematic representation of visual cortex CSD frequency measurements in anesthetized mice. CSD is induced by placement of a cotton pellet containing 1 M KCl on the dura overlaying the visual cortex for a period of 30 min, while CSD events are measured by DC-recording via a glass-electrode placed in the motor cortex. In experiments without physiological monitoring or control, CSD frequency measurements followed CSD threshold measurements (see Methods) (B) Example CSD frequency traces illustrating enhanced visual cortex CSD frequency in male R192Q compared with WT mice in the absence of physiological control using isoflurane-air anesthesia (C) Bar diagram depicting enhanced CSD frequency in the visual cortex in both male and female R192Q compared with WT mice ($^{\dagger}p=0.0001$ and $^{\ddagger}p=0.0001$; one-way ANOVA Bonferroni correction). No CSD frequency difference was observed for male compared with female R192Q mice in experiments without physiological control using isoflurane-air anesthesia.

RESULTS

CSD frequency in the visual cortex is enhanced in R192Q mice without revealing a gender difference, when assessed in the absence of physiological monitoring or physiological control

We determined visual cortex CSD frequency (Figure 1A, B) of male and female R192Q and WT mice using isoflurane-air anesthesia in the absence of physiological monitoring or physiological control. Both female and male R192Q mice showed an enhanced visual cortex CSD frequency compared with WT (female R192Q, 16.4 ± 3.3 CSD/hr, vs female WT, 8.5 ± 3.6 CSD/hr, N=9, $p=0.0001$; male R192Q, 17.0 ± 2.1 CSD/hr, N=10, vs male WT, 8.9 ± 2.8 CSD/hr, N=14, $p=0.0001$). For both R192Q and WT mice no gender difference was observed (female R192Q vs male $p=0.6$; female WT vs male $p=0.7$) (Figure 1C). Table 1 summarizes CSD amplitude and duration characteristics for the different groups. Except for CSD duration, which was longer for female WT compared with female R192Q mice, no statistical differences were observed. Not finding a gender difference in R192Q mice contrasts with published data that revealed that female mutant mice displayed a higher CSD frequency when isoflurane-N₂O/O₂ was used and physiological parameters were controlled (Eikermann-Haerter et al 2009b).

CSD threshold in the visual cortex is reduced in R192Q mice, and more so in male mutants, when assessed in the absence of physiological monitoring and physiological control

A study by Brennan *et al.* (Brennan et al 2007) showed that CSD threshold in the visual cortex was reduced in female compared with WT mice in experiments in which physiological parameters were monitored, and not controlled. We here assessed visual cortex CSD threshold of R192Q and WT mice of both genders, using isoflurane-air anesthesia, without monitoring or controlling physiological parameters. CSD threshold, as assessed by the KCl concentration required to elicit a CSD (Figure 2A), was reduced in both female and male R192Q mice compared with WT mice of the same gender (female R192Q, median=51.8 mM KCl, N=14 vs female WT, median=68.7 mM KCl, N=9; $p=0.01$; male R192Q, median=38.7 mM KCl, N=11 vs female WT, median=58.7 mM KCl, N=14; $p=0.001$) (Figure 2B). Rather unexpectedly, male R192Q mice showed a lower CSD threshold ($p=0.02$) compared with female R192Q mice. CSD threshold did not statistically differ between female and male WT mice, although male WT mice showed a trend towards a lower threshold ($p=0.08$). There were no statistical differences in CSD amplitude or duration between female and male mice, or between genotypes for the visual cortex threshold experiments (Table 1).

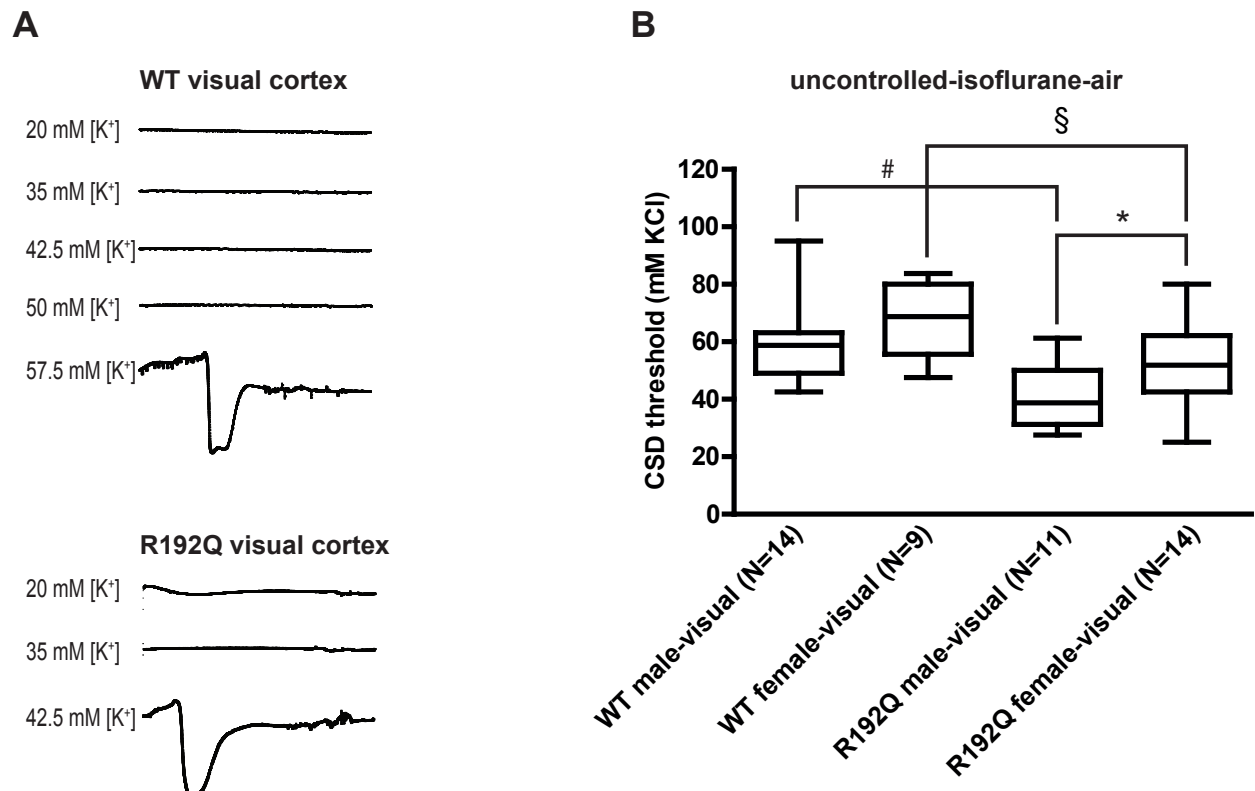


Figure 2. Visual cortex CSD threshold is reduced in R192Q mice compared to WT in the absence of physiological control under isoflurane-air anesthesia, with strongest effect in males.

(A) Specimen recordings of CSD threshold assessments illustrating the lower KCl concentration that is required to induce a CSD in the visual cortex of a male R192Q compared with a WT mouse (B) Box plots depicting lower visual cortex CSD threshold in male R192Q compared with female mice (* $p=0.02$ male R192Q vs female R192Q, Mann-Whitney U-test) and in R192Q male and female mice compared with WT (# $p=0.001$ male R192Q vs WT; § $p=0.01$ female R192Q vs WT, Mann-Whitney U-test).

Table 1. CSD amplitude and duration characteristics of CSD frequency and threshold recordings from visual and motor cortex in R192Q and WT mice for experiments performed in the absence of physiological monitoring or control, using isoflurane-air

CSD Frequency	N	Male		N	Female	
		Amplitude (mV)	Duration (sec)		Amplitude (mV)	Duration (sec)
R192Q visual	10	18.9±3.3	32.4±11.9	14	20.4±2.6 [‡]	25.4±5.0
WT visual	14	20.9±3.0	34.4±18.0	9	23.4±2.6*	46.3±25.1*
R192Q motor	7	14.9±6.2	20.8±7.4	12	15.4±3.9	30.4±11.2
WT motor	10	21.1±4.1 [†]	33.3±8.1	7	10.7±3.4	27.2±10.9
CSD Threshold						
R192Q visual	11	21.9±1.9	71.1±35.2	14	22.2±3.5	63.5±22.8
WT visual	14	25.0±4.3	71.2±39.0	9	25.7±3.1*	72.4±19.5
R192Q motor	8	17.9±5.0	56.2±26.4	12	19.4±2.8	72.3±27.6
WT motor	11	22.7±2.7 [†]	45.8±10.6	10	15.9±3.0	46.8±19.2

Table 1. Values are shown as mean ± SD. CSD duration was measured at half-maximal amplitude. *CSD frequency data:* comparison of CSD characteristics in CSD frequency recordings revealed a lower CSD amplitude in female WT mice for the motor cortex compared with female WT mice for the visual cortex (*p=0.0001), and compared with male WT mice in the motor cortex ([†]p=0.038, one-way ANOVA, Bonferroni correction). CSD amplitude was also reduced in female R192Q mice for the motor cortex compared to the visual cortex ([‡]p=0.049, one-way ANOVA, Bonferroni correction). There were no differences in CSD duration except for a shorter duration in female R192Q mice for the visual cortex compared with female WT mice visual cortex (*p=0.016, one-way ANOVA, Bonferroni correction). *CSD threshold data:* CSD amplitude was reduced in female WT mice for the motor compared to the visual cortex (*p=0.0001) and compared to motor cortex in male WT mice ([†]p=0.0001, one-way ANOVA, Bonferroni correction). There were no differences between groups in CSD duration for CSD threshold measurements.

CSD susceptibility is not affected by gender when assessed in the motor cortex in the absence of physiological monitoring and physiological control

Given reports on visual cortex hyperexcitability in migraine patients (Aurora & Wilkinson 2007), and the suggestion of CSD to initiate preferably in the visual cortex (Hadjikhani et al 2001), we next assessed whether effects of genotype and gender on measures of CSD susceptibility frequency and

threshold are specific to the visual cortex. Therefore, we investigated these CSD measurements also in the motor cortex. Experiments were carried out using isoflurane-air anesthesia without physiological monitoring or physiological control. Regarding a possible effect of genotype, for the motor cortex both male and female R192Q mice exhibited higher CSD frequencies compared with WT mice of the same gender (male R192Q, 14.0 ± 3.6 CSD/hr, $N=7$ vs male WT, 7.6 ± 1.3 CSD/hr, $N=10$, $p=0.0001$; female R192Q, 13.0 ± 3.9 CSD/hr, $N=12$ vs female WT, 5.5 ± 1.7 CSD/hr, $N=7$, $p=0.0001$) (Figure 3A). For CSD threshold however, both male and female R192Q mice showed comparable CSD thresholds as WT mice of the same gender (male R192Q, median= 56.8 mM KCl, $N=9$ vs male WT, median= 57.5 mM KCl, $N=11$, $p=0.8$; female R192Q, median= 59.3 mM KCl, $N=12$ vs female WT, median= 63.1 mM KCl, $N=10$, $p=0.60$) (Figure 3B). With respect to gender, for motor cortex CSD frequency, similar as observed for the visual cortex, no difference was observed between male and female mice for both R192Q ($p=0.5$) and WT mice ($p=0.3$) (Figure 3A). For CSD threshold measurements in the motor cortex, in contrast to the visual cortex, no difference was observed between genders in R192Q mice ($p=0.7$). In WT mice, as seen for the visual cortex, no gender effect was observed for motor cortex CSD threshold ($p=0.8$) (Figure 3B).

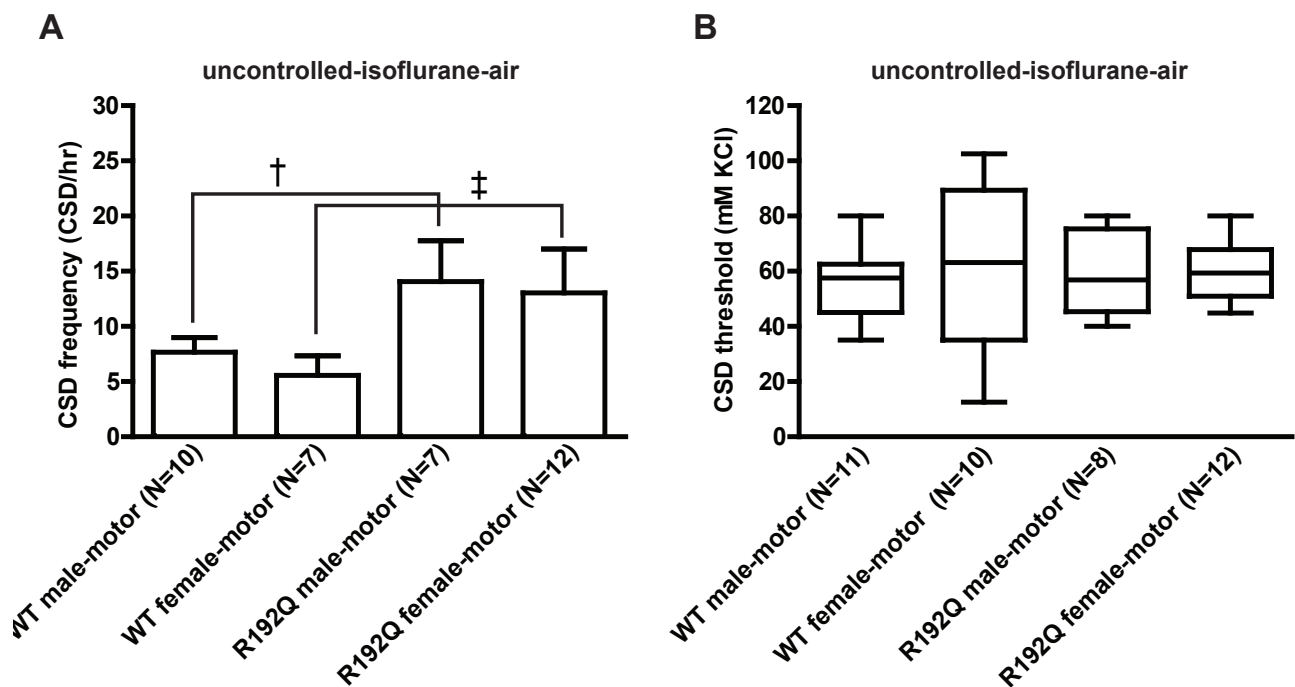


Figure 3. In the absence of physiological control, CSD susceptibility in the motor cortex is not influenced by gender. Experiments were performed in the absence of physiological control under isoflurane-air anesthesia (A) Bar diagrams showing an increased motor cortex CSD frequency for both male ($*p=0.0001$) and female R192Q mice ($*p=0.0001$; one-way ANOVA, Bonferroni correction) compared with WT, with no differences between genders among mice of the same genotype (B) CSD threshold values in the motor cortex were comparable between R192Q and WT mice of both genders in experiments without monitoring or control.

Given these observations, we next assessed whether CSD susceptibility measurements of frequency and threshold may differ *between* the visual and motor cortex, with possible effects of genotype and gender. Between cortical regions, male R192Q mice exhibited comparable CSD frequencies for visual and motor cortex, although a trend towards higher CSD frequency was observed for the visual compared with motor cortex ($p=0.05$). Female R192Q mice displayed a significantly higher CSD frequency in the visual compared with motor cortex ($p=0.02$). CSD frequency was not different for the visual compared with motor cortex in male WT ($p=0.2$) and female WT mice ($p=0.07$) (Figures 1C and 3A). CSD threshold was lower in the visual compared with the motor cortex ($p=0.009$) in male R192Q mice. Female R192Q mice however showed comparable CSD thresholds for both visual and motor cortex ($p=0.1$). In WT mice, CSD threshold was not different between motor and visual cortex in both male ($p=0.6$) and female mice ($p=0.7$) (Figures 2B and 3B). Table 1 summarizes CSD characteristics amplitude and duration for the different groups. For CSD frequency measurements, some differences were observed regarding CSD amplitude. In particular, for female R192Q mice, lower CSD amplitude was observed in motor compared with visual cortex. Furthermore, female WT mice showed lower CSD amplitude in the motor compared with the visual cortex, and compared with male WT mice in the motor cortex. For CSD threshold measurements, no differences were observed except for lower CSD amplitude in female WT mice in the motor compared with the visual cortex.

Ovariectomy has no strong influence on visual cortex CSD susceptibility in experiments without physiological monitoring and physiological control

Although visual cortex CSD frequency was comparable between male and female R192Q mice in physiologically uncontrolled experiments, the enhanced CSD frequency that was observed for female, but not male, R192Q mice in the visual compared with the motor cortex suggests some effect of gender on CSD characteristics in the absence of physiological control. Hence we next determined, in experiments performed in the absence of physiological monitoring and control, whether ovariectomy in female R192Q mice may reduce visual cortex CSD frequency values to those observed for motor cortex. After ovariectomy in female R192Q mice, visual cortex CSD frequency did not show a difference anymore with motor cortex CSD frequency from intact female R192Q mice ($p=0.2$). Nevertheless, visual cortex CSD frequency itself was not significantly reduced by ovariectomy in female R192Q or WT mice (R192Q ovariectomized (Ovx), 15.2 ± 4.0 CSD/hr, $N=8$ vs R192Q intact, 16.4 ± 3.3 CSD/hr, $N=14$, $p=0.8$; WT Ovx, 7.9 ± 2.0 CSD/hr, $N=5$ vs WT intact, 8.5 ± 3.6 CSD/hr, $N=9$, $p=0.7$). Similar as for intact female R192Q compared with WT mice, ovariectomized female R192Q mice showed higher visual cortex CSD frequency compared with ovariectomized WT mice ($p=0.003$). Given the observed, unexpected, higher visual cortex CSD threshold observed for female compared with male R192Q mice, we next determined whether this effect may be influenced by ovariectomy. Similar as for CSD frequency, visual cortex CSD threshold was not influenced by ovariectomy for both female R192Q and WT mice (R192Q Ovx, median= 57.5 mM KCl, $N=7$ vs R192Q intact, median= 51.8 mM KCl, $N=14$, $p=0.3$; WT Ovx, median= 72.5 mM KCl, $N=5$ vs WT intact, median= 68.7 mM KCl,

N=9, $p=0.4$). As a consequence, ovariectomized female R192Q mice still showed a higher visual cortex CSD threshold compared with male R192Q mice ($p=0.01$). The genotype effect on visual cortex CSD threshold was also not influenced by ovariectomy. Ovariectomized R192Q mice showed reduced CSD threshold compared with ovariectomized WT ($p=0.04$). CSD amplitude and duration were not influenced by ovariectomy for both CSD frequency and threshold experiments.

CSD frequency in the visual cortex is enhanced in R192Q mice, and more so in female mutants, when assessed in the presence of physiological monitoring and physiological control

Although our experiments performed without physiological monitoring or physiological control show the reported *genotypic effect* of the R192Q mutation on CSD susceptibility, the absence of a gender effect on visual cortex CSD frequency is not in line with earlier experiments in R192Q mice from Eikermann-Haerter *et al.* that were performed in the presence of physiological control (Eikermann-Haerter *et al.* 2009b). For CSD threshold in WT mice, in contrast to studies from Brennan *et al.* (Brennan *et al.* 2007) we did not observe an effect of gender, and for male R192Q mice we observed an unexpected lower CSD threshold compared with female R192Q mice. Given the variable duration of a CSD threshold paradigm that may have an impact on the studies in mice without physiological control, in our next experiments we choose to use only visual cortex CSD frequency assessment. We performed visual cortex CSD frequency measurements using an experimental paradigm in which isoflurane-N₂O/O₂ anesthesia was used, and in which mice were kept under physiological control, thus following the protocol described in Eikermann-Haerter *et al.* (Eikermann-Haerter *et al.* 2009b). Physiological parameters (pO₂, pCO₂, pH and blood pressure) are shown in Table 2. Both female ($p=0.0002$) and male R192Q mice ($p=0.004$) exhibited a higher CSD frequency compared with WT of the respective gender. In line with published data, CSD frequency was higher in female than in male R192Q mice (female R192Q, 22.8 ± 4.5 CSD/hr, N=7 vs male R192Q, 16.32 ± 1.9 CSD/hr, N=6; $p=0.007$), while no gender difference was observed for WT mice (female WT, 10.42 ± 1.8 CSD/hr, N=5 vs male WT, 12.0 ± 1.7 CSD/hr, N=5; $p=0.1$) (Figure 4). No statistical differences were observed for CSD amplitude and duration among the different groups, except for a longer CSD duration for female WT compared with female R192Q mice and compared with male WT mice (Table 2).

The absence of a gender effect on CSD frequency in experiments that are not physiologically controlled is related to the absence of mechanical ventilation and slight differences in physiology

The observation of a gender effect on visual cortex CSD frequency in R192Q mice in physiologically monitored and controlled experiments raises the question whether this gender effect may also be observed for experiments that are only physiologically monitored, provided that physiological parameters are within ranges. CSD threshold was not considered as a readout measure, given the variable duration of this paradigm. Therefore, we performed visual cortex CSD frequency assessments

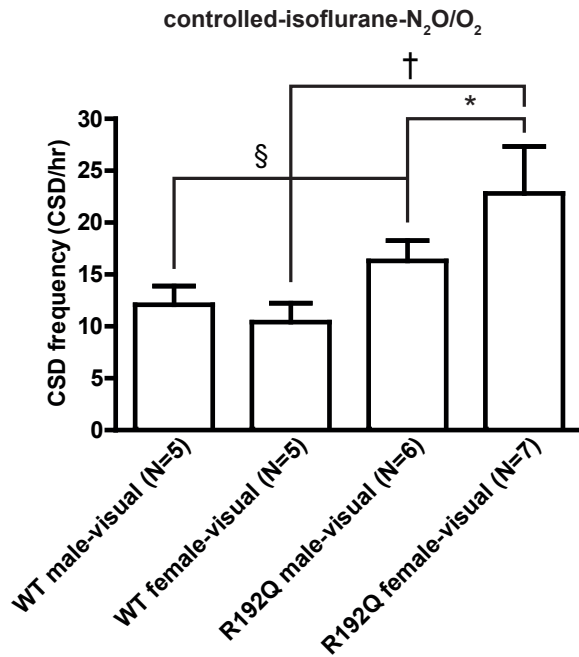


Figure 4. In physiologically controlled experiments performed under isoflurane-N₂O/O₂ anesthesia, visual cortex CSD frequency is enhanced in female R192Q mice compared with males. In agreement with previous findings in which physiological parameters were controlled using mechanical ventilation and isoflurane-N₂O/O₂ anesthesia (Eikermann-Haerter et al 2009b), female R192Q mice exhibited increased visual cortex CSD frequency compared with male R192Q mice (*p=0.007 female vs male R192Q; Student's t-test). Genotypic comparisons revealed a higher CSD frequency for both male and female R192Q mice in comparison with WT (§p=0.004 male R192Q vs male WT; †p=0.0002 female R192Q vs female WT, one-way ANOVA, Bonferroni correction).

Table 2. CSD amplitude and duration and physiological parameters of R192Q and WT mice for CSD frequency experiments performed with physiological monitoring-only, or with physiological monitoring and control

CSD Frequency	N	pH	pO ₂ (mmHg)	pCO ₂ (mmHg)	MABP (mmHg)	Amplitude (mV)	Duration (sec)
Male R192Q monitored-air	6	7.45±0.02 [‡]	97.8±4.0	25.5±2.7	74.2±1.1 [§]	21.1±1.1 [*]	27.1±5.1
Female R192Q monitored-air	6	7.38±0.02 [§]	102.8±5.9	28.6±2.1	77.3±3.3	19.3±2.8 [†]	28.6±11.1
Male R192Q monitored-N ₂ O/O ₂	5	7.41±0.02	133.7±37.7	29.2±3.7	85.0±10.8 [#]	14.8±2.9	26.9±11.1
Female R192Q monitored-N ₂ O/O ₂	6	7.36±0.03 [*]	113.1±10.9	33.2±5.0 [†]	83.5±3.0	19.3±1.1	19.8±2.5
Male R192Q controlled-N ₂ O/O ₂	6	7.40±0.03	123.1±13.3	31.1±1.9 [§]	95.3±9.1	20.3±3.9 [†]	28.2±5.9
Female R192Q controlled-N ₂ O/O ₂	7	7.42±0.04	128.1±23.0 [‡]	27.5±1.9 [#]	94.7±8.9 [§]	22.0±1.9	21.8±4.9 [*]
Male WT Controlled-N ₂ O/O ₂	5	7.39±0.01	132.4±3.4	31.0±1.6	95.2±11.6 [§]	22.9±2.8	27.0±3.9 [†]
Female WT Controlled-N ₂ O/O ₂	5	7.38±0.01	128.7±3.5	31.5±2.4 [§]	99.5±9.0 [‡]	21.6±6.9	45.2±14.0

Table 2. Values are shown as mean \pm SD. CSD duration was measured at half-maximal amplitude. In monitored experiments, physiological parameters were only monitored (via femoral artery catheterization) but not controlled by mechanical ventilation. In these experiments mice were breathing spontaneously using isoflurane with either air or N₂O/O₂. In physiologically controlled experiments, mice were both monitored and mechanically ventilated, using isoflurane-N₂O/O₂ anesthesia. In physiologically controlled experiments physiological parameters were maintained within physiological range by adjusting ventilation guided by femoral artery blood measurements. For some of the experimental groups, differences in CSD amplitude, duration or physiological parameters were observed. For female R192Q and WT mice, CSD amplitude and duration were not different among groups. There were some differences in physiological parameters: pH was higher (*p=0.044) whereas pCO₂ was lower ([†]p=0.020, one-way ANOVA, Bonferroni correction) for the female R192Q controlled-N₂O/O₂ compared to the female R192Q monitored- N₂O/O₂ group. Furthermore, the female R192Q controlled-N₂O/O₂ group exhibited higher pO₂ values ([‡]p=0.031) and higher MABP ([§]p=0.0001, one-way ANOVA, Bonferroni correction) compared to the female R192Q monitored-air group. For male R192Q mice, CSD duration was not different among groups. With respect to amplitude, the male R192Q monitored-N₂O/O₂ group showed a lower CSD amplitude compared to the male R192Q monitored-air group (*p=0.009) and compared to the male R192Q controlled-N₂O/O₂ group ([†]p=0.021, one-way ANOVA, Bonferroni correction). For the male R192Q monitored-air group compared to male R192Q controlled-N₂O/O₂ group, pH was slightly higher ([‡]p= 0.042) and pCO₂ was lower ([§]p=0.013, one-way ANOVA, Bonferroni correction). MABP was higher for the male R192Q controlled-N₂O/O₂ group compared to both male R192Q monitored-air ([§]p=0.0001) and male R192Q monitored-N₂O/O₂ groups ([#]p=0.010, one-way ANOVA, Bonferroni correction). Between genders, the female R192Q monitored- N₂O/O₂ group showed higher CSD amplitude compared to the male R192Q monitored-N₂O/O₂ group ([†]p=0.007, Student's t-test). In addition, the male R192Q monitored-air group exhibited higher pH values compared to the female R192Q monitored-air group ([§]p=0.001, Student's t-test). For the different controlled-N₂O/O₂ groups, some differences were observed in CSD characteristics and physiological parameter values between WT and R192Q mice, for both males and females. Although CSD amplitude for these experiments was comparable among groups, CSD duration was longer for female R192Q compared with female WT mice (*p=0.0001) and for female WT compared to male WT mice ([†]p=0.01, one-way ANOVA, Bonferroni correction). Furthermore, of the controlled-N₂O/O₂ groups female WT mice exhibited higher MABP values compared with female R192Q ([‡]p=0.002) and compared with male WT mice ([§]p=0.005, one-way ANOVA, Bonferroni correction). Lastly, pCO₂ was lower for the controlled-N₂O/O₂ group of female R192Q mice compared to female WT ([§]p=0.038) and compared with male R192Q mice ([#]p=0.027, one-way ANOVA, Bonferroni correction). MABP: mean arterial blood pressure.

in male and female R192Q mice that were physiologically monitored (by femoral artery catheterization) but not controlled (i.e., animals were breathing freely and were not mechanically ventilated). Under these conditions, we compared CSD frequency characteristics between male and female R192Q mice for experiments performed with air (as in our unmonitored and uncontrolled experiments) with experiments performed with N₂O/O₂ (as in the fully controlled experiments). Both with the use of air and N₂O/O₂ in the gas anesthesia mixture, physiologically monitored male and female R192Q mice showed comparable CSD frequencies (isoflurane-air: male R192Q, 17.8 \pm 2.0 CSD/hr, N=6 vs female R192Q, 16.1 \pm 1.7 CSD/hr, N=6, p=0.1; isoflurane-N₂O/O₂: male R192Q, 16.1 \pm 3.0 CSD/hr, N=5 vs female R192Q, 15.4 \pm 2.9 CSD/hr, N=6, p=0.7) (Figure 5A, B). For these monitored experiments, all physiological parameters were within accepted ranges (Table 2). No consistent relationship was apparent between higher or lower CSD frequency values and levels of physiological parameters, with physiological values showing changes in both positive and negative directions.

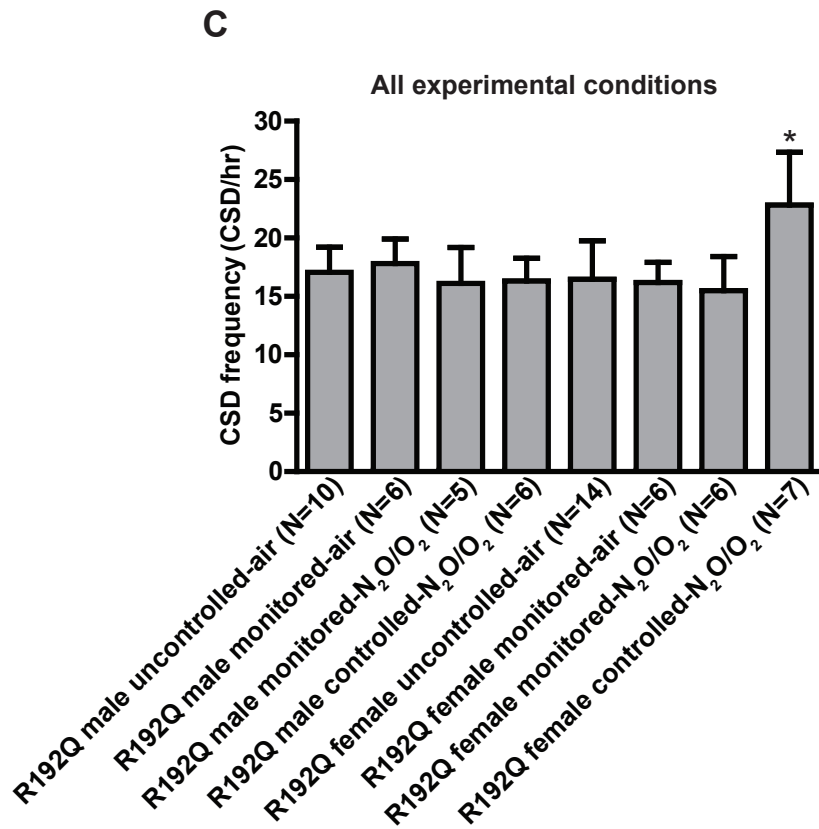
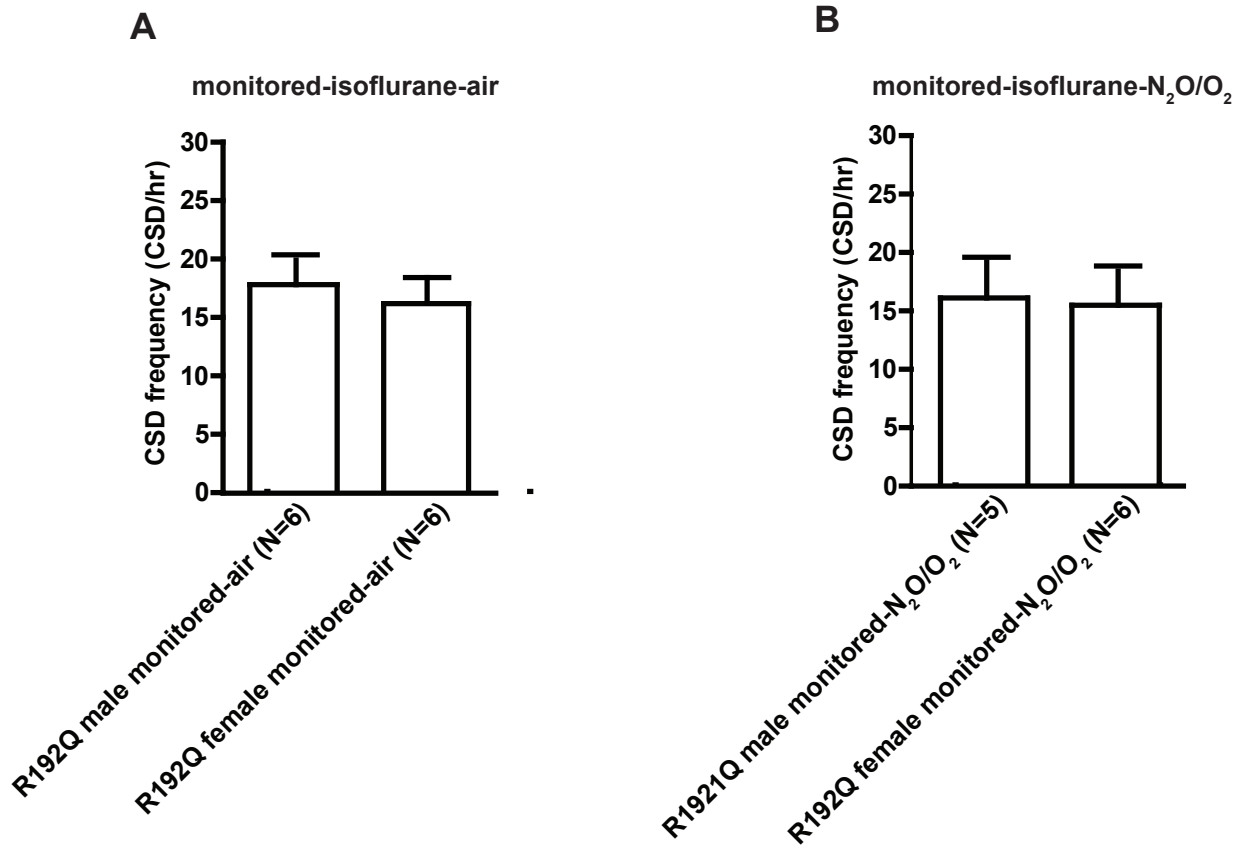


Figure 5. Increased visual cortex CSD frequency in female R192Q mice in experiments with physiological control is not related to the anesthesia gas mixture but to the use of mechanical ventilation.

(A, B) Bar diagrams depicting the lack of a gender effect on visual cortex CSD frequency between male and female R192Q mice for experiments carried out in the presence of physiological monitoring (via the femoral artery), but in the absence of mechanical ventilation (i.e., animals were allowed to breathe spontaneously and were not physiologically controlled), using isoflurane-air anesthesia (A) ($p=0.1$, male vs female R192Q, Student's t-test) and (B) isoflurane-N₂O/O₂ anesthesia ($p=0.7$, male vs female R192Q Student's t-test) (C) Bar diagrams depicting the comparison of the visual cortex CSD frequency data from male and female R192Q mice tested among the different experimental conditions. Grey colour indicates that these data were presented in earlier figures. Male R192Q mice displayed no differences in visual cortex CSD frequency across the 4 different experimental conditions. Female R192Q mice however displayed a significantly increased CSD frequency (indicated by *) in the presence of physiological control (i.e., monitoring via femoral catheterization and mechanical ventilation using isoflurane-N₂O/O₂ anesthesia) in comparison to female R192Q mice that were: i) uncontrolled with isoflurane-air ($p=0.001$); ii) physiologically monitored and not controlled but using isoflurane-air ($p=0.006$); or iii) physiologically monitored and not controlled using isoflurane-N₂O/O₂ ($p=0.005$ one-way ANOVA, Bonferroni correction).

Next, we carried out a direct comparison of the visual cortex CSD frequency data from male and female R192Q mice from the 4 different experimental methodologies used in the present study, i.e., i) uncontrolled-air, ii) monitored-air, iii) monitored-N₂O/O₂, and iv) monitored & controlled-N₂O/O₂. This comparison revealed that for male R192Q mice, CSD frequency was comparable for all 4 conditions. For female R192Q mice however, CSD frequency was significantly higher for the physiologically controlled group in which mice were both monitored and mechanically ventilated using isoflurane-N₂O/O₂ anesthesia (controlled-N₂O/O₂ vs uncontrolled-air $p=0.001$; controlled-N₂O/O₂ vs monitored-air $p=0.006$; controlled-N₂O/O₂ vs monitored-N₂O $p=0.005$; one-way ANOVA, Bonferroni correction) (Figure 5C). Comparison of CSD duration revealed no differences among groups. CSD amplitude however was lower in the male R192Q monitored-N₂O/O₂ group compared to the male R192Q monitored-air and compared to the male R192Q controlled-N₂O/O₂ group. In addition, the female R192Q monitored-N₂O/O₂ group showed higher CSD amplitude compared to the R192Q male monitored-N₂O/O₂ group (Table 2).

Finally, we assessed whether the absence of higher CSD frequency in R192Q female mice that were not physiologically controlled may be associated with differences in physiological parameters (pH, pO₂, pCO₂ and blood pressure) in comparison to experiments under physiological control. For female R192Q mice in the monitoring-only-N₂O/O₂ group, compared to the physiologically controlled-N₂O/O₂ group, pCO₂ values were slightly higher ($p=0.02$) and pH was slightly lower ($p=0.04$). Blood pressure was lower in both the monitoring-only-air and the monitoring-only-N₂O/O₂ groups, compared to the physiologically controlled-N₂O/O₂ group (controlled vs monitoring-only-air $p=0.0001$; controlled vs monitoring-only-N₂O/O₂ $p=0.01$) (Table 2). Physiological parameters were comparable between experiments performed in male R192Q mice with physiological control (using N₂O/O₂) and male R192Q mice that were monitored-only using N₂O/O₂ except for a lower blood pressure in R192Q monitored-N₂O/O₂ compared to R192Q controlled-N₂O/O₂ mice ($p=0.01$).

DISCUSSION

Using CSD frequency as readout for CSD susceptibility, we here showed that in the absence of physiological monitoring and control, R192Q mice exhibit an increased visual cortex CSD frequency compared to WT. In contrast to earlier studies, performed in the presence of physiological control (Eikermann-Haerter et al 2009b), the effect was not more pronounced in females. The absence of a gender effect was not explained by the CSD readout parameter: also with threshold measurements visual cortex CSD susceptibility was not enhanced, and was even increased, for female compared to male R192Q mice. In addition, comparison between visual and motor cortex as sites of CSD induction revealed that also for the motor cortex, CSD frequency was specifically enhanced in R192Q compared with WT mice. CSD threshold however was not different for R192Q compared with WT mice in the motor cortex. Gender had no influence on CSD frequency or threshold in the motor cortex. When comparing the two cortical regions, CSD susceptibility was enhanced in visual compared to motor cortex for CSD threshold in male R192Q mice, and for CSD frequency in female R192Q mice, indicating an effect of gender. Ovariectomy however had no effect on either visual cortex CSD frequency or threshold in female WT and R192Q mice in the absence of physiological control. Experiments performed with physiological monitoring, but without physiological control, revealed that the lack of a gender effect on visual cortex CSD frequency in the absence of control was not related to the use of air instead of N₂O/O₂, but to the absence of mechanical ventilation. In these monitored experiments, slight differences in pH, pCO₂ and blood pressure were observed that may contribute to the lack of enhanced CSD frequency in female compared to male R192Q mice when physiological parameters are not controlled.

Our data indicate that parameters of CSD susceptibility can be masked or unmasked depending on the experimental paradigm used. This has important implications for the interpretation and comparison of experimental CSD studies across laboratories, since it is plausible that certain effects on CSD characteristics are related to the used methodology. Below, we discuss possible implications of certain methodologies with respect to specific CSD characteristics.

The effect of enhanced visual cortex CSD frequency in R192Q mice in the present study for experiments performed using isoflurane-air anesthesia, is in line with findings from earlier work performed in the presence of physiological control and isoflurane-N₂O/O₂ anesthesia (Eikermann-Haerter et al 2009a, Eikermann-Haerter et al 2009b). This indicates that the genotypic effect on CSD frequency is not influenced by the presence or absence of physiological monitoring or control, or by the used anesthesia gas mixture. Our data extend the genotypic effect on CSD frequency also to the motor cortex. The reduced visual cortex CSD threshold in R192Q mice which we observed for both genders in the absence of physiological control is for male mice in line with earlier uncontrolled CSD studies. In those studies urethane was used instead of isoflurane anesthesia, and for threshold assessment electrical stimulation was used (van den Maagdenberg et al 2004, van den Maagdenberg et al 2010) instead of topical KCl application. Gender effects were not studied before in FHM1

mice for CSD threshold. We observed an opposite gender effect in the absence of physiological control, with visual cortex CSD threshold being lower in male compared to female R192Q mice. In addition, contradictory effects were observed for possible regional differences in CSD susceptibility among genders. Furthermore, ovariectomy had no effect on visual cortex CSD frequency or threshold in R192Q mice for physiologically uncontrolled experiments. For CSD frequency this contrasts reported effects of ovariectomy for experiments performed under physiological control (Eikermann-Haerter et al 2009b). It is plausible that in the absence of physiological control, variations occur in physiological parameters that influence CSD susceptibility characteristics, in particular during CSD threshold paradigms with variable durations.

Apart from CSD threshold and frequency, amplitude and duration of CSD events may also be influenced by alterations in physiology. A longer CSD duration for example has been associated with impaired tissue perfusion and recovery in rats (Sukhotinsky et al 2010). In previous studies under physiologically controlled conditions, CSD duration and amplitude were not different for visual cortex CSD frequency recordings between male and female mice for both WT and R192Q mutants (Eikermann-Haerter et al 2009b). In our study, no differences in CSD duration were observed that could contribute to the enhanced CSD frequency for female R192Q mice in the physiologically controlled group. CSD amplitude differences that were observed among some of the experimental groups were not related to differences in CSD frequency. In general, it should be noted that CSD amplitude may not be considered a reliable readout for CSD susceptibility given its dependence on recorded cortical depth.

Enhanced CSD susceptibility of female FHM1 mice is clinically relevant in the context of the higher propensity of women for migraine (Fettes 1999). Underlying mechanisms could involve enhancement of glutamatergic neuronal excitability by estradiol (Kelly et al 2003, Sato et al 2003, Smith 1989, Woolley et al 1997). A direct effect of estradiol on glutamatergic neurotransmission fits the observation of a gender effect only in FHM1 and not in WT mice. The finding that a gender effect in physiologically controlled experiments was observed regardless of estrous cycle, as the phase was not determined, suggests that intrinsic brain differences between males and females (Borsook et al 2014) may contribute to enhanced CSD susceptibility in female FHM1 mice. Interestingly, expression of the subunit of P/Q-type Ca^{2+} channels was shown to be enhanced in the pituitary of female compared to male rodents, and fluctuate during the estrous cycle (Fiordelisio et al. 2007), suggesting a modulation of CSD frequency by female hormones at the level of the mutant Ca^{2+} channels. The observation that a gender effect on CSD frequency was not observed in physiologically uncontrolled experiments suggests that mechanisms underlying the gender effect are influenced by changes in physiology. Although in all monitored experiments physiological parameters were within normal ranges for anesthetized rodents, monitored-only female R192Q mice displayed slightly higher pCO_2 and lower blood pressure values compared to female R192Q mice from the physiologically controlled group. Changes in pCO_2 and related changes in brain pH can modulate neuronal excitability by affecting ion

channels and transporters (Ruusuvuori & Kaila 2014), whereby high $p\text{CO}_2$ and low pH are expected to lower CSD susceptibility (Holland et al 2012). It is thus possible that the absence of a gender effect in monitored-only female R192Q mice relates to the slightly higher $p\text{CO}_2$ for this group. Changes in blood pressure can also affect CSD characteristics (Sukhotinsky et al 2010). Lower blood pressure of monitored-only female R192Q mice, compared to physiologically controlled mice, may thereby have contributed to a lower CSD frequency, thus masking a gender effect in the absence of control. Alternatively, it is possible that the use of mechanical ventilation for physiological control causes certain changes in physiology that are not monitored, but which may influence CSD characteristics. It has been described that mechanical ventilation can affect cerebral blood flow (Milan et al 2009), which has a bi-directional relationship with CSD initiation and propagation (Ayata 2013). Since estradiol can alter the brain's vascular responses to CGRP (Gupta et al 2007), it is possible that vascular effects of mechanical ventilation influence modulation of CSD susceptibility by estradiol.

Our CSD experiments performed in the absence of physiological control suggested that the visual cortex may be more susceptible to CSD than the motor cortex in R192Q, but not in WT mice. If true, this would be in line with neurophysiological studies reporting visual cortex hyperexcitability in migraine patients (Aurora et al 1998, Aurora et al 2003, Aurora & Wilkinson 2007). Further clinical relevance comes from imaging studies in migraine patients suggesting CSD initiation to occur preferably in the visual cortex (Hadjikhani et al 2001). Our data however showed that an effect of cortical region on CSD susceptibility was evident for CSD threshold only in male, and not in female R192Q mice. For CSD frequency, a regional difference was observed only in female, and not in male R192Q mice. Since these observations were made in the absence of physiological monitoring and control it is difficult to assess whether these findings may be confounded by possible changes in physiology during recordings. Studies in WT mice under halothane anesthesia, in the absence of physiological monitoring or control, showed no difference in CSD susceptibility between the occipital and frontal cortex (Godukhin & Obrenovitch 2001), similar to our observations in WT mice. For insight in a putative effect of cortical region on CSD susceptibility, additional experiments with physiological monitoring, and possibly mechanical ventilation for control, would be useful, as well as CSD studies in freely behaving mice that allow for exclusion of possible effects of anesthesia, catheterization or ventilation.

In conclusion, we showed that in experimental CSD studies in mice, control of physiological parameters can influence CSD susceptibility characteristics. Although the mechanisms remain to be unraveled, the occurrence of a gender effect on visual cortex CSD frequency in R192Q mice appeared sensitive to the use of mechanical ventilation and to possible changes in systemic pH, $p\text{CO}_2$ or blood pressure levels. Effects of other factors on CSD susceptibility, such as a putative effect of cortical region, may become apparent in the absence of control if such effects are sensitive to changes in physiology that are influenced by mechanical ventilation. Comparison among CSD studies need to take into account influences of the used methodologies and, ideally, should include studies in awake, unanesthetized animals.

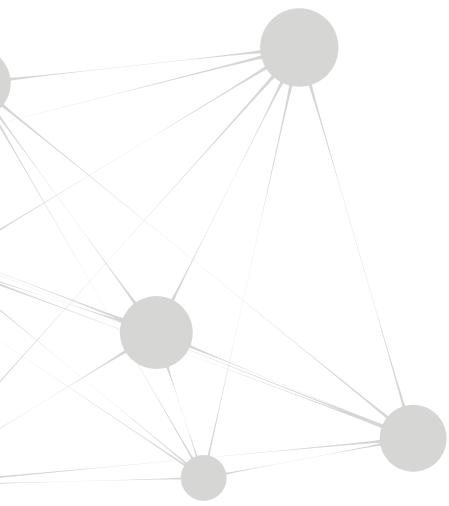
ACKNOWLEDGEMENTS

This work was supported by the EU “EUROHEAD” grant (LSHM-CT-2004-504837; M.D.F. & A.M.J.M.v.d.M.), the EU EUROHEADPAIN grant (nr 602633; M.D.F. & A.M.J.M.v.d.M.), the EU Marie Curie Career Integration Grant (nr 294233; E.A.T.), the Center for Medical Systems Biology (CMSB) established in the Netherlands Genomics Initiative/Netherlands Organisation for Scientific Research (NGI/NWO) (nr 050-060-409; A.M.J.M.v.d.M.), an LUMC Fellowship (E.A.T.) and the CURE SUDEP research award (nr 280560; E.A.T. & A.M.J.M.v.d.M.). The authors would like to thank Dr. Curtis F. Barrett for his contributions to earlier versions of this project, Drs. Cenk Ayata and Katharina Eikermann-Haerter (Boston, USA) for useful discussions.

REFERENCES

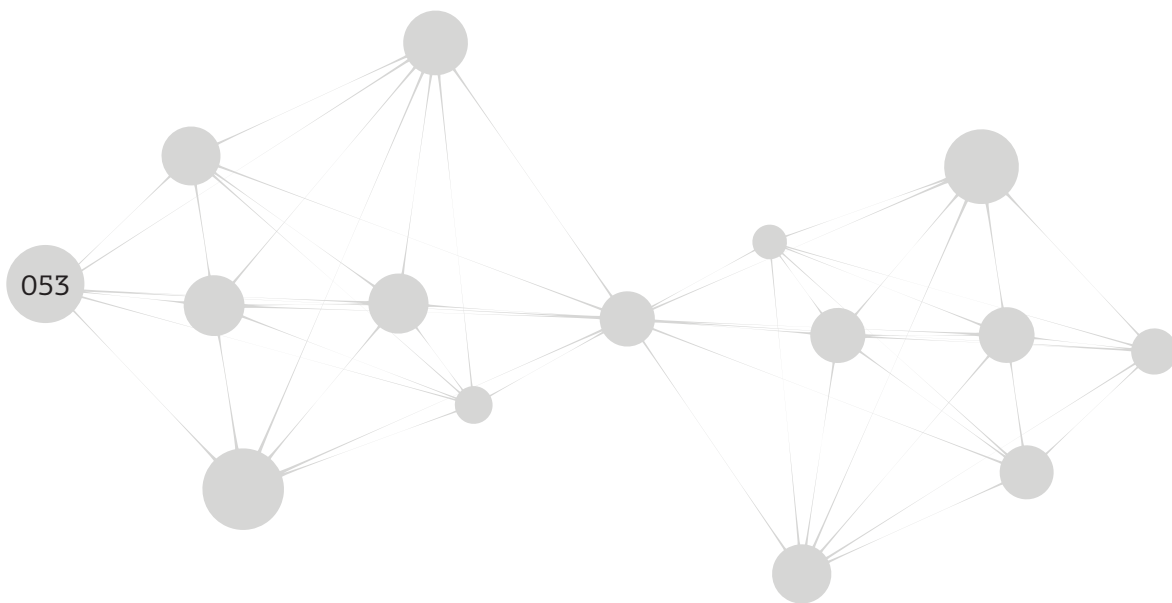
- Aurora SK, Ahmad BK, Welch KM, Bhardhwaj P, Ramadan NM. 1998. Transcranial magnetic stimulation confirms hyperexcitability of occipital cortex in migraine. *Neurology* 50:1111-4
- Aurora SK, Welch KM, Al-Sayed F. 2003. The threshold for phosphenes is lower in migraine. *Cephalalgia* 23:258-63
- Aurora SK, Wilkinson F. 2007. The brain is hyperexcitable in migraine. *Cephalalgia* 27:1442-53
- Ayata C. 2013. Spreading depression and neurovascular coupling. *Stroke* 44:S87-9
- Borsook D, Erpelding N, Lebel A, Linnman C, Veggeberg R, et al. 2014. Sex and the migraine brain. *Neurobiol. Dis.* 68C:200-14
- Brennan KC, Romero Reyes M, Lopez Valdes HE, Arnold AP, Charles AC. 2007. Reduced threshold for cortical spreading depression in female mice. *Ann. Neurol.* 61:603-6
- Eikermann-Haerter K, Baum MJ, Ferrari MD, van den Maagdenberg AM, Moskowitz MA, Ayata C. 2009a. Androgenic suppression of spreading depression in familial hemiplegic migraine type 1 mutant mice. *Ann. Neurol.* 66:564-8
- Eikermann-Haerter K, Dilekoz E, Kudo C, Savitz SI, Waeber C, et al. 2009b. Genetic and hormonal factors modulate spreading depression and transient hemiparesis in mouse models of familial hemiplegic migraine type 1. *J. Clin. Invest.* 119:99-109
- Ferrari MD, Klever RR, Terwindt GM, Ayata C, van den Maagdenberg AM. 2015. Migraine pathophysiology: lessons from mouse models and human genetics. *Lancet Neurol.* 14:65-80
- Fettes I. 1999. Migraine in the menopause. *Neurology* 53:S29-33
- Fiordeliso T, Jimenez N, Baba S, Shiba K, Hernandez-Cruz A. 2007. Immunoreactivity to neurofilaments in the rodent anterior pituitary is associated with the expression of alpha 1A protein subunits of voltage-gated Ca²⁺ channels. *J. Neuroendocrinol.* 19:870-81
- Goadsby PJ, Lipton RB, Ferrari MD. 2002. Migraine--current understanding and treatment. *N. Engl. J. Med.* 346:257-70
- Godukhin OV, Obrenovitch TP. 2001. Asymmetric propagation of spreading depression along the anteroposterior axis of the cerebral cortex in mice. *J. Neurophysiol.* 86:2109-11
- Gupta S, Mehrotra S, Villalon C, De Vries R, Garrelds I, et al. 2007. Effects of female sex hormones on responses to CGRP, acetylcholine, and 5-HT in rat isolated arteries. *Headache* 47:564-75
- Hadjikhani N, Sanchez Del Rio M, Wu O, Schwartz D, Bakker D, et al. 2001. Mechanisms of migraine aura revealed by functional MRI in human visual cortex. *Proc. Natl. Acad. Sci. USA* 98:4687-92
- Holland PR, Akerman S, Andreou AP, Karsan N, Wemmie JA, Goadsby PJ. 2012. Acid-sensing ion channel 1: a novel therapeutic target for migraine with aura. *Ann. Neurol.* 72:559-63

- ICHD. 2004. The International Classification of Headache Disorders: 2nd edition. *Cephalalgia* 24 Suppl 1:9-160
- Kelly MJ, Qiu J, Ronnekleiv OK. 2003. Estrogen modulation of G-protein-coupled receptor activation of potassium channels in the central nervous system. *Ann. N Y Acad. Sci.* 1007:6-16
- Kudo C, Nozari A, Moskowitz MA, Ayata C. 2008. The impact of anesthetics and hyperoxia on cortical spreading depression. *Exp. Neurol.* 212:201-6
- Lauritzen M. 1994. Pathophysiology of the migraine aura. The spreading depression theory. *Brain* 117 (Pt 1):199-210
- Milan A, Freato F, Vanzo V, Chiandetti L, Zaramella P. 2009. Influence of ventilation mode on neonatal cerebral blood flow and volume. *Early Hum. Dev.* 85:415-9
- Ophoff RA, Terwindt GM, Vergouwe MN, van Eijk R, Oefner PJ, et al. 1996. Familial hemiplegic migraine and episodic ataxia type-2 are caused by mutations in the Ca²⁺ channel gene CACNL1A4. *Cell* 87:543-52
- Pietrobon D, Moskowitz MA. 2014. Chaos and commotion in the wake of cortical spreading depression and spreading depolarizations. *Nat. Rev. Neurosci.* 15:379-93
- Ruusuvuori E, Kaila K. 2014. Carbonic anhydrases and brain pH in the control of neuronal excitability. *Subcell. Biochem.* 75:271-90
- Sato K, Matsuki N, Ohno Y, Nakazawa K. 2003. Estrogens inhibit l-glutamate uptake activity of astrocytes via membrane estrogen receptor alpha. *J. Neurochem.* 86:1498-505
- Smith SS. 1989. Estrogen administration increases neuronal responses to excitatory amino acids as a long-term effect. *Brain Res.* 503:354-7
- Sukhotinsky I, Yaseen MA, Sakadzic S, Ruvinskaya S, Sims JR, et al. 2010. Perfusion pressure-dependent recovery of cortical spreading depression is independent of tissue oxygenation over a wide physiologic range. *J. Cereb. Blood Flow Metab.* 30:1168-77
- van den Maagdenberg AM, Pietrobon D, Pizzorusso T, Kaja S, Broos LA, et al. 2004. A Cacna1a knockin migraine mouse model with increased susceptibility to cortical spreading depression. *Neuron* 41:701-10
- van den Maagdenberg AM, Pizzorusso T, Kaja S, Terpolilli N, Shapovalova M, et al. 2010. High cortical spreading depression susceptibility and migraine-associated symptoms in Ca(v)2.1 S218L mice. *Ann. Neurol.* 67:85-98
- Woolley CS, Weiland NG, McEwen BS, Schwartzkroin PA. 1997. Estradiol increases the sensitivity of hippocampal CA1 pyramidal cells to NMDA receptor-mediated synaptic input: correlation with dendritic spine density. *J. Neurosci.* 17:1848-59



Chapter 3

Increased EEG gamma band power and spontaneous cortical spreading depression events in $Ca_v2.1$ R192Q mutant hemiplegic migraine mice



Reinald Shyti^{1‡}, Thijs Houben^{2‡}, Roselin R. Klever², Thijs J.L. Perenboom², Maarten Schenke², Michel D. Ferrari², Katharina Eikermann-Haerter³, Cenk Ayata^{3,4}, Arn M.J.M. van den Maagdenberg^{1,2*}, Else A. Tolner^{2*}

Department of ¹Human Genetics and ²Neurology, Leiden University Medical Center, Leiden, the Netherlands; ³Stroke and Neurovascular Regulation Laboratory, Department of Radiology and Stroke Service and ⁴Neuroscience Intensive Care Unit, Department of Neurology, Massachusetts General Hospital, Harvard Medical School, Charlestown, USA

^{‡,*} equal contributions

In preparation

ABSTRACT

Migraine is an episodic brain disorder for which cortical hyperexcitability has been proposed as one of the key disease mechanisms. Two main subtypes of migraine are distinguished based on the presence of an aura that can accompany headaches in many patients. The aura is likely caused by cortical spreading depression (CSD), a slowly spreading wave of neuronal and glial depolarization. Familial hemiplegic migraine type 1 (FHM1) mutant mice that carry a R192Q missense mutation in the *Cacna1a* gene, which had been previously identified in patients, display enhanced (glutamatergic) neuronal excitability and increased CSD susceptibility. Here we performed continuous day-night DC-EEG and multi-unit activity recordings in visual and motor cortex from freely behaving FHM1 R192Q and wild-type (WT) mice to investigate whether cortical network properties differ between genotypes and whether these can lead to spontaneous CSD events. Parallel experiments under anesthesia were aimed to investigate whether CSD susceptibility differs between the light and dark period and/or between visual and motor cortex. Under freely behaving conditions, FHM1 mice displayed enhanced gamma (30-45 Hz) EEG power in both visual and motor cortex throughout vigilance states (i.e., active waking, REM sleep and non-REM sleep); delta (0.75-5 Hz) power was reduced in motor cortex during REM and non-REM sleep. In 4 out of 10 FHM1 mice, in total 13 spontaneous CSD events occurred that were never observed in WT mice. CSD events occurred both during light and dark periods. For 9 events, the start of CSD was observed first in the visual cortex while for the remaining events the CSD event appeared nearly simultaneously in the visual and motor cortex. Under anesthesia, CSD frequency did not show a correlation with the time-of-day, and was enhanced in both visual and motor cortex for FHM1 mice compared with WT. Taken together, the changes in EEG power and occurrence of spontaneous CSD events in FHM1 mutants are in line with increased cortical network excitability in mutants. Cortical network changes and occurrence of spontaneous CSD events in FHM1 mice provide a unique opportunity to study the episodic nature of migraine attacks.

INTRODUCTION

Migraine is a common episodic brain disorder characterized by recurrent attacks of headache and associated autonomic and neurological symptoms (ICHD 2004, Goadsby et al 2002). In one-third of patients migraine attacks are accompanied, in most cases preceded, by an aura, which typically consists of visual symptoms. Cortical spreading depression (CSD) is the most likely mechanism of migraine aura (Lauritzen 1994, Hadjikhani et al 2001), and a potential trigger of the headache, as suggested by studies in rodents (Bolay et al 2002, Zhang et al 2010, Zhang et al 2011). CSD is defined as a slowly spreading cortical wave of neuronal and glial depolarization that is followed by a temporary suppression of activity (Lauritzen 1994). Clinical and animal data indicate that migraine attacks may be caused by neuronal hyperexcitability (Welch et al 1990, Aurora & Wilkinson 2007, Badawy & Jackson 2012). The visual nature of migraine auras (Eriksen et al 2004), reports of photophobia (Maniyar et al 2015) and structural (Granziera et al 2006) and functional alterations (Aurora et al 1999) in the visual cortex of patients suggest that in the migraine susceptible brain, hyperexcitability may prominently manifest itself in the visual cortex. Moreover, circadian changes in physiology may contribute to the enhanced neuronal excitability (Herzog 2007, Cho 2012) that can explain apparent circadian rhythmicity in the timing of attacks with the majority of the attacks occurring during the active/light period in humans (Fox & Davis 1998, Alstadhaug et al 2008).

To investigate the link between neuronal hyperexcitability and migraine susceptibility, transgenic knock-in mice have been generated that carry the missense mutation R192Q in the *Cacna1a* gene that encodes the α_1 subunit of $\text{Ca}_v2.1$ (P/Q-type) Ca^{2+} channels (van den Maagdenberg et al 2004). In patients, this mutation causes familial hemiplegic migraine type 1 (FHM1) (Ophoff et al 1996). FHM1 R192Q knock-in mice display increased propensity to experimentally induced CSD under anesthesia (van den Maagdenberg et al 2004, Eikermann-Haerter et al 2009, van den Maagdenberg et al 2010), and enhanced glutamatergic neuronal transmission in cortical brain slices (Tottene et al 2009, Vecchia et al 2014).

The well-controlled conditions in which neuronal excitability was studied in brain slices and anesthetized mice exclude studying effects of sleep-wake patterns or interactions of external and internal stimuli with brain physiology. Enhanced neuronal network excitability resulting from such interactions may sporadically create a window of opportunity for the initiation of spontaneous attacks in patients (Stankewitz & May 2009) that can only be identified in freely behaving mice. To assess in what way FHM1 mutations affect ongoing neuronal network activity patterns in the intact awake brain, we performed longitudinal day-night recordings of full-band (DC) EEG and multi-unit activity (MUA) in freely behaving FHM1 R192Q and WT mice. Findings were related to the time-of-day and cortical location (i.e., visual vs motor cortex). In parallel, we compared susceptibility to experimentally induced CSD (i.e., by cortical application of KCl to the exposed dura) performed at the start of the light vs the dark period, as well as between visual and motor cortex, in anesthetized mice under physiological monitoring and control. Our data reveal that freely behaving FHM1 R192Q

mice can display spontaneous CSD events. Observed changes in EEG power are suggestive of overall enhanced cortical excitability. When taking into account also experiments in anesthetized mice, it seems that CSD susceptibility is enhanced independent of the time-of-day in both visual and motor cortex.

MATERIALS AND METHODS

Animals

Male wild-type ('WT') and homozygous *Cacnala* FHM1 R192Q knock-in ('R192Q') (van den Maagdenberg et al 2004) were used that were backcrossed for at least 6 generations with C57BL/6J mice. Prior to experiments, animals were maintained under a 12-hr light/12-hr dark regime unless specifically mentioned. Standard mouse chow and water were available *ad libitum*. All experiments were approved by the Animal Experiments Committee of Leiden University Medical Center and Massachusetts General Hospital Subcommittee on Research Animal Care.

EEG recordings in freely behaving mice

The weight of mice at surgery was 31.2 ± 2.7 gr and 28.4 ± 2.3 gr ($p=0.43$, Student's t-test, $N=10$; WT and R192Q mice, respectively); the age was 145 ± 19 days and 161 ± 75 days, ($p=0.51$, Student's t-test, $N=10$; WT and R192Q mice, respectively). Under isoflurane anesthesia (1.5%), 7 electrodes were stereotactically implanted at the following coordinates (in mm relative to bregma): a pair of Platinum (Pt) electrodes 3.5 posterior/2.0 lateral/0.8 ventral from dura (right visual cortex); a pair of Pt electrodes 1.5 anterior/1.5 lateral/0.8 ventral from dura (right motor cortex); a Silver (Ag) ball-tip electrode 3.5 posterior/2.0 lateral on the dura (left visual cortex); an Ag ball-tip electrode and an Ag-AgCl ball-tip electrode were placed above cerebellum that served as reference and ground electrodes, respectively (Figure 1A). Electrodes were attached to the skull using dental cement (Optibond FL, Kerr, Orange, CA, USA). After a recovery period of 7 days, animals were placed in a shielded recording cage and connected to the recording hardware through a counterbalanced, low-torque custom-built electrical commutator. Epidural and intracortical EEG signals were pre-amplified 3x and were fed into separate amplifiers for DC-EEG and AC-EEG. For DC-EEG, signals were low-pass filtered (500 Hz) and amplified 10x. For AC-EEG, signals were band-pass filtered (0.05 Hz to 500 Hz) and amplified 1200x. Signals were digitized (Power 1401, CED, Cambridge, UK) at a rate of 1000 Hz for DC-EEG and 5000 Hz for AC-EEG. In addition, signals from paired intracortical Pt electrodes were used for detection of multi-unit activity (MUA) by amplifying them differentially (36000x), band-pass filtering them (500 Hz to 5000 Hz) and digitizing them at 25000 Hz. Alongside the EEG and MUA recordings, locomotor activity was recorded using a passive infrared custom-built motion detection sensor and drinking activity was recorded with a custom-built beam-break sensor in front of the drinking bottle.

CSD induction with intracortical KCl infusion

To assess whether our recording technique is able to accurately detect cortical spreading depression, we performed a set of experiments in which we induced CSD using reverse microdialysis with 500 mM KCl. For these experiments, surgery was performed as described above, with two modifications: 1) the posterior pair of intracortical Pt electrodes in the right hemisphere was placed in the somatosensory cortex (1.5 posterior/1.5 lateral/0.8 ventral from dura) and 2) a guide cannula (Brainlink, Groningen, the Netherlands) was placed in a cranial window over the visual cortex (3.5 posterior/2.0 lateral/terminating on dura) (Figure 2D). After the recovery period, recordings were started as described above. On day two of the recording, a microdialysis probe (Brainlink, Groningen, the Netherlands) was placed in the guide cannula with the 1 mm membrane extending from dura to a depth of 1 mm below dura. Microdialysis perfusion with minimal perfusion fluid (140.3 mM Na⁺, 2.7 mM K⁺, 1.2 mM Ca²⁺, 1.0 mM Mg²⁺, and 147.7 mM Cl⁻) was started at a flow rate of 1 μ L/min using a microperfusion syringe pump (Harvard Apparatus Inc, South Natick, MA, USA). On day 4 of the recording, the perfusion fluid was changed to modified minimal perfusion fluid containing 500 mM of KCl (500 mM K⁺, 1.2 mM Ca²⁺, 1.0 mM Mg²⁺, 504.4 mM Cl⁻ in MilliQ water) during a 30-min time window to induce CSD events.

EEG data analysis, scoring of vigilance states and spontaneous CSD detection

For spectral analysis of EEG data, 24 hr of recorded EEG was used that was obtained after at least 24 hr of habituation of the animal to the recording cage. Data were obtained from the second (N=3 WT mice and N=2 R192Q) or third day of recording (N=7 WT and N=8 R192Q). Comparison of power spectra from the first 4 recording days for N=3 WT and N=3 R192Q mice indicated stable EEG power spectra with little variability across recording days for both WT and R192Q mice: Intraclass Correlation Coefficient (Bartko 1966) was higher than 0.9 for visual cortex and motor cortex vigilance state-specific power spectra, for all animals over the first 4 recording days. For the 4 R192Q mice in which spontaneous CSD were observed, EEG analysis was performed on a 24-hr slot during which no CSD was observed, which was the second recording day for two R192Q mice (21 hr after first and only CSD; 27 hr after first CSD, 7 hr before second CSD) and third recording day for the other two R192Q mice (before occurrence of first CSD for both animals).

Signals from the visual and motor cortex were low-pass filtered at 100 Hz and down-sampled to 200 Hz (Spike2 V7, CED, Cambridge, UK). Power spectra were computed using a Fast Fourier Transform (FFT) routine (Hanning window, 0.25 Hz resolution) for each 4-sec epoch of the 24 hr of recording. Epochs containing movement or technical artifacts (typified e.g., by large irregular and often high-frequency waveforms associated with movement in case of movement artifacts, or by irregular clipping of signals or 50 Hz or high-frequency noise) were excluded from further analysis. The overall spectral composition of network activity in the motor and visual cortex was quantified by averaging the power spectral density per cortical region over the entire recording for each animal. For the comparison across genotypes, the total power was calculated for 5 defined spectral bands:

delta (δ , 0.75-5Hz), theta (θ , 5-10Hz), alpha (α , 10-15Hz), beta (β , 15-30Hz), and gamma (γ , 30-45 Hz). As the spectral composition of mouse cortical network activity varies across vigilance states, we also performed a vigilance-state-specific comparison of EEG power spectral composition. For this analysis, only spectra were selected from epochs with clearly defined vigilance states (i.e., active waking, REM sleep and non-REM sleep) that were determined by applying an automated algorithm for defining vigilance state per 4-sec epoch on the basis of the recorded behavioral activity and the spectral composition of the visual cortex EEG signal. In the algorithm, epochs with locomotor or drinking activity were classified as active waking ($19.6 \pm 4.8\%$ for WT, $15.8 \pm 6.8\%$ for R192Q; Student's t-test, $p=0.17$). The first 10 epochs following cessation of behavioral activity were classified as passive waking ($15.1 \pm 2.9\%$ for WT, $16.3 \pm 3.4\%$ for R192Q; Student's t-test, $p=0.40$) (Fisher et al 2012). Remaining epochs were classified as sleeping ($64.6 \pm 6.5\%$ for WT, $67.1 \pm 8.8\%$ for R192Q; Student's t-test, $p=0.49$) and further subdivided into non-REM sleep or REM sleep on the basis of the visual cortex EEG power spectrum: epochs with strong delta activity ($>2x$ average delta power) were classified as non-REM sleep ($30.9 \pm 3.8\%$ for WT, $28.5 \pm 4.2\%$ for R192Q; Student's t-test, $p=0.20$). Epochs with high theta ($>$ average theta power) and low delta ($<$ average delta power) activity were classified as REM sleep ($12.3 \pm 2.7\%$ for WT, $13.0 \pm 4.3\%$ for R192Q; Student's t-test, $p=0.69$). Sleep epochs not fulfilling the above criteria were left unclassified.

The occurrence of spontaneous CSD events was detected on the basis of the following criteria: 1) the presence of a transient negative DC-shift in the DC-EEG signal with an amplitude of 5 mV or more that was detected on multiple recording sites within 60 sec from the first occurrence, 2) a depression of AC-EEG amplitude coinciding with the start of the DC-shift and, if MUA signal was available, 3) multi-unit activity silencing coinciding with the start of the DC-shift. Events were scored as CSD when criterion 1 was met together with either criterion 2 or 3, or all 3 criteria together.

Effect of time-of-day on CSD susceptibility

WT and R192Q mice were randomly assigned to a 'light' or a 'dark' group and acclimatized to the following shifted light/dark regimes for at least 2 weeks before follow-up procedures. Mice in the 'light' group were kept with 'lights on' from 08.30 am until 20.30 pm; mice in the dark group were kept with lights on from 20.30 pm until 08.30 am. All experiments started around 08.15 am, so that mice from the light group just started the light (resting) period at the start of experiment, while mice from the dark group just started the dark (active) period. At least 4 days before the CSD experiment a blood sample ($\sim 20 \mu\text{L}$) was collected by a small tail cut to determine baseline corticosterone plasma levels. Plasma was obtained after centrifugation for 10 min at 4000 rpm at 4°C , temporarily placed on dry ice and stored until used at -80°C . Corticosterone plasma levels were determined using a RIA kit according to manufacturer guidelines (MP Biomedicals Inc., Santa Ana, CA, USA) (Sarabdjitsingh et al 2010).

CSD frequency recordings were carried out under full physiological control as previously described

(Shyti et al 2015). Physiological parameters were maintained within the following ranges; blood pressure: 70-120 mmHg, $p\text{CO}_2$: 30-40 mmHg, $p\text{O}_2$: 80-140 mmHg and pH: 7.30-7.40. The weight of mice at surgery was 25.9 ± 1.2 gr; N=5 for WT and 25.1 ± 1.2 gr; N=5 for R192Q of the 'light' group (Student's t-test, $p=0.3$) and 25.8 ± 1.3 gr; N=7 for WT and 24.4 ± 1.9 gr; N=5 for R192Q mice of the 'dark' group (Student's t-test, $p=0.2$). The age of the mice at surgery was 122.8 ± 13.0 days; N=5 for WT and 123.0 ± 14.0 days; N=5 for R192Q mice of the 'light' group (Student's t-test, $p=0.1$) and 106.6 ± 13.6 days; N=7 for WT and 106.0 ± 7.9 days; N=5 for R192Q mice of the 'dark' group (Student's t-test, $p=0.4$).

For CSD measurements, mice were intubated, muscle paralyzed with an i.p. injection of 0.04 mg/kg body weight pancuronium and mechanically ventilated (SAR-830, CWE Inc, Ardmore, PA, USA). Mice were maintained under 1% isoflurane anesthesia in 20-30% O_2 and 70% N_2O . Blood gas values and mean arterial blood pressure were measured via a catheter in the femoral artery and a blood gas analyser (RapidLab248, Siemens Healthcare Diagnostics Inc., Tarrytown, NY, USA). During the experiment, ventilation parameters were adjusted when necessary to maintain physiological parameters within normal range. Experiments were only included for analysis when physiological parameters were within normal range. Core body temperature was maintained at 37°C using a heating pad (Stoelting, Wood Dale, IL, USA). The mouse was fixed in a stereotaxic frame (David Kopf Instruments, Tujunga, CA, USA) and a midline incision of ~ 2.5 cm was made over the top of the head, the skin was retracted to expose the skull, and the periosteum was removed with cotton-tipped applicator sticks. Two craniotomy windows were prepared at the following coordinates (in mm with respect to Bregma): 3.5 mm posterior/2.0 mm lateral (visual cortex) and 1.5 mm anterior/1.5 mm lateral (motor cortex). Care was taken to keep the dura intact to minimize trauma to the underlying brain tissue. At the recording site a sharp glass capillary electrode (FHC Inc., Bowdoin, ME, USA) filled with 150 mM NaCl was advanced through the dura to a depth of 300 μm . After insertion of the electrode, a drop of mineral oil (~ 5 μL) was applied to the recording site to prevent drying of the cortical tissue. DC-potential signals were measured with respect to an Ag/AgCl reference electrode placed subcutaneously at the neck and amplified 10x (Molecular Devices, Sunnyvale, CA, USA). The DC signal was low-pass filtered at 4 Hz and digitized at 100–200 Hz using PowerLab 16/30 hardware (AD Instruments, Inc., Colorado Springs, CO, USA). Data were recorded and analyzed off-line using LabChart Pro (AD Instruments). Due to the time needed for surgical preparation, CSD frequency measurements started around 09.00 am.

Regional differences in CSD susceptibility

The surgery with full physiological monitoring and control for determining regional differences in CSD susceptibility was performed as described above. The weight of mice at surgery was 26.0 ± 1.3 gr; N=13 and 24.7 ± 1.9 gr; N=16 for WT and R192Q mice (Student's t-test, $p=0.1$), respectively. The age of mice at surgery was 77.1 ± 20.4 days; N=13 and 88.6 ± 18.7 days; N=16 for WT and R192Q mice (Student's t-test, $p=0.1$), respectively. To determine the CSD induction threshold, a cotton

pellet (Interguide Dental Supply, Burlingame, CA, USA) soaked in solution with an increasing K^+ concentration was placed on the dura for 3 min to measure either motor (from bregma: 1.5 mm anterior/1.5 mm lateral or visual (from bregma: 3.5 mm posterior/2 mm lateral) cortex CSD threshold. K^+ concentrations were prepared with 7.5 mM increments, starting at 5 mM, with total osmolarity kept at 300 mOsmol with NaCl. Upon successful induction of a CSD event, the induction site was rinsed thoroughly with 150 mM NaCl.

Subsequently, two additional cranial windows were prepared in the opposite hemisphere in the *same* mouse at the same motor and visual cortex locations as described above to measure CSD threshold in the opposite direction: e.g., motor cortex CSD threshold was measured on the contralateral side in case the visual cortex threshold had been measured first in the other hemisphere or *vice versa* (Figure 4C). After CSD threshold assessments in both hemispheres, CSD frequency was measured in the same hemisphere and location as used for the last CSD threshold measurement by continuous application of a cotton pellet soaked in 1 M KCl on the dura for 30 min (with refreshment of the pellet after 15 min). Only reversible DC deflections with amplitudes larger than 5 mV were considered a CSD event and included in the CSD characteristics analysis.

Nissl and GFAP staining

At the end of the longitudinal EEG/MUA recordings, brains were histologically processed for verification of electrode location and possible inflammatory reaction. Mice were transcardially perfused with 1x PBS and 4% paraformaldehyde (PFA), the brain removed and post-fixed in 4% PFA for at least 2 hr. Subsequently, brains were cryoprotected in consecutive steps of 10.5% (overnight), 10.5% (overnight) and 30% (overnight) sucrose and embedded in 11% gelatin/10% sucrose. Brains were sectioned sagittally at 40 μ m using a cryotome (Leica microsystems, Wetzlar, Germany). Sections were washed for 2 hr in 10% fetal calf serum (FCS) to block endogenous peroxidase activity followed by incubation for 72 hr in primary rabbit polyclonal anti-GFAP antibody (DAKO Cytomation, Copenhagen, Denmark) diluted 1:30000 in 2% FCS and 0.5% TX100. Sections were next treated for 2 hr in the avidin-biotin peroxidase complex (Vectastain ABC peroxidase kit, Vector Laboratories Inc., Burlingame, CA, USA), washed once in 0.1 M Tris-HCl and allowed to react in a solution of 0.02% 3,3'-diaminobenzidine (DAB) in 0.1 M Tris-HCl and 35% H_2O_2 for 10 min. Sections were washed in MilliQ, dehydrated in graded alcohol, cleared in xylene, and coverslipped using permount mounting medium (Thermo Fisher Scientific, Waltham, MA, USA). For Nissl staining, sections were immersed into cresyl violet solution for 3 min followed by consecutive dehydration steps in MilliQ, 50% EtOH, 96% EtOH, 100% EtOH and xylene.

Statistical analysis

For skewed parameters corresponding non-parametric tests were used. For comparison of EEG power in the different spectral bands between genotypes, cortical areas and vigilances states, we used Mann-Whitney U-test with false discovery rate correction (FDR; Benjamini-Hochberg method) to control

for multiple testing. To test whether EEG characteristics varied between different recording days, we calculated the Intraclass Correlation Coefficient (Bartko 1966). Mann-Whitney U-test was also used for comparison of CSD threshold between genotypes and comparison of corticosterone plasma levels between light and dark phases, and Wilcoxon signed ranked test for regional CSD threshold comparisons among mice of the same genotype. CSD frequency data were compared using one-way ANOVA followed by Bonferroni correction. Data are presented as median (CSD threshold, corticosterone plasma values and power spectra) or mean \pm SD (CSD frequency).

RESULTS

EEG spectra of freely behaving R192Q mice display increased gamma power in both visual and motor cortex

To assess effects of the R192Q mutation on neuronal network activity, we recorded longitudinal intracortical EEG from the Pt electrodes in the right hemisphere in 10 freely behaving male R192Q and 10 WT mice (Figure 1A-C). Comparison of 24-hr EEG power spectra from the first 4 recording days of N=3 WT and N=3 R192Q mice revealed that EEG power spectra were stable across recording days with little variability for both R192Q and WT mice (Intraclass Correlation Coefficient > 0.9 for vigilance state specific power spectra, for all animals over the first 4 recording days, for both visual and motor cortex), allowing us to combine data from different days across mice. For comparison between R192Q and WT mice, EEG spectral composition was analyzed from 24 hr EEG recorded on either the second or third day of the recording session (see Materials and Methods), both for the total 24-hr window as well as for separate vigilance states such as active waking, REM and non-REM sleep. The approximate distribution of vigilance states during the 24 hr periods, as determined from the movement sensor and EEG power (see Materials and Methods), is shown in Table 2. No significant differences were observed between R192Q and WT mice regarding the times spent across vigilance states. The total 24-hr EEG power of all frequency bands (0.75-45Hz) did not differ between genotypes in visual or motor cortex ($p>0.05$). In the motor cortex, but not in the visual cortex, we observed that both for the 24-hr average as well as during REM sleep and non-REM sleep, power in the delta band (δ , 0.75-5 Hz) was significantly lower in R192Q than in WT mice (Figure 1E). In the visual cortex and the motor cortex, power in the gamma band (γ , 30-45 Hz) was significantly higher in R192Q than in WT mice, both for the 24-hr average and for the separate vigilance states (Figure 1F).

Power in the theta band was not different in the visual cortex but was significantly reduced in the motor cortex in the 24-hr average during REM sleep and during non-REM sleep. Power in the alpha band was significantly higher in the visual cortex in the 24-hr average and during REM sleep but significantly lower in R192Q mice in motor cortex during non-REM sleep. Power in the beta band was significantly higher in the visual cortex of R192Q mice in the 24-hr average and during REM sleep, non-REM sleep and waking. Beta power was also significantly higher in motor cortex in R192Q mice during waking.

To control for variation in absolute power among individual mice, which can be due to differences in the depth of intracortical EEG electrodes, we next determined the contribution of relative EEG power for the different frequency bands in relation to total EEG power for the overall 24-hr average as well as per vigilance state. For visual cortex recordings of R192Q mice, the relative contribution of delta band activity to the total EEG power was decreased during REM and non-REM sleep, whereas the

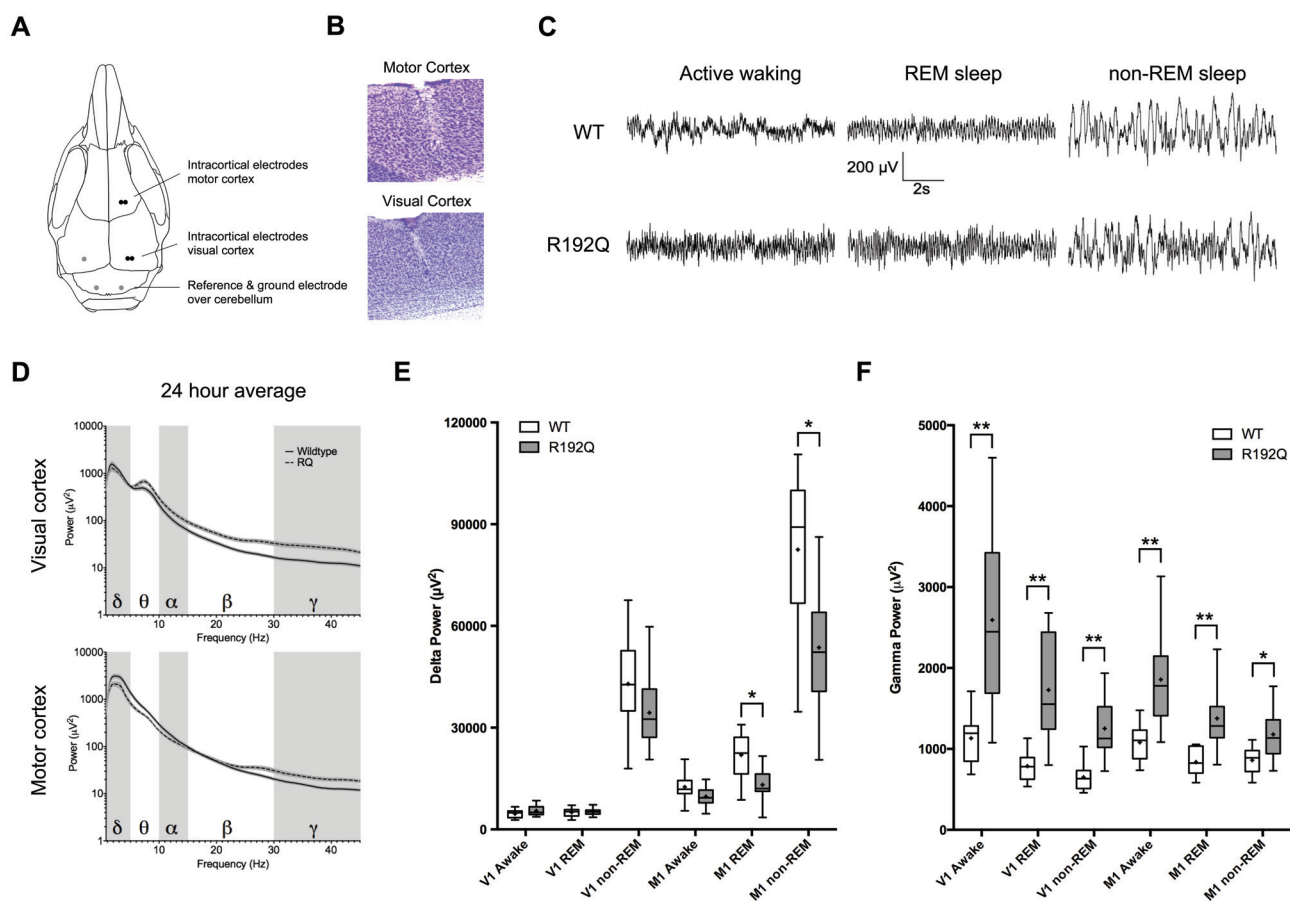


Figure 1. EEG spectral composition shows enhanced power in higher frequency bands in R192Q mutant mice. (A) Schematic depicting electrode locations used for simultaneous recording of intracortical DC-EEG and multi-unit activity from the visual and motor cortex in freely behaving FHM1 R192Q and WT mice. (B) Photomicrograph of sagittal section (Nissl counterstaining) showing histological verification of electrode tracks in middle to deep layers of the motor and visual cortex. (C) Example traces of visual cortex EEG during active waking, REM and non-REM sleep stages in WT and R192Q mice. (D) Averaged 24-hr EEG power spectra from the right hemisphere reveal an overall increased gamma band activity in the visual cortex and motor cortex of R192Q mice (N=10) compared with WT (N=10); δ :0.75-5 Hz, θ :5-10 Hz, α :10-15 Hz, β :15-30 Hz, γ :30-45 Hz. (E) Analysis of delta band activity across specific vigilance states reveal reduced delta power in the motor cortex of R192Q mice during REM and non-REM sleep. (F) In contrast, gamma band activity shows significantly higher power in R192Q mice for all vigilance states in both visual cortex and motor cortex. *corrected p-value <0.05, **corrected p-value <0.01; Mann-Whitney U-test followed by false discovery rate correction (FDR), Benjamini-Hochberg method.

contribution of beta and gamma band was increased in R192Q compared with WT for all vigilance states. The relative contribution of theta and alpha band activity to total EEG power for the visual cortex was comparable between genotypes during active waking and REM sleep, but enhanced for the alpha band activity in R192Q animals during non-REM sleep. For the motor cortex, during active waking and REM sleep, the relative contribution of delta band activity to total EEG power in the motor cortex was decreased in R192Q compared with WT mice. Similar as for the visual cortex, the contribution of beta and gamma band activity to total EEG power was increased for the motor cortex in R192Q compared with WT animals for all vigilance states (Table 1).

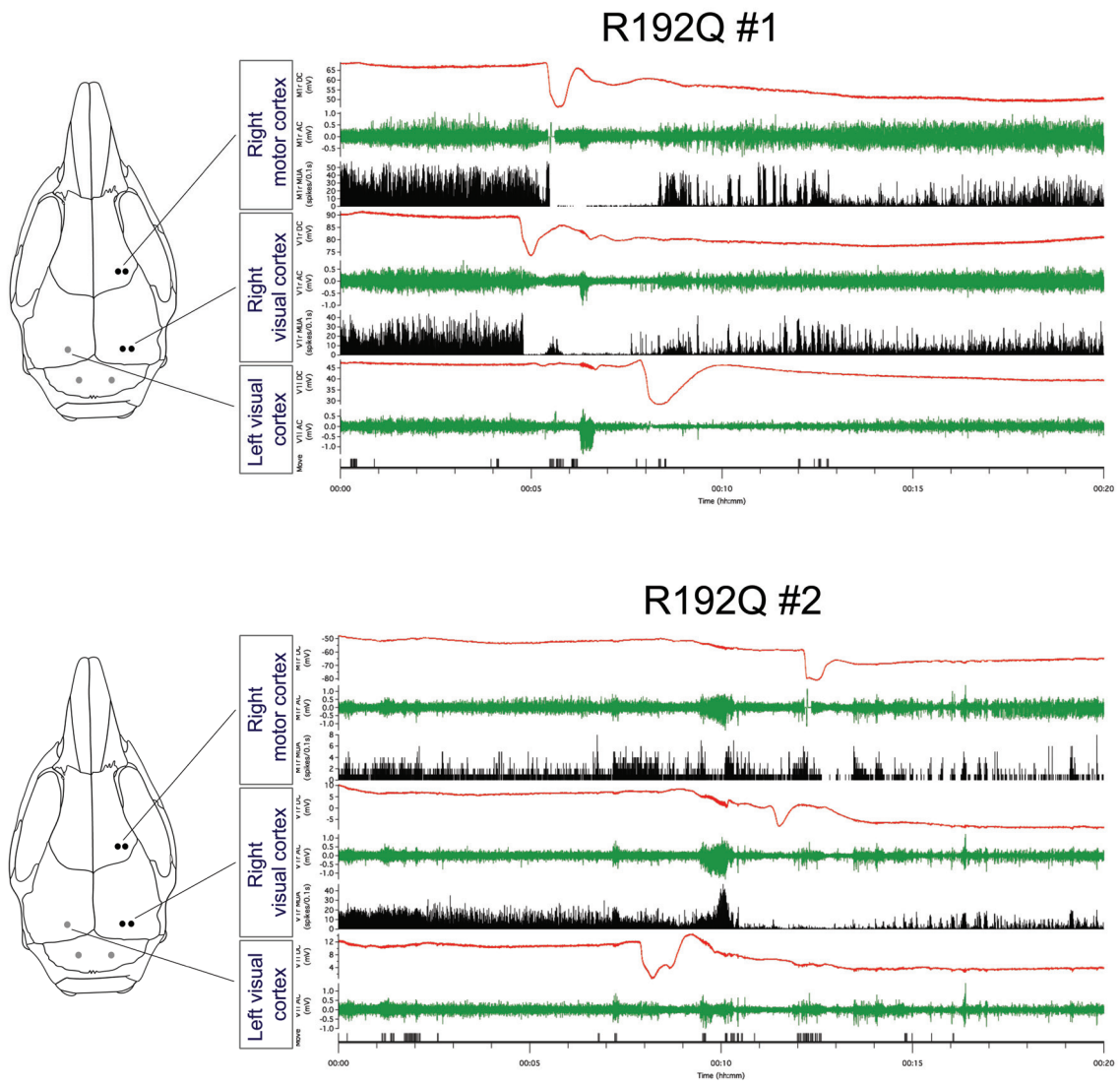
Table 1. Relative EEG power from visual and motor cortex in freely behaving R192Q and WT mice

Visual cortex	δ (0.75-5) Hz		θ (5-10) Hz		α (10-15) Hz		β (15-30) Hz		γ (30-45) Hz	
	R192Q	WT	R192Q	WT	R192Q	WT	R192Q	WT	R192Q	WT
24-hr average	45.9 [31.8,56.9]	55.4 [41.9,66.9]	29.8 [23.8,38.8]	25.0 [20.9,34.9]	9.4 [7.6,12.0]	6.9 [5.0,10.5]	8.1 [6.9,10.3]	5.7 [4.0,8.0]	4.7 [2.8,6.1]	2.6 [1.8,4.4]
Active waking	21.2 [15.7,31.7]	29.5 [17.5,39.8]	39.1 [30.8,50.8]	37.5 [28.2,47.7]	9.6 [7.6,11.2]	10.8 [7.0,14.0]	11.1 [9.8,13.0]	10.0 [9.1,11.6]	9.2 [6.7,16.6]	6.7 [5.7,9.0]
REM	20.5 [14.1,27.6]	30.1 [18.3,35.7]	48.1 [41.6,56.5]	44.0 [36.8,56.6]	9.5 [8.7,12.3]	9.1 [8.7,10.3]	10.1 [8.4,11.3]	7.8 [7.0,10.6]	6.1 [4.8,10.1]	4.4 [3.1,6.9]
non-REM	60.8 [43.6,70.2]	69.1 [53.5,78.2]	22.2 [16.9,33.7]	19.0 [15.1,27.3]	8.1 [6.2,11.9]	5.3 [3.4,10.1]	5.9 [4.6,8.3]	3.8 [2.3,6.7]	2.1 [1.3,2.8]	1.0 [0.6,1.9]

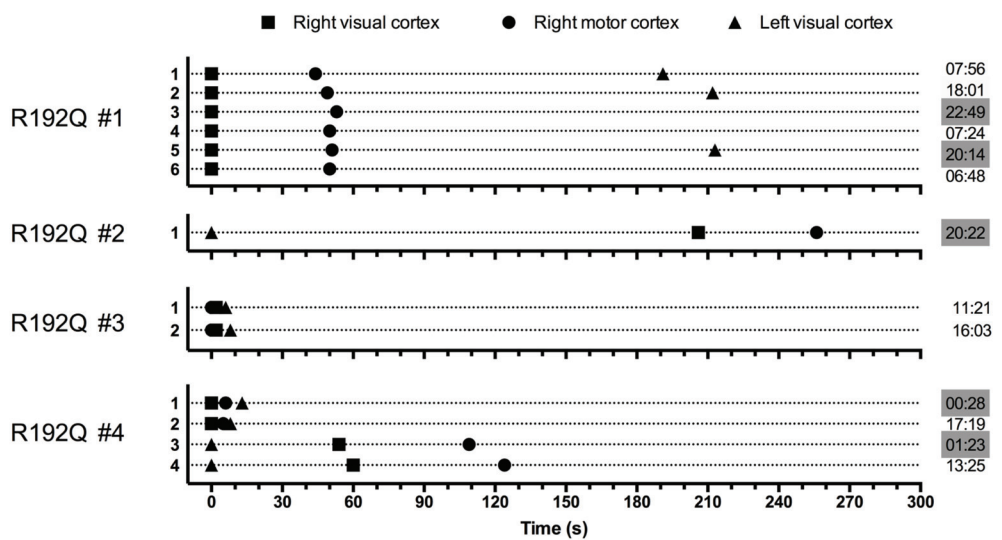
Motor cortex	δ (0.75-5) Hz		θ (5-10) Hz		α (10-15) Hz		β (15-30) Hz		γ (30-45) Hz	
	R192Q	WT	R192Q	WT	R192Q	WT	R192Q	WT	R192Q	WT
24-hr average	57.8 [46.6,65.9]	65.5 [54.0,68.2]	22.4 [18.5,28.2]	22.5 [20.2,29.0]	6.5 [4.5,9.5]	5.6 [4.6,7.6]	6.7 [4.8,8.5]	4.4 [3.4,5.4]	3.0 [2.4,4.0]	1.4 [1.1,2.1]
Active waking	39.8 [30.2,42.9]	46.0 [33.4,52.1]	28.9 [23.4,33.9]	29.6 [26.7,39.3]	6.8 [5.7,10.9]	7.0 [6.3,9.1]	10.0 [8.5,11.2]	7.1 [5.5,8.7]	7.0 [5.5,9.6]	4.0 [2.9,5.6]
REM	43.9 [24.3,52.1]	53.8 [42.3,59.5]	29.3 [24.3,45.3]	29.5 [27.2,37.1]	7.2 [5.9,9.6]	6.9 [5.4,8.3]	8.4 [6.7,10.6]	5.4 [3.8,7.0]	4.7 [3.9,5.5]	2.1 [1.5,2.8]
non-REM	69.4 [58.5,75.6]	73.0 [63.5,75.6]	18.0 [15.5,23.0]	18.9 [16.1,24.0]	5.8 [3.8,8.7]	4.9 [4.0,7.1]	5.2 [3.3,6.8]	3.6 [2.5,4.3]	1.6 [1.0,2.2]	0.7 [0.6,1.1]

Table 1. Data are presented as medians with [min, max values]. Power/frequency band was quantified as percentage of the total power across bands for N=10 R192Q and N=10 WT mice. R192Q mice had a significantly reduced relative delta power compared with WT. This was the case in the visual cortex for the 24-hr average as well as the separate vigilance states, and in the motor cortex for active waking and REM sleep. In contrast, R192Q mice had a significantly increased relative power in the theta and alpha power in the visual cortex for the 24-hr average and non-REM sleep state, and for beta and gamma power for the 24-hr average and for all the separate vigilant states. Beta and gamma power in motor cortex were enhanced in R192Q mice for the 24-hr average as well as for all separate vigilant states. Comparable changes in gamma and delta power described for other transgenic mouse models have been linked to enhanced neuronal excitability (Joho et al 1999, Lau et al 2000). Mann-Whitney U-test followed by false discovery rate correction (FDR), Benjamini-Hochberg method.

A



B



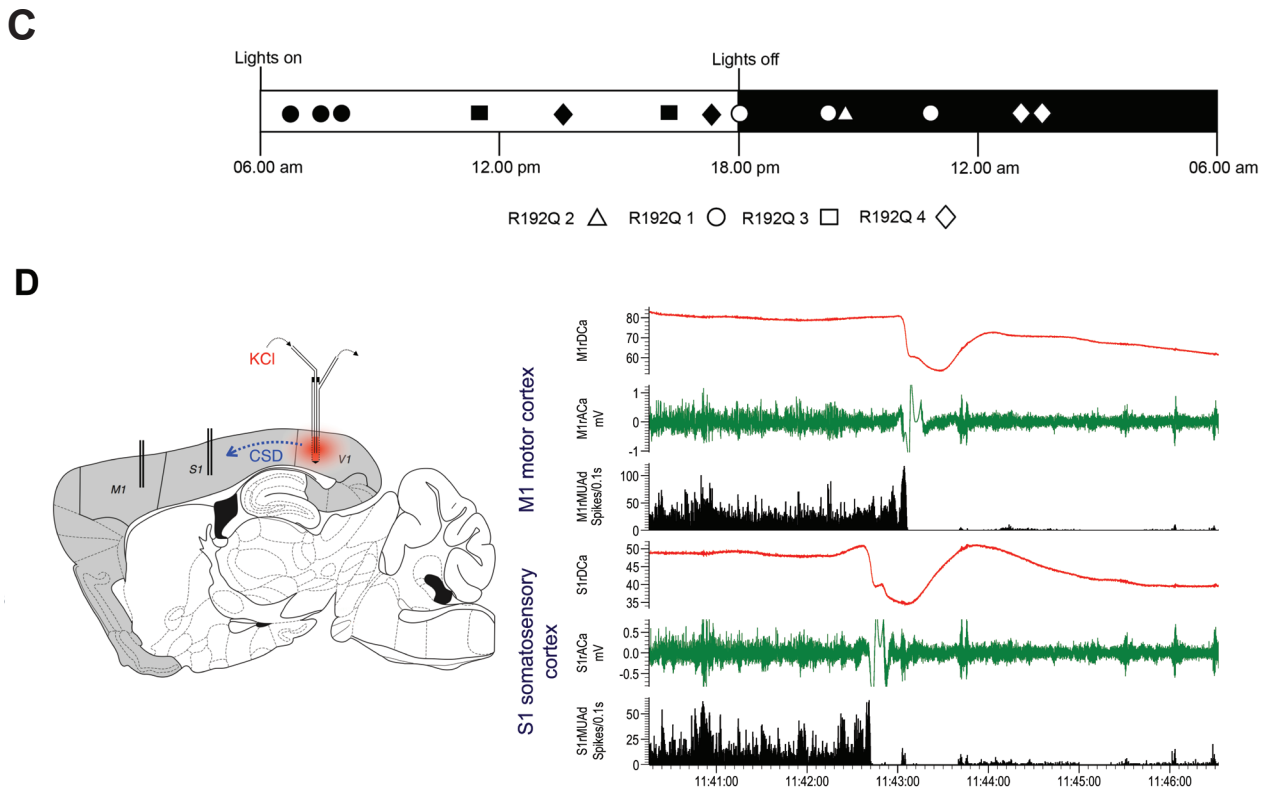


Figure 2. Detection of spontaneous and induced CSD in freely behaving mice using a novel combination of intracortical DC-EEG and Multi-Unit Activity (MUA) recording. (A) Experimental setup with example recordings showing spontaneous CSD events in 2 homozygous R192Q mice. Pre-amplified signals from bipolar Pt electrode pairs in the right cortex are split into multiple channels that are individually amplified and filtered to obtain a DC-EEG (0-500 Hz) channel, an AC-EEG (0.1-500 Hz) channel and a multi-unit activity (MUA, 500-5000 Hz) channel for the right motor cortex and right visual cortex. A single epidural ball-tip electrode placed on the left visual cortex that yields a DC-EEG and an AC-EEG channel but no MUA. During 7 days of recording we detected spreading depolarization coinciding with AC-EEG and MUA suppression in 4 out of 11 homozygous R192Q mice and 0 out of 10 WT mice. In the panel example, the CSD wave appears first in the right visual cortex, then spreads to the right motor cortex and then appears in the left visual cortex. In the example of the bottom panel, the CSD wave first appears in the left visual cortex and then spreads to the right visual cortex and reaches the right motor cortex last. (B) Time course of the observed CSD events in the 4 R192Q animals. In *animal 1*, 5 CSD events were detected, 3 of which were bilateral (including the example depicted in A). In all events in this animal, the CSD wave first appeared in the right visual cortex. In *animal 2* (panel example in A), the CSD wave first appeared in the left visual cortex. In *animal 3*, the start of the negative DC-shift and MUA/EEG silencing was observed within 10 sec from each other in all 3 locations. In *animal 4*, the start of the negative DC-shift and MUA/EEG silencing was observed within 10 sec from each other in all 3 locations in the first two events. For the 3rd and 4th event, the CSD wave started in the left visual cortex and subsequently appeared in the right visual cortex and right motor cortex. (C) Distribution of CSD events over the 24 hr light-dark cycle. Seven out of 13 CSD events occurred during the light phase (between 6 am and 6 pm) whereas 6 out of 13 events happened during the dark phase. (D) To confirm the accuracy of our CSD detection methodology, we performed a separate experiment in which we induced CSD in the visual cortex of freely behaving WT mice by performing reverse microdialysis with a 500 mM KCl solution through a microdialysis probe placed in the V1 visual cortex. Using the same intra-cortical bipolar electrodes as in A, we recorded DC-EEG, AC-EEG and MUA at two locations ipsilateral to the microdialysis probe. Shortly after starting the microdialysis with 500 mM KCl, A transient negative DC-shift coinciding with EEG silencing and MUA suppression appeared first in the somatosensory S1 cortex and then spread to the M1 motor cortex.

R192Q mice exhibit spontaneous CSD events

Notably, during the longitudinal EEG recordings in freely moving mice, we observed a total of 13 spontaneous events resembling CSD in 4 of the 10 recorded R192Q mice (Figure 2A), while no such events were observed in the 10 recorded WT mice. In addition to the intracortical electrodes in the right visual and motor cortex that were used for EEG analysis, an epidural Ag electrode placed on the left visual cortex was used for CSD detection. The events were characterized as CSD on the basis of the occurrence of a transient negative DC-shift exceeding 5 mV, accompanied by a suppression of neuronal multi-unit activity (MUA), and dampening of EEG amplitude, that spread throughout the cortex across the different electrode locations (Figure 2A). Figure 2B shows the order of appearance of the CSD events at the different cortical locations. For 9 events from 3 mice, CSD events were observed first in the visual cortex. Of those, 5 events (from 1 R192Q mouse) were first detected in the right visual cortex before reaching the right motor cortex, followed by the left visual cortex. Three CSD events (from 2 different R192Q mice) were first observed in the left visual cortex before being detected at the right visual cortex and, subsequently, right motor cortex. For 4 events in 2 mice, CSD events were observed in all 3 recording locations near simultaneously (2- to 13-sec time delay). The spontaneous CSD events occurred at different times of the day. Specifically, 5 out of the 13 spontaneous CSD events occurred during the dark (active) period whereas 7 events occurred during the light (resting) period and 1 event occurred during the transition from light to dark (Figure 2C). The amplitude of the CSD events was 12.2 ± 4.6 mV, with duration of 32.1 ± 7.3 sec for the right visual cortex (N=9), and 19.9 ± 8.8 mV with a duration of 30.7 ± 6.9 sec for the right motor cortex (N=13). We validated our methodology for CSD detection in freely behaving mice by experimentally inducing CSD in the visual cortex using micro-infusion of 500 mM KCl solution. Electrophysiological characteristics of evoked CSD events were comparable to spontaneous CSD events with a transient spreading negative DC-shift exceeding 5 mV accompanied by neuronal silencing (evidenced from suppression of MUA) and dampening of EEG amplitude (Figure 2D).

Relation of spontaneous CSD occurrence with EEG spectral changes and vigilance state

Following the spreading transient DC-shift of about 30-sec duration as indicated above, we observed a secondary, longer-lasting negative DC-shift in all animals (Figure 3A). The secondary negative DC-shift had comparable or even larger amplitude as the first shift (17.3 ± 5.4 mV for right visual cortex; 23.1 ± 8.0 mV for right motor cortex) and duration of 20 to 40 min. During the secondary DC-shift, animals were inactive as determined from the movement sensor, and EEG was characterized by high amplitude delta activity (Figure 3B; $140 \pm 28\%$ power in the delta band in the visual cortex between 10 and 30 min after CSD onset compared to the 24-hr average delta power during non REM sleep; paired samples t-test, $p=0.008$). In contrast, power in higher EEG frequency bands and MUA was reduced compared to baseline for up to 60 min after the CSD (Figure 3A and B). Outside the 60-min time window after CSD, the EEG spectra of the R192Q mice with CSD events (N=4) did not show overt differences with the EEG spectra of the N=6 R192Q mice in which no CSD events

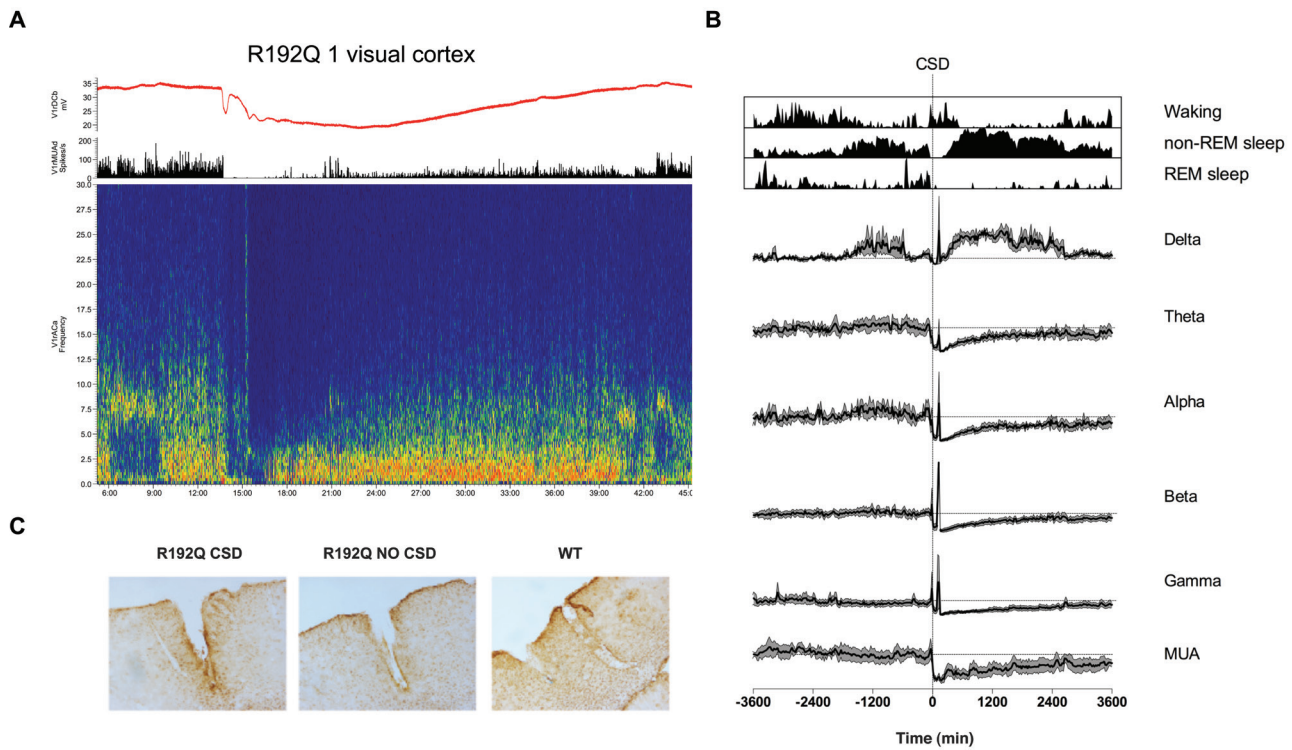


Figure 3. Impact of CSD on cortical network activity and vigilance state. (A) Representative time course of MUA and EEG spectral composition in relation to bi-phasic DC-EEG shift. In line with previous reports on induced CSD under anaesthesia (Chang et al 2010), DC-EEG (top trace, red) in freely behaving R192Q mice showed a biphasic negative DC shift during spontaneous CSD in which the spreading negative depolarization wave (lasting 32.1 ± 7.3 sec) is followed by secondary negative DC shift lasting 20 to 40 min. Following a short MUA burst when the front of the CSD wave reaches the recording electrode, neuronal activity is rapidly suppressed after which it gradually recovers to baseline levels over the course of 30 to 60 min. The time-frequency plot shows the frequency-dependent impact of CSD on EEG power. Red indicates high power and dark blue indicates low power. Note the prominent delta activity from 5 to 30 min after CSD. (B) Averaged time course (averaged from all CSD events in the 4 animals with spontaneous CSD, weighted so each animal has an equal contribution to the overall average) of vigilance state, visual cortex EEG power in the different frequency bands and MUA from 60 min before until 60 min after the start of CSD (time 0, vertical dashed line). Note that post-CSD, delta activity (0.75-5Hz) rapidly recovers to baseline levels (indicated by horizontal dashed lines) and increases to $140 \pm 28\%$ of 24 hr average delta power during non-REM sleep between 10 and 30 min after CSD onset. In contrast, power in higher EEG frequency bands is not elevated post-CSD but instead recovers gradually to baseline in a comparable time frame as MUA. (C) Staining for GFAP revealed comparable levels of astrocyte activation surrounding the electrode in WT animals and in R192Q with and without spontaneous CSD events.

were observed. Vigilance state analysis revealed that the occurrence of CSD events was not limited to a specific vigilance state prior to the CSD. CSD was preceded by waking for 4 events, by non-REM sleep for 5 events and by REM sleep for 4 events. During a CSD event however, in all cases (9 out of 13) where an animal was sleeping prior to the CSD, the animal woke up and displayed locomotor activity. All animals displayed locomotor activity for a period of 1 to 10 min after the start

of CSD, after which they went into a non-REM like sleep state characterized by high amplitude delta oscillations for a period of 20 to 40 min.

To investigate whether the observed spontaneous CSD events in R192Q mice may relate to a genotype-specific tissue inflammatory response, we compared Nissl and glial fibrillary acidic protein (GFAP) stained sections from N=4 R192Q mice in which CSD events were observed with those of N=4 WT and N=4 R192Q mice without CSD events (Figure 3C). Around electrode tracks, enhanced GFAP staining was observed for all animals, with no overt differences between groups. For none of the recorded animals, including the R192Q mice that displayed spontaneous CSD events, signs of tissue damage or bleeding were observed that could relate to inflammatory responses or an infarct.

Table 2. Distribution of vigilance states over 24-hr of EEG recording in freely behaving WT and R192Q mice.

Vigilance states	WT average (N=10)	R192Q average (N=10)	p-value (t-test)
% active waking	19.1 ± 4.3	15.2 ± 7.5	0.17
% NREM	31.3 ± 3.4	29.9 ± 4.1	0.20
% REM	12.3 ± 2.9	12.7 ± 4.0	0.69
% passive waking	15.1 ± 2.5	15.5 ± 3.2	0.40
% sleeping	65.0 ± 5.7	68.7 ± 9.9	0.49
% unclassified sleeping epochs	21.5 ± 6.0	26.1 ± 8.2	0.20
% drinking	0.9 ± 0.4	0.7 ± 0.6	0.87
% artefacts	0.8 ± 0.8	0.3 ± 0.5	0.09

Table 2. Data are presented as mean±SD. R192Q (N=10) and WT (N=10) mice spent a comparable fraction of time across different vigilance states for the analyzed 24-hr EEG windows. Numbers indicate the % of total time spent in a specific vigilance state, determined from 4 sec bins from the analyzed 24-hr window. See Materials and Methods for details and definitions of vigilance states.

Anesthetized R192Q mice kept under full physiological control display enhanced visual cortex CSD frequency compared with WT, both at the start of the light and the start of the dark period

In freely behaving R192Q mice, CSD events occurred both during the dark and during the light period, with a slight majority (7 out of 13) events occurring during the light period. To specifically address whether CSD susceptibility may differ in relation to the light compared with the dark period, we compared the frequency of KCl-induced CSD at the beginning of the light and dark periods. Experiments were performed under isoflurane anesthesia, under continuous physiological monitoring

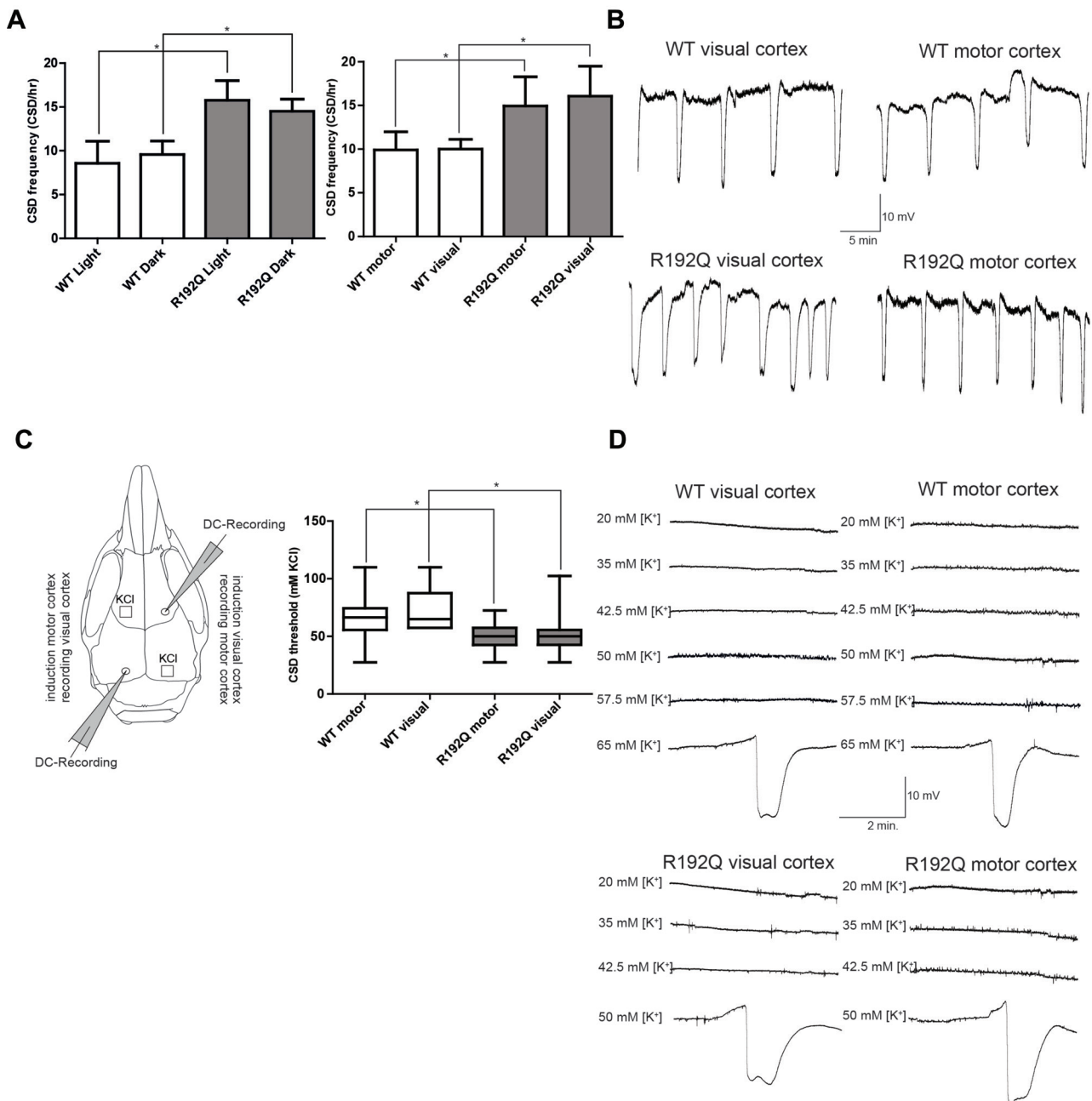


Figure 4. FHM1 R192Q mice display enhanced CSD susceptibility in both visual and motor cortex, independent of the time-of-day. (A left) In R192Q (light; N=5; *p=0.0001, dark; N=5; *p=0.002) mice, visual cortex CSD frequency is increased compared with WT (light; N=5, dark; N=7) with no difference between the start of the light and start of the dark period within the same genotype. (A right) CSD frequency is increased in both the visual (*p=0.005) and motor cortex (*p=0.01) of R192Q (visual; N=6, motor; N=8) mice compared with WT (visual; N=6, motor; N=6). (B) Representative DC-potential traces from CSD frequency recordings from WT and R192Q mice in the visual and motor cortices. (C left) Schematic depicts the KCl application sites and electrode locations for the visual and motor cortex CSD susceptibility assessments. (C right) CSD threshold is reduced in both visual (*p=0.01; in line with previous work; van den Maagdenberg et al 2004) and motor cortex (*p=0.04) of R192Q (visual; N=16, motor; N=16) compared with WT (visual; N=13, motor; N=14) mice. (D) Representative DC-potential traces of CSD threshold assessment. Data are presented as mean \pm SD, except for CSD threshold data that are presented as medians. Statistical differences were determined by one-way ANOVA followed by Bonferroni correction (for CSD frequency) and Mann-Whitney U-test (for CSD threshold).

and control in animals that were accustomed to either regular or shifted day-night regimes. Under these conditions, KCl-induced CSD frequency, assessed in the visual cortex, was compared for R192Q and WT mice at the start of the light and at the start of the dark period. Visual cortex CSD frequency was enhanced in R192Q compared with WT mice at the start of the light period (R192Q, 15.7 ± 2.4 CSD/hr, N=5 vs WT, 8.6 ± 2.5 CSD/hr, N=5; $p=0.0001$, one-way ANOVA Bonferroni correction), and also at the start of the dark period (R192Q, 14.5 ± 1.3 CSD/hr, N=5 vs WT, 9.5 ± 1.5 CSD/hr, N=7; $p=0.002$, one-way ANOVA Bonferroni correction) (Figure 4A). However, within-genotype comparisons revealed similar CSD susceptibility measures for the start of the light ($p=1$, one-way ANOVA Bonferroni correction) as well as the start of the dark period ($p=1$, one-way ANOVA Bonferroni correction), suggesting that the enhanced CSD susceptibility of R192Q compared with WT mice is uniform throughout the day.

To ensure that the mice were in the correct periods after the shifted day-night regimes, corticosterone plasma levels were measured and their motor activity monitored. As expected for nocturnal animals, we found higher corticosterone plasma levels in mice of the dark group compared with mice of the light group (Maywood et al 2007). In particular, R192Q mice of the dark group had higher corticosterone levels compared with R192Q mice of the light group (R192Q dark, 206.8 ± 90.2 ng/mL, N=11 vs R192Q light, 14.4 ± 10.6 ng/mL, N=11; $p=0.0001$, Mann-Whitney U-test). The results were similar for WT mice (WT dark, 135.9 ± 32.6 ng/mL, N=14 vs WT light, 17.7 ± 17.5 ng/mL, N=9; $p=0.001$, Mann-Whitney U-test). There were no differences in corticosterone levels among light and dark groups between R192Q and WT mice (R192Q dark vs WT dark, $p=0.09$; R192Q light vs WT light, $p=0.2$, Mann-Whitney U-test).

Anesthetized R192Q mice kept under full physiological control display enhanced CSD susceptibility in both visual and motor cortex in R192Q compared with WT mice.

We observed that in the majority of cases, spontaneous CSD events in R192Q mice appeared first in the visual cortex, then in the motor cortex, suggesting that the events had originated in the visual cortex. We, therefore, determined whether CSD susceptibility would be different for visual compared with motor cortex by measuring the threshold and frequency of KCl-induced CSD at both locations in anesthetized R192Q and WT mice under full physiological control. CSD threshold was lower ($p=0.001$, Mann-Whitney U-test) in the visual cortex of R192Q compared with WT mice in line with earlier findings (van den Maagdenberg et al 2004). Notably, R192Q mice had a lower CSD threshold also in the motor cortex compared with WT ($p=0.043$, Mann-Whitney U-test). However, within-genotype comparisons revealed similar CSD thresholds for the visual compared with motor cortex in both WT and R192Q mice (Figure 4C). R192Q mice displayed higher CSD frequency values in the visual cortex compared with WT (R192Q, 16 ± 3.4 CSD/hr, N=6 vs WT, 9.9 ± 1.1 CSD/hr, N=6; $p=0.005$, one-way ANOVA Bonferroni correction), in agreement with previous findings (Eikermann-Haerter et al 2009). Again, also in the motor cortex, R192Q mice displayed higher CSD susceptibility as shown by higher frequency values compared with WT (R192Q, 14.9 ± 3.3 CSD/hr,

$N=8$ vs 9.9 ± 2 CSD/hr, $N=6$; $p=0.01$, Mann-Whitney U-test; Figure 4A). Therefore, with 2 different but complementary methods for assessing CSD susceptibility, R192Q mice displayed enhanced CSD susceptibility compared with WT in both the visual and motor the cortex, but did not show a more prominent CSD susceptibility in the visual cortex.

Table 3. Physiological parameters and CSD amplitude and duration values of R192Q and WT mice from CSD threshold and CSD frequency measurements

CSD threshold	N	pH	pCO ₂ (mmHg)	pO ₂ (mmHg)	MABP (mmHg)	Amplitude (mV)	Duration (sec)
R192Q motor	16	7.39 ± 0.05	30.4 ± 5.4	128.6 ± 29.0	91.6 ± 13.7	22.3 ± 6.9	50.9 ± 36.9
R192Q visual	16	7.42 ± 0.04	28.7 ± 3.9	131.8 ± 24.8	91.9 ± 11.4	25.3 ± 5.4 [‡]	51.5 ± 17.6
WT motor	14	7.41 ± 0.04	29.9 ± 3.4	137.2 ± 23.6	91.3 ± 16.7	18.8 ± 4.9	30.4 ± 8.6
WT visual	13	7.41 ± 0.04	31.1 ± 4.5	135.5 ± 26.5	94.2 ± 16.0	25.4 ± 3.3 [†]	41.0 ± 9.1
CSD frequency							
R192Q motor	8	7.36 ± 0.06	31.5 ± 6.4	110.4 ± 20.9	82.5 ± 12.6	17.8 ± 5.8	29.3 ± 15.0
R192Q visual	6	7.38 ± 0.03	31.8 ± 4.2	114.4 ± 10.5	83.6 ± 9.6	20.7 ± 5.2	34.6 ± 9.9
WT motor	6	7.40 ± 0.03	30.2 ± 3.8	124.2 ± 18.0	91.5 ± 13.2	12.8 ± 3.4	21.0 ± 7.3
WT visual	6	7.39 ± 0.03	32.0 ± 4.0	124.6 ± 28.8	84.1 ± 13.2	22.8 ± 3.2 [§]	27.8 ± 5.8
R192Q light	5	7.37 ± 0.02	31.2 ± 6.1	112.2 ± 15.4	84.4 ± 11.2	20.8 ± 2.4	25.4 ± 7.6
R192Q dark	5	7.40 ± 0.03	31.5 ± 2.2	128.9 ± 14.6	85.7 ± 9.0	22.4 ± 2.6	29.9 ± 12.2
WT light	5	7.39 ± 0.03	30.3 ± 2.6	120.7 ± 6.5	87.7 ± 7.0	21.5 ± 1.8	21.4 ± 4.4
WT dark	7	7.40 ± 0.03	32.0 ± 3.0	118.1 ± 9.8	90.5 ± 12.4	23.6 ± 3.3	39.9 ± 13.1 [*]
WT dark	7	7.40 ± 0.03	32.0 ± 3.0	118.1 ± 9.8	90.5 ± 12.4	23.6 ± 3.3	39.9 ± 13.1 [*]

Table 3. Values are shown as mean ± SD. CSD duration was measured at half-maximal amplitude. Mice were physiologically monitored (via femoral artery catheterization) and controlled by mechanical ventilation. Physiological parameters were maintained within normal range by adjusting ventilation parameters. There were no significant differences between groups except for a smaller CSD amplitude in WT motor compared with WT visual ([†] $p=0.01$) and R192Q visual ([‡] $p=0.01$ for both comparisons, one-way ANOVA, Bonferroni correction) for CSD threshold and smaller CSD amplitude in WT motor compared with WT visual ([§] $p=0.008$, one-way ANOVA, Bonferroni correction) for CSD frequency. For time-of-day CSD frequency measurements there was a longer CSD duration in WT dark compared with WT light group (^{*} $p=0.04$, one-way ANOVA, Bonferroni correction). MABP, mean arterial blood pressure.

DISCUSSION

In this study we combined cortical electrophysiological recordings in freely behaving and anesthetized FHM1 R192Q mutant mice to study the effects of FHM1 mutations on cortical network excitability and CSD susceptibility. Analysis of long-term intracortical DC-EEG and MUA recordings in freely behaving mice revealed increased power in the EEG gamma frequency band for both visual and motor cortex in R192Q compared with WT mice. In addition, power in the delta band was reduced for R192Q

mice in motor cortex during REM and non-REM sleep. Spontaneous CSD events were observed in a subset of R192Q, but never in WT mice. The occurrence of CSD events in freely behaving R192Q mice did not show an apparent correlation to the time-of-day. For the majority of events the CSD was observed first in the visual cortex. Parallel DC-recordings performed under anesthesia showed enhanced visual cortex CSD frequency in R192Q mice compared with WT both at the start of the light and at the start of the dark period. CSD susceptibility was enhanced to a comparable extent for both visual and motor cortex in R192Q mice compared with WT. Taken together, our findings indicate that the FHM1 R192Q mutation results in measurable alterations in cortical network activity patterns under freely behaving conditions in both visual and motor cortex that may contribute to the episodic occurrence of CSD.

Neuronal hyperexcitability has been proposed as an underlying mechanism for increased susceptibility to migraine attacks (Welch et al 1990, Vikelis and Mitsikostas 2007, Aurora & Wilkinson 2007). In agreement with this, the gain-of-function FHM1 R192Q mutation results in increased calcium entry into pre-synaptic terminals with concomitant increased glutamate release into the synaptic cleft (Tottene et al 2002, van den Maagdenberg et al 2004, Tottene et al 2009), with apparent little effect on inhibitory neurotransmission (Tottene et al 2009, Vecchia et al 2014). Our present data indicate that these synaptic changes infer significant changes in cortical network activity patterns and predispose the cortex for occurrence of spontaneous CSD events, adding translational value to the FHM1 mouse model.

The spontaneous CSD events showed DC and neuronal activity changes similar to those of induced CSD events (Somjen 2001). Specifically, the spontaneous CSD events showed a characteristic DC-EEG negative deflection coinciding with a peak in neuronal activity, immediately followed by a near-complete suppression of neuronal activity which gradually increase to pre-CSD levels. To our knowledge, the detection of spontaneous CSD events in freely behaving mice is the first report of such events in an animal model. From our recordings, we did not identify factors that may have triggered the spontaneous occurrence of CSD. One possibility that cannot be excluded is that abrupt movements of the mouse might have caused friction of the intracortical electrodes, triggering a mechanically-induced CSD. This, however, seems rather unlikely since there was no correlation between the occurrence of CSD and mouse movements as detected by the movement sensor. In fact, most CSD events were preceded by sleep. It can also not be excluded that an enhanced inflammatory response around the intracortical electrodes may have contributed to the occurrence of the CSD events, since FHM1 R192Q were shown to exhibit a pronounced pro-inflammatory phenotype, at least in trigeminal ganglia neurons (Franceschini et al 2013). Histological analysis of GFAP staining, however, did not reveal overt genotypic differences in tissue reaction to implanted electrodes between R192Q mice that experienced CSD events and those that did not, nor between R192Q and WT mice. Although we cannot exclude that the presence of electrodes in the cortex contributed to occurrence of spontaneous CSD events via some other mechanism, at present, we lack the technical means to reliably detect CSD non-invasively e.g., via stable through-the-skull DC-EEG recordings.

The spontaneous occurrence of CSD events in R192Q mice suggests that such events are initiated by physiological fluctuations in brain activity. Although diurnal and seasonal alterations in neuronal excitability have been reported (Herzog 2007, Farajnia et al 2014), our data did not indicate a particularly enhanced CSD susceptibility in relation to certain times of the day. The overall EEG spectral changes that we observed, in particular enhanced power in the EEG gamma frequency band, are in line with the concept of cortical hyperexcitability. A correlation between enhanced EEG gamma power and decreased delta power with neuronal hyperexcitability is supported by earlier findings in mice deficient of $K_v3.1$ voltage-gated K^+ channels. $K_v3.1$ voltage-gated channels are expressed in cortical GABAergic interneurons that are thought to enhance release of GABA from interneurons (Perney et al 1992, Kanemasa et al 1995). Hence, loss of $K_v3.1$ function is expected to yield hyperexcitability. Indeed 24-hr EEG recordings in $K_v3.1$ deficient mice revealed increased gamma and reduced delta EEG power (Joho et al 1999). These findings indicate that in the context of neuronal ion channel mutations that promote cortical hyperexcitability, as is the case for the R192Q mutation, EEG gamma power is increased whereas delta power may be decreased. Spectral changes in R192Q mice were most pronounced for the EEG gamma band, which showed enhanced power across cortical regions and vigilance states. Notably, in transgenic mice *lacking* functional $Ca_v2.1$ Ca^{2+} channels, i.e., displaying an opposite effect at the cellular level to the gain-of-function effect of the R192Q mutation, a substantial *reduction* in gamma EEG power was observed (Llinas et al 2007). In general, gamma oscillations in neuronal networks are linked to enhanced glutamatergic neurotransmission as illustrated by studies on the generation of gamma oscillations in the hippocampus (Whittington et al 1995, Martin 2001, Herrmann & Demiralp 2005). The association of cortical gamma activity with hyperexcitability is further exemplified by enhanced gamma oscillatory activity during seizure initiation and chronification in epilepsy, a disorder characterized by enhanced neuronal network excitability (Parra et al 2003, Tolner et al 2005).

The question remains whether these findings in R192Q mice have relevance for the understanding of migraine in patients. Early EEG studies in migraine patients have not shown uniform EEG power changes, neither between (interictal) or during (ictal) attacks (Lauritzen et al 1981). More recent reports indicate enhanced interictal theta band activity (Björk et al 2011), and fluctuations in alpha band power (de Tommaso 1998) as well as slowing down of EEG activity in relation to upcoming attacks (Björk et al 2011). Furthermore, a loss of EEG complexity indicative of enhanced EEG synchrony has been reported for migraineurs (Strengé et al 2001). In this context, enhancement of EEG gamma power may be interpreted as an enhancement of cortical network synchrony. Notably, for visual evoked potential responses, enhanced EEG gamma power has been reported for visual evoked potential responses in migraineurs (Coppola et al 2007), which was proposed to be related to a putative functional disconnection of the thalamus to the cortex. In animal models, $Ca_v2.1$ Ca^{2+} channels were shown to play a key role in generation of thalamocortical oscillatory activity (Llinas et al 2007), suggesting that the enhanced EEG gamma power in FHM1 mice may involve altered thalamocortical function. Given the reported integration of visual and nociceptive inputs at the level

of the thalamus in rodents (Noseda et al 2010, Noseda et al 2014), it is tempting to speculate that a combination of sensory triggers and overall (genetically) enhanced cortical excitability may contribute to cyclic occurrence of CSD events.

The majority of observed spontaneous CSD waves appeared first in the visual cortex and then in motor cortex suggesting that the visual cortex might be particularly susceptible to CSD initiation. Our data in anesthetized mice, however, did not reveal a difference in threshold or frequency for KCl-induced CSD between the visual and motor cortex. If indeed spontaneous CSD waves are more readily initiated in the visual cortex, intrinsic changes in the level of neuronal activity in the visual cortex or relative differences in potassium and glutamate buffering capacities between cortical regions may play a role. As we cannot determine the exact point-of-origin of the CSD waves in our experiments, it remains a possibility that CSD waves are initiated in a cortical or even subcortical brain area outside of the visual and motor cortex location. The near-simultaneous occurrence of some CSD events at both visual and motor cortex sites is in line with this idea. Clinical studies indicate that auras can be “silent” and become apparent only when invading the visual cortex (Hansen et al 2013).

The presence of increased gamma power at the cortical network level suggests an elevated baseline cortical network excitability in the migraine susceptible brain. On top of such baseline hyperexcitability, physiological cycles in neuronal activity together with effects of external stimuli may occasionally create the conditions where the threshold for initiation of CSD is exceeded in specific brain regions. The spontaneous occurrence of CSD events in FHM1 mice marks the first evidence for episodic neuronal abnormalities in an animal model for migraine, which allows studying mechanisms of CSD and the migraine aura phase in patients.

ACKNOWLEDGEMENTS

This work was supported by the EU "EUROHEAD" grant (LSHM-CT-2004-504837; M.D.F. & A.M.J.M.v.d.M.), the EU "EUROHEADPAIN" grant (nr 602633; M.D.F. & A.M.J.M.v.d.M.), the EU Marie Curie Career Integration Grant (nr 294233; E.A.T.), the Center for Medical Systems Biology (CMSB) established in the Netherlands Genomics Initiative/Netherlands Organisation for Scientific Research (NGI/NWO) (nr 050 - 060 - 409; A.M.J.M.v.d.M.), an LUMC Fellowship (E.A.T.) and the CURE SUDEP research award (nr 280560; E.A.T. & A.M.J.M.v.d.M.).

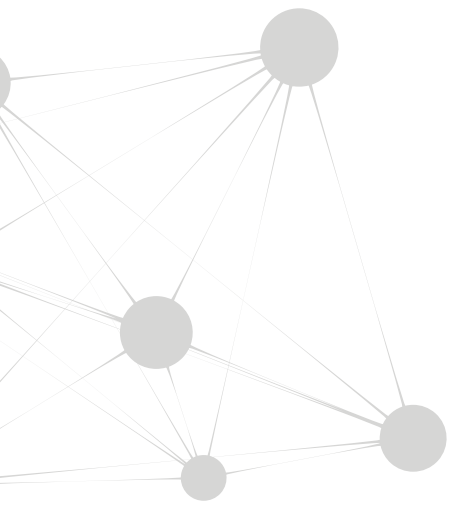
REFERENCES

- Alstadhaug K, Salvesen R, Bekkelund S. 2008. 24-hour distribution of migraine attacks. *Headache* 48:95-100
- Anttila V, Stefansson H, Kallela M, Todt U, Terwindt GM, et al. 2010. Genome-wide association study of migraine implicates a common susceptibility variant on 8q22.1. *Nat. Genet.* 42:869-73
- Aurora SK, Cao Y, Bowyer SM, Welch KM. 1999. The occipital cortex is hyperexcitable in migraine: experimental evidence. *Headache* 39:469-76
- Aurora SK, Wilkinson F. 2007. The brain is hyperexcitable in migraine. *Cephalalgia* 27:1442-53
- Badawy RA, Jackson GD. 2012. Cortical excitability in migraine and epilepsy: a common feature? *J. Clin. Neurophysiol.* 29:244-9
- Bartko JJ. 1966. The intraclass correlation coefficient as a measure of reliability. *Psychol. Rep.* 19:3-11
- Bjørk M, Stovner LJ, Hagen K, Sand T. 2011 What initiates a migraine attack? Conclusions from four longitudinal studies of quantitative EEG and steady-state visual-evoked potentials in migraineurs. *Acta Neurol Scand Suppl.* 191:56-63.
- Bolay H, Reuter U, Dunn AK, Huang Z, Boas DA, Moskowitz MA. 2002. Intrinsic brain activity triggers trigeminal meningeal afferents in a migraine model. *Nat. Med.* 8:136-42
- Chang JC, Shook LL, Biag J, Nguyen EN, Toga AW, et al. 2010. Biphasic direct current shift, haemoglobin desaturation and neurovascular uncoupling in cortical spreading depression. *Brain* 133:996-1012
- Cho CH. 2012. Molecular mechanism of circadian rhythmicity of seizures in temporal lobe epilepsy. *Front. Cell. Neurosci.* 6:55
- Coppola G, Ambrosini A, Di Clemente L, Magis D, Fumal A, et al. 2007. Interictal abnormalities of gamma band activity in visual evoked responses in migraine: an indication of thalamocortical dysrhythmia? *Cephalalgia* 27:1360-7
- Eikermann-Haerter K, Dilekoz E, Kudo C, Savitz SI, Waeber C, et al. 2009. Genetic and hormonal factors modulate spreading depression and transient hemiparesis in mouse models of familial hemiplegic migraine type 1. *J. Clin. Invest.* 119:99-109
- Farajnia S, van Westering TL, Meijer JH, Michel S. 2014. Seasonal induction of GABAergic excitation in the central mammalian clock. *Proc. Natl. Acad. Sci. USA* 111:9627-32
- Fisher SP, Godinho SI, Potheary CA, Hankins MW, Foster RG, Peirson SN. 2012. Rapid assessment of sleep-wake behavior in mice. *J. Biol. Rhythms* 27:48-58
- Fox AW, Davis RL. 1998. Migraine chronobiology. *Headache* 38:436-41
- Franceschini A, Vilotti S, Ferrari MD, van den Maagdenberg AM, Nistri A, Fabbretti E. 2013. TNFalpha levels and macrophages expression reflect an inflammatory potential of trigeminal

- ganglia in a mouse model of familial hemiplegic migraine. *PLoS One* 8:e52394
- Goadsby PJ, Lipton RB, Ferrari MD. 2002. Migraine--current understanding and treatment. *N. Engl. J. Med.* 346:257-70
- Granziera C, DaSilva AF, Snyder J, Tuch DS, Hadjikhani N. 2006. Anatomical alterations of the visual motion processing network in migraine with and without aura. *PLoS Med.* 3:e402
- Hadjikhani N, Sanchez Del Rio M, Wu O, Schwartz D, Bakker D, et al. 2001. Mechanisms of migraine aura revealed by functional MRI in human visual cortex. *Proc. Natl. Acad. Sci. USA* 98:4687-92
- Hansen JM, Baca SM, Vanvalkenburgh P, Charles A. 2013. Distinctive anatomical and physiological features of migraine aura revealed by 18 years of recording. *Brain* 136:3589-95
- Herrmann CS, Demiralp T. 2005. Human EEG gamma oscillations in neuropsychiatric disorders. *Clin. Neurophysiol.* 116:2719-33
- Herzog ED. 2007. Neurons and networks in daily rhythms. *Nat. Rev. Neurosci.* 8:790-802
- ICHD. 2004. The International Classification of Headache Disorders: 2nd edition. *Cephalalgia* 24 Suppl 1:9-160
- Joho RH, Ho CS, Marks GA. 1999. Increased gamma- and decreased delta-oscillations in a mouse deficient for a potassium channel expressed in fast-spiking interneurons. *J. Neurophysiol.* 82:1855-64
- Kanemasa T, Gan L, Perney TM, Wang LY, Kaczmarek LK. 1995. Electrophysiological and pharmacological characterization of a mammalian Shaw channel expressed in NIH 3T3 fibroblasts. *J. Neurophysiol.* 74:207-17
- Lau D, Vega-Saenz de Miera EC, Contreras D, Ozaita A, Harvey M, et al. 2000. Impaired fast-spiking, suppressed cortical inhibition, and increased susceptibility to seizures in mice lacking Kv3.2 K⁺ channel proteins. *J. Neurosci.* 20:9071-85
- Lauritzen M, Trojaborg W, Olesen J. 1981. EEG during attacks of common and classical migraine. *Cephalalgia.* 1:63-6.
- Lauritzen M. 1994. Pathophysiology of the migraine aura. The spreading depression theory. *Brain* 117 (Pt 1):199-210
- Leao A. 1944. Spreading depression of activity in cerebral cortex. *J. Neurophysiol.* 7:359-90
- Llinas RR, Choi S, Urbano FJ, Shin HS. 2007. Gamma-band deficiency and abnormal thalamocortical activity in P/Q-type channel mutant mice. *Proc. Natl. Acad. Sci. USA* 104:17819-24
- Maniyar FH, Sprenger T, Monteith T, Schankin CJ, Goadsby PJ. 2015. The Premonitory Phase of Migraine - What Can We Learn From It? *Headache*
- Martin SJ. 2001. Activation of metabotropic glutamate receptors induces gamma frequency oscillations in the rat dentate gyrus in vivo. *Neuropharmacology* 40:634-7
- Maywood ES, O'Neill JS, Chesham JE, Hastings MH. 2007. Minireview: The circadian clockwork

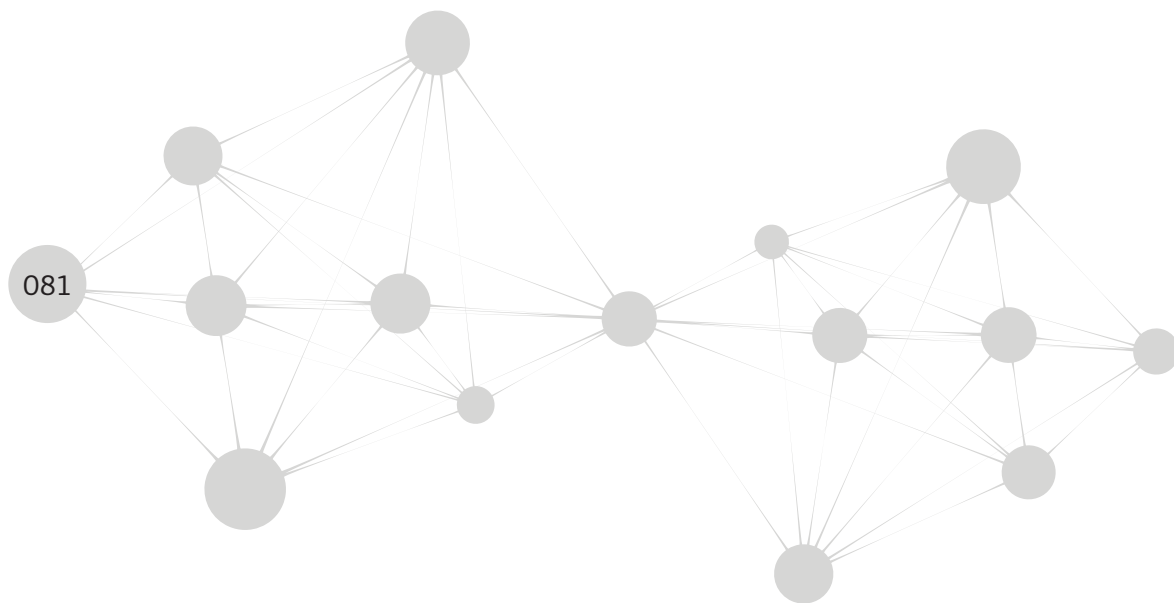
- of the suprachiasmatic nuclei--analysis of a cellular oscillator that drives endocrine rhythms. *Endocrinology* 148:5624-34
- Nosedá R, Kainz V, Borsook D, Burstein R. 2014. Neurochemical pathways that converge on thalamic trigeminovascular neurons: potential substrate for modulation of migraine by sleep, food intake, stress and anxiety. *PloS One* 9:e103929
- Nosedá R, Kainz V, Jakubowski M, Gooley JJ, Saper CB, et al. 2010. A neural mechanism for exacerbation of headache by light. *Nat. Neurosci.* 13:239-45
- Ophoff RA, Terwindt GM, Vergouwe MN, van Eijk R, Oefner PJ, et al. 1996. Familial hemiplegic migraine and episodic ataxia type-2 are caused by mutations in the Ca²⁺ channel gene CACNL1A4. *Cell* 87:543-52
- Parra J, Kalitzin SN, Iriarte J, Blanes W, Velis DN, Lopes da Silva FH. 2003. Gamma-band phase clustering and photosensitivity: is there an underlying mechanism common to photosensitive epilepsy and visual perception? *Brain* 126:1164-72
- Perney TM, Marshall J, Martin KA, Hockfield S, Kaczmarek LK. 1992. Expression of the mRNAs for the Kv3.1 potassium channel gene in the adult and developing rat brain. *J. Neurophysiol.* 68:756-66
- Sarabdjitsingh RA, Conway-Campbell BL, Leggett JD, Waite EJ, Meijer OC, et al. 2010. Stress responsiveness varies over the ultradian glucocorticoid cycle in a brain-region-specific manner. *Endocrinology* 151:5369-79
- Shyti R, Eikermann-Haerter K, van Heiningen SH, Meijer OC, Ayata C, Joëls M, Ferrari MD, van den Maagdenberg AM, Tolner EA. 2015. Stress hormone corticosterone enhances susceptibility to cortical spreading depression in familial hemiplegic migraine type 1 mutant mice. *Exp Neurol* 263:214-220.
- Somjen GG. 2001. Mechanisms of spreading depression and hypoxic spreading depression-like depolarization. *Physiol. Rev.* 81:1065-96
- Stankewitz A, May A. 2009. The phenomenon of changes in cortical excitability in migraine is not migraine-specific--a unifying thesis. *Pain* 145:14-7
- Strengé H, Fritzer G, Göder R, Niederberger U, Gerber WD, Aldenhoff J. 2001. Non-linear electroencephalogram dynamics in patients with spontaneous nocturnal migraine attacks. *Neurosci Lett.* 309:105-8.
- Tolner EA, Kloosterman F, van Vliet EA, Witter MP, Silva FH, Gorter JA. 2005. Presubiculum stimulation in vivo evokes distinct oscillations in superficial and deep entorhinal cortex layers in chronic epileptic rats. *J. Neurosci.* 25:8755-65
- de Tommaso M, Scirucchio V, Guido M, Sasanelli G, Specchio LM, Puca FM. 1998. EEG spectral analysis in migraine without aura attacks. *Cephalalgia.* 18:324-8.
- Tottene A, Conti R, Fabbro A, Vecchia D, Shapovalova M, et al. 2009. Enhanced excitatory transmission

- at cortical synapses as the basis for facilitated spreading depression in Ca(v)2.1 knockin migraine mice. *Neuron* 61:762-73
- Tottene A, Fellin T, Pagnutti S, Luvisetto S, Striessnig J, et al. 2002. Familial hemiplegic migraine mutations increase Ca(2+) influx through single human CaV2.1 channels and decrease maximal CaV2.1 current density in neurons. *Proc. Natl. Acad. Sci. USA* 99:13284-9
- van den Maagdenberg AM, Pietrobon D, Pizzorusso T, Kaja S, Broos LA, et al. 2004. A Cacna1a knockin migraine mouse model with increased susceptibility to cortical spreading depression. *Neuron* 41:701-10
- van den Maagdenberg AM, Pizzorusso T, Kaja S, Terpolilli N, Shapovalova M, et al. 2010. High cortical spreading depression susceptibility and migraine-associated symptoms in Ca(v)2.1 S218L mice. *Ann. Neurol.* 67:85-98
- Vecchia D, Tottene A, van den Maagdenberg AM, Pietrobon D. 2014. Mechanism underlying unaltered cortical inhibitory synaptic transmission in contrast with enhanced excitatory transmission in Ca_v2.1 knockin migraine mice. *Neurobiol. Dis.* 69:225-34
- Vikelis M, Mitsikostas DD. 2007. The role of glutamate and its receptors in migraine. *CNS Neurol Disord Drug Targets.* 6:251-7.
- Welch KM, D'Andrea G, Tepley N, Barkley G, Ramadan NM. 1990. The concept of migraine as a state of central neuronal hyperexcitability. *Neurol. Clin.* 8:817-28
- Whittington MA, Traub RD, Jefferys JG. 1995. Synchronized oscillations in interneuron networks driven by metabotropic glutamate receptor activation. *Nature* 373:612-5
- Zhang X, Levy D, Kainz V, Nosedá R, Jakubowski M, Burstein R. 2011. Activation of central trigeminovascular neurons by cortical spreading depression. *Ann. Neurol.* 69:855-65
- Zhang X, Levy D, Nosedá R, Kainz V, Jakubowski M, Burstein R. 2010. Activation of meningeal nociceptors by cortical spreading depression: implications for migraine with aura. *J. Neurosci.* 30:8807-14



Chapter 4

Stress hormone corticosterone enhances susceptibility to cortical spreading depression in familial hemiplegic migraine type 1 mutant mice



Reinald Shyti¹, Katharina Eikermann-Haerter⁵, Sandra H. van Heiningen¹, Onno C. Meijer², Cenk Ayata^{4,5}, Marian Joëls⁶, Michel D. Ferrari³, Arn M.J.M. van den Maagdenberg^{1,3‡}, Else A. Tolner^{3‡}

Departments of ¹Human Genetics, ²Endocrinology, and ³Neurology, Leiden University Medical Center, Leiden, The Netherlands

⁴Neurovascular Research Laboratory, Department of Radiology and ⁵Stroke Service and Neuroscience Intensive Care Unit, Department of Neurology, Massachusetts General Hospital, Harvard Medical School, Charlestown, USA

⁶Department of Neuroscience and Pharmacology, University Medical Center Utrecht, Rudolf Magnus Institute of Neuroscience, Utrecht, The Netherlands

‡equal contribution

Experimental Neurology 2015;263:214-20

ABSTRACT

Stress is a putative migraine trigger, but the pathogenic mechanisms involved are unknown. Stress and stress hormones increase neuronal excitability by enhancing glutamatergic neurotransmission, but inhibitory effects have also been reported. We hypothesise that an acute rise in stress hormones, such as corticosteroids which are released after stress, increase neuronal excitability and thereby may increase susceptibility to cortical spreading depression (CSD), the mechanism underlying the migraine aura. Here we investigated effects of acute restraint stress and of the stress hormone corticosterone on CSD susceptibility as surrogate migraine marker, in a transgenic mouse model of familial hemiplegic migraine type 1 (FHM1), which displays increased glutamatergic cortical neurotransmission and increased propensity for CSD. We found that 20-min and 3-hr restraint stress did not influence CSD susceptibility in mutant or wild-type mice, despite elevated levels of plasma corticosterone. By contrast, subcutaneous administration of 20 mg/kg corticosterone increased CSD frequency exclusively in mutant mice, while corticosterone plasma levels were similarly elevated in mutants and wild-types. The effect of corticosterone on CSD frequency was normalized by pre-administration of the glucocorticoid receptor (GR) antagonist mifepristone. These findings suggest that corticosteroid-induced GR activation can enhance susceptibility to CSD in genetically susceptible individuals, and may predispose to attacks of migraine. Although corticosterone levels rise also during acute stress, the latter likely triggers a spatiotemporally more complex biological response with multiple positive and negative modulators which may not be adequately modeled by exogenous administration of corticosterone alone.

INTRODUCTION

Migraine is a common disabling brain disorder typically characterised by recurring attacks of severe head pain and associated symptoms of autonomic and neurological dysfunction (Goadsby et al 2002, IHCD 2004). In one-third of patients, attacks are associated with neurological aura symptoms (Launer et al 1999). Migraine auras are likely caused by cortical spreading depression (CSD) that is defined as a slowly spreading cortical wave of neuronal and glial depolarization (Lauritzen 1994). Hyperexcitability of the cortex has been described in migraine patients (Aurora and Wilkinson 2007) compared to healthy controls, but much less is known how migraine attacks come about. It is still unclear whether acute stress is in fact one of the trigger factors for attacks, although often reported by patients (Sauro and Becker 2009, Hauge et al 2011). Moreover, it is unknown *how* hormones that are released upon stress may precipitate attacks (Borsook et al 2012).

Corticosteroid hormones (cortisol in humans and corticosterone in rodents), which are released in high amounts after stress, act by binding to mineralocorticoid (MR) and glucocorticoid receptors (GR) and are known to increase neuronal excitability (Popoli et al 2011, Joels et al 2012). Unlike MRs, GRs are quite abundantly expressed in several layers of the cerebral cortex, and GR pathways are known to mediate excitatory effects of stress hormones on neurotransmission, particularly after acute stress (Joels and Baram 2009). It is therefore plausible that possible effects of stress hormones on cortical excitability in the migraine brain are GR mediated.

Earlier we generated transgenic knock-in mice with an R192Q missense $Ca_v2.1$ (P/Q-type) Ca^{2+} channel mutation (van den Maagdenberg et al 2004), identified in patients with Familial Hemiplegic Migraine type 1 (FHM1; Ophoff et al 1996); these mice are considered a relevant model of migraine. We have shown that the enhanced susceptibility to CSD in mutant animals (van den Maagdenberg et al 2004, Eikermann-Haerter et al 2009) was caused by increased cortical glutamatergic neurotransmission (Tottene et al 2009). In the present study, we used CSD as a migraine-relevant readout for stress-induced changes in cortical hyperexcitability in the FHM1 R192Q mouse model. We investigated whether acute moderate or severe restraint stress may further enhance CSD susceptibility in R192Q mice and whether corticosteroid activation of GR pathways has comparable effects. Our findings provide insight into the mechanisms by which corticosteroids could contribute to triggering migraine attacks via influencing CSD susceptibility.

MATERIALS AND METHODS

Animals

Male homozygous *Cacna1a* FHM1 R192Q knock-in (“R192Q”) and wild type (“WT”) mice of 2-4 months were used. The knock-in mice were generated as previously described by introducing the human FHM1 pathogenic R192Q mutation in the orthologous mouse *Cacna1a* gene using a gene targeting approach (van den Maagdenberg et al 2004). Mice were assigned to the different

experimental groups: (1) 20-min restraint, (2) 3-hr restraint, (3) untreated, (4) corticosterone, (5) vehicle, (6) mifepristone + vehicle or (7) mifepristone + corticosterone. For each of these experimental paradigms, WT and R192Q mice were tested, separately. For most experimental groups, a sample size of 8 animals was used per genotype, except for the WT untreated (N=10), WT 20-min restraint (N=7) and the R192Q corticosterone+THDOC group (N=6). All experiments were approved by the Animal Experiment Ethics Committee of Leiden University Medical Center.

Assessment of corticosterone plasma levels

Mice were habituated to single housing for at least 4 days after which baseline blood samples from the tail (20 μ L) were collected at 10:00 am four days before follow-up procedures. Corticosterone plasma levels were determined by a commercial radioactive immunoassay (MP Biomedicals Inc., Costa Mesa, CA) according to manufacturer's instructions (Sarabdjitsingh et al 2010).

Restraint stress paradigms

Restraint stress experiments were performed in R192Q and WT mice using a single restraint paradigm (Sarabdjitsingh et al 2012) starting between 10:00 and 10:30 am. Mice were restraint in custom made Plexiglas cylinders (3 cm diameter) (1) for a single period of 20 min (moderate restraint) and then returned to the home cage for nearly 3 hr, after which they were prepared for CSD surgery, or (2) for 3 hr (severe restraint), after which they were immediately prepared for CSD surgery. Blood samples for corticosterone plasma measurements were collected prior to the start of CSD surgery (i.e., 3 hr after the end of the 20-min restraint or immediately after the 3-hr restraint procedure) and at the end of CSD recordings. The immediate effect of moderate restraint stress on corticosterone plasma levels (Table 1) was determined in separate groups of R192Q and WT mice by collecting blood samples from the tail 30 min after the end of the 20-min restraint period. In pilot studies, a separate group of animals was weighed ("handled controls") after which blood samples were collected from the tail 30 min later. Since these handled controls showed slightly elevated levels of plasma corticosterone (data not shown), untreated mice were used as controls for the CSD experiments in restraint mice.

Corticosterone, mifepristone and tetrahydrodeoxycorticosterone injections

On the day of the CSD experiment, corticosterone (Sigma-Aldrich, St. Louis, MO; 20 mg/kg, in arachidonic oil) or vehicle was subcutaneously injected between 10:00 and 10:30 am when endogenous corticosterone levels are low (Table 1) after which the mouse was returned to its home cage. A tail blood sample was collected 3 hr after corticosterone or vehicle injection just before surgical preparation. Surgery for CSD measurements started 3 hr after corticosterone or vehicle injection. Mifepristone (10 mg/kg; RU486, Sigma-Aldrich) diluted in 1,2-propanediol was injected subcutaneously 50 min prior to corticosterone/vehicle injection. Tetrahydrodeoxycorticosterone (THDOC; Sigma-Aldrich) was first diluted in 45% hydroxypropyl- β -cyclodextrin (Sigma-Aldrich) in distilled water before further dilution in 0.9% saline, and was injected intraperitoneally at 20 mg/kg shortly after the start of surgery for CSD measurements, approximately 3 hr after corticosterone (20 mg/kg subcutaneously) injection.

Table 1. Corticosterone plasma levels in WT and R192Q mice at baseline, after a 20-min and 3-hr restraint stress paradigm.

Time	Baseline	30 min	3 hr	Post-CSD
WT	14.3 [6,38] (<i>N</i> =11)			
R192Q	15.7 [6,96] (<i>N</i> =9)			
WT 20 min restraint		110 [#] [81,147] (<i>N</i> =4)	59 [14,76] (<i>N</i> =6)	231 [164,271] (<i>N</i> =5)
R192Q 20 min restraint		165 [#] [123,212] (<i>N</i> =5)	27 [6,76] (<i>N</i> =8)	260 [232,338] (<i>N</i> =8)
WT 3 hr restraint			372 [#] [251,556] (<i>N</i> =8)	253 [155,401] (<i>N</i> =8)
R192Q 3 hr restraint			349 [#] [232,621] (<i>N</i> =8)	195 [165,694] (<i>N</i> =8)

Table 1. Values are corticosterone plasma levels in ng/mL, shown as medians with [minimum, maximum] values; group sizes are indicated in italics. Corticosterone plasma levels were determined from tail blood. Blood samples were collected from R192Q and WT mice at baseline, 30 min and 3 hr after 20-min restraint stress and immediately after 3-hr restraint stress. Pairwise comparisons were made using Mann-Whitney U-test corrected for multiple testing (adjusted p-value 0.008). Significant differences compared to baseline are indicated with [#]. Note that 3 hr after 20-min restraint stress corticosterone plasma values had decreased to baseline levels, as indicated by the lack of a significant difference between baseline and the 30 min after 20-min restraint samples. There were no differences between R192Q and WT corticosterone plasma levels at any of the time-points.

CSD recordings under physiological control

CSD susceptibility measurements were performed as described in detail elsewhere (Eikermann-Haerter et al., 2009), under 1% isoflurane anesthesia in 20% O₂/ 80% N₂O with full physiological control (i.e., using a femoral artery lead for continuous blood pressure monitoring and blood sampling, and tracheotomy for artificial ventilation). Arterial blood gases (pCO₂, pO₂) and pH were measured at the start and end of CSD recordings and were maintained within normal limits by adjusting ventilation when necessary (Table 3). For CSD susceptibility measurements, the mouse was transferred into a stereotactic frame after which the skull was exposed and 2 burr holes were prepared over the right hemisphere for (1) CSD recording from the motor cortex (0.5 mm anterior from bregma; 2 mm lateral) and (2) CSD induction on the occipital cortex (3.5 mm posterior, 2 mm lateral). CSD was induced by application of a cotton ball soaked in 300 mM KCl on the occipital cortex for 30 min while DC-potential recordings were made from the motor cortex (Figure 1). Data were sampled

(200 Hz), amplified (10x) and low-pass filtered at 4 Hz and analyzed offline using LabChart (AD Instruments, Colorado Springs, CO).

Statistical analysis

Data are presented as median (corticosterone plasma data and CSD latency) or mean \pm SD. Statistics were calculated using SPSS (version 17; SPSS Inc., Chicago, IL). Effects of moderate (20 min) and severe (3 hr) restraint stress on CSD frequency (Figure 1) as well as the effect of genotype and corticosterone treatment on CSD frequency (Figures 2A, B) were tested with two-way ANOVA and post hoc Bonferroni correction. The effect of corticosterone and THDOC in R192Q mice was tested with one-way ANOVA and post hoc Bonferroni in comparison to the R192Q corticosterone and R192Q vehicle groups only. Systemic physiological data and CSD amplitude and duration (Table 3) were compared among groups using one-way ANOVA and Bonferroni correction. For skewed parameters (corticosterone plasma data and CSD latency), corresponding non-parametric tests were used (Kruskal-Wallis, followed by Mann-Whitney U-test). Significance was set at 0.05 and corrected for multiple testing where applicable.

RESULTS

Acute restraint stress does not influence CSD frequency in FHM1 R192Q and WT mice

We investigated whether an acute moderate or severe stressor influences CSD susceptibility in FHM1 mice, by using a single-restraint stress paradigm of 20 min or 3 hr duration in separate groups of R192Q and WT mice, with untreated mice as controls. Plasma corticosterone levels that were determined 30 min after the end of a moderate stressor (20-min restraint) were elevated compared to baseline in both R192Q and WT mice, with no difference between genotypes. Shortly before the start of the CSD experiments, i.e., 3 hr after the end of the 20-min restraint period, corticosterone plasma levels had normalized to baseline values in both R192Q and WT mice (Table 1). We observed no effect of the 20-min restraint procedure on CSD frequency in R192Q mice (R192Q untreated, 16.6 \pm 1.9 CSD/hr, N=8 vs R192Q 20-min restraint, 16.7 \pm 3.5 CSD/hr, N=8) nor in WT mice (WT untreated, 10.0 \pm 1.9 CSD/hr, N=10 vs WT 20-min restraint, 10.0 \pm 1.1 CSD/hr, N=7; Figure 1). CSD latency (min) was reduced in R192Q untreated compared to WT untreated mice but was not influenced by the 20-min restraint procedure (Table 3).

In contrast to 20 min restraint stress, a more severe 3 hr restraint stress caused increased corticosterone plasma levels compared to baseline levels just prior to CSD measurements (Table 1). In both R192Q and WT, this severe stressor resulted in corticosterone plasma levels close to those obtained after corticosterone injection (Table 2). As with the 20-min paradigm, 3 hr restraint stress did not influence CSD frequency compared to untreated controls in R192Q mice (R192Q untreated, 16.6 \pm 1.9 CSD/hr, N=8 vs R192Q 3-hr restraint 17.1 \pm 2.4 CSD/hr, N=8) or WT (WT untreated, 10.0 \pm 1.9 CSD/hr, N=10 vs WT 3-hr restraint, 9.7 \pm 2.5 CSD/hr, N=8; Figure 1). CSD latency (Table 3) was also not influenced by the restraint procedure compared to untreated mice.

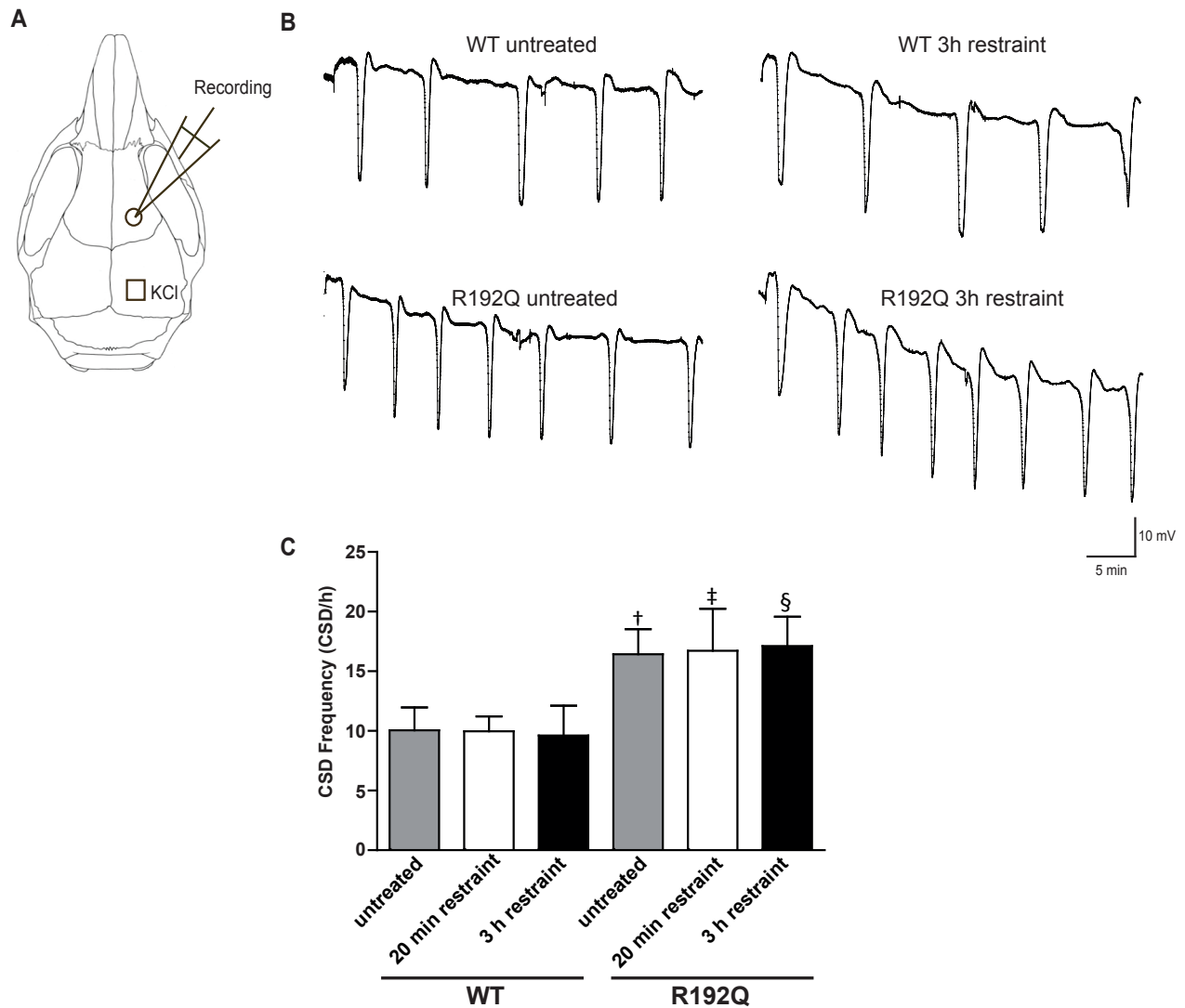


Figure 1. Moderate or severe restraint stress does not influence CSD susceptibility in FHM1 R192Q mice. (A) Schematic of the CSD induction site (KCl application) on the occipital cortex and DC-recording site in the motor cortex. (B) Specimen recordings showing CSD events measured in untreated and 3 hr restraint groups of WT and R192Q mice, illustrating comparable CSD frequencies in untreated compared to the 3-hr restraint animals. Scale bar applies to all traces. (C) Bar diagram (mean \pm SD) showing CSD frequency (number of CSD/hr) results from CSD recordings carried out 4 hr after a 20 min (moderate) and 1 hr after a 3 hr (severe) restraint stress in WT and R192Q mice (WT untreated N=10; R192Q untreated N=8; WT 20 min restraint N=6; R192Q 20 min restraint N=8; WT 3 hr restraint N=8; R192Q 3 hr restraint N=8). Moderate or severe restraint stress did not influence CSD susceptibility in R192Q or WT mice (2-way ANOVA), suggesting that other neurosteroids released during stress may counteract effects of corticosterone on CSD susceptibility in R192Q mice. CSD frequency was increased in R192Q mice compared to WT mice in all treatment groups (untreated [†] $p=0.000$; 20 min restraint [‡] $p=0.000$; 3 hr restraint [§] $p=0.000$).

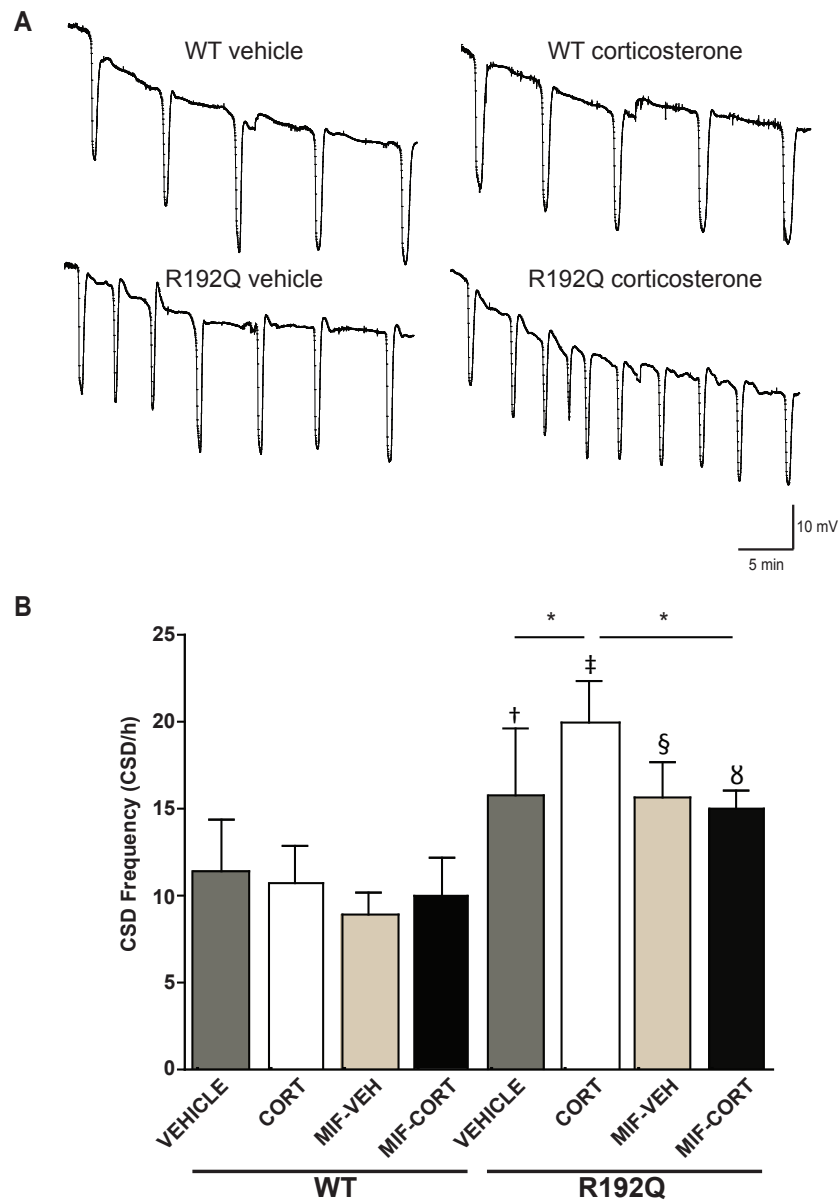


Figure 2. Corticosterone enhances CSD susceptibility in FHM1 R192Q mutant mice via glucocorticoid receptor activation. (A) Specimen recordings showing CSD events measured in the different treatment groups of WT and R192Q mice, illustrating enhanced CSD frequency in R192Q mice that were subcutaneously injected 4 hr earlier with 20 mg/kg corticosterone (CORT). Scale bar applies to all traces. (B) Bar diagram (mean \pm SD) showing CSD frequency (number of CSD/hr) results from R192Q and WT mice in the different treatment groups (N=8 mice/group; except for mifepristone pretreated mice injected with vehicle, MIF-VEH which are N=7 mice/group). Corticosterone administration enhanced CSD frequency in R192Q mice only (* $p=0.02$ vs R192Q VEH), an effect that was prevented by pre-administration of the GR antagonist mifepristone (* $p=0.004$ vs R192Q CORT). There was a significant main effect on CSD frequency of genotype, corticosterone treatment and the interaction between genotype and treatment. Note the higher CSD frequency in the R192Q vehicle group compared to WT vehicle-injected mice ($\dagger p=0.025$), in line with earlier findings from unchallenged R192Q and WT mice (Eikermann-Haerter et al 2009), as well as the higher CSD frequency for R192Q compared to WT mice for the CORT treated ($\ddagger p=0.000$), MIF-VEH treated ($\S p=0.000$) and MIF-CORT treated mice ($\diamond p=0.003$).

After both the 20-min and 3-hr restraint procedure, CSD duration (sec) and amplitude (mV), as well as systemic physiological parameters (i.e., blood pressure, pH, pCO₂, pO₂) were similar to values from untreated animals except for a higher pCO₂ (mm Hg) value in WT untreated compared to R192Q 3-hr restraint mice and a lower MABP (mm Hg) in R192Q 3-hr restraint compared to WT 3-hr restraint mice (Table 3).

Table 2. Corticosterone plasma levels in WT and R192Q mice in the CORT, VEH and MIF treatment groups before and after CSD experiments

Time	3 hr	Post-CSD
WT VEH	33.0 [13,210] (<i>N</i> =7)	158.9 [140,175] (<i>N</i> =8)
R192Q VEH	54.4 [9,90] (<i>N</i> =6)	195.9* [163,339] (<i>N</i> =8)
WT CORT	466.7# [233,1055] (<i>N</i> =5)	215.4# [183,339] (<i>N</i> =8)
R192Q CORT	522.8# [407,668] (<i>N</i> =4)	301.1# [211,562] (<i>N</i> =8)
WT MIF-CORT	1306.2# [699,1600] (<i>N</i> =7)	609.6 [227,1057] (<i>N</i> =8)
R192Q MIF-CORT	1017.3# [755,1648] (<i>N</i> =8)	521.0 [240,739] (<i>N</i> =8)
WT MIF-VEH	332.4 [300,354] (<i>N</i> =7)	226.4 [199,288] (<i>N</i> =7)
R192Q MIF-VEH	326.3 [58,348] (<i>N</i> =7)	286.8 [282,354] (<i>N</i> =7)

Table 2. Values are corticosterone plasma levels in ng/mL, shown as medians with [minimum, maximum] values; group sizes are indicated in italics. Corticosterone plasma levels were determined from tail blood. Blood samples were collected from R192Q and WT mice at 3 hr after a single subcutaneous administration of 20 mg/kg corticosterone (CORT) or vehicle (VEH), with or without pretreatment with the GR antagonist mifepristone (MIF). Post-CSD samples were taken at the end of CSD recordings under isoflurane anesthesia. Group comparisons were done with Kruskal-Wallis test: $\chi^2=51.942$, $p=0.000$. Pairwise comparisons were made using a Mann-Whitney U-test, corrected for multiple testing ($p=0.005$). Significant increases compared to baseline (see Table 1) are indicated by # (Mann-Whitney U-test). For corticosterone-injected animals, corticosterone plasma levels were comparable between R192Q and WT mice in the different treatment groups, including at the end of the experiment, except for post-CSD levels of vehicle-injected mice which showed slightly higher corticosterone plasma levels for R192Q compared to WT mice (* $p=0.0013$ Mann-Whitney U-test). Both for corticosterone and vehicle-injected animals, there was no correlation between corticosterone plasma levels at the end of surgery and CSD frequency (Spearman's $\rho=0.192$, $p=0.224$).

Corticosterone administration increases CSD frequency exclusively in FHMI R192Q mice via GR activation

We next investigated the acute effect of the stress hormone corticosterone on CSD susceptibility, by administering a dose of 20 mg/kg corticosterone in the morning 3 hr before surgery was started to determine CSD frequency in R192Q and WT mice. Corticosterone plasma levels at baseline and after injection of corticosterone were comparable between R192Q and WT mice. In both genotypes, corticosterone injection resulted in strongly elevated corticosterone plasma levels, while no significant plasma corticosterone increase was observed after injection of vehicle (Table 2).

We observed a significant main effect on CSD frequency of genotype ($F[1,54]=105,98$; $p=0.000$), corticosterone treatment ($F[3,54]=5,22$; $p=0.003$), and the interaction between genotype and corticosterone treatment ($F[3, 54]=3.39$; $p=0.024$). Post-hoc testing revealed that corticosterone injection resulted in a significantly increased CSD frequency in R192Q mice (19.9 ± 2.3 CSD/hr; $N=8$) compared to vehicle (15.6 ± 3.8 CSD/hr; $N=8$; $p=0.02$), while there was no effect of corticosterone in WT mice (WT corticosterone, 10.7 ± 2.1 CSD/hr; $N=8$; WT vehicle, 11.4 ± 2.9 CSD/hr; $N=8$; Figure 2A, B).

To investigate a possible role of GR activation on the observed corticosterone effects in R192Q mice, the GR antagonist mifepristone (10 mg/kg) was injected 50 min prior to corticosterone injection. Mifepristone pre-treatment normalized CSD frequency in R192Q mice (15.0 ± 1.0 CSD/hr; $N=8$) to the level of vehicle-controls (15.6 ± 3.8 CSD/hr; $N=8$; Figure 2B). Mifepristone did not influence CSD frequency in vehicle-injected R192Q mice (15.6 ± 2 CSD/hr; $N=7$), vehicle-injected WT mice (8.9 ± 1.2 CSD/hr; $N=7$), or corticosterone-injected WT mice (9.9 ± 2.1 CSD/hr; $N=8$). Since the CSD frequencies of mice in the combined mifepristone with vehicle group were comparable to those in the vehicle-control group, no separate controls for mifepristone injection were included. CSD duration (sec), amplitude (mV), latency (min) and physiological parameters were not influenced by corticosterone, vehicle or mifepristone injection (Table 3).

To investigate whether neurosteroids as a stress mediator may counteract effects of corticosterone on CSD frequency, we administered tetrahydrodeoxycorticosterone (THDOC), a neurosteroid with anticonvulsant properties (Kokate et al 1994, Kokate et al 1996, Reddy and Rogawski 2002) that is synthesized from corticosterone precursor 11-deoxycorticosterone (Kaminski and Rogawski 2011), at a dosage of 20 mg/kg, 40 min prior to CSD measurements in an additional group of R192Q mice ($N=6$) that received a 20 mg/kg corticosterone injection 3 hr earlier. In these mice, corticosterone plasma levels 3 hr after corticosterone injection were strongly elevated (781.3 ± 312.0 ng/mL). The additional administration of THDOC did not change CSD frequency (18.8 ± 3.1 CSD/hr; $N=6$) compared to that observed for the group of R192Q mice injected with corticosterone alone (see above and Figure 2, 19.9 ± 2.3 CSD/hr; $N=8$; $p=1$).

Table 3. Systemic physiological parameters and CSD characteristics in WT and R192Q mice in the different treatment groups

Groups	N	pH	pCO ₂ (mm Hg)	pO ₂ (mmHg)	MABP (mmHg)	CSD Amplitude (mV)	CSD Duration (sec)	CSD Latency (min)
WT untreated	10	7.38±0.03	32.4±1.73 [†]	120.5±12.3	83.9±13.1	16.9±4.1	30.4±9.2	1.3 [1.2-1.5]
R192Q untreated	8	7.39±0.02	31.2±1.6	128.9±11.5	89.8±6.6	20±2.8	21.7±6.2	0.8 [§] [0.5-1.2]
WT 20 min restraint	6	7.39±0.02	32.1±1.9	136.3±19.6	92.6±6.2	18.0±3.3	21.1±4.5	1.3 [1.2-1.4]
R192Q 20 min restraint	8	7.38±0.03	31.7±1.2	129.6±15.1	90.7±3.8	19.6±3.9	22.6±3.82	1.0 [0.2-1.2]
WT 3hr restraint	8	7.37±0.01	30.0±2.0	123.7±13.5	80.1±3.5 [‡]	14.9±2.9	26.4±5.8	1.2 [1.1-2.0]
R192Q 3hr restraint	8	7.36±0.01	29.8±1.5	128.5±17.6	93.7±4.5	17.1±1.7	31.1±6.9	1.0 [0.5-2.5]
WT VEH	8	7.37±0.01	33.9±2.5	127.9±15.1	80.5±6.0	21.7±3.3	23.9±6.0	1.4 [1.3-2.4]
R192Q VEH	8	7.36±0.03	32.2±4.0	119.7±14.3	82.2±7.8	22.6±1.7	22.3±4.0	1.1 [#] [1.0-1.4]
WT CORT	8	7.35±0.01	35.5±2.0	127.9±13.1	85.7±6.8	21.2±4.8	22.9±8.6	1.5 [1.2-2.1]
R192Q CORT	8	7.33±0.01 [*]	31.9±4.1	128.2±19.5	82.1±5.5	21.1±1.9	21.6±2.2	1.2 [#] [1.0-1.3]
WT MIF-VEH	7	7.35±0.02	33.8±3.1	127.7±9	76.1±5.4	18.7±4.3	29.3±5.8	1.4 [1.3-4.5]
R192Q MIF-VEH	7	7.37±0.02	32.7±3	135.6±23.3	84.8.9±7.2	20.1±2.2	26.4±6.3	1.0 [#] [0.5-1.0]
WT MIF-CORT	8	7.36±0.02	32.3±3.1	132.8±09.2	79.0±8.0	23.6±2.8	24.5±5.0	1.4 [1.3-2.1]
R192Q MIF-CORT	8	7.36±0.03	32.3±3.2	127.2±21.4	80.2±7.0	21.0±3.0	25.9±7.3	1.2 [1.1-2.3]

Table 3. Values shown are mean ± SD. Because CSD latency values (min) were not normally distributed and variances were unequal, these are shown as median with [minimum, maximum] values. Physiological parameters during CSD frequency recordings were kept within physiological ranges. In the restraint stress treated mice there were no significant differences in physiological parameters except for a slightly higher pCO₂ value (mm Hg) for WT untreated (indicated by [†]) compared to R192Q 3-hr restraint (p=0.028) and a lower MABP (mean arterial blood pressure; mm Hg) in WT 3-hr restraint (indicated by [‡]) compared to R192Q 3-hr restraint (p=0.013). R192Q untreated mice had a reduced CSD latency compared to WT untreated mice ([§]p=0.009). In the corticosterone injection experiments, there was a slightly lower blood pH in the R192Q CORT group compared to WT VEH (^{*}p=0.03) and R192Q MIF-VEH (p=0.01). Note that lower pH, if effective in the brain, would reduce rather than enhance neuronal excitability. Except for MIF-CORT groups (p=0.08), R192Q mice showed a reduced CSD latency compared to WT across all treatment groups (significance indicated by [#]; CORT p=0.003, VEH p=0.005 and MIF-VEH p=0.0006).

DISCUSSION

Transgenic FHM1 R192Q knock-in mice display an increased susceptibility to experimentally induced CSD (van den Maagdenberg et al 2004, Eikermann-Haerter et al 2009) that can be explained by an enhanced cortical glutamate release (Tottene et al 2009). The enhanced CSD susceptibility serves as a measure of excitability and surrogate migraine marker. Stress and stress hormones can also cause direct changes in glutamatergic neurotransmission, leading to increased neuronal excitability (Popoli et al 2011), but it is not known if this can explain why acute stress may enhance propensity to migraine attacks. Our data show that acute restraint stress does not influence CSD frequency in R192Q or WT mice, despite elevated plasma corticosterone levels. Administration of the stress hormone corticosterone, however, increases CSD frequency within 3-4 hr in R192Q mice and not in WT mice, without affecting blood pressure or blood-gas parameters. The corticosterone-induced increased CSD susceptibility in R192Q mice was prevented by pre-administration of the GR antagonist mifepristone. These findings illustrate that corticosterone-induced GR pathway activation can enhance susceptibility to CSD in genetically susceptible individuals and may predispose to attacks of migraine. Although corticosterone levels rise during acute stress, the latter likely triggers a spatiotemporally more complex biological response with multiple positive and negative modulators (Joels and Baram 2009), which may not be adequately modeled by exogenous administration of corticosterone alone.

The absence of a CSD effect after a 20 min moderate restraint may be related to the fact that corticosterone plasma levels were only transiently increased with this paradigm and had returned to baseline values shortly before start of the CSD experiment. The 3 hr restraint paradigm however did not influence CSD susceptibility either, in both R192Q and WT mice, despite corticosterone plasma levels that were elevated to a similar extent as observed after 20 mg/kg corticosterone injection. It is possible that the biokinetics of corticosterone in case of restraint stress do not mimic those achieved by external corticosterone administration since plasma levels do not necessarily reflect effects at the cortical or cellular level. In addition, in case of an acute stress paradigm apart from corticosterone other stress mediators, such as neurosteroids like THDOC and allopregnanolone (Purdy et al 1991, Zimmerberg and Brown 1998) and the neuropeptide corticotropin-releasing hormone (CRH; Vale et al 1981), are known to be elevated which could have interfered with the effect of corticosterone on CSD. Although THDOC and allopregnanolone have been shown to modulate the physiological response to stress by promoting GABAergic inhibitory neurotransmission (Bitran et al 1995, Stromberg et al 2005) and can suppress hyperexcitability in mouse seizure models (Kokate et al 1994, Kokate et al 1996, Reddy and Rogawski 2002), the administration of THDOC to R192Q mice that were earlier injected with corticosterone did not seem to affect the corticosterone-induced increase in CSD frequency in our study. This outcome is not entirely surprising, since GABAergic agonists in general do not suppress CSD susceptibility (van Harreveld and Stamm 1953, Brand et al 1998, Kitahara et al 2001). Possibly, suppressed release of the endogenous stress hormone CRH in the aftermath of stress

may contribute to the lack of change in CSD frequency upon restraint stress; this would fit with the notion that high levels of CRH generally excite actions (Blank et al 2003).

The exact mechanisms by which corticosterone influences CSD susceptibility in FHM1 mice are unknown, but the involvement of GR suggests interaction at the level of excitatory glutamatergic neurotransmission. GR activation by stress or corticosterone has been shown to influence glutamatergic neurotransmission mainly by increasing postsynaptic glutamate responses (Karst and Joels 2005, Yuen et al 2009) and L-type Ca^{2+} currents (Chameau et al 2007). The FHM1 R192Q gain-of-function mutation leads to increased Ca^{2+} influx pre-synaptically, resulting in increased glutamate release (Tottene et al 2009, van den Maagdenberg et al 2004). When corticosterone is administered to FHM1 R192Q mice, an additive effect of GR activation and the FHM1 $\text{Ca}_v2.1$ gain-of-function on glutamatergic transmission might cause even higher CSD frequencies than achieved by either condition alone. In WT mice, that lack the genetically increased level of glutamatergic neurotransmission, corticosterone apparently does not have sufficient effect by itself to influence CSD susceptibility.

The finding that mifepristone pre-treatment prevented the corticosterone-induced increase in CSD frequency in R192Q mice indicates that the corticosterone effect on CSD susceptibility is specific and mediated by activation of GR pathways. The corticosterone effect emerged in the time-period related to delayed effects mainly involving GR, and not MR, actions (de Kloet et al 2005, Joels and Baram 2009, Joels et al 2012). Observations that mifepristone is generally ineffective in blocking membrane-receptor-mediated events (Di et al 2003, Liu et al 2007, Zhang et al 2012), make it plausible that the observed GR mediated effects on CSD in R192Q mice were genomically mediated, although non-genomic actions cannot be ruled out.

In conclusion, this study showed that an acute stressor does not influence CSD susceptibility in our FHM1 mouse migraine model, while acute administration of corticosterone specifically enhances CSD susceptibility in FHM1 mutants and not in WT. This could reflect the fact that both the FHM1 mutation and corticosterone, via GR activation, exert their effect at the level of glutamatergic neurotransmission, thus providing a possible mechanistic underpinning of their interaction. It can be hypothesised that susceptible individuals may be protected against migraine in cases of acute stress as long as other stress-induced factors counteract GR-mediated actions of corticosteroids on glutamatergic transmission. This protection may fall short when a disbalance between corticosteroids and such other stress hormones occurs. Future work should reveal the complex interplay of corticosterone with other stress mediators in the context of acute stress and CSD susceptibility, as well as mechanisms underlying effects of chronic stress (Borsook et al 2012), as opposed to acute stress, on migraine characteristics.

ACKNOWLEDGEMENTS

This work was financially supported by the Dutch Organization for Scientific Research NWO (Spinoza 2009, M.D.F.; Vici 918.56.602, M.D.F), the EU “Eurohead” grant (LSHM-CT-2004-504837; M.D.F., A.M.J.M.v.d.M), the EU Marie Curie IAPP Program “BRAINPATH” (nr 612360), EU “EUROHEADPAIN” grant (nr 602633) (M.D.F., A.M.J.M.v.d.M), an LUMC Fellowship (E.A.T.), the Marie Curie Career Integration Grant (nr 294233) (E.A.T.) and the Center of Medical System Biology (CMSB) established by the Netherlands Genomics Initiative (NGI)/NWO (A.M.J.M.v.d.M.). The authors thank Menno Hoekstra, Quirijn Dees and Ioannis Zalachoras for help with corticosterone measurements and Brunilda Balliu and Jeanine Houwing-Duistermaat for assistance with statistics.

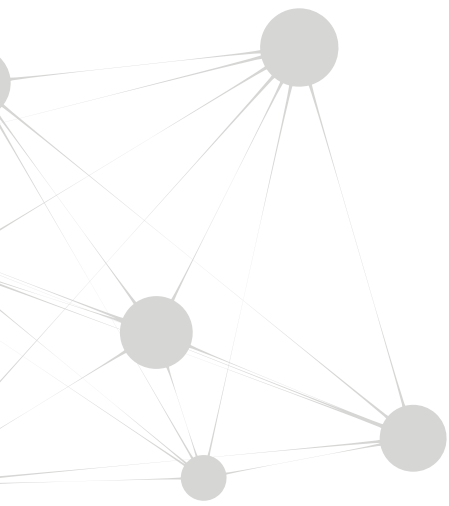
REFERENCES

- The International Classification of Headache Disorders. 2004 2nd edition. *Cephalalgia* 24:Suppl 1: 9-160
- Aurora SK, Wilkinson F. 2007. The brain is hyperexcitable in migraine. *Cephalalgia* 27:1442-1453
- Bitran D, Shiekh M, McLeod M. 1995. Anxiolytic effect of progesterone is mediated by the neurosteroid allopregnanolone at brain GABAA receptors. *J. Neuroendocrinol.* 7:171-177
- Blank T, Nijholt I, Grammatopoulos DK, Randeva HS, Hillhouse EW, Spiess J. 2003. Corticotropin-releasing factor receptors couple to multiple G-proteins to activate diverse intracellular signaling pathways in mouse hippocampus: role in neuronal excitability and associative learning. *J. Neurosci.* 23:700-707
- Borsook D, Maleki N, Bercerra L, McEwen B. 2012. Understanding Migraine through the Lens of Maladaptive Stress Responses: A Model Disease of Allostatic Load. *Neuron* 73:219-234
- Brand S, Fernandes de Lima VM, Hanke W. 1998. Pharmacological modulation of the refractory period of retinal spreading depression. *Naunyn-Schmiedeberg's Arch. Pharmacol.* 357:419-425
- Chameau P, Qin Y, Spijker S, Smit G, Joels M. 2007. Glucocorticoids specifically enhance L-type calcium current amplitude and affect calcium channel subunit expression in the mouse hippocampus. *J. Neurophysiol.* 97:5-14
- de Kloet ER, Joels M, Holsboer F. 2005. Stress and the brain: from adaptation to disease. *Nat. Rev. Neurosci.* 6:463-475
- Di S, Malcher-Lopes R, Halmos KC, Tasker JG. 2003. Nongenomic glucocorticoid inhibition via endocannabinoid release in the hypothalamus: a fast feedback mechanism. *J. Neurosci.* 23:4850-4857
- Eikermann-Haerter K, Dilekoz E, Kudo C, Savitz SI, Waeber C, et al. 2009. Genetic and hormonal factors modulate spreading depression and transient hemiparesis in mouse models of familial hemiplegic migraine type 1. *J. Clin. Invest.* 119:99-109
- Goadsby PJ, Lipton RB, Ferrari MD. 2002. Migraine--current understanding and treatment. *N. Engl. J. Med.* 346:257-270
- Hauge AW, Kirchmann M, Olesen J. 2011. Characterization of consistent triggers of migraine with aura. *Cephalalgia* 31:416-438
- Joels M, Baram TZ. 2009. The neuro-symphony of stress. *Nat. Rev. Neurosci.* 10:459-466
- Joels M, Sarabdjitsingh RA, Karst H. 2012. Unraveling the time domains of corticosteroid hormone influences on brain activity: rapid, slow, and chronic modes. *Pharmacol. Rev.* 64:901-938
- Kaminski RM, Rogawski MA. 2011. 11beta-Hydroxylase inhibitors protect against seizures in mice by increasing endogenous neurosteroid synthesis. *Neuropharmacology* 61:133-137
- Karst H, Joels M. 2005. Corticosterone slowly enhances miniature excitatory postsynaptic current

- amplitude in mice CA1 hippocampal cells. *J. Neurophysiol.* 94:3479-3486
- Kitahara Y, Taga K, Abe H, Shimoji K. 2001. The effects of anesthetics on cortical spreading depression elicitation and c-fos expression in rats. *J. Neurosurg. Anesthesiol.* 13:26–32
- Kokate TG, Svensson BE, Rogawski MA. 1994. Anticonvulsant activity of neurosteroids: correlation with gamma-aminobutyric acid-evoked chloride current potentiation. *J. Pharmacol. Exp. Ther.* 270:1223-1229
- Kokate TG, Cohen AL, Karp E, Rogawski MA. 1996. Neuroactive steroids protect against pilocarpine- and kainic acid-induced limbic seizures and status epilepticus in mice. *Neuropharmacology* 35:1049-1056
- Launer LJ, Terwindt GM, Ferrari MD. 1999. The prevalence and characteristics of migraine in a population-based cohort: the GEM study. *Neurology* 53:537-542
- Lauritzen, M. 1994. Pathophysiology of the migraine aura. The spreading depression theory. *Brain* 117 (Pt 1):199-210.
- Liu L, Wang C, Ni X, Sun J. 2007. A rapid inhibition of NMDA receptor current by corticosterone in cultured hippocampal neurons. *Neurosci. Lett.* 420:245-250
- Ophoff RA, Terwindt GM, Vergouwe MN, van Eijk R, Oefner PJ, et al. 1996. Familial hemiplegic migraine and episodic ataxia type-2 are caused by mutations in the Ca²⁺ channel gene CACNL1A4. *Cell* 87:543-552
- Popoli M, Yan Z, McEwen BS, Sanacora G. 2011. The stressed synapse: the impact of stress and glucocorticoids on glutamate transmission. *Nat. Rev. Neurosci.* 13:22-37
- Purdy RH, Morrow AL, Moore PH, Paul SM. 1991. Stress-induced elevations of gamma-aminobutyric acid type A receptor-active steroids in the rat brain. *Proc. Natl. Acad. Sci. USA* 88:4553-4557
- Reddy DS, Rogawski MA. 2002. Stress-induced deoxycorticosterone-derived neurosteroids modulate GABA(A) receptor function and seizure susceptibility. *J. Neurosci.* 22:3795-3805
- Sarabdjitsingh RA, Isenia S, Polman A, Mijalkovic J, Lachize S, et al. 2010. Disrupted corticosterone pulsatile patterns attenuate responsiveness to glucocorticoid signaling in rat brain. *Endocrinology* 151:1177-1186
- Sarabdjitsingh RA, Kofink D, Karst H, de Kloet ER, Joels M. 2012. Stress-induced enhancement of mouse amygdalar synaptic plasticity depends on glucocorticoid and ss-adrenergic activity. *PLoS One* 7:e42143
- Sauro KM, Becker WJ. 2009. The stress and migraine interaction. *Headache* 49:1378-1386
- Stromberg J, Backstrom T, Lundgren P. 2005. Rapid non-genomic effect of glucocorticoid metabolites and neurosteroids on the gamma-aminobutyric acid-A receptor. *Eur. J. Neurosci.* 21:2083-2088
- Tottene A, Conti R, Fabbro A, Vecchia D, Shapovalova M, et al. 2009. Enhanced excitatory transmission at cortical synapses as the basis for facilitated spreading depression in Ca(v)2.1

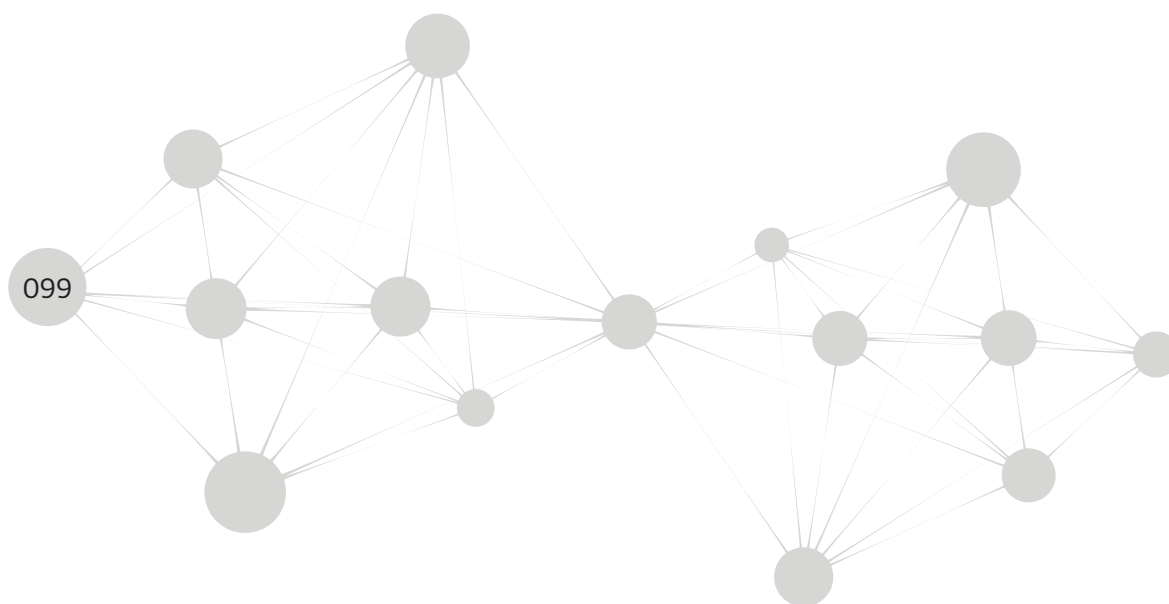
knockin migraine mice. *Neuron* 61:762-773

- Vale W, Spiess J, Rivier C, Rivier J. 1981. Characterization of a 41-residue ovine hypothalamic peptide that stimulates secretion of corticotropin and beta-endorphin. *Science* 213:1394-1397
- van den Maagdenberg AM, Pietrobon D, Pizzorusso T, Kaja S, Broos LA, et al. 2004. A Cacna1a knockin migraine mouse model with increased susceptibility to cortical spreading depression. *Neuron* 41:701-710
- Van Harreveld A, Stamm JS. 1953. Effect of pentobarbital and ether on the spreading cortical depression. *Am. J. Physiol.* 173:164-170
- Yuen EY, Liu W, Karatsoreos IN, Feng J, McEwen BS, Yan Z. 2009. Acute stress enhances glutamatergic transmission in prefrontal cortex and facilitates working memory. *Proc. Natl. Acad. Sci. USA* 106:14075-14079
- Zhang Y, Sheng H, Qi J, Ma B, Sun J, Li S, Ni X. 2012. Glucocorticoid acts on a putative G protein-coupled receptor to rapidly regulate the activity of NMDA receptors in hippocampal neurons. *Am. J. Physiol. Endocrinol. Metab.* 302:E747-758
- Zimmerberg B, Brown RC. 1998. Prenatal experience and postnatal stress modulate the adult neurosteroid and catecholaminergic stress responses. *Int. J. Dev. Neurosci.* 16:217-228



Chapter 5

Imaging mass spectrometry to visualize biomolecule distributions in mouse brain tissue following hemispheric cortical spreading depression



Emrys A. Jones^{*1}, Reinald Shyti^{*2}, René J.M. van Zeijl¹, Sandra H. van Heiningen², Michel D. Ferrari³, André M Deelder¹, Else A. Tolner^{2,3}, Arn M.J.M. van den Maagdenberg^{2,3,‡}, Liam A. McDonnell^{1,‡}

¹Biomolecular Mass Spectrometry Unit, Department of Parasitology, Leiden University Medical Center, Leiden, the Netherlands

²Department of Human Genetics, Leiden University Medical Center, Leiden, the Netherlands

³Department of Neurology, Leiden University Medical Center, Leiden, the Netherlands

^{*,‡} equal contributions

Journal of Proteomics 2012;75:5027-35

ABSTRACT

MALDI mass spectrometry can simultaneously measure hundreds of biomolecules directly from tissue. Using essentially the same technique but different sample preparation strategies, metabolites, lipids, peptides and proteins can be analyzed. Spatially correlated analysis, imaging MS, enables the distributions of these biomolecular ions to be simultaneously measured in tissues. A key advantage of imaging MS is that it can annotate tissues based on their MS profiles and thereby distinguish biomolecularly distinct regions even if they were unexpected or are not distinct using established histological and histochemical methods e.g., neuropeptide and metabolite changes following transient electrophysiological events such as cortical spreading depression (CSD), which are spreading events of massive neuronal and glial depolarisations that occur in one hemisphere of the brain and do not pass to the other hemisphere, enabling the contralateral hemisphere to act as an internal control. A proof-of-principle imaging MS study, including 2D and 3D datasets, revealed substantial metabolite and neuropeptide changes immediately following CSD events which were absent in the protein imaging datasets. The large high dimensionality 3D datasets make even rudimentary contralateral comparisons difficult to visualize. Instead non-negative matrix factorization (NNMF), a multivariate factorization tool that is adept at highlighting latent features, such as MS signatures associated with CSD events, was applied to the 3D datasets. NNMF confirmed that the protein dataset did not contain substantial contralateral differences, while these were present in the neuropeptide dataset.

INTRODUCTION

Matrix-assisted laser desorption/ionization mass spectrometry (MALDI MS) can generate biomolecular profiles directly from tissue that contain hundreds of distinct biomolecular ions (Chaurand et al 2004). Spatially-correlated analysis, imaging MS, can simultaneously record the distribution of each of these ions in heterogeneous tissue samples (Cornett et al 2007, McDonnell & Heeren 2007). There is growing evidence that imaging is having an impact in disease detection and investigation (McDonnell et al 2010, Schwamborn & Caprioli 2010). By combining imaging MS with histology the differential MS profiles found in specific histopathological entities can be used to identify candidate biomarkers (Cazares et al 2009).

A major advantage of imaging MS is that it can annotate tissues based on their MS profiles and thereby distinguish biomolecularly distinct regions even if they are not distinct using established histological and histochemical methods (Mathur et al 2009). Imaging MS-based molecular histology has been used to differentiate histologically overlapping/identical tumors, identify patient subgroups (Willems et al 2010), reveal intratumor heterogeneity that may indicate clonal development (Deininger et al 2008, Jones et al 2011, Willems et al 2010) and uncovered evidence of early infiltration at tumor interface zones (Kang et al 2010, Oppenheimer et al 2010). These capabilities offer enormous potential to investigate the biomolecular changes that take place prior to, or without, morphological change, or for which a molecular specific stain is unavailable. This may be especially true for metabolic and neuropeptide changes following transient events, for instance for neurological diseases such as migraine or epilepsy that are defined by their episodic nature, and which may lack histopathological features and stains for specific metabolites/neuropeptides.

In many neurological diseases the pathophysiology is not entirely known and would benefit from systematic investigations of the biomolecular differences between diseased and healthy tissue. Information of such biomolecular differences can guide the search for reliable biomarkers in neurological diseases that are currently lacking.

Cortical Spreading Depression (CSD) is a self-propagating wave of intense neuronal and glial cell depolarization that occurs in one hemisphere of the cerebral cortex which is followed by a marked neuronal silencing (Leao 1944, Somjen 2001), which in humans is associated with for instance the aura phase during migraine attacks (Hadjikhani et al 2001, Lauritzen 1994). Apart from migraine, spreading depression can occur in brain tissue in relation to ischemic insults or seizures (Dreier et al 2012, Lauritzen et al 2011, Somjen 2001). CSD can be easily induced experimentally in animals by local stimulation of the cortex by current injection or by topical application of a high concentration of K^+ on the brain surface (Lauritzen 1994, Somjen 2001). When induced in one hemisphere, CSD does not cross to the other hemisphere (Eikermann-Haerter et al 2009, Somjen 2001). Previous studies have described a number of neuropeptides and metabolites that are transiently released after CSD such as changes in lactate (Scheller et al 1996) and glutamate (Fabricius et al 1993). However the

spatial distributions of these peptides and metabolites, and the evolution of their spatiotemporal signatures, have not been established.

Here we report the results of a proof-of-principle imaging MS study of the biomolecular changes following CSD, including metabolites, neuropeptides and proteins. CSD was unilaterally induced, enabling the contralateral hemisphere to be used as an internal control, as introduced by Andrén and workers for Parkinson's disease research (Nilsson et al 2007, Sköld et al 2006) and recently used by (Hanreider et al. 2011). A SHAM-operated mouse, in which Na⁺ instead of K⁺ is applied to the brain surface and which does not result in CSD events, is included to control for possible changes related to the surgical procedures.

METHODS

CSD Experiments

Two male C57Bl/6 mice of 3 months of age were used. In one animal 7 CSDs were evoked by repeated application of 1 M KCl onto the right visual cortex with a 5-min interval. The other animal received SHAM treatment by repeated application of 1 M NaCl which does not induce CSDs. CSD induction and monitoring was carried out by topical KCl application as described previously (Eikermann-Haerter et al 2011) with some modifications. In short, surgery was carried out using 1.5% isoflurane anesthesia in surgical air. After preparing a cranial window above the occipital cortex of the right hemisphere (ca. 3.5 mm posterior, 2 mm lateral from bregma) 7 CSD were evoked with a 5-min interval between two successive applications. For this, a cotton ball soaked in 1 M KCl was placed for 30 sec on the dura overlaying the occipital cortex followed by a wash with 150 mM NaCl. The CSDs were monitored by recording cortical DC-potential changes via a glass microelectrode placed in the frontal sensorimotor cortex (0.5 mm anterior, 2 mm lateral from bregma; depth 300 μ m). Immediately after the 7th CSD the mouse was decapitated, the brain was removed and flash-frozen on dry ice in less than 1 min and stored at -80 °C. The SHAM-treated mouse underwent the same procedure with NaCl application instead of KCl.

Imaging MS Data Acquisition

For the MALDI imaging MS experiments 12 μ m thick tissue sections were cut at -20 °C and thaw-mounted onto conductive glass slides (Delta Technologies, Stillwater, MN, USA). The tissues were then slowly brought to room temperature in a desiccator and prepared for MALDI analysis.

Peptide imaging

A uniform coating of α -cyano-4-hydroxycinnamic acid (CHCA) was added using an ImagePrep device (Bruker Daltonics, Bremen, Germany) and a solution of 10 mg/ml CHCA in 70:30 AcN: 0.1% TFA(aq.). MALDI imaging MS was then performed using an UltrafleXtreme MALDI-ToF/ToF (Bruker Daltonics), 100 mm pixel size, and 800 laser shots per pixel (50 laser shots per position of a random walk within each pixel). Data acquisition, preprocessing (smoothing and baseline

subtraction of each pixel's MALDI mass spectrum), and data visualization were performed using the Flex software suite (FlexControl 3.3, FlexAnalysis 3.3, FlexImaging 2.1). The SavitskyGolay algorithm was used for mass spectral smoothing (width 0.02 m/z , 2 cycles) and the TopHat algorithm used for baseline subtraction.

Protein imaging

The tissues were washed in isopropanol and sinapinic acid (SA) matrix added using the ImagePrep device and a solution of 20 mg/ml SA in 70% isopropanol: 0.1% TFA(aq.). MALDI Imaging MS experiments were then performed using an Autoflex III MALDI-ToF (Bruker Daltonics), 100 mm pixel size, and 600 laser shots per pixel (50 laser shots per position of a random walk within each pixel). Data acquisition, preprocessing and data visualization were performed using the Flex software suite (FlexControl 3.0, FlexAnalysis 3.0, FlexImaging 2.1). The Gaussian algorithm was used for mass spectral smoothing (width 2 m/z , 4 cycles) and a ConvexHullV3 for baseline subtraction.

Metabolite Imaging

A uniform coating of 9-aminoacridine was added using the ImagePrep and a solution of 10 mg/ml 9-aminoacridine 7:3 MeOH:H₂O. Metabolite imaging MS experiments were performed using an UltrafleXtreme MALDI-ToF/ToF in negative-ion mode, a 100 mm pixel size with 500 laser shots per pixel (100 laser shots per position of a random walk within each pixel). Data acquisition, preprocessing and data visualization were performed using the Flex software suite (FlexControl 3.3, FlexImaging 2.1, FlexAnalysis 3.3). The SavitskyGolay algorithm was used for mass spectral smoothing (width 0.005 m/z , 2 cycles) and the TopHat algorithm for baseline subtraction.

After the imaging MS experiments the remaining matrix was removed and the tissues stained with Hematoxylin & Eosin (H&E) (Schwamborn et al 2007). High resolution optical images of the H&E stained tissues were then aligned to the imaging MS datasets.

3D Imaging MS Reconstruction

Approximately 20 coronal tissue sections, sampled in 200 mm steps – covering a region in between the CDS induction and CSD recording sites, between 0.5 mm anterior and 3.5 mm posterior from bregma - were analyzed to create 3D imaging MS datasets of the biomolecular changes that occur between the occipital cortex (where the CSDs were initiated) and the sensorimotor cortex (location of the recording site of cortical DC-potential changes related to CSD). The 3D imaging MS dataset was reconstructed from the serial 2D imaging MS datasets by first aligning each individual tissue section's imaging MS dataset to an optical image of the H&E stained tissue, and then aligning the serial sections on the basis of their histology. The coordinates of the pixels in each tissue's imaging MS dataset were then converted into the aligned 3D space.

In order to efficiently analyze the full 3D imaging MS datasets automated feature identification and extraction was used to reduce the imaging MS data to the MS features with a S/N>5. First an automated feature identification routine was applied to each tissue section's imaging MS dataset (McDonnell et

al 2010). The peak-lists obtained from each tissue were then collated into a final 3D-project peak list, which was then used to extract all MS features ($S/N > 5$) from every tissue's imaging MS dataset. Thus the final reduced 3D imaging dataset contains the coordinates of each pixel, a peak list of all MS peaks with a $S/N > 5$, and the intensity of each of the peaks in every pixel.

To identify regions of the 3D imaging MS datasets containing similar MS profiles Non-Negative Matrix Factorization (NNMF) was applied to the reduced 3D imaging MS dataset using the David Ross's (University of Toronto: <http://www.cs.toronto.edu/~dross/>) implementation of Lee & Seung's Non-Negative Matrix Factorization algorithm (Lee & Seung 1999). The number of iterations was set to 100 and typically resulted in a stable solution. NNMF decomposes the data into a sum of additive non-negative components (explicit requirement, scores and loadings must be non-negative) (Lee & Seung 1999). 3D score plots of NNMF were obtained by projecting each pixel's NNMF score onto its pixel coordinates.

RESULTS AND DISCUSSION

The non-targeted nature of imaging MS led us to investigate whether it could be used to investigate the chemical and spatial extent of the disturbances that follow CSD, evoked in one hemisphere leaving the other contralateral hemisphere as an internal control. Seven CSD, spaced 5 min apart, were evoked in one hemisphere of C57Bl/6 mice, after which the animals were immediately sacrificed and the brains removed and flash frozen (< 1 min postmortem time).

MALDI Imaging MS is able to analyze different molecular classes using essentially the same technique but different sample preparation strategies, and in which the mass spectrometer is optimized for the mass range of the molecular class of interest. Figure 1 shows examples of metabolite, neuropeptide and protein imaging MS results obtained after CSD. The mean average mass spectrum, displaying which peaks were detected, and a selection of MS images is displayed for each molecular class. CSD was invoked in the right hemisphere of each tissue section.

Each peak in the average mass spectra corresponds to a distinct biomolecular ion, the spatial distribution of which is contained in the imaging MS datasets. It is evident that a large number of metabolite, peptide and protein ions were obtained, and that marked changes in the distributions of specific metabolites and peptides were present in the ipsilateral hemisphere in which CSD was induced. Contralateral differences were evident in cortical structures, but less so in the subcortical structures far away from the cortex in any of the datasets, e.g., the peptide ion detected at m/z 1635. Figure 2 shows 3D MS images of proteins following CSD, as well as a schematic of the alignment procedure. Coronal tissue sections spaced 200 μm through the middle region of the cortex of the mouse brain, in between the sites of CSD induction and CSD recording - were analyzed. The placement of the thin tissue sections on the conductive glass slides for the MALDI imaging MS experiments leads to significant variability in placement and orientation. The tissues were first approximately aligned by aligning their midpoints and rotating the tissues into a common orientation. The relative tissue positions were then fine adjusted on the basis of their anatomical structure (as revealed by H&E

staining). The offsets and rotations applied to each tissue section was then transposed into the imaging MS coordinate system and used to create the 3D imaging MS datasets.

The 3D imaging MS data demonstrate the high reproducibility of the MALDI imaging MS protocol. The visualization of 3D datasets has been performed using a thresholded surface rendering function – if the intensity of the peak is below threshold then that voxel (3D pixel) is set to transparent; if the intensity is above threshold then the intensity is set to 1. A smoothed surface is then fitted to the voxels containing the peak of interest. The advantage of such a surface rendering is that it efficiently depicts the 3D locations containing the MS peak, the disadvantage is that it does not communicate the relative intensity of the MS peak within the surface enclosed area. Caprioli and coworkers have used single color gradients (Andersson et al 2008) and heat maps (Sinha et al 2008) to depict relative concentrations in relatively simple 3D structures, but these are less suited to the highly structured surfaces such as those shown in Figure 2.

3D imaging MS datasets consist of a many individual 2D imaging MS datasets (of tissue sections), each of which contains a very large number of mass spectra and discrete MS peaks. It was found that even a rudimentary contralateral comparison of the CSD hemisphere relative to the control hemisphere was complicated by the large number of peaks and tissue sections, making it difficult to visualize specific molecular features. Instead the multivariate factorization technique non-negative matrix factorization (Lee & Seung 1999) (NNMF) was used to summarize the latent molecular classes, each defined by specific MS profiles, which were found in the 3D imaging MS dataset, as shown in Figure 3. NNMF of the 3D protein imaging MS dataset distinguished multiple distinct regions of the mouse brain but differences between the ipsi- and contralateral side were not detected.

The NNMF calculation was performed using an NVidia Tesla C2070 Graphical Processing Unit to provide the high processing speed necessary to analyze these very large datasets (Jones et al 2012). The corrected Akaike information criterion was used to estimate the number of classes present in the dataset, as has been reported previously (Hanselmann et al 2008). Increasing the number of factors could generate latent class images that included apparent contralateral differences but were prone to over-fitting of the data; the Akaike information criterion guards against over-fitting of the data by increasing the cost of models with increased parameter space – the NNMF factor analysis that led to contralateral differences were significantly disfavored by the Akaike information criterion.

Figure 4 shows 3D imaging MSI images of neuropeptides obtained from an animal after CSD. The peptide at m/z 2273 shows no ipsi vs contralateral differences in the cortex, and only very minor differences in subcortical regions. In contrast the peptide at m/z 2220 shows differences between the ipsi- and contralateral sides in the cortex.

The triggering of CSD waves involves a surgical procedure; a cotton ball soaked in 1 M KCl is applied topically on the dura overlying the visual cortex through a cranial window, followed by a wash with NaCl. CSDs were monitored using a microelectrode placed in the frontal cortex. To differentiate changes due to the surgical procedure, but not CSD, 3D analysis of SHAM-operated

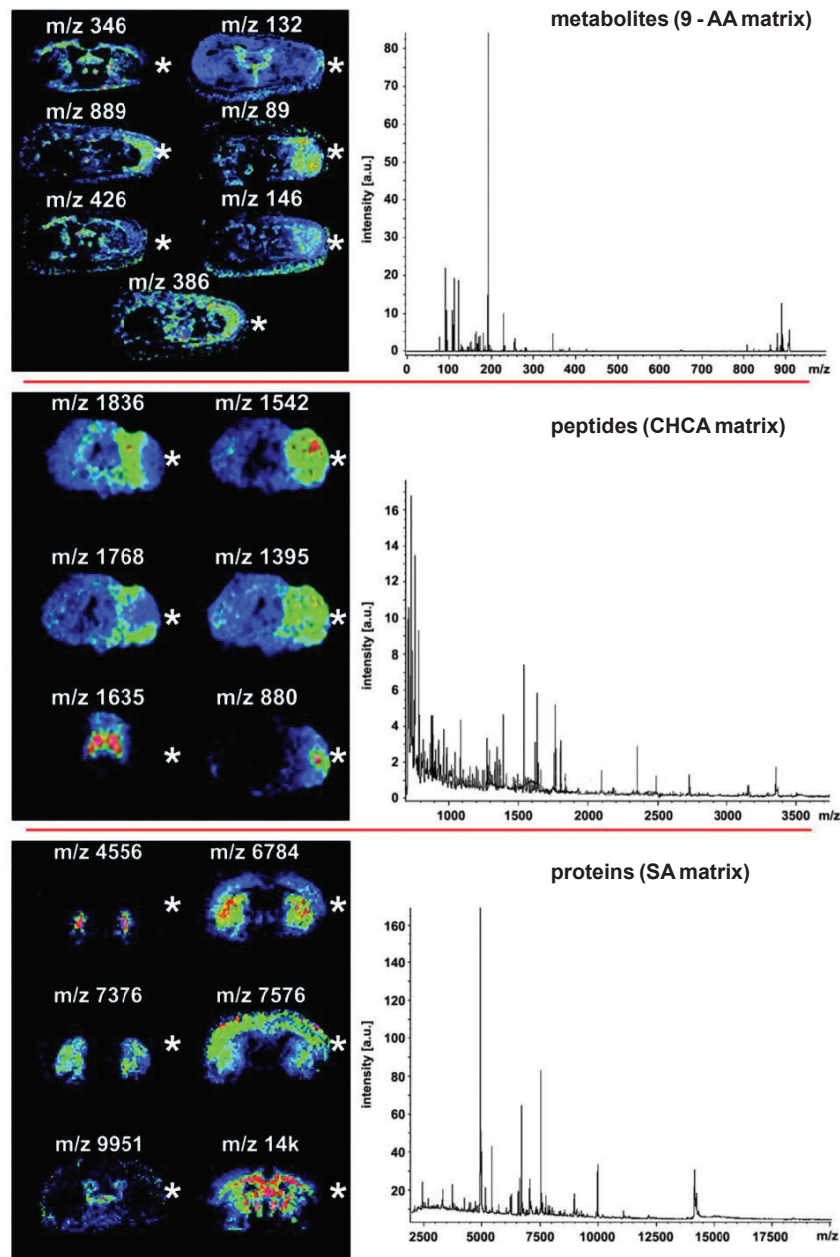


Figure 1. MALDI imaging MS datasets of metabolites (top), peptides (middle) and proteins (bottom) after cortical spreading depression in wild type mice. Figures on the left show example images with the 2D distribution of different metabolites, peptides or proteins. * indicates CSD side. The metabolite dataset was recorded in negative ion mode with a reflectron ToF and using 9-aminoacridine as the matrix. The peptide dataset was recorded in positive ion mode with a reflectron ToF and using α -cyano-4-hydroxycinnamic acid as the matrix. The protein dataset was recorded in positive ion mode in linear ToF mode using sinapinic acid as the matrix. CSD was invoked in the right hemisphere of each tissue. Contralateral differences are evident in both the metabolite and peptide datasets but not in the protein dataset. Assignments of the metabolite peaks based on previous MALDI imaging MS of metabolites using the same matrix [36,42]:- m/z 89, lactate; m/z 132, aspartate; m/z 146, glutamate; m/z 346, adenosine monophosphate; m/z 386, dCDP; m/z 426 adenosine diphosphate.

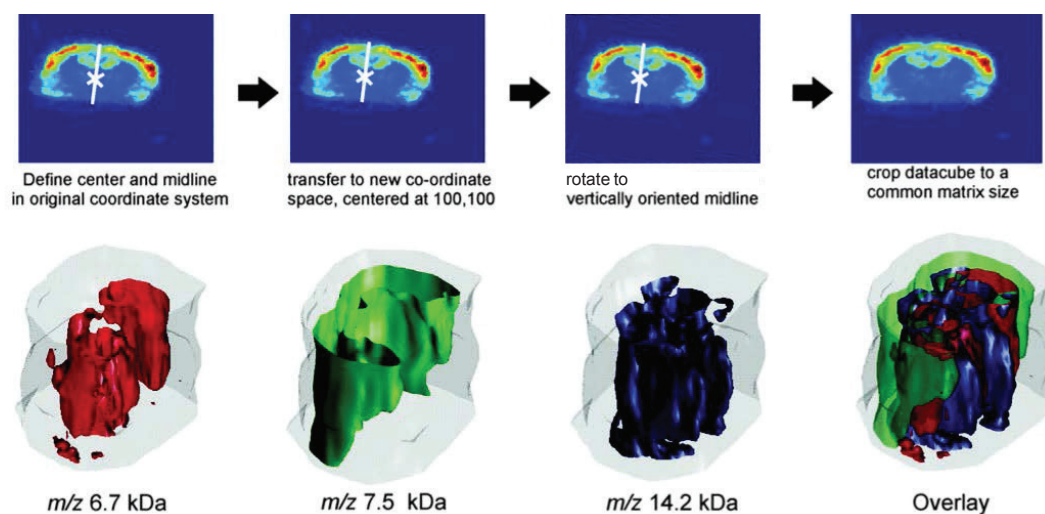


Figure 2. Top row: preliminary alignment procedure for generation of 3D imaging MS datasets. Each tissue is first centered and then aligned to a common orientation. Fine alignment of the tissues is then performed on the basis of their anatomical structure, and the final transformation applied to each tissue's imaging MS dataset. Bottom row. Examples of 3D protein imaging MS datasets of a wild-type mouse brain following CSD.

animals was also performed. The SHAM animals underwent an identical procedure except KCl was replaced with NaCl, which does not induce CSD. Figure 5 shows examples of 3D distributions that are unchanged between sham and CSD, as well as peptides that were detected at higher levels only in the CSD hemisphere of the KCl-treated animal.

Changes in protein content have previously been detected following CSD (Kawahara et al 1999, Obrenovitcha et al 2002) but have involved longer intervals between CSD induction and animal sacrifice, thus allowing sufficient time for the expression of new proteins. The very short time delay (45-60 min) in the current experiments limits significant expression of new proteins in response to CSD. The changes after CSD observed for neuropeptides are consistent with the vesicular release of neuropeptides from (sub)cellular vesicles and presynaptic terminals after depolarization of neuronal membranes during initiation of CSD.

These results represent a proof-of-concept study that forms the foundation for a larger study on the consequences of CSD, for instance in relation to migraine, which will involve multiple animals in each group and multiple genotypes. The proof of concept is essential as all previous imaging MS studies have focused on biomolecular changes associated with either distinct histopathological entities or with known, irreversible changes e.g., cell death in the CA3 layer of the hippocampus following kainate induced seizures (Sugiura et al 2011). The CSD results represent the first example of imaging MS being used to reveal transient biomolecular changes. The 3D analysis demonstrates the high reproducibility that can be obtained, within a single animal, and the recent biomarker discovery experiments provide ample evidence of the inter-patient/animal reproducibility that may be attained

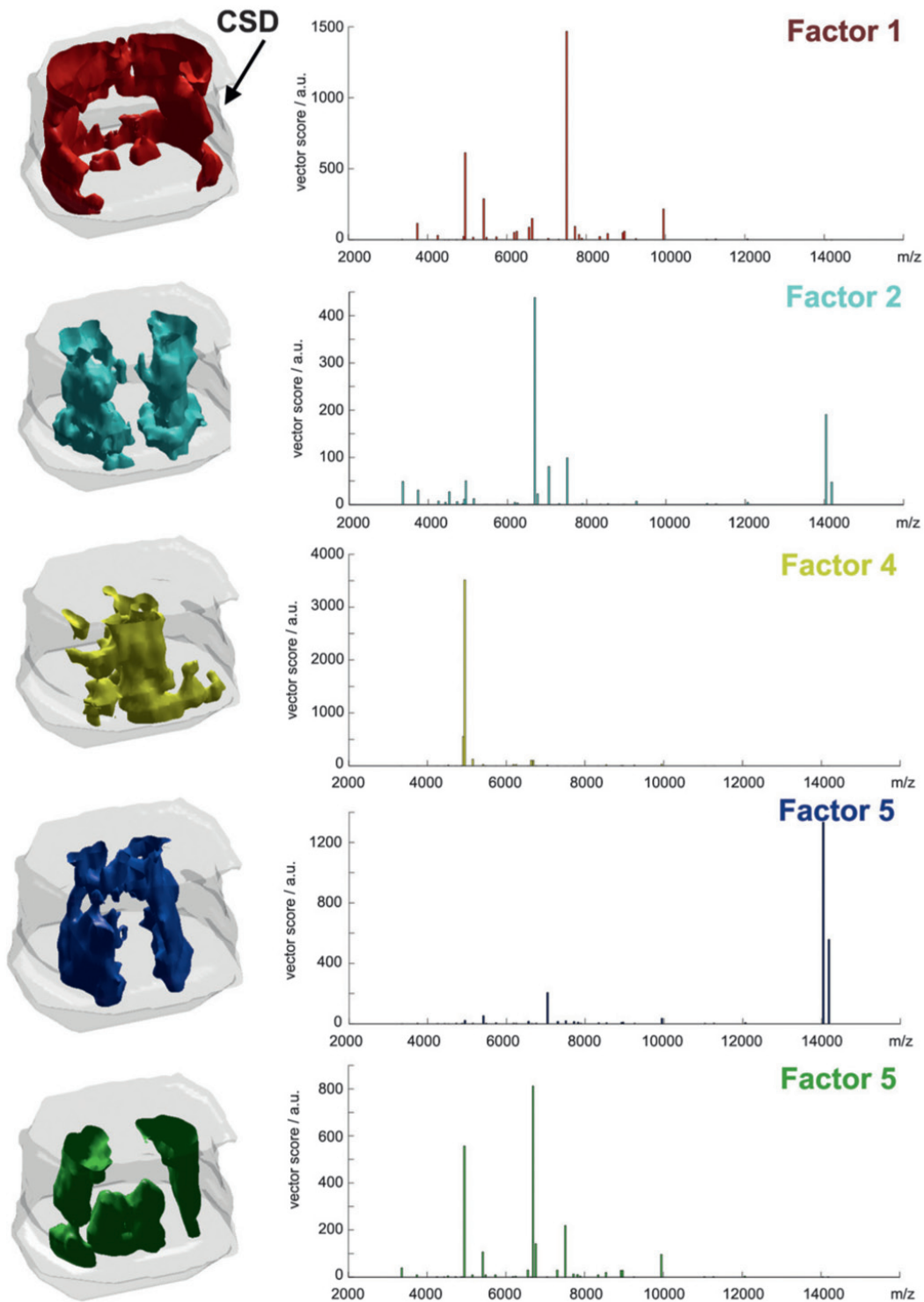


Figure 3. Non-negative matrix factorization of the 3D protein imaging MS dataset of a mouse brain following CSD did not reveal cortical contralateral differences. Note: factor 3 revealed background signals of the target slide and so is not included here.

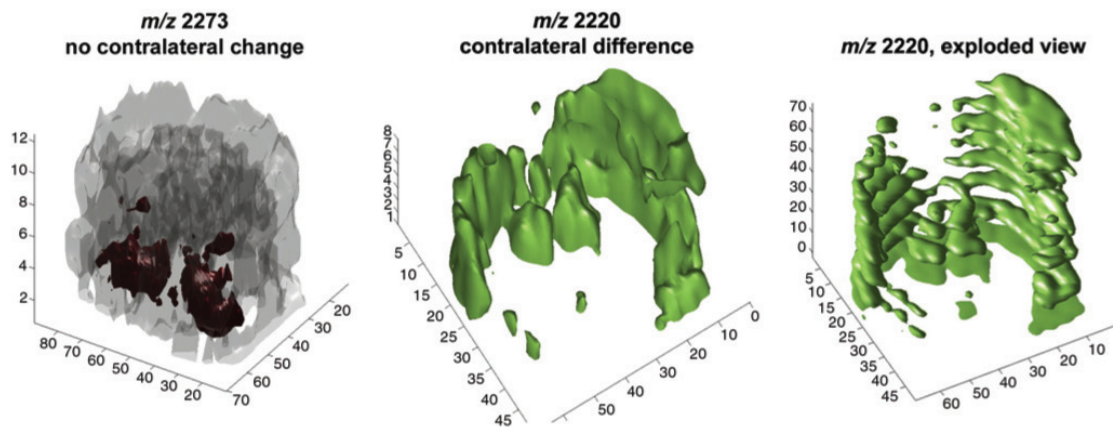


Figure 4. Example of 3D peptide imaging MS datasets of a wild-type mouse brain following CSD. The peptide ion detected at m/z 2273 was primarily detected far away from the cortical spreading depression, consequently no contralateral differences are observed. In contrast the peptide ion detected at m/z 2220 is located in the cortex and displays significant contralateral differences following CSD. A blown-up 3D figure is also provides to display the results of each tissue section's individual imaging MS dataset.

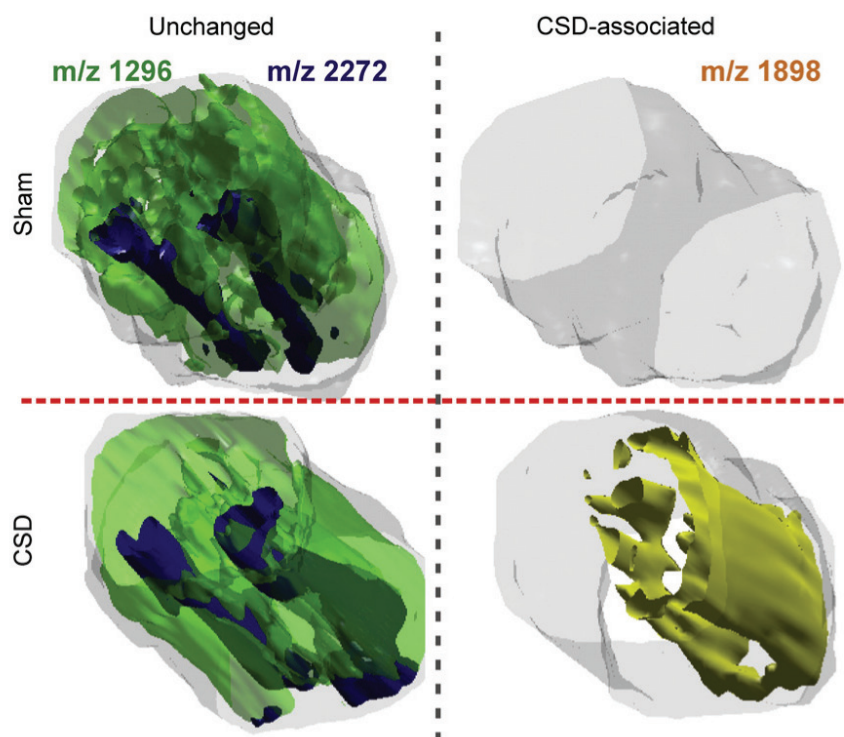


Figure 5. Exclusion matrix of 3D peptide imaging MS data for highlighting peptide ions related to CDS. Left hand side; peptide ions not specific to CSD are observed in the sham and CSD operated mouse, and do not exhibit contralateral differences. Right hand side; CSD associated peptide ions are detected at higher levels in the CSD animal and CSD hemisphere.

(Meding et al 2012).

Since its introduction by Crecelius et al. (Crecelius et al 2005) 3D MALDI imaging MS experiments have grown in popularity, but at a much slower pace than 2D imaging MS experiments owing to the much greater demands placed on experimental reproducibility and data handling (Seeley & Caprioli 2012). Andersson et al. have published an experimental workflow (Andersson et al 2008), and alignment procedures have been reported to combine 3D imaging MS with 3D magnetic resonance imaging (Sinha et al 2008) and 3D optical imaging techniques (Chughtai et al 2012). These studies have focused on reproducing the histo-architectures of the tissues, such as mouse or crustacean brain architecture (Andersson et al 2008, Crecelius et al 2005, Chen et al 2009) and localizing tumors (Sinha et al 2008).

CONCLUSION

The results reported here represent the first 3D MALDI imaging MS that explicitly targets biomolecular changes that are not associated with distinct morphological features, and which includes the first multivariate analysis of 3D MALDI imaging MS datasets. The 2D and 3D imaging MS investigations revealed metabolite and peptide disturbances immediately following CSD in wild-type mice, but the analogous protein datasets did not show similar profound changes. The short time between CSD and animal sacrifice is insufficient for appreciable protein synthesis in response to CSD; metabolic pathways are able to respond much more rapidly to changing conditions and increased neuropeptide signals are consistent with peptide release from (sub)cellular vesicles following depolarization associated with CSD. These results indicate that the molecular histology capabilities of MALDI imaging MS may be used to reveal spatial extent of transient biomolecular disturbances that do not result in morphological change.

ACKNOWLEDGEMENTS

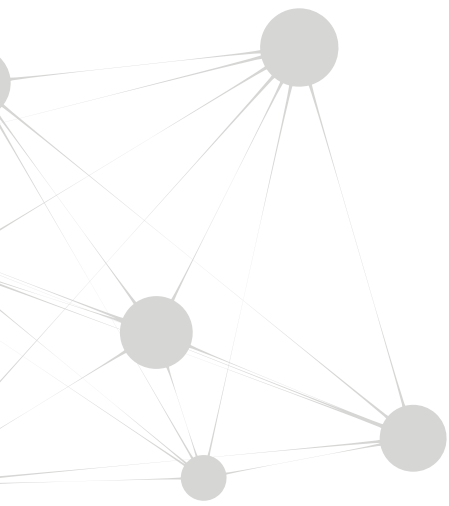
This work is financially supported by NWO Horizon project 93511027, the ICT consortium COMMIT project “e-biobanking with Imaging”, the Cyttron II project “Imaging Mass Spectrometry”, the Vici award 918.56.602, and the Center of Medical System Biology (CMSB) established by the Netherlands Genomic Initiative/Netherlands Organisation for Scientific Research (NGI/NOW) and Community.

REFERENCES

- Andersson M, Groseclose MR, Deutch AY, Caprioli RM. 2008. Imaging mass spectrometry of proteins and peptides: 3D volume reconstruction. *Nat. Methods* 5:101-08
- Cazares LH, Troyer D, Mendrinós S, Lance RA, Nyalwidhe JO, et al. 2009. Imaging Mass Spectrometry of a Specific Fragment of Mitogen-Activated Protein Kinase/Extracellular Signal-Regulated Kinase Kinase 2 Discriminates Cancer from Uninvolved Prostate Tissue. *Clin. Cancer Res.* 15:5541-51
- Chaurand P, Sanders ME, Jensen RA, Caprioli RM. 2004. Proteomics in diagnostic pathology-Profilng and imaging proteins directly in tissue sections. *Am. J. Pathol.* 165:1057-68
- Chen R, Hui L, Sturm RM, Li L. 2009. Three dimensional mapping of neuropeptides and lipids in crustacean brain by mass spectral imaging. *J. Am. Soc. Mass Spectrom.* 20:1068-77
- Chughtai K, Jiang L, Greenwood TR, Klinkert I, Amstalden van Hove ER, et al. 2012. Fiducial markers for combined 3-dimensional mass spectrometric and optical tissue imaging. *Anal. Chem.* 84:1817-23
- Cornett DS, Reyzer ML, Chaurand P, Caprioli RM. 2007. MALDI imaging mass spectrometry: molecular snapshots of biochemical systems. *Nat. Methods* 4:828-33
- Crecelius AC, Cornett DS, Caprioli RM, Williams B, Dawant BM, Bodenheimer B. 2005. Three-Dimensional Visualization of Protein Expression in Mouse Brain Structures Using Imaging Mass Spectrometry. *J. Am. Soc. Mass Spectrom.* 16:1093-99
- Deininger S-O, Ebert MP, Fütterer A, Gerhard M, Röcken C. 2008. MALDI Imaging Combined with Hierarchical Clustering as a New Tool for the Interpretation of Complex Human Cancers. *J. Proteome Res.* 7:5230-36
- Eikermann-Haerter K, Yuzawa I, Qin T, Wang Y, Baek K, et al. 2011. Enhanced subcortical spreading depression in familial hemiplegic migraine type 1 mutant mice. *J. Neurosci.* 31:5755-63
- Fabricius M, Jensen LH, Lauritzen M. 1993. Microdialysis of interstitial amino acids during spreading depression and anoxic depolarization in rat neocortex. *Brain Res.* 28:61-69
- Hanrieder J, Ljungdahl A, Fälth M, Mammo SE, Bergquist J, Andersson M. 2011. L-DOPA-induced dyskinesia is associated with regional increase of striatal dynorphin peptides as elucidated by imaging mass spectrometry. *Mol. Cell. Proteomics* 10(10):M111.009308
- Hanselmann M, Kirchner M, Renard BY, Amstalden ER, Glunde K, et al. 2008. Concise Representation of Mass Spectrometry Images by Probabilistic Latent Semantic Analysis. *Anal. Chem.* 80:9649-58
- Jones EA, van Remoortere A, van Zeijl RJM, Hogendoorn PCW, Boveé JVMG, et al. 2011. Multiple Statistical Analysis Techniques Corroborate Intratumor Heterogeneity in Imaging Mass Spectrometry Datasets of Myxofibrosarcoma. *PLoS ONE* 6:e24913
- Jones EA, Zeijl RJMv, Deelder AM, Andrén PE, Wolters L, McDonnell LA. 2012. High Speed Data

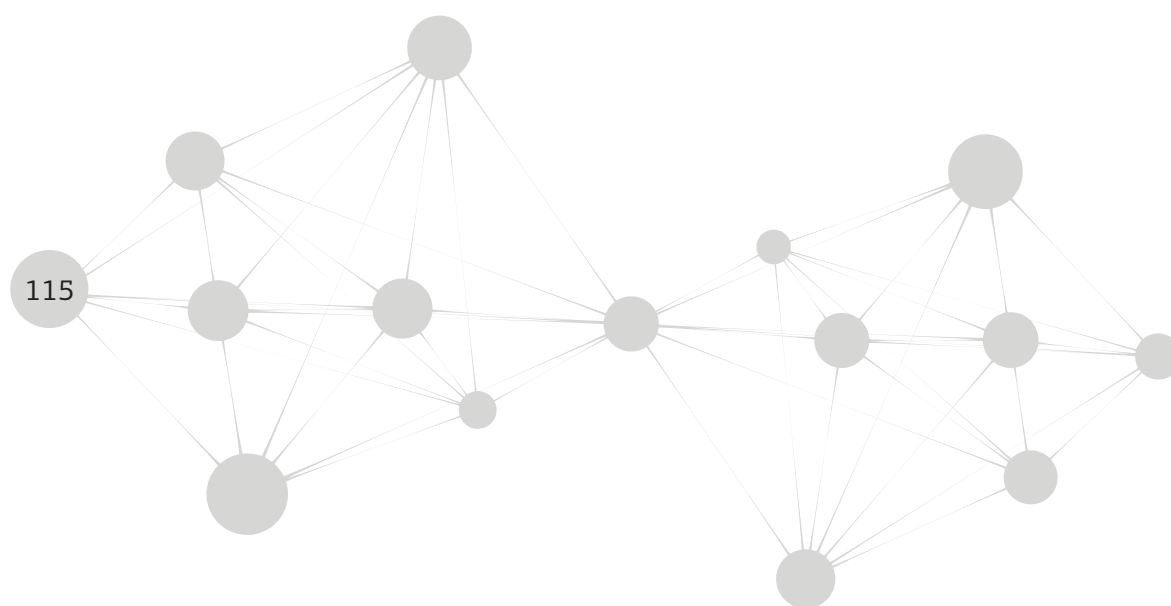
- Processing for Imaging MS-Based Molecular Histology Using Graphical Processing Units. *J. Am. Soc. Mass Spectrom.* 23:745-52
- Kang S, Shim HS, Lee JS, Kim DS, Kim HY, et al. 2010. Molecular Proteomics Imaging of Tumor Interfaces by Mass Spectrometry. *J. Proteome Res.* 9:1157-64
- Kawahara N, Ruetzler CA, Mies G, Klatzo I. 1999. Cortical spreading depression increases protein synthesis and upregulates basic fibroblast growth factor. *Exp. Neurol.* 158:27-36
- Kors E, Terwindt G, Vermeulen F, Fitzsimons R, Jardine P, et al. 2001. Delayed cerebral edema and fatal coma after minor head trauma: role of the CACNA1A calcium channel subunit gene and relationship with familial hemiplegic migraine. *Ann. Neurol.* 49:753-60
- Lauritzen M, Hansen AJ, Kronborg D, Wieloch T. 1990. Cortical Spreading Depression is Associated with Arachidonic-Acid Accumulation and Preservation of Energy-Charge. *J. Cereb. Blood Flow Metab.* 10:115-22
- Leão AAP. 1944. Pial circulation and spreading depression of activity in the cerebral cortex. *J. Neurophysiol.* 7:391-96
- Lee DD, Seung HS. 1999. Learning the Parts of Objects by Non-Negative Matrix Factorization. *Nature* 401:788-91
- Mathur BN, Caprioli RM, Deutch AY. 2009. Proteomic Analysis Illuminates a Novel Structural Definition of the Claustrum and Insula. *Cereb. Cortex* 19:2372-79
- McDonnell LA, Heeren RMA. 2007. Imaging Mass Spectrometry. *Mass Spectrom. Rev.* 26:606-43
- McDonnell LA, van Remoortere A, de Velde N, van Zeijl RJM, Deelder A. 2010a. Imaging Mass Spectrometry Data Reduction: Automated Feature Identification and Extraction. *J. Am. Soc. Mass Spectrom.* 21:1969-78
- McDonnell LA, Willems SM, Corthals GL, van Remoortere A, van Zeijl RJM, Deelder AM. 2010b. Imaging Mass Spectrometry in Cancer Research: Past Experiences and Future Possibilities. *J. Proteomics* 73:1921-44
- Meding S, Nitsche U, Balluff B, Elsner M, Rauser S, et al. 2012. Tumor Classification of Six Common Cancer Types Based on Proteomic Profiling by MALDI Imaging. *J. Proteome Res.* 11:1996-2003
- Nilsson A, Sköld K, Sjögren B, Svensson M, Pierson J, et al. 2007. Increased Striatal mRNA and Protein Levels of the Immunophilin FKBP-12 in Experimental Parkinson's Disease and Identification of FKBP-12-Binding Proteins. *J. Proteom. Res.* 6:3952-61
- Ohrenovitcha TP, Godukhina OV, Chazotb PL. 2002. Repetitive spreading depression induces nestin protein expression in the cortex of rats and mice. Is this upregulation initiated by N-methyl-d-aspartate receptors? *Neurosci. Lett.* 320:161-63
- Ophoff R, Terwindt G, Vergouwe M, van Eijk R, Oefner P, et al. 1996. Familial hemiplegic migraine and episodic ataxia type-2 are caused by mutations in the Ca²⁺ channel gene CACNL1A4. *Cell* 87:543-52

- Oppenheimer SR, Mi D, Sanders ME, Caprioli RM. 2010. Molecular Analysis of Tumor Margins by MALDI Mass Spectrometry in Renal Carcinoma. *J. Proteome Res.* 9:2182-90
- Rausser S, Deininger S-O, Suckau D, Höfler H, Walch A. 2010. Approaching MALDI Molecular Imaging for Clinical Proteomic Research: Current State and Fields of Application. *Expert Rev. Proteomic* 7:927-41
- Scheller D, Kolb J, Peters U, Tegtmeier F. 1996. The measurement of extracellular inorganic phosphate gives a more reliable indication for severe impairment of cerebral cell function and cell death than the measurement of extracellular lactate. *Acta neurochir. Suppl.* 67:28-30
- Schwamborn K, Caprioli RM. 2010. Molecular imaging by mass spectrometry - looking beyond classical histology. *Nat. Rev. Cancer* 10:639-46
- Schwamborn K, Krieg RC, Reska M, Jakse G, Knuechel R, Wellmann A. 2007. Identifying Prostate Carcinoma by MALDI-Imaging. *Int. J. Mol. Med.* 20:155-59
- Seeley EH, Caprioli RM. 2012. 3D Imaging by Mass Spectrometry: A New Frontier. *Anal. Chem.* 84:2105-10
- Sinha TK, Khatib-Shahidi S, Yankeelov TE, Mapara K, Ehtesham M, et al. 2008. Integrating spatially resolved three dimensional MALDI IMS with in vivo magnetic resonance imaging. *Nat. Methods* 5:57-59
- Sköld K, Svensson M, Nilsson A, Zhang X, Nydahl K, et al. 2006. Decreased striatal levels of PEP-19 following MPTP lesion in the mouse. *J. Proteom. Res.* 5:262-69
- Somjen GG. 2001. Mechanisms of spreading depression and hypoxic spreading depression-like depolarization. *Physiol Rev.* 81:1065-96
- Sugiura Y, Taguchi R, Setou M. 2011. Visualization of Spatiotemporal Energy Dynamics of Hippocampal Neurons by Mass Spectrometry during a Kainate-Induced Seizure. *PLoS ONE* 6:e17952
- van den Maagdenberg A, Pietrobon D, Pizzorusso T, Kaja S, Broos LAM, et al. 2004. A Ca_v1a knockin migraine mouse model with increased susceptibility to cortical spreading depression. *Neuron* 41:701-10
- van den Maagdenberg AMJM, Pizzorusso T, Kaja S, Terpolilli N, Shapovalova M, et al. 2010. High Cortical Spreading Depression Susceptibility and Migraine-Associated Symptoms in Ca_v1.1 S218L Mice. *Ann. Neurol.* 67:85-98
- Wahl M, Schilling L, Parsons A, Kaumann A. 1994. Involvement of calcitonin gene-related peptide (CGRP) and nitric oxide (NO) in the pial artery dilatation elicited by cortical spreading depression. *Brain Res.* 637:204-10
- Willems SM, van Remoortere A, van Zeijl R, Deelder AM, McDonnell LA, Hogendoorn PCW. 2010. Imaging Mass Spectrometry of Myxoid Sarcomas Identifies Proteins and Lipids Specific to Tumor Type and Grade, and Reveals Biochemical Intratumor Heterogeneity. *J. Pathol.* 222:400-09



Chapter 6

Large-scale mass spectrometry imaging investigation of consequences of cortical spreading depression in a transgenic mouse model of migraine



Ricardo J. Carreira^{1,*}, Reinald Shyti^{2,*}, Benjamin Balluff¹, Walid M. Abdelmoula³, Sandra H. van Heiningen², Rene J. van Zeijl¹, Jouke Dijkstra³, Michel D. Ferrari⁴, Else A. Tolner⁴, Liam A. McDonnell^{1,5,‡}, Arn M.J.M. van den Maagdenberg^{2,4,‡}

¹ Center for Proteomics and Metabolomics, Leiden University Medical Center, Leiden, Netherlands

² Department of Human Genetics, Leiden University Medical Center, Leiden, Netherlands

³ Division of Image Processing, Department of Radiology, Leiden University Medical Center, Leiden, Netherlands

⁴ Department of Neurology, Leiden University Medical Center, Leiden, Netherlands

⁵ Fondazione Pisana per la Scienza ONLUS, Pisa, Italy

^{*,‡}equal contributions

ABSTRACT

Cortical spreading depression (CSD) is the electrophysiological correlate of migraine aura. Transgenic mice carrying the R192Q missense mutation in the *Cacnala* gene, which in patients causes familial hemiplegic migraine type 1 (FHM1), exhibit increased propensity to CSD. Herein, mass spectrometry imaging (MSI) was applied for the first time to an animal cohort of transgenic and wild type mice to study the biomolecular changes following CSD in the brain. Ninety six coronal brain sections from 32 mice were analyzed by MALDI-MSI. All MSI datasets were registered to the Allen Brain Atlas reference atlas of the mouse brain so that the molecular signatures of distinct brain regions could be compared. A number of metabolites and peptides showed substantial changes in the brain associated with CSD. Among those, different mass spectral features showed significant (Student's t-test, $p < 0.05$) changes in the cortex, 146 and 377 Da; and in the thalamus, 1820 and 1834 Da, of the CSD-affected hemisphere of FHM1 R192Q mice. Our findings reveal CSD-and genotype-specific molecular changes in the brain of FHM1 transgenic mice that may further our understanding about the role of CSD in migraine pathophysiology. The results also demonstrate the utility of aligning MSI datasets to a common reference atlas for large-scale MSI investigations.

INTRODUCTION

Matrix-assisted laser desorption/ionization (MALDI) mass spectrometry imaging (MSI) is a label-free technique capable of analyzing hundreds of biomolecular ions directly from tissue in a spatially correlated manner (Caprioli et al 1997). Main factors contributing to the increasing popularity of this technology include the ability to (1) analyze a large range of molecular classes (proteins, peptides, lipids, metabolites, pharmaceuticals); (2) reveal disease-related biomolecular changes in highly localized regions; and (3) unravel changes that are invisible to established histopathological methods (McDonnell & Heeren 2007, McDonnell et al 2012, Norris & Caprioli 2013).

MSI has been applied to a multitude of tissues from various tumor tissues (Balluff et al 2011, McDonnell et al 2010) to plant tissues (Kaspar et al 2011), but rodent brain (Henrieder et al 2013, Shariatgorji et al 2014) is still the most frequently analyzed tissue type because of its widespread availability and use in neurological research (Hafezparast et al 2002). For instance, MALDI-MSI has been used to visualize spatiotemporal disturbances in rodent models of seizure (Sugiura et al 2011), stroke (Miura et al 2010), Alzheimer's disease (Rohner et al 2005, Stoeckli et al 2006) and Parkinson's disease (Ljungdahl et al 2011, Nilsson et al 2007, Pierson et al 2004). These studies demonstrate the potential of MSI for neurological research, and which have been further validated by studies using small animal cohorts (Henrieder et al 2013). The application of MSI to preclinical investigations of neurological disorders requires considerable multidisciplinary capabilities: MSI, statistics and knowledge of brain anatomy. The latter aspect is exacerbated by the high degree of variation in brain region size that exists between animals (Hager et al 2012) and the variability introduced during tissue sectioning and mounting. We recently demonstrated how MSI data could be automatically aligned to the Allen Brain Atlas, which allows the analyst to ensure all tissue sections of animals are obtained from a similar region of the mouse brain and to extract the mass spectral signatures from identical brain regions (Abdelmoula et al 2014). Here we demonstrate how this registration pipeline enables larger-scale preclinical investigations of neurological disorders. This first demonstration of such a cohort studied and analyzed by MSI concerns migraine.

Migraine is a common, severe episodic brain disorder that is characterized by attacks of severe unilateral throbbing headache associated with nausea, vomiting, photo- and phonophobia (Goadsby et al 2002, ICHD 2004). An aura, which consists of transient neurological symptoms, including visual and sensory disturbances, can accompany a migraine attack in one-third of patients. The aura is caused by cortical spreading depression (CSD), a slow, self-propagating wave of neuronal and glial cell depolarization in the cerebral cortex of one hemisphere followed by neuronal depression (Hadjikhani et al 2001, Lauritzen 1994, Pietrobon & Moskowitz 2013). CSD causes a temporary dramatic failure of brain homeostasis, efflux of neurotransmitters, and changes in metabolism. Several metabolites, such as labile phosphate compounds (ATP, ADP, AMP, their cyclic analogues, cGMP, and phosphocreatine) and glycolytic metabolites (lactate, pyruvate, glucose and glycogen) have been associated with CSD (Selman et al 2004).

In 2012 Jones et al. (Jones et al 2012) reported a proof-of-concept MALDI-MSI investigation of the biomolecular changes in C57BL/6J wild-type (WT) mouse brain following CSD. The study included 2D- and 3D-MSI datasets, including an exclusion matrix to highlight apparent CSD-related changes, but omitted any form of statistical analysis because of the small number of animals involved in the study. Accordingly, the results obtained provided limited information regarding the biological aspects and changes associated with CSD. Here we report, for the first time, the application of MSI to a large scale animal cohort of a neurological disease, in particular CSD as the neurobiological correlate of the migraine aura. To this end, we make use of a relevant mouse model of migraine, (i.e., knock-in transgenic mice carrying the pathogenic human R192Q missense mutation in the *Cacna1a* gene that encodes the α_1 subunit of voltage-gated neuronal $\text{Ca}_v2.1 \text{ Ca}^{2+}$ channels (Ferrari et al 2015, van den Maagdenberg et al 2004). $\text{Ca}_v2.1 \text{ Ca}^{2+}$ channels with a R192Q-mutated α_1 subunit cause familial hemiplegic migraine type 1 (FHM1) (Ophoff et al 1996), a monogenic subtype of migraine with aura characterized by a prominent transient hemiparesis during the aura (ICHD 2004). FHM1 R192Q mice exhibit an increased propensity to CSD, most likely because of an enhanced glutamatergic neurotransmission (Eikermann-Haerter et al 2009, Ferrari et al 2015, Tottene et al 2009, van den Maagdenberg et al 2004). In addition, unlike in WT mice, CSD waves can reach subcortical areas in R192Q mice, which correlate with the clinical phenotype (Eikermann-Haerter et al 2011). We hypothesized that CSD could induce the expression of different biomolecular profiles in the brains of R192Q mice compared with wild-type. We measured and compared the biomolecular profiles of both mouse strains at specific cortical and subcortical brain regions and were able to show different consequences of CSD on the brains of R192Q and wild-type mice.

MATERIALS AND METHODS

Animals

Male 2-to 4-month-old transgenic FHM1 R192Q mice (carrying the human pathogenic missense mutation R192Q) and corresponding non-transgenic wild-type (WT) mice were used. Transgenic mice were generated by introducing the human pathogenic mutation in the mouse *Cacna1a* gene using a gene targeting approach, as described in (van den Maagdenberg et al 2004). All mice were kept in a normal 12:12 light/dark regime and food and water were available *ad libitum*. The 32 animals used in this study were divided into different groups according to the experimental conditions: WT-Naïve (5 animals); WT-Sham (6 animals); WT-CSD (5 animals); R192Q-Naïve (5 animals); R192Q-Sham (6 animals); R192Q-CSD (5 animals). All experiments were approved by the Animal Experiment Ethics Committee of Leiden University Medical Center.

CSD experiments

CSD experiments were performed as previously described (Jones et al 2012). In brief, the mice were anesthetized with 4% isoflurane in pressurized air (21% O_2 and 79% N_2) and mounted on a stereotactic frame (David Kopf, Tujunga, CA, USA); 1.5% isoflurane was used for maintenance of

the anesthesia. A midline incision was made to expose the skull. Two burr holes were drilled over the following coordinates (from bregma): 0.5 mm anterior, 2 mm lateral for DC recordings and 3.5 mm posterior, 2 mm lateral for KCl or NaCl application. Seven CSDs were induced by applying a cotton ball soaked in 1M KCl (CSD) or NaCl (Sham) for 30 sec followed by extensive saline washing. The interval between two successive applications was 5 min. DC-potential signals were measured with respect to an Ag/AgCl reference electrode placed subcutaneously in the neck and amplified 10x (Molecular Devices, Sunnyvale, CA, USA). The DC signal was low-pass filtered at 4 Hz and digitized at 100–200 Hz using PowerLab 16/30 hardware (AD Instruments, Inc., Colorado Springs, CO, USA). Data were recorded and analyzed off-line using LabChart Pro (AD Instruments).

Sample collection and tissue preparation

Following 7 CSD/Sham events the mice were decapitated 5 min after the last CSD/Sham event, the brains quickly removed (within < 2 min), immediately snap-frozen on powdered dry ice and stored at -80°C until further processing. Coronal tissue sections, 12- μ m thick, were cut at -12°C using a cryostat microtome (Leica Microsystems, Wetzlar, Germany), thaw-mounted onto poly-L-lysine coated indium-tin-oxide (ITO) glass slides (Bruker Daltonics, Bremen, Germany), and stored at -80°C. In order to exclude the effect of electrode insertion and KCl or NaCl application only sections from the middle part of the brain (posterior from bregma, in between locations -1.22 and -1.94 mm) were used for MSI analysis. For the selection of sections in this part of the brain, the brain was trimmed in 25 μ m slices and individual sections were visually inspected under a microscope and compared with the Paxinos Mouse Brain Atlas reference (3rd Edition; ISBN 978-0-12-374244-5) to judge their location along the anteroposterior axis, based on histological landmarks. Once the level corresponding to the location -1.22 posterior from Bregma was reached, 12 μ m thick coronal sections were collected for the MSI experiments. For each animal, consecutive tissue sections were collected on different ITO slides for the analysis of proteins, peptides and metabolites. Each ITO slide contained tissue sections from four animals. A semi-supervised block randomization was used to distribute the sections in a random way across and within slides while maximizing the group heterogeneity within a slide. This included the position of each sample on the MALDI slides and the measurement order within a slide – in order to minimize any potential sources of bias during MSI data acquisition (see Supplementary Information for the pseudo-code).

Mass spectrometry imaging

Tissue sections were collected from storage at -80°C and equilibrated to room temperature (RT, 23°C) for 30 min in a vacuum desiccator. The slides were prepared for MALDI-MSI according to the molecular class to be analyzed. For peptide and protein imaging the tissue sections were washed as follows: (1) dip in 70% ethanol for 30 sec; (2) dip in 96% ethanol for 30 sec; (3) five short dips in deionized water; (4) dip in 70% ethanol for 30 sec; (5) dip in 96% ethanol for 30 sec; and finally (6) dried in a vacuum desiccator for 15 min. No washing procedure was applied to the samples used for the analysis of metabolites. MALDI matrix was uniformly applied over the brain sections using

the SunCollect sprayer (SunChrom, Friedrichsdorf, Germany) according to the analyzed molecular class: sinapinic acid (SA; 5 mg/mL in 50% acetonitrile/ 0.3% TFA) was used for proteins; α -cyano-4-hydroxycinnamic acid (CHCA; 5 mg/mL in 50% acetonitrile/ 0.3% TFA) was used for peptides; and 9-aminoacridine (9AA; saturated solution in 70% methanol) was used for metabolites. MSI analyses of peptides (600 – 2000 Da) and metabolites (50 – 1000 Da) were performed using an UltrafleXtreme MALDI-TOF/TOF (Bruker Daltonics) in the reflectron positive (for peptides) or negative (for metabolites) ion mode with 100 μ m raster width, 500 laser shots per pixel. MSI of proteins (3000 – 20,000 Da) was performed in an Autoflex III MALDI-TOF (Bruker Daltonics) in the linear positive ion mode with 100 μ m raster width, 500 laser shots per pixel. Data acquisition, pre-processing and visualization were performed using the flex software package from Bruker Daltonics: flexImaging 3.0 was used for experiment definition; flexControl 3.4 was used for data acquisition; and flexAnalysis 3.4 was used for on-the-fly mass spectral processing – metabolite/peptide datasets were preprocessed using a Gauss smoothing algorithm (width 0.02 m/z , 2 cycles) and a TopHat baseline subtraction algorithm; protein MSI spectra were preprocessed identically except the parameters of the Gauss smoothing algorithm were adapted for the lower mass resolution (width 2 m/z , 4 cycles).

After the MSI experiments, the matrix was washed off with 70% ethanol and the tissue samples stained with cresyl violet (Nissl staining). High-resolution histological images were recorded using a Panoramic MIDI digital slide scanner (3D Histech, Budapest, Hungary).

Processing and reduction of MSI datasets

High-resolution histological images were co-registered to the MSI data with flexImaging using fiducial markers applied at defined positions on each ITO slide with water-based correction fluid (Tipp-Ex, Ecolutions, BIC, Clichy, France) before MSI analyses. A list of all mass spectra contained within each brain section was extracted into an XML file for further processing in MATLAB R2011a (MathWorks, Natick, MA, USA). The preprocessed mass spectra contained in the MSI datasets were then read into Matlab.

Metabolite datasets: the spectra were normalized to their total-ion-count (TIC) on a pixel-by-pixel basis and aligned on common peaks that are present in at least 85% of the samples. Peak picking and feature extraction was performed using the global base peak mass spectrum (McDonnell et al 2010). Briefly, this routine distills the original MSI data into an image cube containing the spatial distribution of every detected peak. Finally, a logarithmic-based variance-stabilizing transformation was applied to the peak intensities in order to reduce the impact of Poisson noise in the datasets (Keenan et al 2004, Veselkov et al 2014).

Peptide and protein datasets: except for the logarithmic transformation of peak intensities, which was not performed for these datasets, all processing steps were as described above including TIC normalization on a pixel-by-pixel basis, with minor modifications in the thresholds used for peak

picking to account for the different characteristics of the peptide and protein datasets.

Image processing and registration to the mouse Allen Brain Atlas

The reduced MSI datasets and the aligned histological images were registered to the mouse Allen Brain Atlas (ABA; <http://www.brain-map.org/>) using our recently developed pipeline (Abdelmoula et al 2014). In brief, the histological images are first preprocessed to reduce background noise and acquisition artifacts. Then the ABA corresponding histological image is selected based on the maximum cord length of the hippocampus. Image registration is performed by applying a rigid affine transformation (correct for translation, shearing, rotation and scaling), followed by non-linear registration based on a B-Spline transform (correct for local deformations). Finally, the transformation matrix used to register the sample and ABA histological images is applied to the respective MSI datasets.

Anatomy driven data analysis

The anatomic annotations contained in the ABA were used to define four anatomical regions of interest (ROI) in the MSI datasets: cortex (C), striatum (S), hippocampus (H) and thalamus (T). MS data were extracted from each ROI from every ABA-aligned MSI dataset for statistical analysis: (1) a non-paired Student's t-test was used for comparisons between independent groups; and (2) a paired Student's t-test was used for comparisons (left vs right hemispheres) within each independent group of animals. The Benjamini-Hochberg procedure was used to correct for multiple testing. All statistical analyses were done in R (R Foundation for Statistical Computing, Vienna, Austria) and Matlab, in which p-values < 0.05 were considered statistically significant.

RESULTS

CSD induction and MSI analysis

Seven CSD events were evoked each with a 5 min interval in the occipital cortex of WT and transgenic FHM1 R192Q mice; equivalent Sham experiments utilizing aqueous NaCl instead of aqueous KCl, which does not evoke a CSD, were performed in parallel so as to clearly differentiate CSD-related from non-CSD-related biomolecular changes. As shown in Table S1 (Supplementary Information), there were no significant differences between R192Q and WT mice regarding the CSD characteristics and time under anesthesia. All animals were sacrificed 5 min after the last CSD event and the brains were immediately removed and frozen on dry ice to limit post-mortem degradation effects. Previous studies have indicated that the analysis of metabolites can be significantly impaired by post-mortem degradation (Blatherwick et al 2013, Hattori et al 2010, Sugiura et al 2014). These results indicated that labile metabolites, such as AMP, ADP and ATP that act as energy reserves in the brain can be used as a measure of the post-mortem degradation effects. We measured the AMP/ATP ratios across the different mouse brains but found no correlation with the short post-mortem times of these experiments, which indicated that any variability associated with the isolation of the mouse brain had a negligible effect on the MSI data.

Alignment of MSI datasets to a single reference system

Preclinical studies typically compare a number of animals per test group to guard against the individual variation in any animal population. We have analyzed a total of 96 mouse brain sections from 32 animals from 16 R192Q and 16 WT mice. We registered all histological images and MSI datasets to the mouse brain reference atlas contained within the Allen Brain Atlas (Abdelmoula et al 2014) in order to (1) reduce the impact of variance attributable to differences in brain region size (Hager et al 2012); (2) check if all tissue sections came from a similar region of the brain; and (3) correct for any tissue-processing artifacts introduced during the experiment (e.g., folds, tears). The 96 brain sections were registered to just 3 of 132 different coronal sections present in the ABA reference atlas, corresponding to a tissue-section sampling accuracy between animals of 200 μm , and thus indicating we sampled similar regions of the mouse brain. The registration itself was performed with an accuracy of less than 30 μm , which is below the spatial resolution used for the MSI measurements (100 μm) (see Figure 5, reference Abdelmoula et al 2014). A scheme of the workflow is presented in Figure 1.

Anatomy based data-analysis

The distribution of proteins, peptides and metabolites after CSD and Sham operations was investigated across the whole brain and in four particular brain regions that are of relevance to migraine pathophysiology (Eikermann-Haerter et al 2011): cortex, striatum, hippocampus and thalamus. Electrophysiology measurements indicate that when induced in one hemisphere CSD does not cross to the other hemisphere (Eikermann-Haerter et al 2009, Somjen 2001), accordingly the left (unaffected) hemisphere was used as control for the CSD/Sham-affected right hemisphere.

Protein datasets

Comparison between right (CSD-affected) and left (control) hemispheres within the R192Q-CSD group revealed moderate differences in the distribution of m/z feature 11,302 Da and statistically significant differences in the distribution of m/z feature 11,344 Da ($p < 0.05$, Student's t-test), as shown in Figure 2. In both cases, the ion intensities are lower in the CSD-affected hemisphere (R). These changes were not observed in the WT and Sham groups. Poté et al. (Poté et al 2013) have previously identified the same molecular features as histone H4 and respective acetylated form while analyzing hepatocellular carcinoma. Although their experiment concerned human tissue samples, a Basic Local Alignment Search Tool (BLAST) search (in UniProt database) revealed 100% homology with murine histone H4.

Peptide datasets

Intra-group comparison between right (CSD-affected) and left (control) hemispheres showed significant differences occurring in the thalamus region for m/z features 1819.96 Da and 1833.96 Da ($p < 0.05$, Student's t-test) only in R192Q-CSD mice (Figure 3). A decrease in ion intensities was observed in the CSD-affected brain hemisphere in both cases. Similarly to the protein dataset, also these biomolecular features share the same spatial distribution and are separated by 14 Da, which

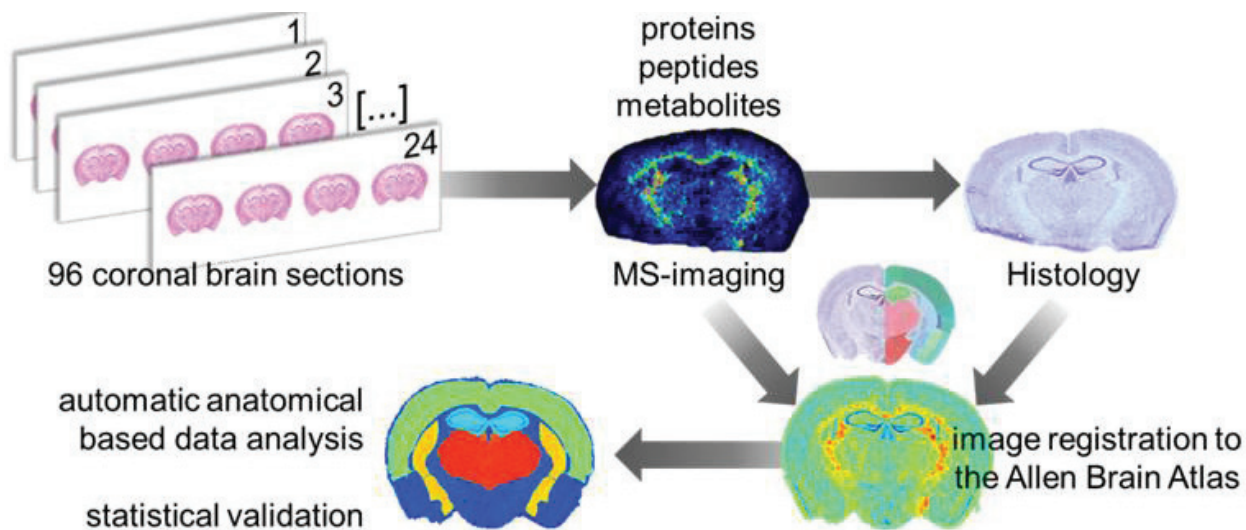


Figure 1. Schematic of workflow developed to analyze the effect of CSD in WT and R192Q mouse brains. Ninety-six coronal brain sections were obtained from a total of 32 mouse brains (3 consecutive sections per animal). Proteins, peptides and metabolites were independently analyzed by MSI using optimized sample treatment for each molecular class as described in the Materials and Methods section. Each section was stained with Nissl reagent after matrix removal and the MSI datasets, and histological images were aligned to the Allen Brain Atlas of mouse brain (Abdelmoula et al 2014). Automatic anatomical annotation of regions of interest allowed the extraction of MSI data from specific brain regions of interest and statistical analysis.

is compatible with a methylation post-translational modification. Moderate differences were also observed in the R192Q mouse brains after CSD, in particular m/z 1713.8 with increased expression in the cortex of the CSD-affected hemisphere, and m/z 1754.85 and its K^+ adduct m/z 1792.85 with decreased expression in the striatum of the CSD hemisphere. No significant biomolecular changes were observed for the Sham and Naïve mouse groups.

Metabolite datasets

Intra-group comparisons between control and CSD-affected hemispheres revealed differences associated with CSD in WT and R192Q mice (Supplementary Information, Figure S1). Biomolecular features present at 89.03 Da showed an increase in signal intensity in the CSD-affected hemisphere, whereas m/z features at 146.07 Da, 339.01 Da, 360.97 Da and 376.97 Da presented a decrease in intensity in the CSD-affected hemisphere. Interestingly, significant changes were only found in the distribution of 2 m/z features for R192Q-CSD mice ($p < 0.05$, Student's t-test), particularly m/z 146.07 Da and 376.97 Da as shown in Figure 4. In order to more confidently assign the m/z features observed we performed high-resolution MS analysis by MALDI Fourier transform ion cyclotron resonance (FTICR) directly from tissue. Accurate masses were then searched in the metabolite database METLIN revealing the presence of glutamate ($[M-H]^-$ 146.0459 Da), fructose 1,6-bisphosphate ($[M-H]^-$ 338.9888 Da) and fructose 1,6-bisphosphate K^+ adduct ($[M+K-2H]^+$ 376.9447 Da) among other isobaric species.

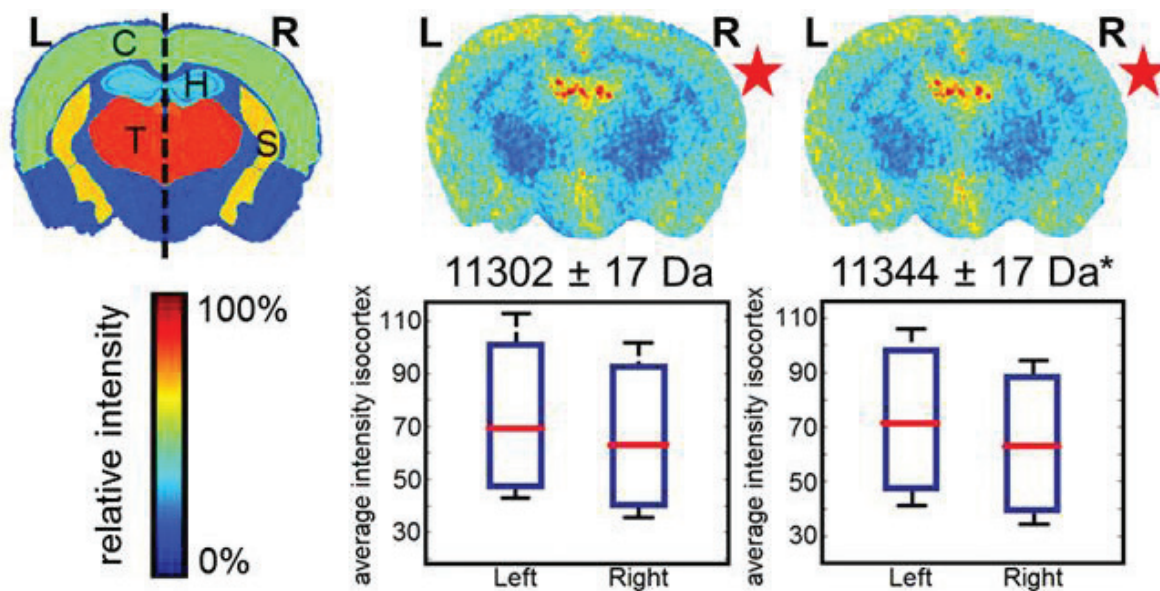


Figure 2. Protein MSI dataset: differences between CSD (right, R) and control hemisphere (left, L) in R192Q-CSD mouse brain. Each image corresponds to the visualization of the average distribution of a particular m/z feature in five mouse brains after alignment to the ABA. (* $p < 0.05$, Student's t -test). C: cortex, T: thalamus; H: hippocampus, S: Striatum.

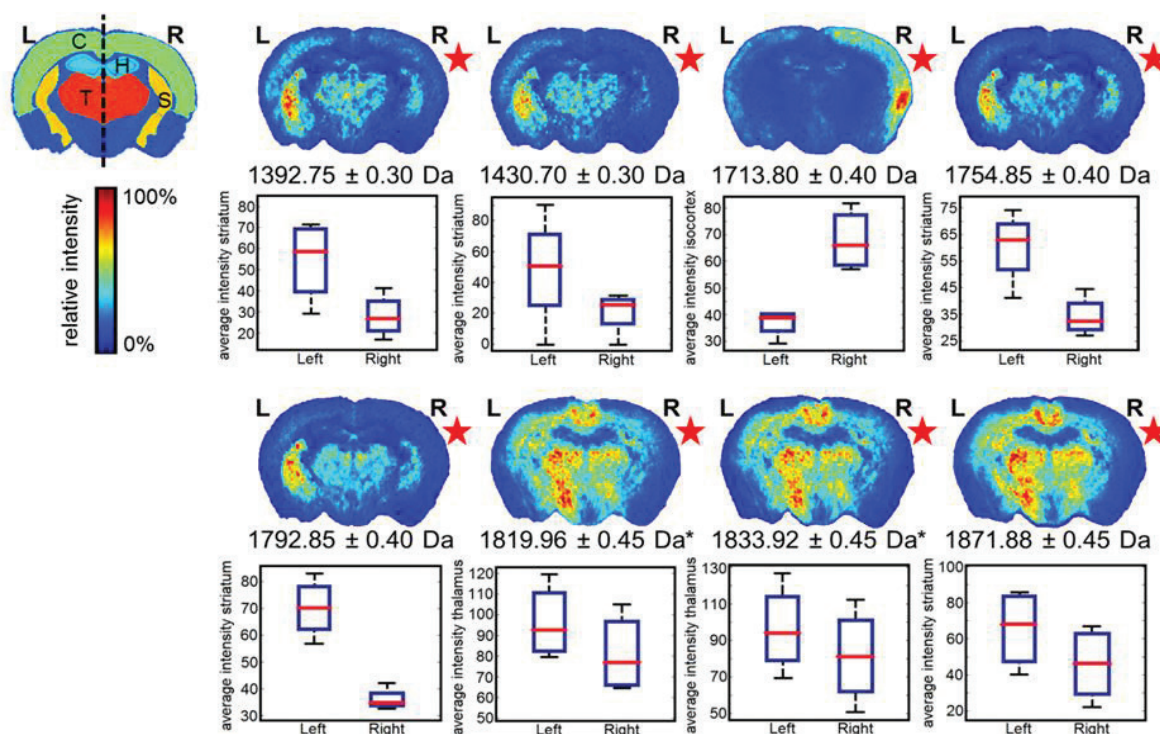


Figure 3. Peptide MSI dataset: differences between CSD (right, R) and control hemisphere (left, L) in R192Q-CSD mouse brain. Each image corresponds to the visualization of the average distribution of a particular m/z feature in five mouse brains after alignment to the ABA. (* $p < 0.05$, Student's t -test) C: cortex, T: thalamus; H: hippocampus, S: Striatum.

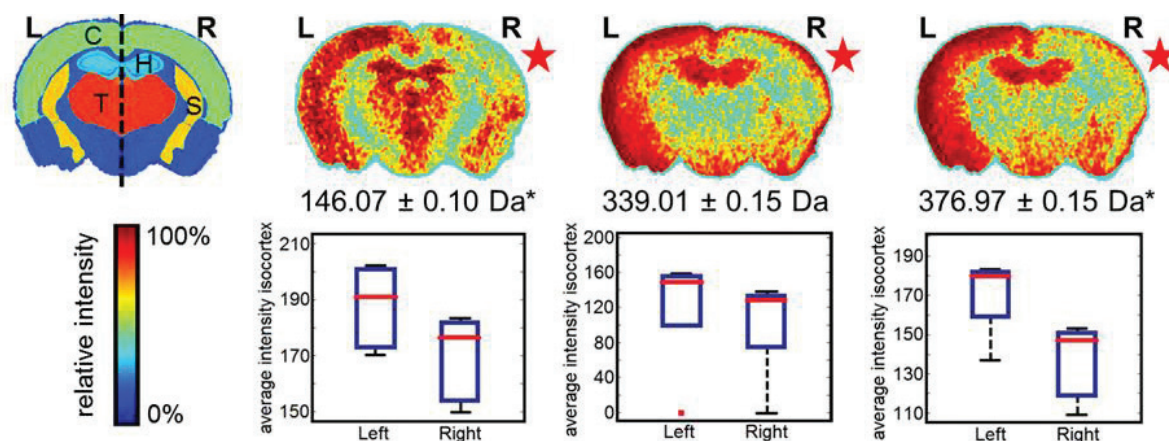


Figure 4. Metabolite MSI dataset: differences between CSD (right, R) and control hemisphere (left, L) in R192Q-CSD mouse brain. Each image corresponds to the visualization of the average distribution of a particular m/z feature in five mouse brains after alignment to the ABA. (* $p < 0.05$, Student's t-test). C: cortex, T: thalamus; H: hippocampus, S: Striatum.

DISCUSSION

MSI is a non-targeted methodology that allows the analysis of different biomolecular classes directly from tissue. One of the main advantages of MSI is its ability to unravel biomolecular changes independently of histology. This is of particular interest to the study of migraine, a neurological disorder characterized by recurrent attacks and lack of clear histopathological features. Many metabolites, amino acids and neuropeptides have been measured in the brain during and after CSD experiments (Selman et al 2004). However, the effects of CSD are still not fully understood, namely: (1) How are the proteome, peptidome and metabolome profiles affected by CSD? (2) How are the CSD changes affected by the genetic background of the mice (i.e., a comparison between mice with a genetic predisposition to migraine and WT mice)? And (3) does CSD induce biomolecular changes in subcortical areas? To answer these questions, we measured and compared the biomolecular profiles of FHM1 R192Q and WT mice after CSD induction in the occipital cortex.

The biomolecular profiles recorded by MSI presented disturbances that may be associated with the CSD wave progression only in R192Q mouse brain. Given the short time between CSD induction and animal sacrifice, ca. 40 min after the first CSD event, significant changes in protein expression level were not expected. Indeed, the only significant change revealed by MSI is associated with a post-translational modification in histone H4: acetylated histone H4 (11,344 Da) showed a decreased intensity in the cortical region of the CSD-affected hemisphere. Likewise, previous reports showed that CSD induction in rats affected methylation levels in the cortex, although this was evident 24 hr following CSD induction (Passaro et al 2010, Rana et al 2012). Histone modifications, such as acetylation, methylation, ubiquitination, and phosphorylation have an important role in the epigenetic regulation of transcription and have been associated with neurological diseases such as Alzheimer's

disease, Huntington's disease and Parkinson's disease (Konsoula & Barile 2012). Therefore, the effect of CSD on post-translational modification of histones, and consequently on the transcription mechanisms, may have relevance to migraine.

It is well known that CSD triggers the release of vasoactive peptides (Colonna et al 1994, Tozzi et al 2012). Trigeminal axons that innervate the dural vessels and are activated during CSD release calcitonin gene related peptide (CGRP), substance P (SP) and neurokinin- α (NKA), which all are potent vasodilators (Bolay et al 2002, Colonna et al 1994, Ho et al 2010, Raddant & Russo 2011, Wahl et al 1994). These vasoactive peptides are believed to be mediators of neurogenic inflammation, which is thought to be a mechanism relevant to the generation of migraine headache (Bolay et al 2002). Interestingly, levels of CGRP and SP in the blood of migraine patients were found increased between and during attacks (Fusayasu et al 2007, Gallai et al 1995, Goadsby et al 1990). Although we did not observe significant changes in any of these compounds, the MSI peptide datasets revealed moderate differences in the distributions of a few biomolecular features (1392.75 Da; 1713.80 Da, 1754.85 Da; 1871.88 Da) in mouse brain hemispheres affected by CSD, which is in agreement with the idea that CSD induction triggers a substantial redistribution of peptides in the extracellular space. Additionally, a significant decrease in the intensity of m/z features 1819.96 Da and 1833.92 Da was observed only in the thalamus region of R192Q mice. Although the identity of these m/z features is currently unknown, their similar distribution and m/z shift consistent with a methylation post-translational modification indicate that these may be different forms of the same peptide.

In the peptide datasets, we detected changes in subcortical regions (striatum and thalamus) as a result of CSD. This is in agreement with previously published data indicating that CSD induction in the cortex may also easily spread to subcortical regions in FHM1 R192Q but not WT mice (Eikermann-Haerter et al 2011). Therefore, the differential distribution of peptides in the striatum, thalamus and hippocampus identified after CSD might reflect a subcortical spread of CSD waves. Yet, the possibility for a transport of peptides released in the cortex to subcortical structures cannot be excluded at this time.

Several metabolites, such as ATP, ADP, AMP, cGMP, lactate, pyruvate, glucose and glycogen have been associated with CSD (Selman et al 2004). In addition, CSD can also trigger the release of amino acids and change their brain regional distribution. During single episodes of CSD in rat brain, interstitial levels of several amino acids (e.g., alanine, arginine, aspartate, glutamate, glycine) were found to be elevated, highlighting the massive changes in biomolecular distribution that occur in the brain during episodes of CSD (Fabricius et al 1993). Our MSI metabolite datasets revealed a significant decrease in the intensity of m/z feature 146.07 in the cortical region of R192Q mice after CSD. Owing to the high number of isobaric molecules in this mass region, it is virtually impossible to identify small metabolites directly from tissue with MS/MS analysis. Yet, after high-resolution MS analysis and assignment based on previous reports, this biomolecule was assigned as glutamate. Glutamate plays a major role in CSD and elevated levels of glutamate and glutamic acids have been detected in plasma (Ferrari et al 1990) and cerebrospinal fluid (CSF) (Martinez et al 1993, Peres et

al 2004) of migraine patients. Of note, pharmacological targeting of glutamate receptors is currently being explored as a potential migraine therapy (Andreou & Goadsby 2009). Glutamate is a well-known trigger of CSD (Van Harreveld 1959), and during CSD propagation in the cortex there is a release of glutamate to the extracellular space (Basarsky et al 1999, Fabricius et al 1993). Given the above, the down-regulation of glutamate in cortex of CSD affected brain hemispheres observed by MSI analysis may seem contradictory, at first. Previous quantitative proteomics studies in naïve FHM1 R192Q mice, however, revealed an up-regulation of major glutamate transporters, EAAT1 and EAAT2, when compared to WT mice (Klychnikov et al 2010). These findings, together with the MSI results reported here, suggest that a compensatory mechanism in the brain might be in place to clear excessive glutamate from the synaptic space by glial cells using glutamate transporters.

Besides the putative identification of glutamate changes, our MSI data revealed significant differences in the spatial localization of m/z 376.96 Da in the R192Q brain after CSD. Database search based on high-resolution MS indicated that this molecular feature is probably associated with different forms of fructose 1,6-biphosphate, which is a byproduct of fructose and glucose metabolism common to all cells. In a previous publication, this m/z feature was also assigned as fructose 1,6-bisphosphate by MSI in a rat model of ischemic stroke (Miura et al 2010). Interestingly, the distribution of fructose 1,6-biphosphate and glutamate in the ischemic brain is similar to the distribution observed after CSD in both R192Q and WT mice. Recently Eikermann-Haerter et. al. (Eikermann-Haerter et al 2012) studied the link between stroke and migraine using the same transgenic FHM1 R192Q mice and demonstrated that FHM mutations do not only enhance susceptibility to CSD but also to ischemic depolarizations, leading to stroke. Therefore, the MSI results reported here in combination with previous work by Miura et al. (Miura et al 2010) seem to suggest that there is indeed a link between CSD and stroke events, although more work is required to prove this hypothesis.

CONCLUSIONS

Here we used MALDI-MSI combined with a newly developed pipeline that allows the automatic registration of MS datasets to mouse data contained in the Allen Brain Atlas (Abdelmoula et al 2014), to investigate the biomolecular distribution in the brain after CSD in a relevant mouse model of migraine. Our results revealed that CSD events affect the distribution of metabolites, peptides and proteins, not only in the cortex but also in subcortical structures. The finding that changes in biomolecules distribution were only evident in R192Q mice that had undergone CSD indicates that these changes are both genotype- and CSD-specific. Future work should reveal the identities of biomolecules that are affected by CSD events and might provide more in-depth insights in migraine pathophysiology. In conclusion, our results show that CSD induction in FHM1 R192Q mice is associated with a substantial redistribution of biomolecules in the brain and highlight that MALDI-MSI can be instrumental in preclinical animal models of disease.

ACKNOWLEDGEMENTS

The authors acknowledge support for this work by the ZonMW Zenith project Imaging Mass Spectrometry-Based Molecular Histology: Differentiation and Characterization of Clinically Challenging Soft Tissue Sarcomas (No. 93512002; LMD), Cyttron II (to L.M.D.), Commit (to L.M.D.), Centre for Medical Systems Biology (CMSB) in the framework of the Netherlands Genomics Initiative (NGI) (to A.vdM.), Marie Curie Action ENIGMAS FP7-PEOPLE-2011-IEF (No. 303344; to R.C.), Marie Curie Action SITH FP7-PEOPLE-2012-IEF (No. 331866; to B.B.), Marie Curie Career Integration Grant (No. 294233; to E.A.T.), FP7 EUROHEADPAIN (No. 602633; to A.vdM. & M.D.F.), Marie Curie IAPP Program BRAINPATH (No. 612360; to A.vdM. & E.A.T.), an LUMC Fellowship (to E.A.T.), and CURE SUDEP research award (nr. 280560) (to E.A.T.).

REFERENCES

- Abdelmoula WM, Carreira RJ, Shyti R, Balluff B, van Zeijl RJ, et al. 2014. Automatic registration of mass spectrometry imaging data sets to the Allen brain atlas. *Anal. Chem.* 86:3947-54
- Andreou AP, Goadsby PJ. 2009. Therapeutic potential of novel glutamate receptor antagonists in migraine. *Expert Opin. Investig. Drugs* 18:789-803
- Balluff B, Schöne C, Höfler H, Walch A. 2011. MALDI imaging mass spectrometry for direct tissue analysis: technological advancements and recent applications. *Histochem. Cell Biol.* 136:227-44
- Basarsky TA, Feighan D, MacVicar BA. 1999. Glutamate release through volume-activated channels during spreading depression. *J. Neurosci.* 19:6439-45
- Blatherwick EQ, Svensson CI, Frenguelli BG, Scrivens JH. 2013. Localisation of adenine nucleotides in heat-stabilised mouse brains using ion mobility enabled MALDI imaging. *Int. J. Mass Spectrom.* 345:19-27
- Bolay H, Reuter U, Dunn AK, Huang Z, Boas DA, Moskowitz MA. 2002. Intrinsic brain activity triggers trigeminal meningeal afferents in a migraine model. *Nat. Med.* 8:136-42
- Caprioli RM, Farmer TB, Gile J. 1997. Molecular imaging of biological samples: localization of peptides and proteins using MALDI-TOF MS. *Anal. Chem.* 69:4751-60
- Colonna DM, Meng W, Deal DD, Busija DW. 1994. Calcitonin gene-related peptide promotes cerebrovascular dilation during cortical spreading depression in rabbits. *Am. J. Physiol.* 266:H1095-102
- Eikermann-Haerter K, Dilekoz E, Kudo C, Savitz SI, Waeber C, et al. 2009. Genetic and hormonal factors modulate spreading depression and transient hemiparesis in mouse models of familial hemiplegic migraine type 1. *J. Clin. Invest.* 119:99-109
- Eikermann-Haerter K, Lee JH, Yuzawa I, Liu CH, Zhou Z, et al. 2012. Migraine mutations increase stroke vulnerability by facilitating ischemic depolarizations. *Circulation* 125:335-45
- Eikermann-Haerter K, Yuzawa I, Qin T, Wang Y, Baek K, et al. 2011. Enhanced subcortical spreading depression in familial hemiplegic migraine type 1 mutant mice. *J. Neurosci.* 31:5755-63
- Fabricius M, Jensen LH, Lauritzen M. 1993. Microdialysis of interstitial amino acids during spreading depression and anoxic depolarization in rat neocortex. *Brain Res.* 612:61-9
- Ferrari MD, Klever RR, Terwindt GM, Ayata C, van den Maagdenberg AM. 2015. Migraine pathophysiology: lessons from mouse models and human genetics. *Lancet Neurol.* 14:65-80
- Ferrari MD, Odink J, Bos KD, Malessy MJ, Bruyn GW. 1990. Neuroexcitatory plasma amino acids are elevated in migraine. *Neurology* 40:1582-6
- Fusayasu E, Kowa H, Takeshima T, Nakaso K, Nakashima K. 2007. Increased plasma substance P and CGRP levels, and high ACE activity in migraineurs during headache-free periods. *Pain* 128:209-14
- Gallai V, Sarchielli P, Floridi A, Franceschini M, Codini M, et al. 1995. Vasoactive peptide levels in the plasma of young migraine patients with and without aura assessed both interictally and ictally.

Cephalalgia 15:384-90

- Goadsby PJ, Edvinsson L, Ekman R. 1990. Vasoactive peptide release in the extracerebral circulation of humans during migraine headache. *Ann. Neurol.* 28:183-7
- Goadsby PJ, Lipton RB, Ferrari MD. 2002. Migraine-current understanding and treatment. *N. Engl. J. Med.* 346:257-70
- Hadjikhani N, Sanchez Del Rio M, Wu O, Schwartz D, Bakker D, et al. 2001. Mechanisms of migraine aura revealed by functional MRI in human visual cortex. *Proc. Natl. Acad. Sci. USA* 98:4687-92
- Hafezparast M, Ahmad-Annur A, Wood NW, Tabrizi SJ, Fisher EM. 2002. Mouse models for neurological disease. *Lancet Neurol.* 1:215-24
- Hager R, Lu L, Rosen GD, Williams RW. 2012. Genetic architecture supports mosaic brain evolution and independent brain-body size regulation. *Nat. Commun.* 3:1079
- Hanrieder J, Phan NTN, Kurczy ME, Ewing AG. 2013. Imaging Mass Spectrometry in Neuroscience. *ACS Chem. Neurosci.* 4:666-79
- Hattori K, Kajimura M, Hishiki T, Nakanishi T, Kubo A, et al. 2010. Paradoxical ATP elevation in ischemic penumbra revealed by quantitative imaging mass spectrometry. *Antioxid. Redox Signal.* 13:1157-67
- Ho TW, Edvinsson L, Goadsby PJ. 2010. CGRP and its receptors provide new insights into migraine pathophysiology. *Nat. Rev. Neurol.* 6:573-82
- ICHD. 2004. The International Classification of Headache Disorders: 2nd edition. *Cephalalgia* 24 Suppl 1:9-160
- Jones EA, Shyti R, van Zeijl RJ, van Heiningen SH, Ferrari MD, et al. 2012. Imaging mass spectrometry to visualize biomolecule distributions in mouse brain tissue following hemispheric cortical spreading depression. *J. Proteomics* 75:5027-35
- Kaspar S, Peukert M, Svatos A, Matros A, Mock H-PP. 2011. MALDI-imaging mass spectrometry - An emerging technique in plant biology. *Proteomics* 11:1840-50
- Keenan MR, Kotula PG. 2004. Accounting for Poisson noise in the multivariate analysis of ToF-SIMS spectrum images. *Surf. Interface Anal.* 36:203-12
- Klychnikov OI, Li KW, Sidorov IA, Loos M, Spijker S, et al. 2010. Quantitative cortical synapse proteomics of a transgenic migraine mouse model with mutated Ca(V)2.1 calcium channels. *Proteomics* 10:2531-5
- Lauritzen M. 1994. Pathophysiology of the migraine aura. The spreading depression theory. *Brain* 117 (Pt 1):199-210
- Ljungdahl A, Hanrieder J, Fälth M, Bergquist J, Andersson M. 2011. Imaging mass spectrometry reveals elevated nigral levels of dynorphin neuropeptides in L-DOPA-induced dyskinesia in rat model of Parkinson's disease. *PLoS one* 6(9):e25653.

- Martinez F, Castillo J, Rodriguez JR, Leira R, Noya M. 1993. Neuroexcitatory amino acid levels in plasma and cerebrospinal fluid during migraine attacks. *Cephalalgia* 13:89-93
- McDonnell LA, Corthals GL, Willems SM, van Remoortere A, van Zeijl RJ, Deelder AM. 2010a. Peptide and protein imaging mass spectrometry in cancer research. *J. Proteomics* 73:1921-44
- McDonnell LA, Heeren RM, Andrén PE, Stoeckli M, Corthals GL. 2012. Going forward: Increasing the accessibility of imaging mass spectrometry. *J. Proteomics* 75:5113-21
- McDonnell LA, Heeren RMA. 2007. Imaging mass spectrometry. *Mass Spectrom. Rev.* 26:606-43
- McDonnell LA, van Remoortere A, de Velde N, van Zeijl RJ, Deelder AM. 2010b. Imaging mass spectrometry data reduction: automated feature identification and extraction. *J. Am. Soc. Mass Spectrom.* 21:1969-78
- Miura D, Fujimura Y, Yamato M, Hyodo F, Utsumi H, et al. 2010. Ultrahighly sensitive in situ metabolomic imaging for visualizing spatiotemporal metabolic behaviors. *Anal. Chem.* 82:9789-96
- Nilsson A, Sköld K, Sjögren B, Svensson M, Pierson J, et al. 2007. Increased striatal mRNA and protein levels of the immunophilin FKBP-12 in experimental Parkinson's disease and identification of FKBP-12-binding proteins. *J. Proteome Res.* 6:3952-61
- Norris JL, Caprioli RM. 2013. Analysis of tissue specimens by matrix-assisted laser desorption/ionization imaging mass spectrometry in biological and clinical research. *Chem. Rev.* 113:2309-42
- Ophoff RA, Terwindt GM, Vergouwe MN, van Eijk R, Oefner PJ, et al. 1996. Familial hemiplegic migraine and episodic ataxia type-2 are caused by mutations in the Ca²⁺ channel gene CACNL1A4. *Cell* 87:543-52
- Passaro D, Rana G, Piscopo M, Viggiano E, De Luca B, Fucci L. 2010. Epigenetic chromatin modifications in the cortical spreading depression. *Brain Res.* 1329:1-9
- Peres MF, Zukerman E, Senne Soares CA, Alonso EO, Santos BF, Faulhaber MH. 2004. Cerebrospinal fluid glutamate levels in chronic migraine. *Cephalalgia* 24:735-9
- Pierson J, Norris JL, Aerni HR, Svenningsson P, Caprioli RM, Andrén PE. 2004. Molecular Profiling of Experimental Parkinson's Disease: Direct Analysis of Peptides and Proteins on Brain Tissue Sections by MALDI Mass Spectrometry. *J. Proteome Res.* 3:289-95
- Pietrobon D, Moskowitz MA. 2013. Pathophysiology of migraine. *Annu. Rev. Physiol.* 75:365-91
- Poté N, Alexandrov T, Le Faouder J, Laouirem S, Léger T, et al. 2013. Imaging mass spectrometry reveals modified forms of histone H4 as new biomarkers of microvascular invasion in hepatocellular carcinomas. *Hepatology* 58:983-94
- Raddant AC, Russo AF. 2011. Calcitonin gene-related peptide in migraine: intersection of peripheral inflammation and central modulation. *Expert Rev. Mol. Med.* 13:e36
- Rana G, Donizetti A, Virelli G, Piscopo M, Viggiano E, et al. 2012. Cortical spreading depression differentially affects lysine methylation of H3 histone at neuroprotective genes and retrotransposon

- sequences. *Brain Res.* 1467:113-9
- Rohner TC, Staab D, Stoekli M. 2005. MALDI mass spectrometric imaging of biological tissue sections. *Mech. Ageing Dev.* 126:177-85
- Selman WR, Lust WD, Pundik S, Zhou YN, Ratcheson RA. 2004. Compromised metabolic recovery following spontaneous spreading depression in the penumbra. *Brain Res.* 999:167-74
- Shariatgorji M, Svenningsson P, Andrén PE. 2014. Mass spectrometry imaging, an emerging technology in neuropsychopharmacology. *Neuropsychopharmacology* 39:34-49
- Somjen GG. 2001. Mechanisms of spreading depression and hypoxic spreading depression-like depolarization. *Physiol. Rev.* 81:1065-96
- Stoekli M, Knochenmuss R, McCombie G, Mueller D, Rohner T, et al. 2006. MALDI MS imaging of amyloid. *Methods Enzymol.* 412:94-106
- Sugiura Y, Honda K, Kajimura M, Suematsu M. 2014. Visualization and quantification of cerebral metabolic fluxes of glucose in awake mice. *Proteomics* 14:829-38
- Sugiura Y, Taguchi R, Setou M. 2011. Visualization of spatiotemporal energy dynamics of hippocampal neurons by mass spectrometry during a kainate-induced seizure. *PloS one* 6:e17952
- Tottene A, Conti R, Fabbro A, Vecchia D, Shapovalova M, et al. 2009. Enhanced excitatory transmission at cortical synapses as the basis for facilitated spreading depression in Ca(v)2.1 knockin migraine mice. *Neuron* 61:762-73
- Tozzi A, de Iure A, Di Filippo M, Costa C, Caproni S, et al. 2012. Critical role of calcitonin gene-related peptide receptors in cortical spreading depression. *Proc. Natl. Acad. Sci. USA* 109:18985-90
- Van den Maagdenberg AM, Pietrobon D, Pizzorusso T, Kaja S, Broos LA, et al. 2004. A Cacna1a knockin migraine mouse model with increased susceptibility to cortical spreading depression. *Neuron* 41:701-10
- Van Harreveld A. 1959. Compounds in brain extracts causing spreading depression of cerebral cortical activity and contraction of crustacean muscle. *J. Neurochem.* 3:300-15
- Veselkov KA, Mirnezami R, Strittmatter N, Goldin RD, Kinross J, et al. 2014. Chemo-informatic strategy for imaging mass spectrometry-based hyperspectral profiling of lipid signatures in colorectal cancer. *Proc. Natl. Acad. Sci. USA.* 111:1216-21
- Wahl M, Schilling L, Parsons AA, Kaumann A. 1994. Involvement of calcitonin gene-related peptide (CGRP) and nitric oxide (NO) in the pial artery dilatation elicited by cortical spreading depression. *Brain Res.* 637:204-10
- Zacharoula K, Frank AB. 2012. Epigenetic histone acetylation and deacetylation mechanisms in experimental models of neurodegenerative disorders. *J. Pharmacol. Toxicol. Methods* 66(3):215-2

SUPPLEMENTARY INFORMATION

Table S1. CSD characteristics and average time under anesthesia for the different mouse groups. Seven CSD events were evoked by topical application of 1M KCl in the occipital cortex of the right hemisphere of the brain with 5 minutes interval (equivalent Sham experiments were performed with topical application of 1M NaCl). Significant differences between R192Q and WT mice regarding the CSD characteristics and time under anesthesia were not observed.

Group	N	Amplitude (mV)	Duration (sec)	Time anesthesia (min)
WT-CSD	5	22.9±2.4	44.2±19.4	62.0±6.3
WT-Sham	6			62.0±2.2
R192Q-CSD	5	22.0±1.2	31.2±3.3	61.5±2.9
R192Q-Sham	6			65.1±4.3

Pseudo-code of the semi-supervised block randomization

- s = number of samples
- Define $n * m$ experimental design matrix M
 - m = maximum number of samples that can be placed on a slide
 - n = number of slides needed for the project = $\text{ceiling}(s/m)$
- Sort groups into list L according to amount of samples
- Fill up M iteratively by column
 - As long as there are empty places in a column, do
 - select next group from L
 - draw randomly x samples from the selected group where $x \leq m$
 - place the selected samples randomly within the empty positions in the column
 - delete already taken samples from the initial sample list
- When done, permute samples within slides

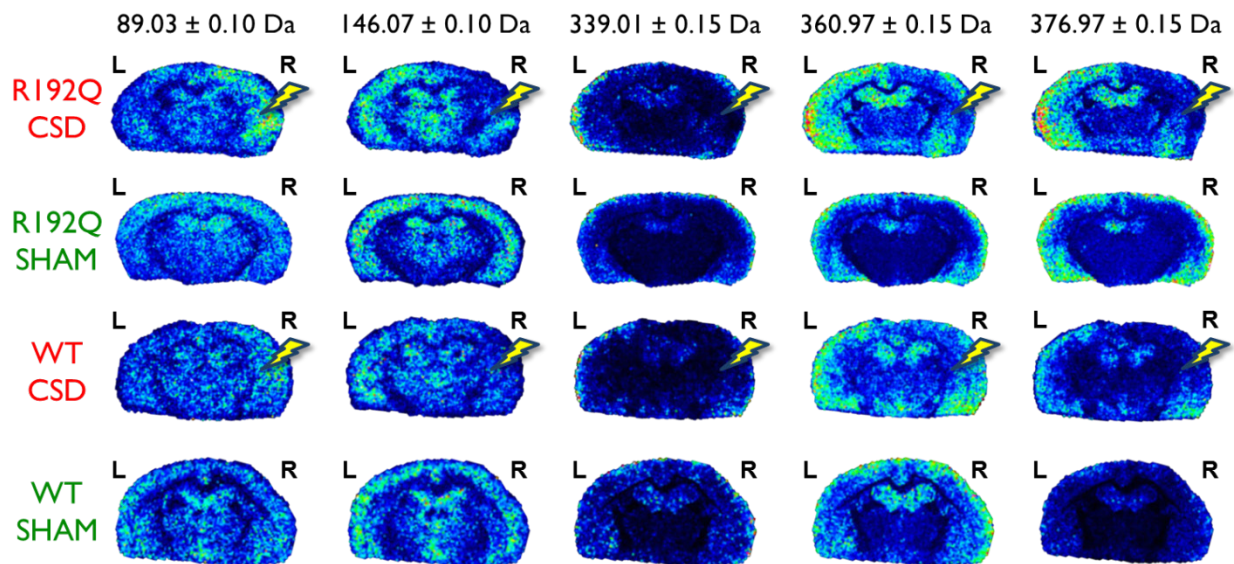


Figure S1: The effect of CSD on the distribution of a number of metabolites in coronal sections of WT and R192Q mouse brain. Seven CSDs (and equivalent Sham experiments) were evoked in the right (R) hemisphere of WT and R192Q mouse brain. Twelve μm thick coronal brain sections were homogeneously sprayed with 9AA matrix and analyzed by MALDI-TOF-MS in the negative mode. MS-images refer to a single mouse example per experimental group. Lightning bolt indicates the hemisphere (right hemisphere) where the CSD event was evoked.

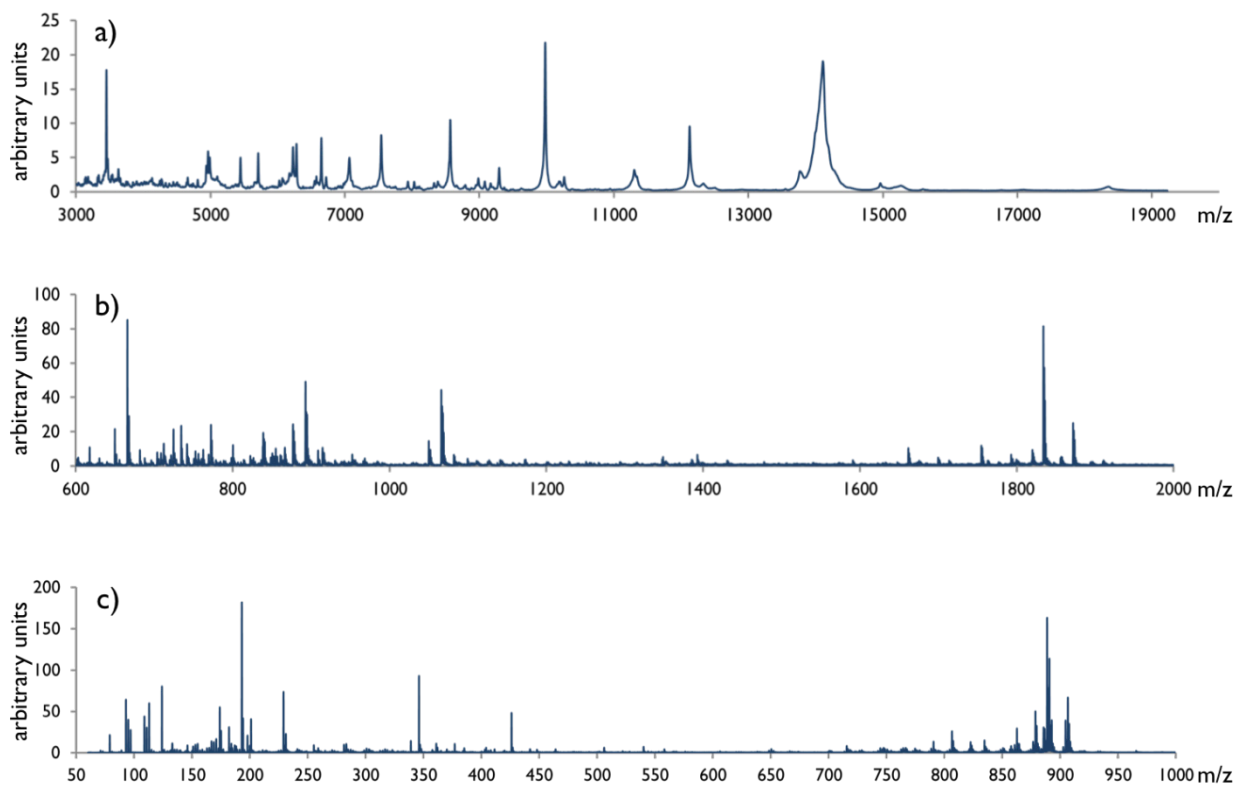
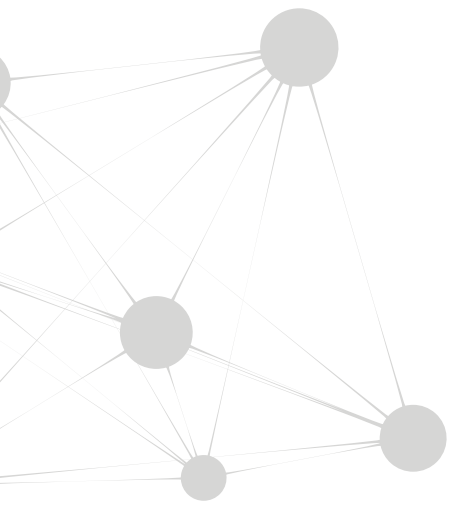
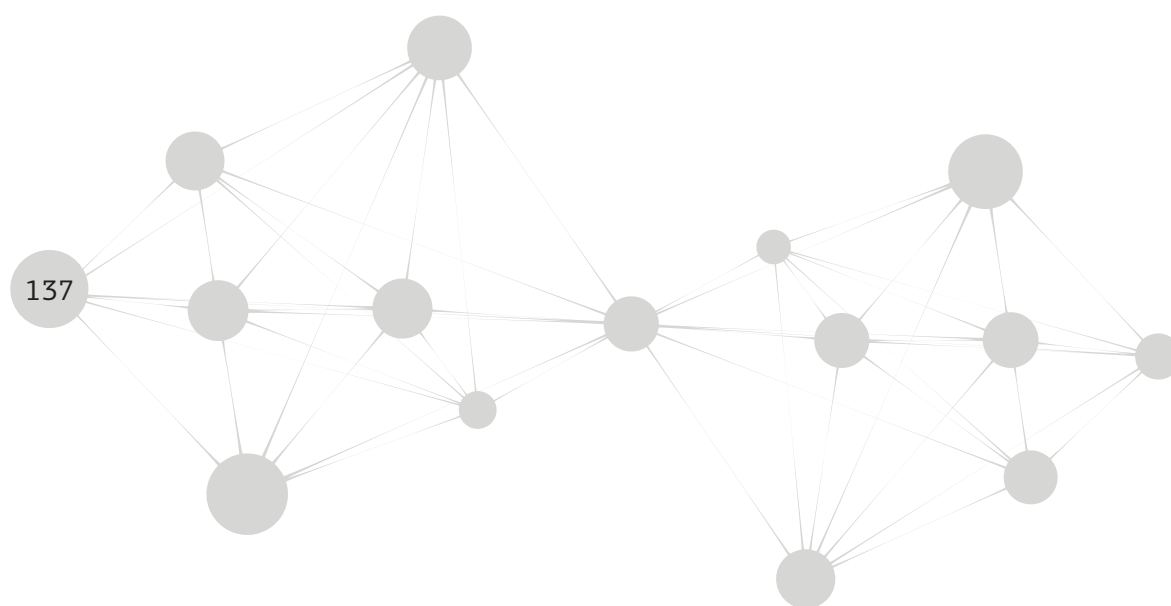


Figure S2: Representative spectra from different MSI datasets. **A)** Protein dataset – positive linear mode; 2000 – 20 000 Da. **B)** Peptide dataset – positive reflectron mode; 600 – 2000 Da. **C)** Metabolite dataset – negative reflectron mode; 50 – 1000 Da.



Chapter 7

Plasma metabolic profiling after cortical spreading depression in a transgenic mouse model of hemiplegic migraine by capillary electrophoresis - mass spectrometry



Reinald Shyti^{a,*}, Isabelle Kohler^{b,*}, Bart Schoenmaker^b, Rico J. E. Derks^b, Michel D. Ferrari^c, Else A. Tolner^c, Oleg A. Mayboroda^{b,‡}, Arn M.J.M. van den Maagdenberg^{a,c,‡}

^aDepartment of Human Genetics, Leiden University Medical Center, Leiden, The Netherlands

^bCenter for Proteomics and Metabolomics, Leiden University Medical Center, Leiden, The Netherlands

^cDepartment of Neurology, Leiden University Medical Center, Leiden, The Netherlands

^{*,‡}equal contribution

Molecular BioSystems 2015;11:1462-71

ABSTRACT

Migraine is a common brain disorder characterized by recurrent attacks of severe headaches and other neurological symptoms. In one-third of patients headaches are accompanied by auras, which consist of transient visual and sensory disturbances, believed to be caused by cortical spreading depression (CSD). CSD is characterized by a wave of neuronal and glial depolarization with concomitant changes in metabolite concentrations in the brain and cerebrospinal fluid. It remains unknown whether CSD-induced brain metabolic changes can be captured outside the central nervous system, i.e., in peripheral fluids. This study investigated plasma metabolic changes in transgenic mice that harbor a gene mutation in voltage-gated $\text{Ca}_v2.1 \text{ Ca}^{2+}$ channels previously identified in patients with familial hemiplegic migraine, a subtype of migraine with aura. The use of a mouse model allows investigation of molecular changes occurring shortly after CSD, which is notoriously difficult in patients. Capillary electrophoresis - mass spectrometry was used for the analysis of plasma samples to obtain, for the first time, a comprehensive view of molecular changes immediately after experimentally induced CSD. Multivariate data analysis showed a clear distinction between profiles of transgenic and wild-type animals after CSD. Two metabolites considered important for this discrimination were tentatively identified as being lysine and its by-product pipecolic acid with additional confidence provided by hydrophilic interaction chromatography combined with tandem mass spectrometry. The changed metabolites suggest a compensatory increase in GABAergic neurotransmission upon enhanced excitatory neurotransmission. These results show that CSD induces metabolic remodeling in transgenic migraine mice that can be captured and measured in plasma.

INTRODUCTION

Migraine is a common debilitating brain disorder characterized by episodic recurrent attacks of severe headaches often accompanied by nausea, vomiting, photophobia, and phonophobia (Goadsby et al 2002, ICHD 2004). In one-third of patients attacks are accompanied by transient neurological dysfunction called an aura that consists of visual, sensory or aphasic symptoms. Familial hemiplegic migraine (FHM), a monogenic subtype of migraine with aura with reversible pronounced motor weakness during the aura, is considered a valid model for common forms of migraine (Ferrari et al 2015). FHM type 1 is caused by mutations in the *CACNA1A* gene that encodes the pore-forming α_1 subunit of neuronal $\text{Ca}_v2.1$ (P/Q-type) voltage-gated calcium channels (de Vries et al 2009, Ducros et al 2001, Ophoff et al 1996, van den Maagdenberg et al 2007). The underlying cause of the aura is cortical spreading depression (CSD), which consists of a wave of glial and neuronal depolarization that slowly propagates through the cortex and is followed by a long-lasting (ca. 1 hr) neuronal silencing. Experiments in animals have shown that CSD can activate trigeminovascular pathways in the brainstem involved in headache generation (Karatas et al 2013, Zhang et al 2011), but such evidence is lacking in humans. CSD leads to a disruption of cellular ionic balance and is associated with changes in extracellular levels of ions, neurotransmitters, and metabolites (Davies et al 1995, Somjen 2001). Furthermore, it has been shown that a CSD event can change blood-brain barrier permeability (Gursoy-Ozdemir et al 2004), which may indicate that CSD events and their consequences may be traced beyond the central nervous system (CNS), e.g., in peripheral fluids such as blood or urine. Metabolomics appears a logical approach for testing this assumption; indeed, the response of an organism to any biological effect is ultimately reflected in alterations of metabolic composition of body fluids. Profiling of CSD-induced molecular changes may give relevant molecular insight into the pathophysiological mechanisms of migraine and lead to relevant (putative) biomarkers for diagnosis, monitoring, or prognosis of migraine events in patients. Surprisingly, even though the clinical importance of metabolomics-based studies has been widely demonstrated for various neurological disorders, migraine remains a largely unexplored area (Lionetto et al 2013).

Performing metabolomics studies in mice poses technical challenges that need to be addressed. For instance, non-terminal blood collection provides only minute amounts (i.e., few μL) of plasma, a miniaturized analytical workflow is thus mandatory. Capillary electrophoresis hyphenated to mass spectrometry (CE-MS) presents numerous advantages, including high-separation efficiency and selectivity, as well as low sample and solvent consumption. The feasibility of CE-MS as an analytical method for metabolic profiling of the volume-restricted samples has been shown multiple times; it is particularly well-suited for the analysis of polar and ionizable compounds, such as amino acids, phosphorylated compounds, tricarboxylic acid cycle intermediates, as well as nucleosides and nucleotides in biosamples (Bonvin et al 2012, Hirayama et al 2014, Kohler et al 2013, Kok et al 2014). The high sensitivity and resolution required for such bioanalytical applications can be reached by using online sample preconcentration techniques and a sheathless nanospray ionization interface.

A prototype based on a porous sheathless interface, first proposed by Moini (Moini 2007), has been successfully used for metabolomics applications (Hirayama et al 2012, Nevedomskaya et al 2010, Ramautar et al 2012). This sheathless interface was shown to display a mass-flux sensitive response at flow rates lower than 25 nL min^{-1} , suggesting a maximum sensitivity and reduced ion suppression at very low flow rates usually observed with CE (Busnel et al 2010).

In this study, CE-MS was used for metabolic profiling of plasma from a FHM1 transgenic mouse model carrying a R192Q missense mutation that was introduced in the *CACNA1A* gene (van den Maagdenberg et al 2004). The mutant mice exhibit migraine-relevant features including an increased susceptibility to CSD that is the consequence of enhanced excitatory neurotransmission due to hyperactive $\text{Ca}_v2.1$ channels (Eikermann-Haerter et al 2009, Tottene et al 2009, van den Maagdenberg et al). CSD-induced metabolite changes significantly differed between mutants and wild-type (WT) control animals. Hydrophilic interaction chromatography (HILIC) combined with tandem mass spectrometry (MS/MS) was used for platform-independent and orthogonal confirmation of the identity of lysine and pipercolic acid (PA), the two metabolites that were considered important for the discrimination of mutant and WT metabolite profiles. Changed levels of lysine and PA may reflect a compensatory increase in GABAergic neurotransmission as a consequence of enhanced excitatory neurotransmission that is particularly prominent in mutant mice upon CSD.

MATERIALS AND METHODS

Chemicals

Potassium chloride, sodium chloride, sodium hydroxide, methanol (MeOH), ethanol (EtOH), isopropanol (i-PrOH), 28% ammonium hydroxide (m/v), L-lysine monohydrochloride, and L-PA were of analytical grade and purchased from Sigma-Aldrich (Schnelldorf, Germany). Water and acetonitrile (MeCN) were of LC-MS grade and were obtained from Sigma-Aldrich. Formic and acetic acid were of ULC-MS grade and were purchased from Biosolve (Valkenswaard, The Netherlands).

Animals

Male 2- to 4-months-old FHM1 R192Q and WT control mice were used and genotyped as previously described (van den Maagdenberg et al 2004). Mice were kept in a standard 12:12 light dark cycle; water and food were available *ad libitum*. All the animal experiments were approved by the Animal Experiment Ethics Committee of Leiden University Medical Centre.

Induction and recording of cortical spreading depression

Mice were anesthetized using 4% isoflurane in pressurized air (20% O_2 and 80% N_2) for induction and 1.5% for maintenance. Mice were placed in a stereotactic frame (David Kopf, Tujunga, CA, USA) and a midline incision was made to expose the skull. Two burr holes were drilled with a microdriller at the following coordinates from bregma: 3.5 mm posterior and 2 mm lateral for CSD induction in the occipital cortex and 0.5 mm anterior and 2 mm lateral for CSD recording in the frontal cortex.

CSD events were induced by application of a cotton ball soaked in 1M KCl over the dura for 30 sec, immediately removed prior to thorough washing with saline solution. In sham-operated mice, a cotton ball soaked in 1M NaCl was applied for 30 sec, immediately removed prior to thorough washing with saline solution. This procedure was repeated 7 times each with a 5-min interval for both CSD- and sham-operated mice. The experimental design, illustrated in Figure S1, included 24 mice, i.e., two groups consisting of 12 sham- and 12 CSD-operated mice, each group containing 6 WT and 6 R192Q animals. CSD events were measured as DC-potential changes that were recorded at 300 μm depth using a glass electrode filled with 150 mM NaCl in the frontal cortex. Data were sampled at 200 Hz, amplified (10x) and low-pass-filtered (100 Hz) using a Powerlab (AD Instruments Inc, Colorado Springs, CO, USA).

Sample collection and preparation

Five minutes after the 7th CSD (in the case of KCl application) or 7th sham (in the case of NaCl application), mice were decapitated and a minimum of 40 μL of blood was collected from the trunk in heparinized blood collection capillaries (Sarstedt Microvette CB 300, Nümbrecht, Germany). Plasma samples were obtained after centrifugation of blood for 10 min with 4000 rpm at 4°C and then snap-frozen in liquid N₂ and stored at -80°C. Prior to CE-MS analysis, plasma samples were thawed at room temperature. Protein precipitation (PP) was carried out with addition of cold EtOH to the plasma (3:1, v/v) followed by vortex agitation. After 20 min, samples were centrifuged for 10 min at 4000 rpm prior to the collection of supernatant and its evaporation to dryness. The obtained dried extracts were dissolved by addition of 100 mM ammonium acetate at pH 4.0 to a volume corresponding to the original one. The prepared samples were randomized prior to CE-MS analysis, which also included quality control (QC) samples consisting of a pool of all plasma samples prepared in the same way to evaluate the analytical variability of the CE-MS experimental set-up.

Capillary electrophoresis – mass spectrometry

CE-MS experiments

CE experiments were performed using a PA800 Plus instrument (Beckman Coulter, Brea, CA, USA) equipped with a temperature-controlled sample tray, capillary cooling liquid, and a power supply able to deliver up to 30 kV. CE separations were carried out with neutrally-coated capillaries (30 μm i.d. 150 μm o.d. 100 cm) consisting of a bilayer with polyacrylamide as the outer layer and the end proximal to the mass analyzer made porous to ion flow, in development and supplied by Beckman Coulter at the time of this study. CE was hyphenated to a MaXis 4G UHR-TOF mass analyzer (Bruker Daltonics, Bremen, Germany) *via* a porous CE-electrospray (ESI)-MS sheathless interface. The prototype interface set up as well as daily system suitability tests are described in details elsewhere (Busnel et al 2010, Heemskerk et al 2012). The background electrolyte (BGE) was composed of 10% acetic acid (v/v). Samples were hydrodynamically introduced at 2.5 psi for 65 sec (corresponding to 3% of the capillary volume, 25 nL) using a transient isotachopheresis (t-ITP) online pre-concentration previously described (Heemskerk et al 2012). Separation was carried out in

65 min with an applied voltage of 25 kV and a pressure of 2 psi to ensure the ESI spray stability. MS acquisition was performed in ESI positive mode over the range 50 to 1500 m/z with an acquisition rate of 1 Hz. ESI capillary voltage was set at -1200 V and drying flow rate and temperature at 2 L/min and 180°C, respectively. A hydro-organic solution of H₂O/i-PrOH 50:50 (v/v) containing sodium formate clusters was infused at the beginning of each analysis to allow for mass recalibration.

Data analysis

All MS data files were recalibrated based on sodium formate m/z clusters. The CE-MS data files were exported in *mzxml* format and aligned with the in-house developed alignment algorithm *msAlign2* available on www.ms-utils.org/msalign2 (Nevedomskaya et al 2009). Peak picking was performed with XCMS package (The Scripps Research Institute, La Jolla, CA, USA) based on the *centWave* algorithm using the following settings: maximal tolerated m/z deviation in consecutive scans, 5 ppm; electrophoretic peak width, 5-15 sec; scan range to process, 70-1500 m/z ; noise, 15,000; prefilter step, at least 3 peaks with intensity >20,000; m/z center of the feature, *wMean* (intensity weighted mean of the feature m/z values); signal-to-noise ratio threshold, 50; minimum difference in m/z for peaks with overlapping migration time, 0.05 min; integration method, peak limits found through descent on the Mexican hat filtered data; no Gaussian fitted to each peak (Smith et al 2006, Tautenhahn et al 2008). Probabilistic Quotient Normalization method was used to account for the dilution of the samples (Dieterle et al 2006). Data were mean centered and a square root transformation was used to correct for the heteroscedasticity.

Principal component analysis (PCA), partial least squares discriminant analysis (PLS-DA), and orthogonal partial least squares discriminant analysis (OPLS-DA) were computed using SIMCA-P+ software version 12.0 (Umetrics, Umeå, Sweden). The validity of the PLS-DA model was checked using a permutation test containing 200 iterations. Features responsible for the separation between classes in OPLS-DA were determined based on the S-plot visualization method and the Variable Influence on Projection (VIP) values, which both highlight the importance of the variables for the classification. In order to identify the classifiers of interest, rational chemical formulae were generated based on the internally calibrated monoisotopic mass within 5 ppm mass error and submitted to METLIN Metabolite Search (<http://metlin.scripps.edu>; Smith et al 2005) and the Human Metabolome Database (HMDB, <http://www.hmdb.ca>; Wishart et al 2009). The confirmation of the identity of metabolites of interest was carried out by HILIC-MS/MS.

Hydrophilic interaction chromatography-tandem mass spectrometry

HILIC-MS/MS experiments were performed with a LC-MS Advance™ UHPLC hyphenated to an EVOQ Elite™ Triple Quadrupole (QqQ), both from Bruker Daltonics. Confirmatory analyses were carried out with a Luna NH₂ column (Phenomenex, Utrecht, The Netherlands) of 100 mm 2.00 mm i.d., 3 μm, and 100 Å. The mobile phase was composed of a 20 mM ammonium acetate buffer at pH 9.0 (A) and MeCN (B). The flow rate was set to 600 μL min⁻¹ with the following gradient profile: 95%

B for 1 min, 95-5% B for 5 min, and 5% B for 1 min. Equilibration of the column was performed with 95% B for 5 min. Analyses were carried out at 40°C. MS/MS experiments were performed in positive ESI mode with a collision energy of 10 eV and a dwell time of 200 ms. ESI source parameters were: an ESI capillary voltage of 4500 V, a cone gas voltage of 20 V, a cone gas temperature of 25 °C, a probe gas voltage of 20 V, a probe gas temperature of 300 °C, and a nebulizer gas pressure of 200 psi. N₂ was used for collision-induced dissociation at a pressure of 1.5 mTorr. Sample preparation included plasma PP prior to solid-phase extraction (SPE). PP was carried out by adding 1.5 mL of MeOH to 500 µL of pooled plasma collected from naïve WT control mice and centrifuged at 13000 rpm for 10 min. The supernatant was collected and basified (*ca.* pH 12) by adding 2 mL of a mixture of NH₄OH/H₂O 5:95 (v/v). SPE was performed on precipitated sample with Strata Strong Anion Mixed Mode (Strata-X-A, Phenomenex) cartridges containing 100 mg sorbent mass. SPE cartridges were first conditioned with 1 mL MeOH and equilibrated with 1 mL of NH₄OH/H₂O 5:95 (v/v) prior to the loading of basified sample. The first and second washing step were performed with 1 mL of NH₄OH/H₂O 5:95 (v/v) and 1 mL of MeOH, respectively. Compounds of interest were then eluted with 1 mL of a mixture of HCOOH/MeOH 2:98 (v/v). The organic eluate was evaporated to dryness and reconstituted in 25 µL of a solution of MeCN/0.1 M HCl 9:1 (v/v). Two µL of this solution were eventually injected for subsequent HILIC-MS/MS experiments.

RESULTS AND DISCUSSION

Plasma metabolic profiling by CE-MS

In order to reach the highest sensitivity and separation efficiency, leading to an enhanced plasma metabolic coverage, an integrated CE nanospray MS approach was used in combination with t-ITP online pre-concentration (Heemskerk et al 2012). The use of neutrally-coated capillaries, which almost entirely suppress the electro-osmotic flow (EOF), also allowed for the highest separation efficiencies while keeping the CE effluent to very low flow rates (<25 nL min⁻¹) which are necessary to observe a mass-flux sensitive detector response (Busnel et al 2010). A typical base peak electropherogram obtained with the analysis of precipitated mouse plasma is shown in Figure 1.

Compared to widely used chromatographic techniques, CE-MS, especially at very low EOF, suffers from a poorer migration time repeatability which can affect the statistical data analysis and, eventually, the identification of putative compounds of interest. Therefore, most of the available algorithms and software packages previously developed for LC-MS and routinely used for non-linear correction of retention times are usually not fully adapted to CE-MS data. Prior to subsequent data pre-processing and analysis, CE-MS data were thus aligned using a dedicated, in-house, and open source alignment tool, msalign2 (Nevedomskaya et al 2009).

The analytical consistency of the CE-MS workflow was evaluated *via* analysis of QCs composed of a pool of all samples repeatedly analyzed at regular intervals throughout the sequence runs (Dunn et al 2012, Naz et al 2014). To this end, a PCA model was built on the whole data set, i.e., 20 samples

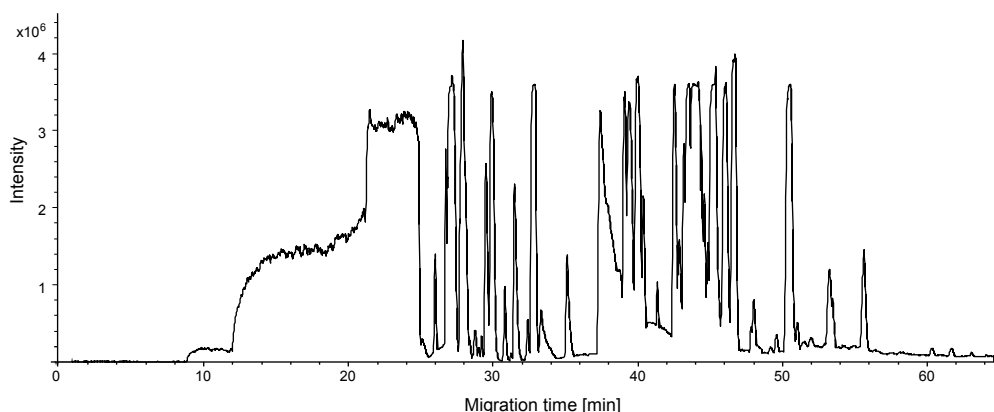


Figure 1: Base peak electropherogram obtained by CE-ESI-MS for the analysis of 25 nL of precipitated mouse plasma. See Section 2.5 for experimental conditions.

and all QCs. Four samples, i.e., two from the CSD and two from the sham group, were discarded prior to the data analysis as no satisfactory data were acquired due to instrumental issues. As shown by the score plot obtained for the first two principal components (covering 50% of the total variation) presented in Figure S2, the variation present in the group of mouse samples was much larger than the variation between QCs. The analytical variability was thus considered having a negligible influence on the data matrix. QCs were then removed from the data set for subsequent data analysis.

The initial PCA analysis of the entire data set did not show any trend or tendency relevant to the experimental design (data not shown). Thus, in order to dissect CSD-triggered differences in the metabolic composition of plasma samples of FHM1 R192Q mice in comparison to WT mice, the PCA models were built for sham and CSD mice separately (Figure 2). Visual inspection of the PCA plots revealed important differences between the models. Figure 2A presents the score-plot of the first two principal components for PCA obtained for the combined FHM1 R192Q and WT sham group where the samples were randomly distributed. This result was anticipated as no CSD event was induced in this group of mice. However, the PCA score plot obtained for the combined FHM1 R192Q and WT CSD group (Figure 2B) showed a clear trend in sample clustering. Two PLS-DA models (i.e., for sham and CSD groups) with WT and FHM1 R192Q mice as class identifiers were built to confirm these observations. As expected, the PLS-DA model built on sham samples proved to be statistically poor, while the statistical descriptors of the CSD data indicated a solid model ($\text{cum} = 0.417$, $\text{cum} = 0.996$, $\text{cum} = 0.712$). Figure 3A presents the cross-validated score-plot PLS-DA model built on CSD data. The metabolites responsible for this classification were highlighted by OPLS-DA regression and the derived S-plot (Figure 3B). The S-plot is a visualization method that combines the modelled covariance (X -axis) and modelled correlation (Y -axis) from the OPLS-DA on a scatter plot, allowing for pinpointing of interesting variables. The variables showing the highest p and p

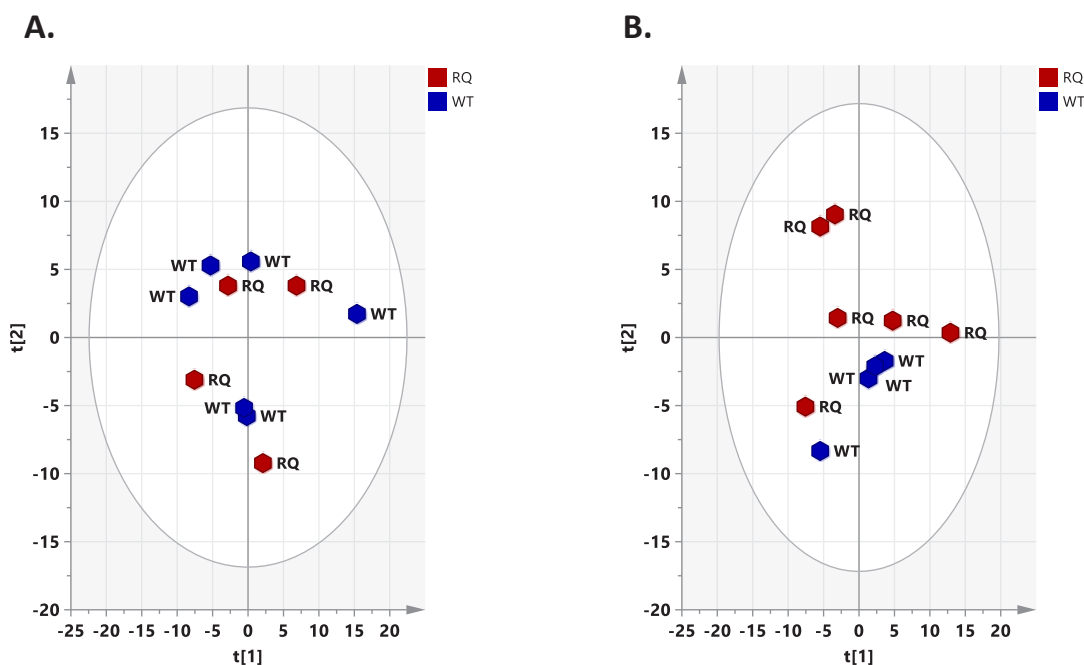


Figure 2: PCA score plots with experimental condition as a class identifier. (A) Sham-operated group and (B) CSD-operated group. Samples are colored according to their phenotype; RQ (red diamonds), plasma from transgenic mice carrying the FHM1 R192Q mutation; WT (blue diamonds), plasma from wild-type non-transgenic mice. t -scores represent the score vectors for the first ($t[1]$) and the second ($t[2]$) principal components after PCA. The first two principal components cover 48% and 42% of the total variability in (A) and (B), respectively.

(*corr*) values are considered the most relevant metabolites for the classification between samples. According to the S-plot and Variable Importance on Projection (VIP) values, two metabolites were ranked as the most important variables responsible for the separation between FHM1 R192Q and WT groups after CSD. The first metabolite (VIP value = 4.1), measured at m/z 130.0860 with a migration time of 14.5 min, showed a higher peak area in FHM1 R192Q group relative to WT controls, after CSD. Based on the monoisotopic mass, the isotope distribution, the nitrogen rule, the hydrogen/carbon ratio rule (Kind & Fiehn 2007), as well as research in METLIN Metabolite Search and HMDB public databases, this metabolite was tentatively identified as pipercolic acid ($C_6H_{11}NO_2$, exact m/z 130.0863, $\Delta = 2$ ppm), a non-protein imino acid. Another important metabolite responsible for the samples classification (VIP values = 1.1 and 2.1 for most abundant and second most abundant isotope, respectively), biochemically correlated to PA and detected at m/z 147.1128 with a migration time of 14.2 min was determined as being lysine ($C_6H_{14}N_2O_2$, exact m/z 147.1128, $\Delta = 0$ ppm), which showed a significantly lower peak area in FHM1 R192Q samples compared to WT after CSD. Figure 4 shows the box-plots constructed for both metabolites with integrated peak areas, highlighting the significant difference observed between FHM1 R192Q and WT plasma after CSD, with significantly higher peak areas for PA (Figure 4A) and lower areas for lysine (Figure 4B), respectively, in the FHM1 R192Q group compared to WT control.

Confirmatory analysis by HILIC-MS/MS

The use of an orthogonal analytical technique such as liquid chromatography, i.e., based on a different mechanism of separation than CE, as well as information on the fragmentation pattern *via* MS/MS experiments provides an additional confidence of the identification of both compounds (Sumner et al 2007). Contrary to widely used reversed-phase liquid chromatography, where a poor retention and selectivity are usually observed for metabolites analysis, the HILIC chromatographic mode is well-suited for the analysis of relatively polar compounds (Buszewski & Noga 2012, Hemstrom & Irgum 2006, Kohler & Guillarme 2014, Rainville et al 2014).

HILIC-MS/MS experiments were carried out on a QqQ mass analyzer with standard solutions of L-PA and L-lysine and naïve WT control mouse plasma. As the basal concentration of PA was observed to be relatively low in the plasma of WT mice, a sample preconcentration was necessary to reach the sufficient limit of detection for both compounds. The 20-fold preconcentration obtained with the developed PP-SPE procedure based on anion-exchange mechanism allowed for the detection of both

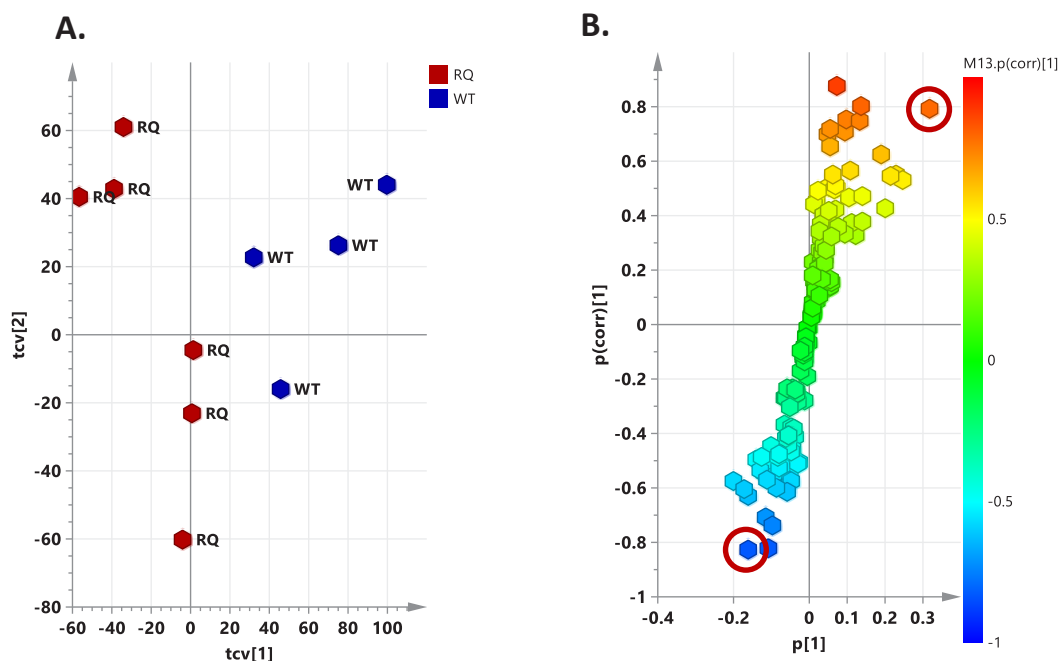


Figure 3: Cross-validated PLS-DA model and S-plot obtained from OPLS-DA regression. (A) Cross-validated PLS-DA model built on CSD sub-group with $\text{cum} = 0.417$, $\text{cum} = 0.996$, and $\text{cum} = 0.712$; samples are colored according to their phenotype; RQ (red diamonds), plasma from transgenic mice carrying the FHM1 R192Q mutation; WT (blue diamonds), plasma from wild-type non-transgenic mice. (B) S-plot obtained from OPLS-DA model. t -scores represent the cross-validated score vectors for the first (tcv[1]) and second (tcv[2]) principal components after cross-validated PLS-DA model.

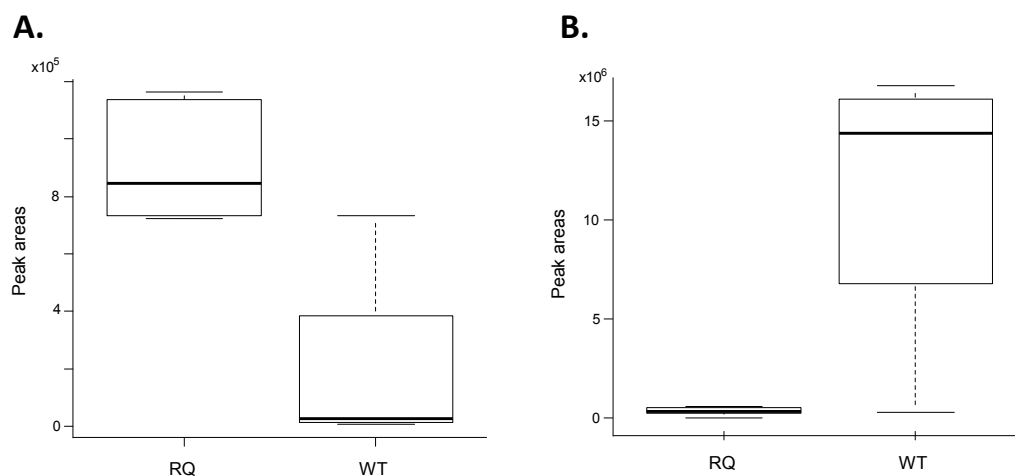


Figure 4: Box-plots displaying the differences in integrated peak areas observed for the two metabolites of interest after CSD events between the transgenic mice carrying the FHM1 R192Q mutation (labelled RQ) and the WT control group (labelled WT). Whiskers represent the standard deviation. (A) m/z 130.0860, corresponding to pipecolic acid. (B) m/z 147.1128, corresponding to lysine.

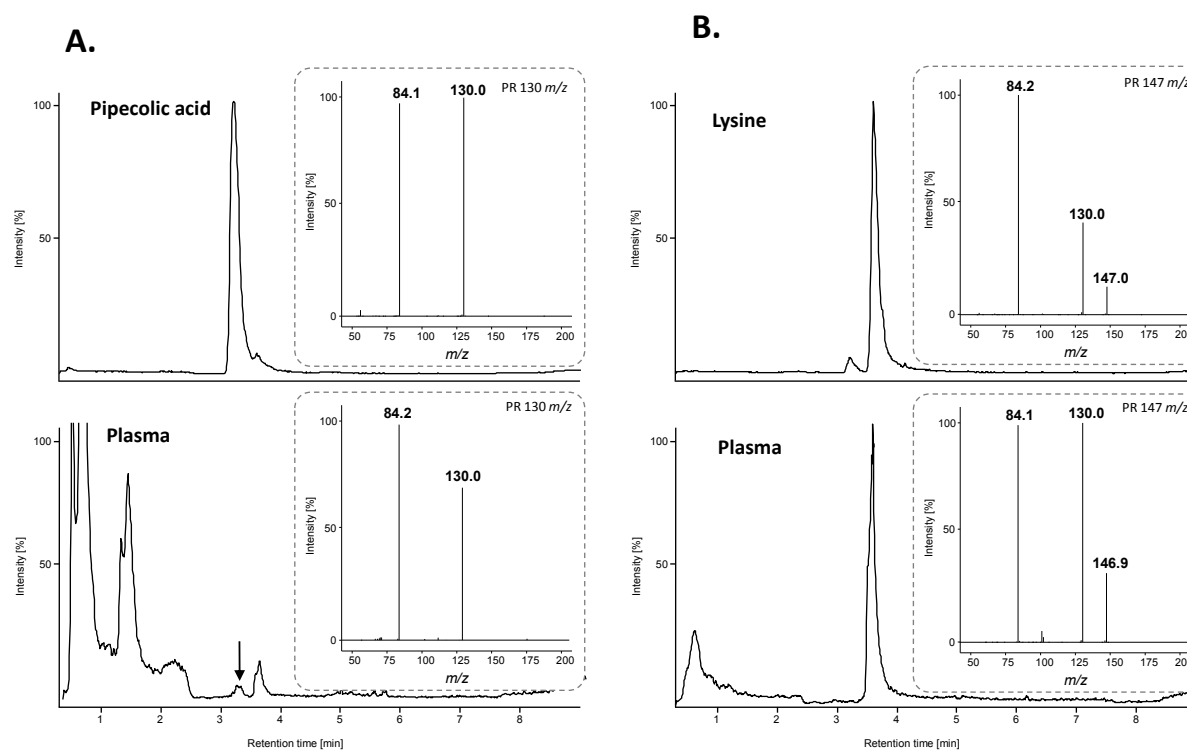


Figure 5: Extracted ion chromatograms (EICs) and MS/MS spectra obtained for both compounds for standard solutions at $100 \mu\text{g mL}^{-1}$ (upper EIC) and the prepared plasma sample (lower EIC). (A) Pipecolic acid, product ion (PR) MS/MS experiments on m/z 130. (B) Lysine, PR experiments on m/z 147. See Section 2.6 for experimental conditions.

compounds in plasma sample. Product ion scan (PR) mode, i.e., where the first quadrupole of the QqQ selects the parent ion(s) then fragmented in the collision cell prior to the detection of fragments in the third quadrupole operating in the full-scan mode, was used for MS/MS acquisition. Figure 5 shows the extracted ion chromatograms (EICs) obtained for PA (Figure 5A) and lysine (Figure 5B) in the plasma sample with their respective MS/MS spectra obtained with a collision of energy of 10 eV. The EICs obtained for m/z 130 and m/z 147 showed similar retention times for both compounds in plasma samples and standard solutions, i.e., 3.22 min and 3.61 min for PA and lysine, respectively. The identity of the compounds was confirmed by comparing the MS/MS spectra obtained for m/z 130 and m/z 147 in plasma sample *vs* standard spectra. The MS/MS spectrum observed for PA in plasma showed the molecular ion at m/z 130 as well as a fragment at m/z 84, which corresponds to the loss of the carboxyl functional group. The MS/MS spectrum of lysine showed the molecular ion at m/z 147 as well as fragments at m/z 130 and m/z 84. The fragment at m/z 130 is obtained with the loss of the secondary amine prior to cyclization of the molecule into PA (Argirov et al 2005) and, rationally, the subsequent loss of the carboxyl group to obtain the fragment at m/z 84. According to the Metabolomics Standards Initiative, a definitive (i.e., level 1) compound identification may be obtained by comparing two or more orthogonal properties (e.g., retention time, m/z ratio, fragmentation mass spectrum) of an authentic chemical standard *vs* the metabolite(s) of interest (Dunn et al 2013, Gika et al 2014). Due to the restricted sample volume available from mice, the orthogonal confirmatory analysis was performed on a WT material only. Therefore, additional studies may be required to increase the confidence in the identification of PA and lysine, although CE data usually provide a strong context for identification of amino acids, and lysine in particular.

Lysine and pipercolic metabolism and biological implications

In animals and humans, L-lysine has been shown to be predominantly metabolized to saccharopine (ϵ -[glutaryl-2]-L-lysine) in peripheral tissues, including liver and kidney, while the brain appears to mainly metabolize this amino acid to the intermediate of reaction L-PA. Both pathways lead to the formation of α -amino adipic semialdehyde (α -ASAA), α -amino adipic acid, and eventually acetyl-Co-A. The primary metabolic function of PA in human and mammals, however, is unknown. Nevertheless, PA was shown to be associated with several diseases, such as pyridoxine-dependent epilepsy, α -ASAA dehydrogenase deficiency, inherited peroxisomal disorders, and chronic liver dysfunction (Dalazen et al 2014, Sadilkova et al 2009).

Peroxisomal disorders are characterized by a defect in peroxisome formation, leading to a deficiency or little activity of the peroxisomal PA oxidase, the enzyme responsible for oxidation of PA. A significant elevation of L-PA plasma concentration (normal range 0.1-4.0 $\mu\text{mol L}^{-1}$) is observed and used for diagnosis purpose in combination with the determination of plasma very-long-chain fatty acids and plasmalogens (Peduto et al 2004, Poll-The & Gardner 2012, Stockler et al 2011).

Pyridoxine-dependent epilepsy (PDE) is a recessive inherited condition that affects the γ -aminobutyric acid (GABA) pathway and is characterized by epileptic seizures that are not controlled with antiepileptic

drugs but stop with administration of pharmacological doses of pyridoxine (vitamin B₆) (Baxter 2003, Plecko et al 2005, Stockler et al 2011). Due to α -ASAA dehydrogenase deficiency caused by pathogenic mutations in the *ALDH7A1* gene, elevated levels of α -ASAA are observed in plasma, CSF, and urine in patients with PDE. Increased concentrations of L-PA have also been observed in plasma (4.3 - 15.3 fold) and CSF (5.6 – 37.2 fold) of patients with PDE (Plecko et al 2000, 2005). *In vitro* experiments revealed that L-PA serves as a modulator of GABAergic neurotransmission by stimulating GABA release in the synaptic cleft, decreasing its uptake by the synaptosomes, and/or enhancing GABA_A receptor response likely by binding to another site on GABA_A receptor (Beitz & Larson 1985, Bernasconi et al 1986, Charles 1986, Gutierrez et al 1989, Kase et al 1980, Matsumoto et al 2003). PDE remains up to now the only paroxysmal episodic disorder for which a correlation between plasma PA concentrations and brain events has been shown.

To the best of our knowledge, this is the first time that the lysine degradation pathway is suggested to be involved in migraine pathophysiology. Any relevance for migraine mainly comes from the observation that changes in plasma levels of lysine and PA were different in FHM1 R192Q mutant vs WT control mice after CSD induction only, and not after sham treatment. The higher level of PA after CSD induction in FHM1 R192Q mutant may hypothetically point towards a compensatory mechanism to counteract the effect of excessive glutamatergic neurotransmission *via* an enhancement of inhibitory GABAergic synaptic transmission; perhaps to restore the imbalance in cortical excitatory-inhibitory transmission that occurs with CSD. In this scenario, increased GABAergic synaptic transmission may be an attempt of the brain to restore homeostasis. Increased GABAergic synaptic transmission may be the mere consequence of the excessive glutamatergic neurotransmission and subsequent activation of GABAergic neurons, without direct changes at the level of GABAergic transmission. Indeed, it has been already shown that the FHM1 R192Q mutation increases excitatory glutamatergic neurotransmission while having no effect on inhibitory GABAergic transmission (Tottene et al 2009). Enhanced glutamatergic neurotransmission was shown to underlie the increased susceptibility to CSD in FHM1 R192Q mutant mice (Tottene et al 2009). Finally, a proteomic analysis of synaptosomes from cortical neurons of FHM1 R192Q mutant mice showed compensatory up-regulation of glutamate transporters (Klychnikov et al 2010). These features seem to suggest that although GABAergic neurotransmission seems not primarily affected in FHM1 R192Q mice, it may kick in as part of the consequences of the enhanced excitatory transmission and may be involved in compensatory actions attempting to restore brain homeostasis, a hypothesis which would fit the episodic nature of migraine. This study also brings out that the mechanisms underlying CSD events can be captured beyond the CNS, for instance in plasma. It thus suggests that the investigation of metabolic changes in peripheral fluids may provide a useful strategy to monitor pathophysiological effects related to migraine that occur in the brain.

CONCLUDING REMARKS

This study investigated the metabolic profiling in the plasma of transgenic migraine mice carrying the FHM1 R192Q mutation and WT controls following induction of multiple CSD events. Plasma samples collected after CSD induction were analyzed by CE-MS and highlighted significant changes in the concentration of two metabolites in FHM1 R192Q mutant that were tentatively identified as lysine and PA. The relative changes of PA concentration observed in FHM1 mutant mice compared to WT are consistent with the previously shown correlation between PA and inhibitory GABAergic neurotransmission, which in theory may serve to counteract the neuronal excitability and promote homeostasis recovery upon CSD in FHM1 mutant mice. Notably, CSD events appear to induce a metabolic remodeling in peripheral fluids such as plasma. This opens new perspectives in the discovery of putative biomarkers in easily-accessible body fluids to improve the diagnosis and prognosis in migraine, as well as in proposing novel biomolecular targets for the development of new therapies. Further experiments are required to investigate the longitudinal evolution of the metabolic profile underlying CSD in peripheral fluids.

ACKNOWLEDGEMENTS

This work was financially supported by the Dutch Organization for Scientific Research, EU Marie Curie IAPP Program “BRAINPATH” (nr 612360) (A.M.J.M.v.d.M.), EU “EUROHEADPAIN” grant (nr 602633) (M.D.F., A.M.J.M.v.d.M), an LUMC Fellowship (E.A.T.), Marie Curie Career Integration Grant (nr 294233) (E.A.T.) and the Center of Medical System Biology (CMSB) established by the Netherlands Genomics Initiative (NGI)/NWO (A.M.J.M.v.d.M.). I.K. was a recipient of a fellowship (P2GEP3_155633) supported by the Swiss National Scientific Foundation. Jeff D. Chapman from Beckman Coulter/AB Sciex is acknowledged for the kind loan of CE-MS sheathless prototype and valuable discussions.

REFERENCES

- Argirov OK, Leigh ND, Ortwerth BJ. 2005. Specific MS/MS fragmentation of lysine, arginine, and ornithine glycation products provides an opportunity for their selective detection in protein acid hydrolysates and enzymatic digest. *Ann. N Y Acad. Sci.* 1043:903
- Baxter P. 2003. Pyridoxine-dependent seizures: a clinical and biochemical conundrum. *Biochim. Biophys. Acta* 1647:36-41
- Beitz AJ, Larson AA. 1985. Inhibition of intrathecally administered picrotoxin- and bicuculline-induced convulsions in mice by pipercolic acid or GABA. *Eur. J. Pharmacol.* 114:181-7
- Bernasconi R, Jones RS, Bittiger H, Olpe HR, Heid J, et al. 1986. Does pipercolic acid interact with the central GABA-ergic system? *J. Neural Transm.* 67:175-89
- Bonvin G, Schappler J, Rudaz S. 2012. Capillary electrophoresis-electrospray ionization-mass spectrometry interfaces: fundamental concepts and technical developments. *J. Chromatogr. A.* 1267:17-31
- Busnel JM, Schoenmaker B, Ramautar R, Carrasco-Pancorbo A, Ratnayake C, et al. 2010. High capacity capillary electrophoresis-electrospray ionization mass spectrometry: coupling a porous sheathless interface with transient-isotachopheresis. *Anal. Chem.* 82:9476-83
- Buszewski B, Noga S. 2012. Hydrophilic interaction liquid chromatography (HILIC)--a powerful separation technique. *Anal. Bioanal. Chem.* 402:231-47
- Charles AK. 1986. Pipercolic acid receptors in rat cerebral cortex. *Neurochem. Res.* 11:521-5
- Dalazen GR, Terra M, Jacques CE, Coelho JG, Freitas R, et al. 2014. Pipercolic acid induces oxidative stress in vitro in cerebral cortex of young rats and the protective role of lipoic acid. *Metab. Brain Dis.* 29:175-83
- Davies JA, Annels SJ, Dickie BG, Ellis Y, Knott NJ. 1995. A comparison between the stimulated and paroxysmal release of endogenous amino acids from rat cerebellar, striatal and hippocampal slices: a manifestation of spreading depression? *J. Neurol. Sci.* 131:8-14
- de Vries B, Frants RR, Ferrari MD, van den Maagdenberg AM. 2009. Molecular genetics of migraine. *Hum. Genet.* 126:115-32
- Dieterle F, Ross A, Schlotterbeck G, Senn H. 2006. Probabilistic quotient normalization as robust method to account for dilution of complex biological mixtures. Application in 1H NMR metabonomics. *Anal. Chem.* 78:4281-90
- Ducros A, Denier C, Joutel A, Cecillon M, Lescoat C, et al. 2001. The clinical spectrum of familial hemiplegic migraine associated with mutations in a neuronal calcium channel. *N. Engl. J. Med.* 345:17-24
- Dunn WB, Erban A, Weber RJM, Creek DJ, Brown M, et al. 2013. Mass appeal: metabolite identification in mass spectrometry-focused untargeted metabolomics. *Metabolomics* 9:S44-S66

- Dunn WB, Wilson ID, Nicholls AW, Broadhurst D. 2012. The importance of experimental design and QC samples in large-scale and MS-driven untargeted metabolomic studies of humans. *Bioanalysis* 4:2249-64
- Eikermann-Haerter K, Dilekoz E, Kudo C, Savitz SI, Waeber C, et al. 2009. Genetic and hormonal factors modulate spreading depression and transient hemiparesis in mouse models of familial hemiplegic migraine type 1. *J. Clin. Invest.* 119:99-109
- Ferrari MD, Klever RR, Terwindt GM, Ayata C, Van den Maagdenberg AM. 2015. Migraine pathophysiology: lessons from genetic mouse models and human genetics. *Lancet Neurol.* 14:65-80
- Gika HG, Theodoridis GA, Plumb RS, Wilson ID. 2014. Current practice of liquid chromatography-mass spectrometry in metabolomics and metabonomics. *J. Pharm. Biomed. Anal.* 87:12-25
- Goadsby PJ, Lipton RB, Ferrari MD. 2002. Migraine--current understanding and treatment. *N. Engl. J. Med.* 346:257-70
- Gursoy-Ozdemir Y, Qiu J, Matsuoka N, Bolay H, Berman D, et al. 2004. Cortical spreading depression activates and upregulates MMP-9. *J. Clin. Invest.* 113:1447-55
- Gutierrez MC, Delgado-Coello BA. 1989. Influence of pipercolic acid on the release and uptake of [3H]GABA from brain slices of mouse cerebral cortex. *Neurochem. Res.* 14:405-8
- Heemskerk AA, Busnel JM, Schoenmaker B, Derks RJ, Klychnikov O, et al. 2012. Ultra-low flow electrospray ionization-mass spectrometry for improved ionization efficiency in phosphoproteomics. *Anal. Chem.* 84:4552-9
- Hemstrom P, Irgum K. 2006. Hydrophilic interaction chromatography. *J. Sep. Sci.* 29:1784-821
- Hirayama A, Tomita M, Soga T. 2012. Sheathless capillary electrophoresis-mass spectrometry with a high-sensitivity porous sprayer for cationic metabolome analysis. *Analyst* 137:5026-33
- Hirayama A, Wakayama M, Soga T. 2014. Metabolome analysis based on capillary electrophoresis-mass spectrometry. *TrAC* 61:215-22
- ICHD. 2004. The International Classification of Headache Disorders: 2nd edition. *Cephalalgia* 24 Suppl 1:9-160
- Karatas H, Erdener SE, Gursoy-Ozdemir Y, Lule S, Eren-Kocak E, et al. 2013. Spreading depression triggers headache by activating neuronal Panx1 channels. *Science* 339:1092-5
- Kase Y, Takahama K, Hashimoto T, Kaisaku J, Okano Y, Miyata T. 1980. Electrophoretic study of pipercolic acid, a biogenic imino acid, in the mammalian brain. *Brain Res.* 193:608-13
- Kind T, Fiehn O. 2007. Seven Golden Rules for heuristic filtering of molecular formulas obtained by accurate mass spectrometry. *BMC Bioinformatics* 8:105
- Klychnikov OI, Li KW, Sidorov IA, Loos M, Spijker S, et al. 2010. Quantitative cortical synapse proteomics of a transgenic migraine mouse model with mutated Ca(V)2.1 calcium channels.

Proteomics 10:2531-5

- Kohler I, Guillarme D. 2014. Multi-target screening of biological samples using LC-MS/MS: focus on chromatographic innovations. *Bioanalysis* 6:1255-73
- Kohler I, Schappler J, Rudaz S. 2013. Highly sensitive capillary electrophoresis-mass spectrometry for rapid screening and accurate quantitation of drugs of abuse in urine. *Anal. Chim. Acta* 780:101-9
- Kok MGM, Somsen GW, de Jong G. 2014. The role of capillary electrophoresis in metabolic profiling studies employing multiple analytical techniques. *TrAC* 61:223-35
- Lionetto L, Gentile G, Bellei E, Capi M, Sabato D, et al. 2013. The omics in migraine. *J. Headache Pain* 14:55
- Matsumoto S, Yamamoto S, Sai K, Maruo K, Adachi M, et al. 2003. Pipecolic acid induces apoptosis in neuronal cells. *Brain Res.* 980:179-84
- Moini M. 2007. Simplifying CE-MS operation. 2. Interfacing low-flow separation techniques to mass spectrometry using a porous tip. *Anal. Chem.* 79:4241-6
- Naz S, Vallejo M, Garcia A, Barbas C. 2014. Method validation strategies involved in non-targeted metabolomics. *J. Chromatogr. A.* 1353:99-105
- Nevedomskaya E, Derks R, Deelder AM, Mayboroda OA, Palmblad M. 2009. Alignment of capillary electrophoresis-mass spectrometry datasets using accurate mass information. *Anal. Bioanal. Chem.* 395:2527-33
- Nevedomskaya E, Ramautar R, Derks R, Westbroek I, Zondag G, et al. 2010. CE-MS for metabolic profiling of volume-limited urine samples: application to accelerated aging TTD mice. *J. Proteome Res.* 9:4869-74
- Ophoff RA, Terwindt GM, Vergouwe MN, van Eijk R, Oefner PJ, et al. 1996. Familial hemiplegic migraine and episodic ataxia type-2 are caused by mutations in the Ca²⁺ channel gene CACNL1A4. *Cell* 87:543-52
- Peduto A, Baumgartner MR, Verhoeven NM, Rabier D, Spada M, et al. 2004. Hyperpipecolic acidemia: a diagnostic tool for peroxisomal disorders. *Mol. Genet. Metab.* 82:224-30
- Plecko B, Hikel C, Korenke GC, Schmitt B, Baumgartner M, et al. 2005. Pipecolic acid as a diagnostic marker of pyridoxine-dependent epilepsy. *Neuropediatrics* 36:200-5
- Plecko B, Stockler-Ipsiroglu S, Paschke E, Erwa W, Struys EA, Jakobs C. 2000. Pipecolic acid elevation in plasma and cerebrospinal fluid of two patients with pyridoxine-dependent epilepsy. *Ann. Neurol.* 48:121-5
- Poll-The BT, Gartner J. 2012. Clinical diagnosis, biochemical findings and MRI spectrum of peroxisomal disorders. *Biochim. Biophys. Acta* 1822:1421-9
- Rainville PD, Theodoridis G, Plumb RS, Wilson ID. 2014. Advances in liquid chromatography coupled to mass spectrometry for metabolic phenotyping. *TrAC* 61:181-91

- Ramautar R, Shyti R, Schoenmaker B, de Groote L, Derks RJ, et al. 2012. Metabolic profiling of mouse cerebrospinal fluid by sheathless CE-MS. *Anal. Bioanal. Chem.* 404(10):2895-900
- Sadilkova K, Gospe SM, Jr., Hahn SH. 2009. Simultaneous determination of alpha-aminoadipic semialdehyde, piperidine-6-carboxylate and pipercolic acid by LC-MS/MS for pyridoxine-dependent seizures and folinic acid-responsive seizures. *J. Neurosci. Methods* 184:136-41
- Smith CA, O'Maille G, Want EJ, Qin C, Trauger SA, et al. 2005. METLIN: a metabolite mass spectral database. *Ther. Drug Monit.* 27:747-51
- Smith CA, Want EJ, O'Maille G, Abagyan R, Siuzdak G. 2006. XCMS: processing mass spectrometry data for metabolite profiling using nonlinear peak alignment, matching, and identification. *Anal. Chem.* 78:779-87
- Somjen GG. 2001. Mechanisms of spreading depression and hypoxic spreading depression-like depolarization. *Physiol. Rev.* 81:1065-96
- Stockler S, Plecko B, Gospe SM, Jr., Coulter-Mackie M, Connolly M, et al. 2011. Pyridoxine dependent epilepsy and antiquitin deficiency: clinical and molecular characteristics and recommendations for diagnosis, treatment and follow-up. *Mol. Genet. Metab.* 104:48-60
- Sumner LW, Amberg A, Barrett D, Beale MH, Beger R, et al. 2007. Proposed minimum reporting standards for chemical analysis Chemical Analysis Working Group (CAWG) Metabolomics Standards Initiative (MSI). *Metabolomics* 3:211-21
- Tautenhahn R, Bottcher C, Neumann S. 2008. Highly sensitive feature detection for high resolution LC/MS. *BMC Bioinformatics* 9:504
- Tottene A, Conti R, Fabbro A, Vecchia D, Shapovalova M, et al. 2009. Enhanced excitatory transmission at cortical synapses as the basis for facilitated spreading depression in Ca(v)2.1 knockin migraine mice. *Neuron* 61:762-73
- van den Maagdenberg AM, Haan J, Terwindt GM, Ferrari MD. 2007. Migraine: gene mutations and functional consequences. *Curr. Opin. Neurol.* 20:299-305
- van den Maagdenberg AM, Pietrobon D, Pizzorusso T, Kaja S, Broos LA, et al. 2004. A Cacna1a knockin migraine mouse model with increased susceptibility to cortical spreading depression. *Neuron* 41:701-10
- Wishart DS, Knox C, Guo AC, Eisner R, Young N, et al. 2009. HMDB: a knowledgebase for the human metabolome. *Nucleic Acids Res.* 37:D603-10
- Zhang X, Levy D, Kainz V, Nosedá R, Jakubowski M, Burstein R. 2011. Activation of central trigeminovascular neurons by cortical spreading depression. *Ann. Neurol.* 69:855-65

SUPPLEMENTARY INFORMATION

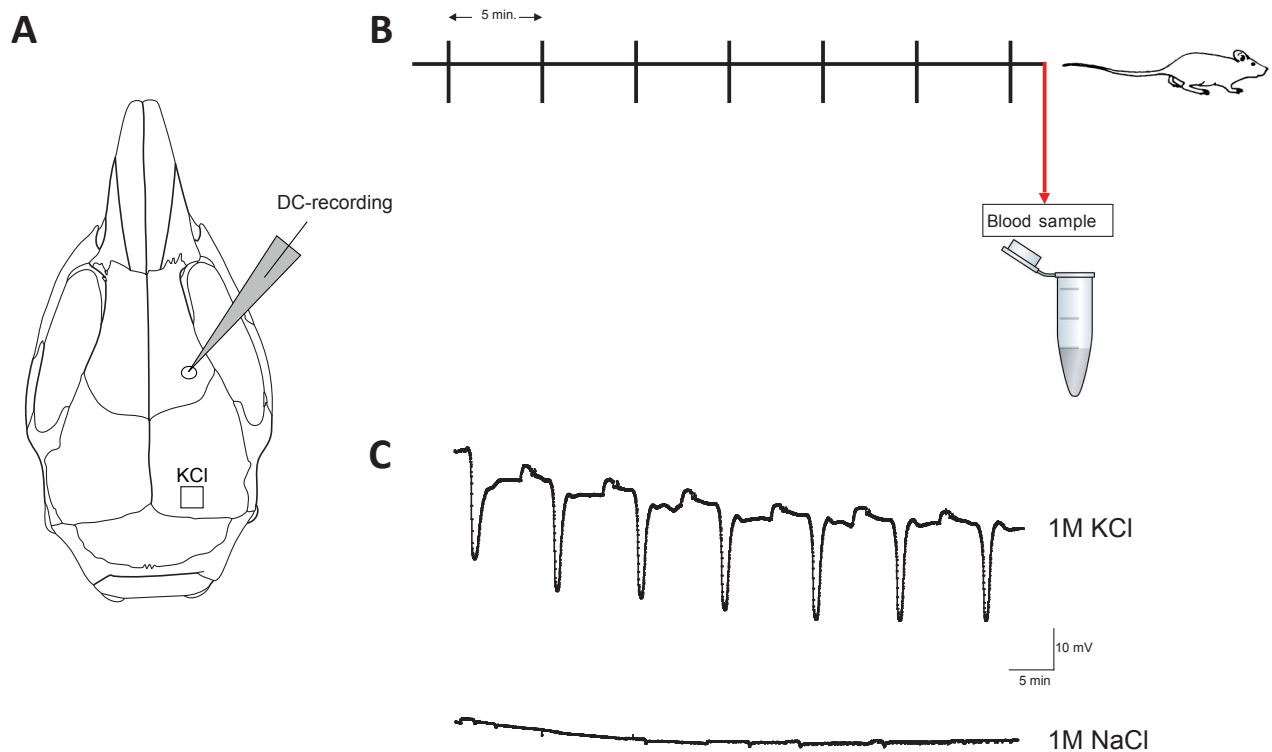


Figure S1. Illustration of the experimental design. (A) Mouse skull depicting the locations of KCl application (i.e., occipital cortex) and DC-potential recordings (i.e., frontal cortex). (B) Induction of 7 CSDs by application of 1M KCl with a 5-min interval. At the end of the CSD induction, *ca.* 40 μ L of blood was collected from the mouse trunk. (C) Specimen example traces recordings following application of 1M KCl (upper part) and 1M NaCl (lower part) in FHM1 R192Q and WT mice.

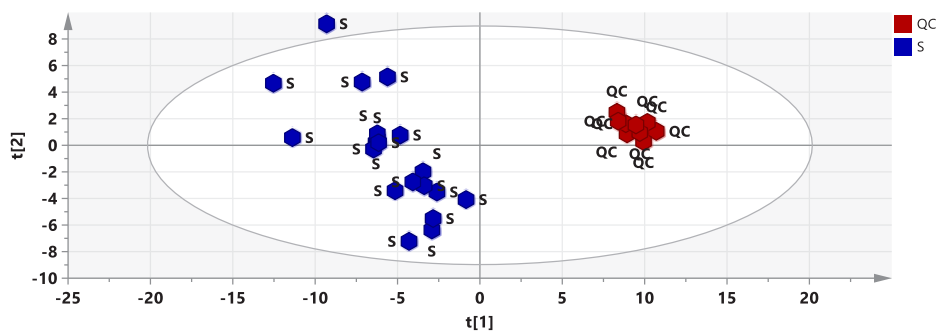
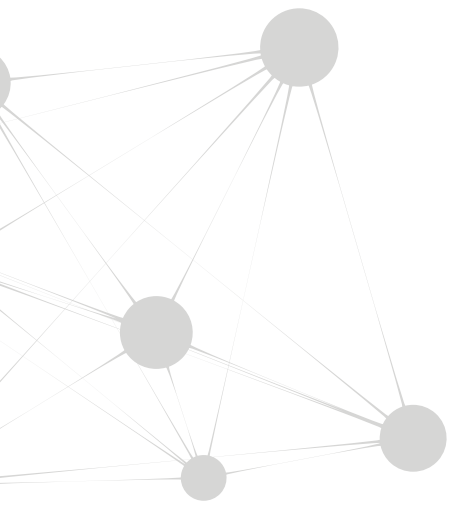
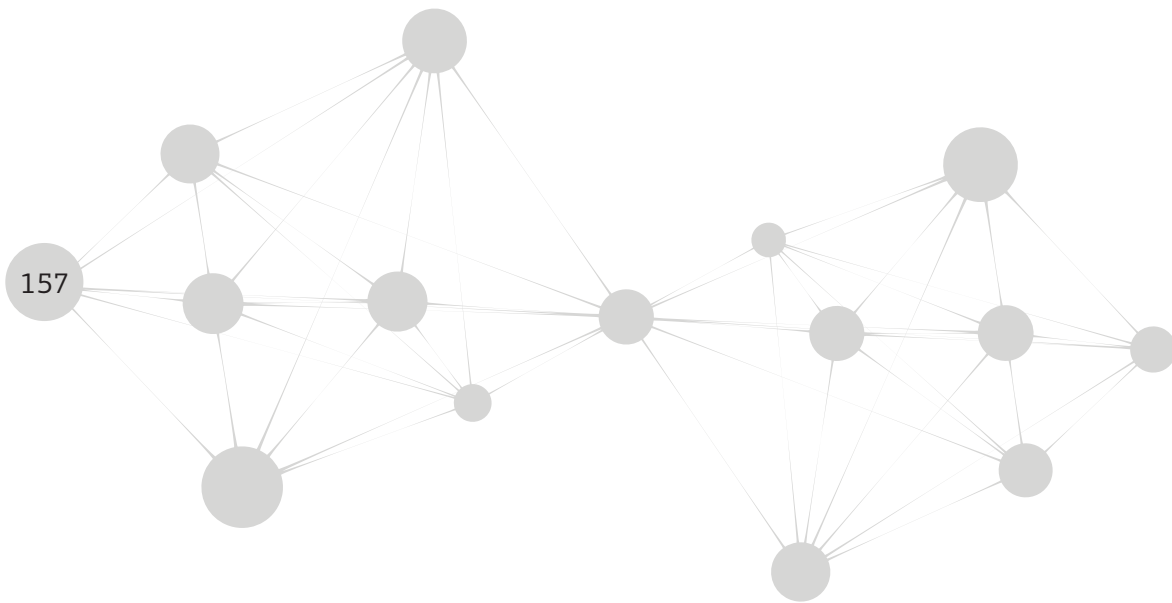


Figure S2. PCA score plot of the whole data set, including mice samples (labelled S, blue diamonds) and quality controls (labelled QC, red diamonds). The first two principal components cover 50% of the total variation.



Chapter 8

General discussion



Migraine is a common brain disorder that is characterized by attacks of severe unilateral headaches and associated neurological symptoms. In about one third of patients, attacks are accompanied by an aura that is likely caused by cortical spreading depression (CSD). In this thesis, transgenic FHM1 R192Q mice were used as a relevant migraine model to investigate mechanisms underlying the effects of CSD modulating factors, as well as the consequences of CSD (Figure 1). FHM1 mice carry an R192Q missense mutation in the α_1 subunit of voltage-gated $\text{Ca}_v2.1$ channels (van den Maagdenberg et al 2004), which was previously identified in patients with familial hemiplegic migraine (Ophoff et al 1996). The experimental approaches and outcomes as described in the chapters of this thesis are discussed below, also in relation to relevant literature and with a look forward to future research.

8.1 Should CSD susceptibility measurements be performed in anesthetized or in freely behaving mice?

Technical progress has made it possible to investigate CSD in relation to cortical activity and behavior in freely behaving animals. Nevertheless, for certain research questions anesthesia can be the preferred regime. Possibilities and caveats of performing experiments under anesthesia and in freely behaving animals were investigated in various chapters of this thesis and are discussed in the paragraphs below.

8.1.1 CSD studies under anesthesia

Under anesthesia, CSD induction and monitoring are technically easier to control than in the longitudinal chronic recordings lasting days-weeks in freely behaving mice. Anesthesia was used for experiments where a fixed number of CSD events was induced by topical KCl application on the dura to study modulatory factors and consequences of CSD, in **Chapters 5, 6 and 7**. The possibility to precisely time CSD events is a great advantage when administering drugs/modulators, as performed for stress modulators in experiments described in **Chapter 4**. Moreover, when drugs are administered under anesthesia, stress and discomfort of the mice is avoided to a large extent. A drawback, however, is that anesthetics affect critical parameters of animal physiological status, such as blood pressure (BP), blood gases and pH, in particular during long-duration experiments. Changes in these parameters are known to affect properties of brain tissue that are relevant to initiate and sustain CSD (Somjen 2001). The implementation of *physiological monitoring* in **Chapter 2** yields important information on physiological parameters in relation to CSD characteristics, and makes possible the exclusion of animals in which physiological parameters are out-of-range. The use of *physiological control* by adjusting breathing patterns by mechanical ventilation is superior to the use of monitoring alone in the sense that it ensures a more comparable physiological status between mice; especially when experimental designs are used in which anesthesia last longer. Physiological control was performed for experiments to assess effects of gender (**Chapter 2**), diurnal rhythm (**Chapter 3**) and stress hormone (**Chapter 4**). Physiological control may however influence CSD characteristics and can sometimes act as a double-edged sword. By keeping physiological parameters within tight ranges, these parameters are kept comparable across experiments. However, if the experimental

readout itself *depends* on differences in physiological parameters, controlling them will logically interfere with the experimental outcome. This is illustrated in **Chapter 2**, in which the increased CSD frequency in female compared with male FHM1 R192Q mice, as reported by Eikermann-Haerter et al. (Eikermann-Haerter et al 2009b), was only revealed in the presence of physiological control. In an opposite way, in **Chapter 3**, physiological control appeared to mask a putative effect of a difference in CSD susceptibility between the visual and motor cortex in mutant mice; an effect that was observed *only* when experiments were performed in an uncontrolled and non-monitored manner (**Chapter 2**). Since anesthetics suppress neuronal activity (Hertle et al 2013), CSD and its characteristics will be affected by anesthetics, and in many instances masked. Common anesthetics such as isoflurane, which is used in the CSD experiments of this thesis, in particular in combination with N₂O (used in CSD experiments under full physiological control described in **Chapters 2, 3 and 4**) are known to suppress CSD susceptibility (Kudo et al 2013, Takagaki et al 2014). Anesthesia may also directly interfere with the experimental intervention, e.g., when studying effects of drugs that influence GABAergic function, which is known to be modulated by many anesthetics (Hoffmann et al 2011). There seems to be no ideal anesthetic to investigate the susceptibility of CSD.

8.1.2 CSD studies in freely behaving mice

Studying CSD characteristics in freely behaving mice can overcome some of the disadvantages of studies under anesthesia. Since both autonomous and central functions are retained, the physiology and brain functions of the mouse are more likely to mimic the situation in patients. With chronic implantation of miniaturized electrodes and a counter-balanced EEG/MUA-cable with swivel, it has been possible to record both EEG and MUA activity from the cortex with minimal discomfort to the mouse for multiple days to weeks (**Chapter 3**). Such recordings in freely behaving mice enable correlations between CSD characteristics and changes in neuronal network activity, vigilance states and other behavioral characteristics that are not possible under anesthesia. In rats, a similar awake electrophysiology approach has been used to correlate induced events of spreading depression to migraine-relevant pain pathways (Fioravanti et al 2011, Tepe et al 2015) and epilepsy (Broberg et al 2014). Our studies in **Chapter 3** show that the freely behaving approach is now also feasible in mice. Thus, we could demonstrate the occurrence of spontaneous CSD events in FHM1 R192Q mice, which were not observed in WT mice. Studies on spontaneous CSD events in freely behaving mice will allow investigating how natural triggers and modulatory factors of migraine (e.g., changes in sleep patterns, stress, and light) affect CSD susceptibility, thus enabling better translation of observations from and to the clinic. Because recordings are possible for several days to weeks, multiple trigger paradigms and modulators can be studied in a single animal. This include the possibility for intra-individual vehicle controls and assessment of repeatability.

However, experiments in awake, freely behaving mice have also disadvantages. Chronic electrode implantation can cause variation among animals with respect to electrode depth and location. Furthermore, an inflammatory response of the brain to chronic electrode implantation (as discussed

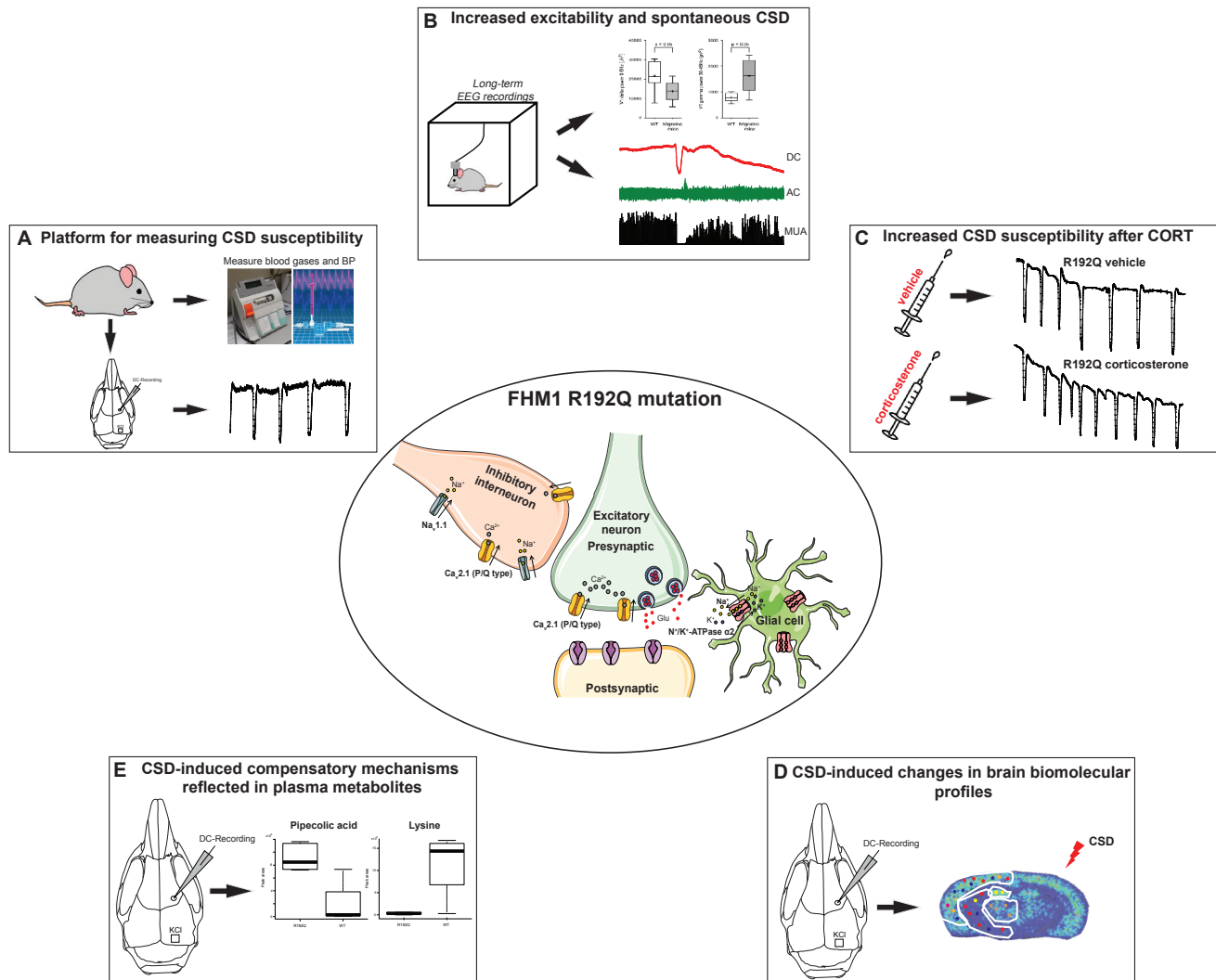


Figure 1. Overview of key experimental findings in FHM1 R192Q mice described in this thesis. (Center) FHM1 R192Q gain-of-function mutation increases neuronal Ca²⁺ influx via P/Q-type Ca_v2.1 Ca²⁺ channels that leads to increased release of excitatory neurotransmitters in the synaptic cleft. (A) We established an experimental platform to measure CSD susceptibility in anesthetized mice under continuous monitoring and control of critical physiological parameters, such as blood pressure and blood gases (**Chapter 2**). (B) In awake freely moving mice, long-term EEG recordings revealed increased cortical excitability and spontaneous CSD events in a subgroup of FHM1 R192Q mice but not in WT (**Chapter 3**). (C) Corticosterone injection in FHM1 R192Q mice increased CSD susceptibility compared to vehicle injection, via a GR-mediated mechanism (**Chapter 4**). (D) CSD induction resulted in changes of metabolite, peptide and protein distribution in the cortex and subcortical brain areas that were genotype-and CSD-specific (**Chapter 6**). (E) CSD induction in the cortex of FHM1 R192Q mice triggered an activation of compensatory mechanisms likely to restore inhibition/excitation imbalance that occurred following CSD and this could be measured in plasma (**Chapter 7**).

in **Chapter 3**) may affect CSD characteristics (Sukhotinsky et al 2011). Another difficulty with experiments in awake mice is that implanted electrodes and the EEG cable may increase levels of stress hormones, which can affect CSD characteristics (**Chapter 4** and see **Section 10.2.3**). What remains challenging as well is to standardize CSD induction paradigms in freely behaving animals. This is illustrated by the KCl infusion paradigm used in **Chapter 3**, which does not induce a single CSD but multiple CSD events with high variability. Due to their larger size, and willingness to be handled, it is easier to overcome such problems in rats when an implanted cannula for KCl infusion is used (Fioravanti et al 2011, Tepe et al 2015). The strength of an experimental CSD design lies in overcoming technical disadvantages by the integration of experimental platforms for the induction and monitoring of CSD that either use or do not use anesthesia, as illustrated in **Chapter 3**. Finally, the advent of novel technologies for modulation of neuronal activity, such as optogenetics (Williams & Deisseroth 2013), is expected to overcome at least some of the disadvantages thus far associated with chronic recordings. This is well illustrated by the recent implementation of optogenetics for induction of CSD in freely behaving mice (Tolner et al 2015).

8.2 Factors that modulate CSD susceptibility

8.2.1 Gender

It is well established that women are more susceptible to migraine than men (Finocchi & Strada 2014, Lipton et al 2001). The higher frequency of experimentally induced CSD events observed for female FHM1 R192Q mice in experiments with physiological control (**Chapter 2**) is in line with previous data (Eikermann-Haerter et al 2009b). A potential underlying mechanism for the higher CSD susceptibility in female mice (and the female preponderance of migraine) may be the response to female gonadal hormones changes (Borsook et al 2014). It is hypothesized that a sudden drop in estradiol level just before the start of menstruation (Somerville 1972a, Somerville 1972b) is involved in initiating attacks. This drop may lead to direct enhancement of glutamatergic neuronal excitability via up-regulation of NMDA receptor expression, down-regulation of glutamate uptake by astrocytes, and increasing the dendritic spine number (Kelly et al 2003, Sato et al 2003, Smith 1989, Woolley et al 1997). Vascular changes may also be involved in the effect of female hormones on CSD frequency in FHM1 R192Q mice. This is supported by the observation that a gender effect was only noticed in mutant mice when mechanical ventilation was performed and thus physiological parameters were controlled. A gender effect remained masked in physiologically monitored but not controlled mice that had a lower blood pressure (**Chapter 2**). It is known that mechanical ventilation can reduce brain blood volume and blood flow (Milan et al 2009), which in turn may have affected CSD characteristics (Ayata 2013). In addition, direct changes in vascular function may occur in relation to gender, since estradiol was shown to alter vascular responses to calcitonin gene-related peptide (CGRP) (Gupta et al 2007). In this context it is plausible that different neurovascular responses between physiologically controlled and uncontrolled experiments in female mice may be the reason that a gender effect on CSD frequency was observed only in the presence of physiological control. This gender effect in

mutant mice was detected irrespective of the phase in the estrous cycle, as mice were not investigated at a specific phase in the cycle (**Chapter 2** and Eikermann-Haerter et al 2009b), which suggests that the increased CSD susceptibility in female mutant mice may in fact be due to intrinsic brain differences between females and males (Borsook et al 2014) and perhaps less to a sudden drop in estrogen level during a phase of the cycle.

8.2.2 Diurnal changes

Observations that sleep (Holland 2014) and hypothalamic function (Moulton et al 2014) are linked to migraine support the idea that attacks may be influenced by diurnal rhythm (Fox & Davis 1998). Analysis of 24-hr EEG periods in freely behaving FHM1 R192Q mice in **Chapter 3** revealed an increased EEG gamma power, which had been related to increased neuronal excitability (Joho et al 1999, Lau et al 2000). This finding fits earlier data that excessive neuronal excitability underlies the increased susceptibility to CSD in these mutant animals (Tottene et al 2009). The idea of hyperexcitability has been proposed as a mechanism underlying migraine attack susceptibility in humans (Aurora & Wilkinson 2007). Notably, we could show that a subset of FHM1 R192Q, but not WT mice showed spontaneous (i.e., not experimentally-triggered) CSD events. The majority of the spontaneous CSD events occurred within 2 hr in the transition from *dark-to-light* or from *light-to-dark* phases in the animal facility. Paradoxically, results of parallel experiments, performed under anesthesia with physiological control, seem to rule out that CSD susceptibility is specifically increased at the start of the light or the dark phase. It cannot however be excluded that the anesthesia or mechanical ventilation used in the experiments may have caused changes in the animal's physiology that mask a putative diurnal difference in CSD susceptibility. Further studies are needed to assess whether, in addition to the overall increase in EEG gamma power, other changes may be detected from EEG recordings that are present before or during these diurnal transitions that can be related to changes in cortical excitability.

We hypothesize that diurnal fluctuations in hormones and neurotransmitters that occur around these transitions may contribute to changes in neuronal excitability leading to CSD events. It is tempting to speculate that the high level of corticosterone that is present at *the beginning of the dark period* (Maywood et al 2007) may correlate with an enhanced CSD susceptibility at that time point. Notably, adenosine, a neuromodulator that induces sleep and decreases neuronal excitability (Nehlig et al 1992), exhibits a diurnal pattern opposite to that of corticosterone, with high levels at *the beginning of the light period* (and low levels at *the beginning of the dark period*) (Basheer et al 2004). FHM1 R192Q mice were reported to be less sensitive to exogenous modulation of adenosinergic inhibition and exhibit an increase of waking episodes during the dark period (Deboer et al 2013). One can therefore rationalize that a reduction in inhibitory adenosinergic response in mutant animals can lead to transiently enhanced neuronal excitability leading to enhanced CSD susceptibility, particularly when adenosine levels are high, i.e., at the beginning of the light period.

8.2.3 Stress

The majority of migraine patients report stress as a prominent trigger for their migraine attacks (Hauge et al 2011), although one might argue that such self-reported information is not very reliable. As stress is a complex response of the body and involves multiple neurotransmitters and hormones with different dynamics, it is not known which aspects of the body's stress response, if any at all, may bring about migraine attacks. In **Chapter 4**, we could show that administration of stress hormone corticosterone (cortisol in humans) specifically increased CSD frequency in FHM1 R192Q mice and that this occurred via a glucocorticoid receptor-mediated mechanism. Given that corticosterone had no effect in WT mice, and it is thought to increase glutamatergic neurotransmission (Popoli et al 2011), suggest that corticosterone may have further enhanced the already present intrinsically enhanced (glutamatergic) excitability in FHM1 mice (Tottene et al 2009). It is tempting to speculate that in freely behaving mice, external triggers such as sensory inputs (e.g., light, sound) may cause enhanced levels of corticosterone (Ishida et al 2005, Kim et al 2008) and thereby enhanced excitation of thalamo-cortical pathways (Noseda et al 2010). The combined sensory input and intrinsically enhanced neuronal excitability in FHM1 R192Q mice may result in spontaneous CSD events, as described in **Chapter 3**.

Effects of natural stressors on CSD susceptibility seem harder to identify since exposure of FHM1 R192Q mice to mild or even severe restraint stress did not seem to affect CSD susceptibility. In **Chapter 4**, we provide evidence that such lack of an effect is not simply due to suppressive actions of neuromodulators such as tetrahydrodeoxycorticosterone, which like corticosterone is released during restraint stress. Although corticosterone levels rise both after exogenous administration and as a consequence of acute stress, the latter triggers a much more complex response with effects that may either enhance or suppress CSD susceptibility.

It is speculated that in patients the recovery from chronic stress, and not so much from acute stress, triggers a migraine attack (Lipton et al 2014). The concept of a 'rebound' effect after stress refers to the emergence of a stress effect following a period of recovery after chronic exposure to a stressor or after chronic glucocorticoid administration. While acute stress has been shown to induce analgesia, thus having anti-nociceptive effects, effects of chronic stress or chronically elevated glucocorticoid levels appear less predictable (McEwen & Kalia 2010). The direct effect of chronic administration of glucocorticoids in rats was an increase in pain threshold (Pinto-Ribeiro et al 2009). This observation is in line with studies in chronically stressed patients that suffer from chronic back pain, which reported less pain in a series of pain tests in comparison to healthy controls (Clark et al 1986). However, children that were chronically stressed due to abdominal pain (Dufton et al 2008) were reported to exhibit an increased reaction to a pain test (i.e., hyperalgesia). The variable results of chronic stress studies may relate to a rebound-after-stress effect, either because of fluctuations in stress levels in patients or because of different time-points after chronic stress at which readout effects were measured. In a study in which rats were measured 24 hr following exposure to chronic stress, the pain threshold

was shown to be reduced (Gamaro et al 1998). In line with the variable reports of chronic stress effects on pain, effects of chronic stress on glutamatergic transmission are also variable with studies indicating both enhancement (Kerr et al 1991, Joëls et al 2004, Raudensky & Yamamoto 2007) and suppression (Moghaddam 2002, Yuen et al 2012) of glutamatergic transmission following chronic stress. The variation in outcome may relate to differences in the studied brain regions, with e.g., the prefrontal cortex showing a reduction and hippocampal regions typically showing an enhancement of glutamatergic function (Joëls et al 2007, Yuen et al 2012). In these experimental studies on chronic stress, measurements were performed directly after the chronic stress paradigm, and did not provide information on glucocorticoid levels *at the end* of the chronic stress paradigm. Taken together, thus far, not much is known about mechanisms that could explain a possible rebound effect of (chronic) stress on triggering a migraine attack.

To gain insight into the rebound-after-stress phenomenon, we performed pilot experiments to investigate whether a time-delay after chronically elevated corticosterone levels affects CSD susceptibility (Figure 2). In brief, male WT and FHM1 R192Q mice were implanted with corticosterone or control pellets for a time period of 21 days. After the 3-week period, the pellet was removed and CSD frequency was tested either directly (on day 21) or 4 or 7 days later, at days 25 or 28 respectively (Figure 2A). High corticosterone plasma levels were shown to be maintained for 21 days when corticosterone pellets were implanted. After pellet removal at day 21, corticosterone plasma levels were decreased by day 28 in WT, but not in FHM1 R192Q mice in which corticosterone levels were found to remain high (Figure 2B). At none of the chosen time points after the 3-week corticosterone treatment however, CSD frequency was different in either WT or FHM1 mice in comparison to the respective frequency in naïve WT and FHM1 R192Q mice (Figure 2C, D). These preliminary findings suggest that a chronic elevation of systemic corticosterone levels followed by withdrawal is not a sufficient trigger to modulate CSD susceptibility. Since corticosterone levels remained elevated for several days after pellet removal in FHM1 R192Q mice, the rebound-after-stress paradigm may not have been sufficient to modulate CSD susceptibility. One may need to first determine the time point when corticosterone plasma levels show the steepest decline, and then assess CSD susceptibility around this transition point.

In this context, our findings raise an important issue regarding the translation of observations on the time-relationship between stress and migraine in humans to the time-line of stress paradigms in mice. In humans, a decline in perceived stress was recently shown to correlate with an increased probability to experience a migraine attack in the subsequent 6, 12 and 18 hr (Lipton et al 2014). In our study, corticosterone plasma levels were still elevated several days after corticosterone pellet removal, more so in R192Q mice. Although no information was available on cortisol levels in the human study, it is possible that the dynamics of the stress response differs between humans and mice. Alternatively, it may be that recovery from chronically elevated levels of glucocorticoids is less relevant as a stress factor in migraine, if adaptation occurs in the period of chronic stress or in the period of recovery. In an animal model, after 3 weeks of daily restraint, adaptation was shown to occur as evidenced from

plasma corticosterone levels that were no longer elevated (Joëls et al 2007). Overall, it is important to emphasize the complexity of physiological responses to chronic exposure to stress and glucocorticoids (Borsook et al 2012, Maleki et al 2012, Resmini et al 2013), some of which may cause compensatory effects at the level of neuronal excitation and CSD susceptibility.

8.3 Insight in migraine pathophysiology from investigating modulators of CSD

Better insight in the modulating effects of e.g., female hormones, diurnal or circadian rhythm and stress on CSD susceptibility can give mechanistic insight in the interaction of various neurobiological systems relevant to migraine. Enhanced susceptibility to various migraine modulators, e.g., sleep, food intake and anxiety, which affect various neurochemical pathways, seem to converge at the level of thalamus (Nosedá et al 2014). In addition, intrinsic differences in neuronal network excitability properties in specific brain regions may render the migraine brain more susceptible to attacks. As an example, neuroimaging studies have shown structural and functional alterations in the visual cortex of migraineurs (Aurora et al 1999, Granziera et al 2006), which may have relevance to explain the clinical observation that the far majority of migraine auras are visual (Eriksen et al 2005). Certain experiments in **Chapter 2** seem to indicate that in FHM1 R192Q mice the visual cortex is more susceptible to CSD than the motor cortex. This difference, however, was only seen when experiments were carried out in the absence of physiological monitoring and control. Under other experimental conditions cortical regions, as tested for motor and visual cortex in the presence of physiological control in **Chapter 3**, appear equally susceptible to CSD induction, and cannot explain a preference for auras being visual. This finding fuels the idea that silent auras' may exist (Ayata 2010; Denuelle et al 2008), i.e., spreading depression waves may affect (and may be initiated in) a cortical (or even non-cortical) brain region that does not lead to an abnormal visual perception (Hansen et al 2013) and could have relevance for migraine without aura patients. Relevant to this idea are also first observations made in freely behaving mice in **Chapter 3** that indicate that not all spontaneous CSD events are first observed in the visual cortex (sometimes they are first seen in the motor cortex), suggesting that a CSD may start at different brain locations.

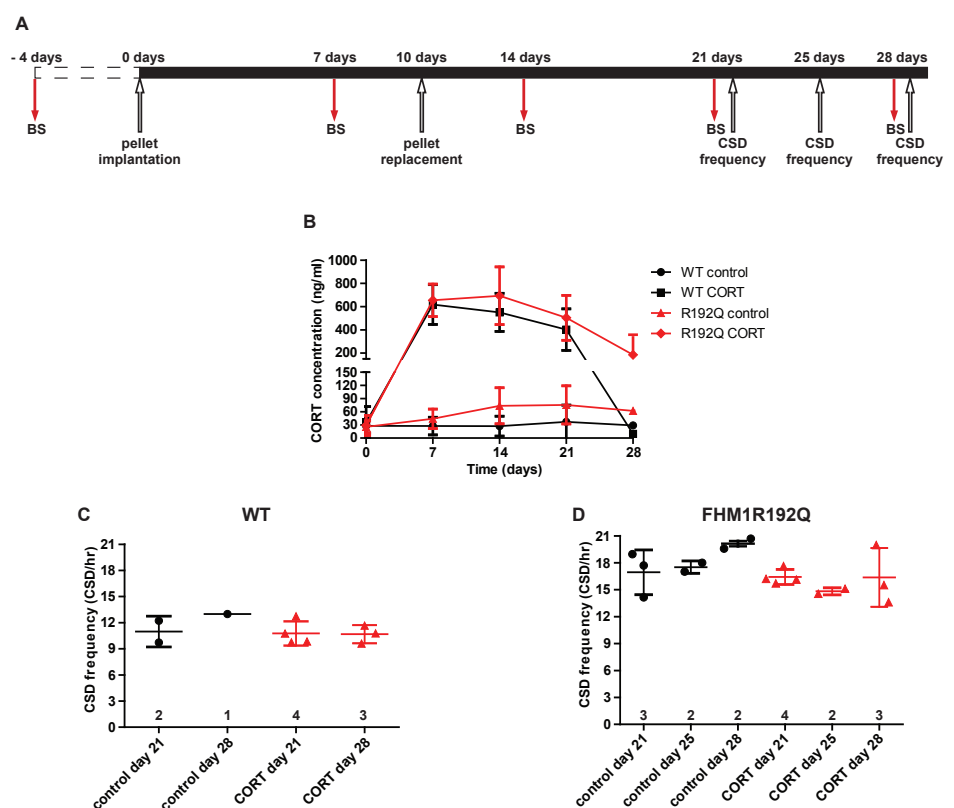
8.4 CSD-induced changes in biomolecular profiles detected by mass spectrometry imaging in the brains of mice

Mass spectrometry imaging (MSI) is an advanced bioanalytical method that allows the simultaneous detection of hundreds of biomolecules from different molecular classes directly from brain tissue (McDonnell & Heeren 2007). MSI therefore offers great potential in revealing—in an untargeted manner—biomolecular changes in the brain that are related to migraine gene mutations, CSD, or migraine-relevant triggers, while preserving spatial information of the distribution of these compounds. In **Chapter 5**, we demonstrated in a proof-of-principle study the applicability of MSI by the identification of changes in brain metabolite and peptide profiles upon CSD induction. In **Chapter 6**, we implemented the matrix-assisted laser desorption/ionization (MALDI) MSI approach

in a larger study to investigate biomolecular changes in the brain following CSD in FHM1 R192Q mice. CSD triggered specific brain changes in metabolite, peptide and protein profiles in FHM1 R192Q mice, which were not observed in WT brains that underwent the CSD procedure nor in WT and FHM1 R192Q brains that underwent a sham procedure (in which no CSDs were evoked). Metabolite *m/z* 146.0593, which was putatively identified as L-glutamate, appeared down-regulated in the CSD-affected hemisphere in FHM1 R192Q mice. This finding suggests an increased clearance of glutamate by the action of glial cells and glutamate transporters or an adaptation of glutamate

Figure 2. CSD susceptibility upon chronic corticosterone exposure.

(A) Experimental design of chronic corticosterone experiments. At least 4 days prior to pellet implantation a blood sample (BS) was collected from a tail cut to measure corticosterone levels at baseline. Additional blood samples were collected every week to measure corticosterone plasma levels following pellet implantation. The corticosterone pellet (50 mg corticosterone/50 mg cholesterol) was implanted subcutaneously in the flank of the mouse while it was under brief isoflurane anesthesia. Control mice were implanted with a pellet containing 100 mg cholesterol. To maintain stable corticosterone release the pellet was replaced at day 10. The pellet was removed at



day 21 and CSD frequency was measured at day 21, day 25, or day 28 to test for possible rebound effects following corticosterone pellet removal. (B) No significant differences in corticosterone plasma levels were detected between WT and FHM1 R192Q mice. Corticosterone plasma levels in mice implanted with the control pellet were low as expected (0, 7, 14, 21 days: WT N=5, R192Q N=4; 28 days: WT N=1, R192Q N=1). In mice implanted with corticosterone pellets, corticosterone plasma levels were strongly elevated in the first 14 days and then gradually dropped at day 21 and even more at day 28. Note the drop at day 28 in corticosterone plasma level (9.5 ng/mL) in the WT mouse below the level reported for stressed animals (i.e., 50 ng/mL). In contrast, in FHM1 R192Q mice corticosterone plasma levels remained high for 2 of 3 mice with particularly high corticosterone plasma levels at day 28 (~270 ng/mL; in line with values reported for stressed animals (Zalachoras et al 2013) (0, 7, 14, 21 days: WT N=6, R192Q N=8; 28 days: WT N=1, R192Q N=3). (C, D) Scatter plots (mean \pm SD) depict CSD frequency measured at different time-points in WT (C) and FHM1 R192Q (D) mice. There was no significant differences in CSD frequency for WT ($p=0.1$) and FHM1 R192Q ($p=0.14$, one-way ANOVA Bonferroni correction) for any of the days following corticosterone compared to control pellet removal. Group sizes are shown on the x-axis.

release, in reaction to the intense metabolic and synaptic demand during repeated CSD induction. Such compensatory mechanisms in FHM1 R192Q mice might already be in place under naive conditions, since cortical synaptosomes from naive FHM1 R192Q mice showed an up-regulation of both major glutamate transporters, EAAT1 and EAAT2 (Klychnikov et al 2010). Notably, the same m/z 146.0593 compound was found down-regulated in the occluded cortical hemisphere in a rat middle cerebral artery occlusion model (Miura et al 2010). For the protein dataset, we detected a down-regulation of unidentified protein m/z 11343 following CSD in the ipsilateral hemisphere, only in FHM1 R192Q mice. The short time between the 7th CSD and sacrifice of the mouse 5 min later suggests that this mass likely represents a protein modification of an already synthesized protein. In addition, several peptides were found to be down- or up-regulated following CSD in mutant mice in cortex and several subcortical regions relevant to migraine pathophysiology (i.e., cortex, hippocampus, striatum and thalamus). The finding of robust changes in the peptide dataset seem in line with reports showing peptide concentration changes associated with both migraine attacks in humans and with CSD induction in animals. Relevant peptides include calcitonin gene related peptide (CGRP), substance P (SP) and neurokinin A (NKA), of which levels were found to be altered in the cortical extracellular space of rodents after CSD (Bolay et al 2002, Colonna et al 1994, Tozzi et al 2012, Wahl et al 1994) and in blood plasma of patients (Fusayasu et al 2007, Gallai et al 1995, Goadsby et al 1990). The observation of peptide changes in subcortical areas after cortical induction of CSD in our study is perhaps not so surprising when considering the spread of CSD waves to subcortical areas, such as striatum and hippocampus, as was shown for FHM1 R192Q mice (Eikermann-Haerter et al 2011). Future experiments are expected to reveal the identity of the compounds that were differentially regulated after CSD.

8.5 CSD-induced biomolecular changes captured in blood plasma of mice

Changes in metabolite composition perhaps best reflect the response of an organism to a biological change. Relevant biomolecule changes that occur in brain may also be captured in cerebrospinal fluid (CSF), and even blood. Experiments in **Chapter 7** revealed specific changes, obtained by capillary electrophoresis-mass spectrometry (CE-MS), in plasma metabolite profiles of FHM1 R192Q mice following CSD. Such changes were not observed in WT mice that underwent the same procedure. In particular, a decreased plasma level of lysine and an increased level of pipecolic acid (a by-product of lysine catabolism) were found. Given the involvement of pipecolic acid in GABA-ergic neurotransmission (Gutierrez & Delgado-Coello 1989, Kase et al 1980), the observed changes in plasma, if reflecting similar metabolite changes in the brain, may indicate a compensatory response to effects of neuronal hyperexcitability in FHM1 R192Q mice. An inhibitory compensatory reaction seems in line with the observed down-regulation of L-glutamate following the same CSD induction paradigm in the MSI study from **Chapter 6**. When paralleled with microdialysis studies in freely behaving animals (Rogers et al 2013) and studies of plasma (Guldiken et al 2009), urine (Jacobsen et al 2013) or CSF (Fonteh et al 2011) obtained from patients, the analysis of CSD-induced changes in

plasma or other peripheral body fluids from migraine mice has great potential for migraine biomarker identification.

8.6 New knowledge with respect to migraine-relevant pathways

Events such as CSD trigger intense neurometabolic activity in the brain and are likely to affect the body in various ways. Our findings show that CSD induction causes specific changes of biomolecular distribution and gene expression in the brain, as well as specific changes in levels of metabolites in peripheral body fluid (i.e., plasma). Notably, some of the observed changes after CSD were different and/or only seen in FHM1 R192Q mice compared with WT mice, which suggest that these changes reflect specific CSD-induced changes relevant to migraine pathophysiology.

Changes in brain biomolecular distribution, as revealed by MSI, and profiling of metabolites in plasma using CE-MS, pointed towards the activation of compensatory mechanisms in FHM1 R192Q mice following CSD induction. A reduced m/z value (likely L-glutamate) in the CSD-affected hemisphere and an increased plasma level of pipecolic acid (with a presumed function in GABAergic neurotransmission) in FHM1 R192Q mice suggests that the induction of CSD triggers a body defense mechanism in order to restore the inhibition/excitation misbalance following CSD events. Our experiments cannot determine whether the observed reduction in glutamate is caused by an increased clearance of glutamate from glial cells by glutamate transporters, such as EAAT1 and EAAT2. The increased expression of EAAT1 and EAAT2 that was seen in the naïve brain of FHM1 R192Q mice using a proteomics approach on synaptosome preparations (Klychnikov et al 2010), provides some support for this scenario. Notably, previous studies in brain slices proposed increased glutamatergic neurotransmission as a key underlying mechanism of increased CSD susceptibility in FHM1 R192Q mice, whereas GABAergic neurotransmission was considered unaffected by the gene mutation (Tottene et al 2009).

Our results seem to indicate that the body is coping or counteracting the excess glutamatergic neurotransmission by: (i) increasing GABAergic neurotransmission, perhaps best reflected by the increased plasma level of pipecolic acid, and (ii) removal of excess glutamate from the synaptic cleft possibly by glutamate transporters as shown in **Chapter 6**. A recent *in vitro* study on cortical tissue from FHM1 R192Q mice showed that the enhanced glutamatergic transmission caused enhanced recruitment of inhibitory neuronal networks (Vecchia et al 2014). This is in line with reports on a possible compensatory inhibitory response in the cortex of migraine patients (Cosentino et al 2014).

Table 1.

<i>Migraine-related features</i>	FHM1 R192Q	Reference	Remarks
Photophobia	Present	Chanda et al 2013	Modified elevated plus maze was used for behavioural studies; mutant mice spent more time in open arms compared with brightly illuminated closed safe arms.
Hemiplegia	Present	Eikermann-Haerter et al 2009	Hemiplegia was observed and lasted 20 min or more after recovery from a single CSD event induced under anesthesia. S218 mutants were more severely affected.
CSD susceptibility	Increased	van den Maagdenberg et al 2004, 2010, Eikermann-Haerter et al 2009b, Chapters 2 & 3	In Chapters 2 & 3 CSD susceptibility (frequency and threshold) was increased compared to WT both for experiments with and without physiological monitoring or control. S218L mice display enhanced CSD frequency compared to R192Q mutants (Eikermann-Haerter et al 2009b, van den Maagdenberg et al 2010).
Female preponderance	Present	Eikermann-Haerter et al 2009, Chapter 2	In S218L mice CSD frequency is also enhanced for female compared to male mice. In Chapter 2 , gender effect on CSD frequency in R192Q mice is only observed for experiments with physiological monitoring and control.
Neuronal hyperexcitability	Present	Tottene et al 2009, Hullugundi et al 2014, Vecchia et al. 2014, Vecchia et al 2015, Chapter 3	In Tottene <i>et al.</i> and Vecchia <i>et al.</i> (2014) cortical slices and neuronal cultures were analysed <i>in vitro</i> ; Vecchia <i>et al.</i> (2015) shows most severe effects in S218L homozygous mice; in Hullugundi <i>et al.</i> cultured trigeminal ganglia neurons <i>in vitro</i> , and in Chapter 3 EEG activity was analysed <i>in vivo</i> .

Signs of headache	Present	Langford et al 2010, Chanda et al 2013	In Chanda et al. signs of headache were associated with novelty stress; S218L mutants showed stronger blink responses compared to R192Q mice.
Signs of inflammation	Present	Franceschini et al 2013	In Franceschini et al. trigeminal ganglia were analyzed
Impaired learning and memory	Present	Dilekoz et al 2015	R192Q mice exhibited enhanced excitatory transmission and LTP in the hippocampus but impaired learning and memory

Migraine triggers

Stress	Effective	Chapter 4	Acute administration of corticosterone, but not a 3h restraint stress, results in enhanced CSD frequency within 3 hrs.
Circadian rhythm shift	Effective	van Oosterhout et al 2008	R192Q mice showed enhanced phase resetting to 6-hr advance shifts of the light/dark cycle in freely behaving electrophysiology studies of EEG and SCN activity; no differences between mutants and WT mice were observed in <i>in vitro</i> recordings of the suprachiasmatic nucleus.

Table 1. The FHM1 mouse model is a relevant animal model for migraine Summary of experimental findings that highlight the relevance of FHM1 R192Q mice as a useful animal model for FHM, and perhaps also for the common forms of migraine. FHM1 R192Q mice exhibit key migraine-related features, such as signs of headache, photophobia and increased susceptibility to CSD including occurrence of spontaneous CSD. In addition, the FHM1 R192Q mice phenotype can be modulated by relevant migraine triggers such as stress hormones or circadian phase shifts. For several readouts, as indicated in the remarks, the phenotype was more severe or effects were stronger in FHM1 S218L compared to FHM1 R192Q mice.

8.7 Relevance of FHM1 R192Q mice as a useful animal model to study migraine pathophysiology

Migraine is a brain disorder with symptoms varying considerably between individuals (Goadsby et

al 2002), but there are core features of the disease. A good animal model of a disorder should ideally replicate (and allow the investigation) of such core features. The FHM1 R192Q mouse model used in this thesis displays various features that seem not only relevant to FHM but also to the common forms of migraine (Table 1).

In brief, FHM1 R192Q mice exhibit:

signs of photophobia and unilateral headache (Chanda et al 2013), which are prominent symptoms in migraine patients (ICHD 2004).

transient hemiplegia following induction of CSD (Eikermann-Haerter et al 2009b), thus mimicking the characteristic motor problems in patients with FHM.

enhanced CSD susceptibility and spontaneous CSD events, as both FHM1 transgenic mouse models exhibit enhanced CSD susceptibility compared to WT. Furthermore, as recorded, in this thesis for the first time, in freely behaving mutant mice (**Chapter 3**), which forms a reassuring translational paradigm to mimic the episodic nature of migraine.

a CSD phenotype in FHM1 R192Q mice that is more pronounced in females, in line with the higher propensity of migraine in women; this can be explained by modulation by gender hormones and gonadectomy as shown by effects of ovariectomy in females (Eikermann-Haerter et al 2009b, **Chapter 2**) and orchietomy in males (Eikermann-Haerter et al 2009a).

neuronal hyperexcitability as identified in cortical brain slices (Tottene et al 2009), cortical neuronal cultures (Vecchia et al 2014; Vecchia et al 2015) and, in this thesis, at the neuronal network level in freely behaving mice (**Chapter 3**), which is in agreement with the concept that hyperexcitability (Aurora & Wilkinson 2007), and possibly dynamic changes in neuronal excitability (Cosentino et al 2014) underlies migraine.

signs of inflammation, as shown for trigeminal ganglia (Franceschini et al 2013)

signs of impaired learning and memory, which may explain cognitive changes associated with FHM and, possibly, common forms of migraine (Dilekoz et al 2015).

enhancement of migraine-relevant readouts in response to triggers of migraine, such as stress (and stress hormones) and sudden shifts in circadian rhythms, as shown by increased CSD susceptibility to acute corticosterone administration (**Chapter 4**) and an enhanced circadian adaptation (van Oosterhout et al 2008).

Several of the functional readouts are impacted by allele dosage, and, most importantly, by the type of FHM1 mutation: strongest effects of the mutations are observed for S218L homozygous mice in comparison to homozygous R192Q mice (Eikermann-Haerter et al 2009b, van den Maagdenberg et al

2010, Chanda et al 2013, Vecchia et al 2014, Vecchia et al 2015, Dilekoz et al 2015). The observation of a more severe phenotype in S218L compared to R192Q mice is in line with the clinical presentation of symptoms in patients (Haan et al 2005, Stam et al 2009), thus underscoring the usefulness of FHM1 mice for studying mechanisms of migraine pathophysiology. The finding that effects of FHM1 mutations can differ among neurons of specific brain regions (Fioretti et al 2011, Inchauspe et al 2010) and, as shown for cortex, have strong effects on excitatory but not inhibitory neurons (Tottene et al 2009, Vecchia et al 2014, Vecchia et al 2015) provides a mechanistic basis for dissecting the role of various neuronal networks in migraine pathophysiology.

8.8 Future perspectives

An important finding in this thesis is the identification of spontaneous CSD events occurring in FHM1 R192Q mice but not WT mice. Future experiments should focus on revealing changes in neuronal firing properties and changes of neuronal network properties that precede spontaneous CSD events. Revealing such changes will be instrumental for a better understanding of neurobiological mechanisms that explain characteristics of CSD and migraine headache, and in combination with the identification of biomolecules and disease mechanisms, e.g., using the molecular tools used in this thesis, can be exploited to design novel therapies for migraine.

Whereas our data revealed an increased susceptibility to CSD in FHM1 R192Q mice upon an acute, strong elevation in corticosterone plasma levels, we did not see an effect on CSD susceptibility when mutant mice were subjected to a single restraint stress (that also increased corticosterone levels) or chronically elevated corticosterone levels. These findings seem to indicate corticosterone exerts multiple effects on biological systems and that the administration of corticosterone does not faithfully mimic the exact consequence to a physiological stressor. In humans, stress has a strong subjective component and often consists of small every day stressors, instead of a single major stressor. Perhaps only their cumulative effects may sufficiently modulate the threshold for CSD. Clinical data indicate that the “let-down” of stress can increase the likelihood of a migraine attack (Lipton et al 2014). Future research should focus on identifying every day (milder) stressors, which presumably affect factors in addition to cortisol, to better understand how stress affects migraine. From a clinical point of view it may still be relevant to identify the time point of corticosterone reduction following chronically high corticosterone levels (glucocorticoid withdrawal) and assess whether CSD susceptibility is changed at that transition. In addition, to stress and corticosterone, future experiments may also address effects of other known migraine-relevant trigger factors, such as drugs overuse (e.g., triptans overuse), changes in sleep patterns or specific foods, in modulating characteristics of CSD and other migraine-relevant outcomes.

Finally, the identification of reliable disease biomarkers is important; not only for diagnosis of the disease but also for pinpointing potential novel drug targets. Such biomarkers do not exist for migraine, yet. The identification, in this thesis, of specific compounds that are differentially regulated following CSD induction in an animal model of migraine in peripheral body fluid and brain tissue, may have relevance to migraine biomarker discovery. Future research may use these compounds as

a starting point to perform a systematic targeted analysis and identify whether similar compounds are abnormally regulated during and between migraine attacks in patients. Such targeted approach may further our understanding of migraine pathophysiology and may aid in the development of more effective treatments for migraine.

REFERENCES

- Aurora SK, Cao Y, Bowyer SM, Welch KM. 1999. The occipital cortex is hyperexcitable in migraine: experimental evidence. *Headache* 39:469-76
- Aurora SK, Wilkinson F. 2007. The brain is hyperexcitable in migraine. *Cephalalgia* 27:1442-53
- Basheer R, Strecker RE, Thakkar MM, McCarley RW. 2004. Adenosine and sleep-wake regulation. *Prog. Neurobiol.* 73:379-96
- Bolay H, Reuter U, Dunn AK, Huang Z, Boas DA, Moskowitz MA. 2002. Intrinsic brain activity triggers trigeminal meningeal afferents in a migraine model. *Nat. Med.* 8:136-42
- Borsook D, Erpelding N, Lebel A, Linnman C, Veggeberg R, et al. 2014. Sex and the migraine brain. *Neurobiol. Dis.* 68C:200-14
- Borsook D, Maleki N, Becerra L, McEwen B. 2012. Understanding Migraine through the Lens of Maladaptive Stress Responses: A Model Disease of Allostatic Load. *Neuron* 73:219-34
- Broberg M, Pope KJ, Olsson T, Shuttleworth CW, Willoughby JO. 2014. Spreading depression: Evidence of five electroencephalogram phases. *J. Neurosci. Res* 92:1384-94
- Chanda ML, Tuttle AH, Baran I, Atlin C, Guindi D, et al. 2013. Behavioral evidence for photophobia and stress-related ipsilateral head pain in transgenic *Cacna1a* mutant mice. *Pain* 154:1254-62
- Clark WC, Yang JC, Janal MN. 1986. Altered pain and visual sensitivity in humans: the effects of acute and chronic stress. *Ann. N. Y. Acad. Sci.* 467:116-29
- Colonna DM, Meng W, Deal DD, Busija DW. 1994. Calcitonin gene-related peptide promotes cerebrovascular dilation during cortical spreading depression in rabbits. *Am. J. Physiol.* 266:H1095-102
- Cosentino G, Fierro B, Vigneri S, Talamanca S, Paladino P, et al. 2014. Cyclical changes of cortical excitability and metaplasticity in migraine: evidence from a repetitive transcranial magnetic stimulation study. *Pain* 155:1070-8
- Deboer T, van Diepen HC, Ferrari MD, Van den Maagdenberg AM, Meijer JH. 2013. Reduced sleep and low adenosinergic sensitivity in *cacna1a* R192Q mutant mice. *Sleep* 36:127-36
- Denuelle M, Fabre N, Payoux P, Chollet F, Geraud G. 2008. Posterior cerebral hypoperfusion in migraine without aura. *Cephalalgia* 28:856-62
- Dilekoz E, Houben T, Eikermann-Haerter K, Balkaya M, Lenselink AM, et al. 2015. Migraine mutations impair hippocampal learning despite enhanced long-term potentiation. *J. Neurosci.* 35:3397-402
- Dufton LM, Konik B, Colletti R, Stanger C, Boyer M, et al. 2008. Effects of stress on pain threshold and tolerance in children with recurrent abdominal pain. *Pain* 136:38-43
- Eikermann-Haerter K, Baum MJ, Ferrari MD, van den Maagdenberg AM, Moskowitz MA,

- Ayata C. 2009a. Androgenic suppression of spreading depression in familial hemiplegic migraine type 1 mutant mice. *Ann. Neurol.* 66:564-8
- Eikermann-Haerter K, Dilekoz E, Kudo C, Savitz SI, Waeber C, et al. 2009b. Genetic and hormonal factors modulate spreading depression and transient hemiparesis in mouse models of familial hemiplegic migraine type 1. *J. Clin. Invest.* 119:99-109
- Eikermann-Haerter K, Yuzawa I, Qin T, Wang Y, Baek K, et al. 2011. Enhanced subcortical spreading depression in familial hemiplegic migraine type 1 mutant mice. *J. Neurosci.* 31:5755-63
- Eriksen MK, Thomsen LL, Olesen J. 2005. The Visual Aura Rating Scale (VARS) for migraine aura diagnosis. *Cephalalgia* 25:801-10
- Finocchi C, Strada L. 2014. Sex-related differences in migraine. *Neurol. Sci.* 35 Suppl 1:207-13
- Fioravanti B, Kasasbeh A, Edelmayer R, Skinner DP, Jr, Hartings JA, et al. 2011. Evaluation of cutaneous allodynia following induction of cortical spreading depression in freely moving rats. *Cephalalgia* 31:1090-100
- Fioretti B, Catacuzzeno L, Sforza L, Gerke-Duncan MB, van den Maagdenberg AM, et al. 2011. Trigeminal ganglion neuron subtype-specific alterations of CaV2.1 calcium current and excitability in a Cacna1a mouse model of migraine. *J. Physiol.* 589:5879-95
- Fonteh AN, Chung R, Sharma TL, Fisher RD, Pogoda JM, et al. 2011. Cerebrospinal fluid phospholipase C activity increases in migraine. *Cephalalgia* 31:456-62
- Fox AW, Davis RL. 1998. Migraine chronobiology. *Headache* 38:436-41
- Franceschini A, Vilotti S, Ferrari MD, van den Maagdenberg AM, Nistri A, Fabbretti E. 2013. TNFalpha levels and macrophages expression reflect an inflammatory potential of trigeminal ganglia in a mouse model of familial hemiplegic migraine. *PloS One* 8:e52394
- Fusayasu E, Kowa H, Takeshima T, Nakaso K, Nakashima K. 2007. Increased plasma substance P and CGRP levels, and high ACE activity in migraineurs during headache-free periods. *Pain* 128:209-14
- Gallai V, Sarchielli P, Floridi A, Franceschini M, Codini M, et al. 1995. Vasoactive peptide levels in the plasma of young migraine patients with and without aura assessed both interictally and ictally. *Cephalalgia* 15:384-90
- Gamaro GD, Xavier MH, Denardin JD, Pilger JA, Ely DR, et al. 1998. The effects of acute and repeated restraint stress on the nociceptive response in rats. *Physiol. Behav.* 63:693-7
- Goadsby PJ, Edvinsson L, Ekman R. 1990. Vasoactive peptide release in the extracerebral circulation of humans during migraine headache. *Ann. Neurol.* 28:183-7
- Goadsby PJ, Lipton RB, Ferrari MD. 2002. Migraine--current understanding and treatment. *N.Engl. J. Med.* 346:257-70
- Granziera C, DaSilva AF, Snyder J, Tuch DS, Hadjikhani N. 2006. Anatomical alterations of the

- visual motion processing network in migraine with and without aura. *PLoS Med.* 3:e402
- Guldiken B, Demir M, Guldiken S, Turgut N, Ozkan H, et al. 2009. Asymmetric dimethylarginine and nitric oxide levels in migraine during the interictal period. *J. Clin. Neurosci.* 16:672-4
- Gupta S, Mehrotra S, Villalon C, De Vries R, Garrelds I, et al. 2007. Effects of female sex hormones on responses to CGRP, acetylcholine, and 5-HT in rat isolated arteries. *Headache* 47:564-75
- Gutierrez MC, Delgado-Coello BA. 1989. Influence of pipercolic acid on the release and uptake of [3H]GABA from brain slices of mouse cerebral cortex. *Neurochem. Res.* 14:405-8
- Haan J, Kors EE, Vanmolkot KR, van den Maagdenberg AM, Frants RR, Ferrari MD. 2005. Migraine genetics: an update. *Curr. Pain Headache Rep.* 9:213-20.
- Hansen JM, Baca SM, Vanvalkenburgh P, Charles A. 2013. Distinctive anatomical and physiological features of migraine aura revealed by 18 years of recording. *Brain* 136:3589-95
- Hauge AW, Kirchmann M, Olesen J. 2011. Characterization of consistent triggers of migraine with aura. *Cephalalgia* 31:416-38
- Hertle D, Werhahn L, Beynon C, Zweckberger K, Vienenkötter B, et al. 2013. Depression of neuronal activity by sedatives is associated with adverse effects after brain injury. *Brain Res.* 1510:1-9
- Hoffmann U, Dilekoz E, Kudo C, Ayata C. 2011. Oxcarbazepine does not suppress cortical spreading depression. *Cephalalgia* 31:537-42
- Holland PR. 2014. Headache and sleep: Shared pathophysiological mechanisms. *Cephalalgia* 34:725-44
- Hullugundi SK, Ferrari MD, van den Maagdenberg AM, Nistri A. 2013. The mechanism of functional up-regulation of P2X3 receptors of trigeminal sensory neurons in a genetic mouse model of familial hemiplegic migraine type 1 (FHM-1). *PloS One* 8:e60677
- ICHD The International Classification of Headache Disorders: 2nd edition. 2004. *Cephalalgia* 24 Suppl 1:9-160
- Inchauspe CG, Urbano FJ, Di Guilmi MN, Forsythe ID, Ferrari MD, et al. 2010. Gain of function in FHM-1 Ca(V) 2.1 knock-in mice is related to the shape of the action potential. *J. Neurophys.* 104:291-9
- Ishida A, Mutoh T, Ueyama T, Bando H, Masubuchi S, et al. 2005. Light activates the adrenal gland: timing of gene expression and glucocorticoid release. *Cell Metab.* 2:297-307
- Jacobsen LM, Winsvold BS, Romundstad S, Pripp AH, Holmen J, Zwart JA. 2013. Urinary albumin excretion as a marker of endothelial dysfunction in migraine sufferers: the HUNT study, Norway. *BMJ open* 3: e003268
- Joëls M, Karst H, Alfarez D, Heine VM, Qin Y, et al. 2004 Effects of chronic stress on structure and

- cell function in rat hippocampus and hypothalamus. *Stress* 7:221-31.
- Joëls M, Karst H, Krugers HJ, Lucassen PJ. 2007. Chronic stress: implications for neuronal morphology, function and neurogenesis. *Front. Neuroendocrinol.* 28:72-96
- Joho RH, Ho CS, Marks GA. 1999. Increased gamma- and decreased delta-oscillations in a mouse deficient for a potassium channel expressed in fast-spiking interneurons. *J. Neurophysiol.* 82:1855-64
- Kase Y, Takahama K, Hashimoto T, Kaisaku J, Okano Y, Miyata T. 1980. Electrophoretic study of pipercolic acid, a biogenic imino acid, in the mammalian brain. *Brain Res.* 193:608-13
- Kelly MJ, Qiu J, Ronnekleiv OK. 2003. Estrogen modulation of G-protein-coupled receptor activation of potassium channels in the central nervous system. *Ann. N. Y. Acad. Sci.* 1007:6-16
- Kerr DS, Campbell LW, Applegate MD, Brodish A, Landfield PW. 1991 Chronic stress-induced acceleration of electrophysiologic and morphometric biomarkers of hippocampal aging. *J. Neurosci.* 11:1316-24.
- Kim JY, Kang HH, Ahn JH, Chung JW. 2008. Circadian changes in serum corticosterone levels affect hearing in mice exposed to noise. *Neuroreport* 19:1373-6
- Klychnikov OI, Li KW, Sidorov IA, Loos M, Spijker S, et al. 2010. Quantitative cortical synapse proteomics of a transgenic migraine mouse model with mutated Ca(V)2.1 calcium channels. *Proteomics* 10:2531-5
- Kudo C, Toyama M, Boku A, Hanamoto H, Morimoto Y, et al. 2013. Anesthetic effects on susceptibility to cortical spreading depression. *Neuropharmacology* 67:32-6
- Lau D, Vega-Saenz de Miera EC, Contreras D, Ozaita A, Harvey M, et al. 2000. Impaired fast-spiking, suppressed cortical inhibition, and increased susceptibility to seizures in mice lacking Kv3.2 K⁺ channel proteins. *J. Neurosci.* 20:9071-85
- Lipton RB, Buse DC, Hall CB, Tennen H, Defreitas TA, et al. 2014. Reduction in perceived stress as a migraine trigger: testing the “let-down headache” hypothesis. *Neurology* 82:1395-401
- Lipton RB, Stewart WF, Diamond S, Diamond ML, Reed M. 2001. Prevalence and burden of migraine in the United States: data from the American Migraine Study II. *Headache* 41:646-57
- Maleki N, Becerra L, Borsook D. 2012. Migraine: maladaptive brain responses to stress. *Headache* 52 Suppl 2:102-6
- Maywood ES, O'Neill JS, Chesham JE, Hastings MH. 2007. Minireview: The circadian clockwork of the suprachiasmatic nuclei--analysis of a cellular oscillator that drives endocrine rhythms. *Endocrinology* 148:5624-34
- McDonnell LA, Heeren RM. 2007. Imaging mass spectrometry. *Mass Spectrom. Rev.* 26: 606-43
- McEwen BS, Kalia M. 2010. The role of corticosteroids and stress in chronic pain conditions.

Metabolism 59 Suppl 1:S9-15

- Miura D, Fujimura Y, Yamato M, Hyodo F, Utsumi H, et al. 2010. Ultrahighly sensitive in situ metabolomic imaging for visualizing spatiotemporal metabolic behaviors. *Anal. Chem.* 82:9789-96
- Moghaddam B. 2002. Stress activation of glutamate neurotransmission in the prefrontal cortex: implications for dopamine-associated psychiatric disorders. *Biol. Psychiatry* 51:775-87
- Moulton EA, Becerra L, Johnson A, Burstein R, Borsook D. 2014. Altered hypothalamic functional connectivity with autonomic circuits and the locus coeruleus in migraine. *PloS One* 9:e95508
- Nehlig A, Daval JL, Debry G. 1992. Caffeine and the central nervous system: mechanisms of action, biochemical, metabolic and psychostimulant effects. *Brain Res. Brain Res. Rev.* 17:139-70
- Nosedá R, Kainz V, Borsook D, Burstein R. 2014. Neurochemical pathways that converge on thalamic trigeminovascular neurons: potential substrate for modulation of migraine by sleep, food intake, stress and anxiety. *PloS One* 9:e103929
- Nosedá R, Kainz V, Jakubowski M, Gooley JJ, Saper CB, et al. 2010. A neural mechanism for exacerbation of headache by light. *Nat. Neurosci.* 13:239-45
- Pinto-Ribeiro F, Moreira V, Pego JM, Leao P, Almeida A, Sousa N. 2009. Antinociception induced by chronic glucocorticoid treatment is correlated to local modulation of spinal neurotransmitter content. *Mol. Pain* 5:41
- Popoli M, Yan Z, McEwen BS, Sanacora G. 2011. The stressed synapse: the impact of stress and glucocorticoids on glutamate transmission. *Nat. Rev. Neurosci.* 13:22-37
- Raudensky J, Yamamoto BK 2007 Effects of chronic unpredictable stress and methamphetamine on hippocampal glutamate function. *Brain Res.* 1135:129-35.
- Resmini E, Santos A, Gomez-Anson B, Lopez-Mourelo O, Pires P, et al. 2013. Hippocampal dysfunction in cured Cushing's syndrome patients, detected by (1) H-MR-spectroscopy. *Clin. Endocrinol.* 79:700-7
- Rogers ML, Feuerstein D, Leong CL, Takagaki M, Niu X, et al. 2013. Continuous online microdialysis using microfluidic sensors: dynamic neurometabolic changes during spreading depolarization. *ACS Chem. Neurosci.* 4:799-807
- Sato K, Matsuki N, Ohno Y, Nakazawa K. 2003. Estrogens inhibit l-glutamate uptake activity of astrocytes via membrane estrogen receptor alpha. *J. Neurochem.* 86:1498-505
- Smith SS. 1989. Estrogen administration increases neuronal responses to excitatory amino acids as a long-term effect. *Brain Res.* 503:354-7
- Somerville BW. 1972a. The influence of progesterone and estradiol upon migraine. *Headache* 12:93-102
- Somerville BW. 1972b. The role of estradiol withdrawal in the etiology of menstrual migraine.

Neurology 22:355-65

- Somjen GG. 2001. Mechanisms of spreading depression and hypoxic spreading depression-like depolarization. *Physiol. Rev.* 81:1065-96
- Stam AH, Luijckx GJ, Poll-Thé BT, Ginjaar IB, Frants RR, et al. 2009. Early seizures and cerebral oedema after trivial head trauma associated with the CACNA1A S218L mutation. *J. Neurol. Neurosurg. Psychiatry* 80:1125-9
- Sukhotinsky I, Dilekoz E, Wang Y, Qin T, Eikermann-Haerter K, et al. 2011. Chronic daily cortical spreading depressions suppress spreading depression susceptibility. *Cephalalgia* 31:1601-8
- Takagaki M, Feuerstein D, Kumagai T, Gramer M, Yoshimine T, Graf R. 2014. Isoflurane suppresses cortical spreading depolarizations compared to propofol--implications for sedation of neurocritical care patients. *Exp. Neurol.* 252:12-7
- Tepe N, Filiz A, Dilekoz E, Akcali D, Sara Y, et al. 2015. The thalamic reticular nucleus is activated by cortical spreading depression in freely moving rats: prevention by acute valproate administration. *Eur. J. Neurosci.* 41:120-8
- Tolner EA, Houben T, Terwindt GM, de Vries B, Ferrari MD, van den Maagdenberg AM. 2015. From migraine genes to mechanisms. *Pain* 156 Suppl 1:S64-74
- Tottene A, Conti R, Fabbro A, Vecchia D, Shapovalova M, et al. 2009. Enhanced excitatory transmission at cortical synapses as the basis for facilitated spreading depression in Ca(v)2.1 knockin migraine mice. *Neuron* 61:762-73
- Tozzi A, de Iure A, Di Filippo M, Costa C, Caproni S, et al. 2012. Critical role of calcitonin gene-related peptide receptors in cortical spreading depression. *Proc. Natl. Acad. Sci. USA* 109:18985-90
- van den Maagdenberg AM, Pietrobon D, Pizzorusso T, Kaja S, Broos LA, et al. 2004. A Cacna1a knockin migraine mouse model with increased susceptibility to cortical spreading depression. *Neuron* 41:701-10
- van den Maagdenberg AM, Pizzorusso T, Kaja S, Terpolilli N, Shapovalova M, et al. 2010. High cortical spreading depression susceptibility and migraine-associated symptoms in Ca(v)2.1 S218L mice. *Ann. Neurol.* 67:85-98
- van Oosterhout F, Michel S, Deboer T, Houben T, van de Ven RC, et al. 2008. Enhanced circadian phase resetting in R192Q Cav2.1 calcium channel migraine mice. *Ann. Neurol.* 64:315-24
- Vecchia D, Tottene A, van den Maagdenberg AM, Pietrobon D. 2014. Mechanism underlying unaltered cortical inhibitory synaptic transmission in contrast with enhanced excitatory transmission in CaV2.1 knockin migraine mice. *Neurobiol. Dis.* 69:225-34.
- Vecchia D, Tottene A, van den Maagdenberg AM, Pietrobon D. 2015. Abnormal cortical

- synaptic transmission in CaV2.1 knockin mice with the S218L missense mutation which causes a severe familial hemiplegic migraine syndrome in humans. *Front. Cell. Neurosci.* 9:8
- Wahl M, Schilling L, Parsons AA, Kaumann A. 1994. Involvement of calcitonin gene-related peptide (CGRP) and nitric oxide (NO) in the pial artery dilatation elicited by cortical spreading depression. *Brain Res.* 637:204-10
- Williams SC, Deisseroth K. 2013. Optogenetics. *Proc. Natl. Acad. Sci. USA* 110:16287
- Woolley CS, Weiland NG, McEwen BS, Schwartzkroin PA. 1997. Estradiol increases the sensitivity of hippocampal CA1 pyramidal cells to NMDA receptor-mediated synaptic input: correlation with dendritic spine density. *J. Neurosci.* 17:1848-59
- Yuen EY, Wei J, Liu W, Zhong P, Li X, Yan Z. 2012. Repeated stress causes cognitive impairment by suppressing glutamate receptor expression and function in prefrontal cortex. *Neuron* 73:962-77
- Zalachoras I, Houtman R, Atucha E, Devos R, Tijssen AM, et al. 2013. Differential targeting of brain stress circuits with a selective glucocorticoid receptor modulator. *Proc. Natl. Acad. Sci. USA* 110:7910-5

SUMMARY

The research in this thesis was aimed at identifying and understanding mechanisms underlying modulating factors for and consequences of cortical spreading depression (CSD), the pathophysiological substrate for migraine aura that occurs in one-third of migraine patients. In this thesis, experimental studies on CSD were performed in wild-type (WT) and transgenic migraine mice, which express $\text{Ca}_v2.1 \text{ Ca}^{2+}$ channels with a mutated α_1 subunit that contains the R192Q missense mutation. The R192Q mutation was previously identified in patients with familial hemiplegic migraine type 1 (FHM1) and causes gain-of-function effects in terms of neuronal Ca^{2+} influx, neurotransmission, and susceptibility to experimentally induced CSD. Using various experimental strategies, in this thesis, the FHM1 R192Q mouse model was used to study pathophysiological mechanisms of the initiation and modulation of CSD as well as of neurobiological and molecular changes that accompany CSD events. In **Chapter 2** we investigated in what way physiological factors that vary in animals during surgery affect readouts of CSD experiments, CSD frequency and threshold. We determined to what extent the composition of the gas mixture and the choice of the experimental paradigm, i.e., monitoring or controlling physiological parameters pO_2 , pCO_2 , pH and blood pressure, or no monitoring at all, affected the CSD readouts in FHM1 R192Q and WT animals. The physiological monitoring paradigm entails that physiological parameters are measured in femoral artery blood; the physiological control paradigm ensures that variations in physiological parameters are adjusted via subtle changes of the breathing condition of the animal by making adjustments in the mechanical ventilation using tracheotomy. We showed that physiological control unmasks a gender effect on visual cortex CSD susceptibility in R192Q mice that remained hidden when physiological parameters of the animal were not controlled. This finding indicates that the CSD readouts appear sensitive to changes in pH, pO_2 , pCO_2 or blood pressure. We could also show that CSD readouts differed between visual versus motor cortex and showed a gender difference in R192Q mice, when the experiments were performed in the absence of physiological control. All in all, our study demonstrates that parameters of CSD susceptibility may be masked or unmasked depending on the experimental paradigm used. Although controlling the physiological status of an animal seems the preferred experimental paradigm, it has the risk that certain characteristics of CSD susceptibility in mutant mice are missed, when they depend on differences in physiological status between R192Q and WT mice.

A way to overcome the methodological issues related to CSD susceptibility measurements in anesthetized animals is to perform recordings of brain activity under freely behaving conditions. Therefore, in **Chapter 3** we investigated mechanisms underlying CSD susceptibility in freely behaving FHM1 R192Q and WT mice. Long-term cortical DC-EEG recordings revealed an increase in cortical EEG gamma power in both the visual and motor cortex of R192Q compared with WT mice, which suggests that the mutant brain displays an overall enhanced cortical excitability. Notably, R192Q mice were found to display spontaneous CSD events, evidenced by characteristic changes in patterns of electrical activity, that were never observed in WT mice. Unfortunately, an insufficient

number of spontaneous CSD events has been recorded until now to demonstrate whether these events occur at a particular time of day, which may be expected considering reports from patients indicating a circadian component in the occurrence of their attacks. Parallel CSD frequency recordings carried out under anesthesia in the presence of physiological control, at least, did not reveal that the enhanced susceptibility of FHM1 R192Q mice for CSD was different between the start of the day and the start of the night. Our observations provide evidence that cortical hyperexcitability contributes to the enhanced susceptibility to experimentally induced and spontaneous CSD in FHM1 mice.

Many migraine patients report stress as a prominent factor that brings about their migraine attacks. In **Chapter 4** we investigated the link between stress and CSD susceptibility, as surrogate for a migraine attack. In FHM1 R192Q and WT mice two paradigms were tested: behavioral restraint stress and administration of stress hormone corticosterone. Whereas subjecting mice to 20 min or even 3 hr restraint stress did not change CSD susceptibility, the administration of a single injection of corticosterone increased CSD susceptibility in R192Q mice, but not WT mice. Our finding suggests that a sudden rise in stress hormone may lead to a migraine attack when this occurs in the context of a brain that is prone to display increased excitatory neurotransmission, like it is the case when specific genetic mutations are present. It remains an enigma why natural stress - such as the restraint stress paradigm used, in which corticosterone levels also rise, does not cause a change in CSD susceptibility. It may be that in response to natural stress a spatiotemporally more complex biological response with multiple modulators is needed before an effect on CSD susceptibility can be detected. Also, it may be that such a response takes longer than the 3 hr paradigm that was used in this experiment.

In **Chapters 5 and 6** we investigated effects of CSD on biomolecular profiles in brain using various mass spectrometry (MS) technologies. MS imaging (MSI) was combined with matrix-assisted laser desorption/ionisation (MALDI) for the analysis of brain sections to unravel molecular consequences of CSD in the brain of mice while maintaining spatial resolution of these compounds.

Chapter 5 described the applicability of MALDI MSI in identifying molecular changes in the brains of WT mice that were subjected to CSD. CSD-related differences in metabolite and peptide composition were observed in the hemisphere in which 7 CSD events had been induced by topical application of KCl on the dura. No changes were observed in protein composition, which can be explained by the fact that changes in protein expression take longer than the duration of the experiment. Observed changes in metabolites and peptides were CSD-related as they were absent in sham controls, in whom KCl was replaced by NaCl, which does not induce CSD.

In **Chapter 6** we used the applicability of MALDI MSI from **Chapter 5** to investigate whether migraine-relevant molecular changes had occurred in the brains of FHM1 R192Q after experimentally induced CSD. CSD events were associated with various changes in the content of three molecular classes (i.e., metabolites, peptides and proteins); molecular changes were observed in cortex as well as subcortical areas. When in future research the identity of the molecules is revealed, these may pinpoint (novel) neurobiological pathways involved in migraine pathophysiology. At the moment,

the findings only demonstrate that CSD events in R192Q and WT mice are associated with different molecular profiles, shown as differences in m/z values.

In **Chapter 7**, MS technology was combined with capillary electrophoresis (CE) to assess changes in plasma metabolite composition in FHM1 R192Q and WT mice following experimentally induced CSD. We could show that specific metabolite changes can be captured in peripheral body fluid. Compared with WT mice, CSD events induced in R192Q mice were associated with a lower level of lysine and a higher level of pipecolic acid, the by-product of lysine catabolism. The study holds the promise that metabolic changes that occur in the brains of migraine patients may be measured in plasma, which is accessible in clinical research. If proven correct, metabolic changes in plasma of migraine patients could serve as potential disease biomarkers.

Chapter 8 provides a general discussion of the main findings in this thesis.

NEDERLANDSE SAMENVATTING

Het onderzoek beschreven in dit proefschrift heeft als doel het identificeren en begrijpen van de mechanismen die ten grondslag liggen aan modulerende factoren en gevolgen van het fenomeen “cortical spreading depression” (CSD), het pathofysiologische substraat voor migraine aura dat optreedt in één derde van de migraine patiënten. Voor dit proefschrift werden experimentele studies naar CSD uitgevoerd in wild-type (WT) en transgene migraine muizen, die $Ca_v2.1$ Ca^{2+} kanalen tot expressie brengen met een $\alpha 1$ subunit die de R192Q mutatie bevat. Deze R192Q mutatie is in het verleden geïdentificeerd bij patiënten met familiale hemiplegische migraine type 1 (FHM1), en veroorzaakt “gain-of-function” effecten met betrekking tot neuronale Ca^{2+} influx, glutamaterge neurotransmissie, en gevoeligheid voor experimenteel geïnduceerde CSD. Met behulp van verschillende experimentele strategieën, beschreven in dit proefschrift, werd het FHM1 R192Q muismodel gebruikt om pathofysiologische mechanismen van de initiatie en modulatie van CSD te bestuderen, evenals de neurobiologische en moleculaire veranderingen die gepaard gaan met CSD. In **hoofdstuk 2** onderzochten we op welke manier de fysiologische factoren die in dieren kunnen variëren tijdens de operatie bij gebruik van verschillende experimentele methodologieën, van invloed zijn op de resultaten van CSD experimenten, met name ten aanzien van de frequentie en drempel voor het opwekken van CSD. We hebben vastgesteld in welke mate de samenstelling van het gasmengsel voor de anesthesie en de keuze van de bewaking van fysiologie tijdens de anesthesie, door middel van het controleren van fysiologische parameters zoals pO_2 , pCO_2 , pH en bloeddruk, van invloed zijn op CSD parameters in FHM1 R192Q en WT dieren. Voor de fysiologische bewaking werden parameters gemeten in arterieel (femorale) bloed. Het fysiologische controle paradigma verzekert dat variaties in fysiologische parameters worden aangepast via subtiele veranderingen in de ademhalingscondities van het dier, door aanpassingen in de mechanische ventilatie met behulp van tracheotomie. We toonden aan dat het fysiologische controle paradigma een geslachts-specifiek effect bloot legt ten aanzien van CSD gevoeligheid in de visuele cortex in R192Q muizen, en dat dit effect niet zichtbaar was wanneer de fysiologische parameters van de dieren niet werden gecontroleerd. Deze bevinding geeft aan dat CSD parameters gevoelig zijn voor veranderingen in pH, pCO_2 of bloeddruk. We konden ook aantonen dat er verschillen zijn tussen de visuele en de motorische cortex in de CSD resultaten en dat er ook een geslachtverschil in R192Q muizen is wanneer de experimenten werden uitgevoerd zonder fysiologische controle. Al met al blijkt uit onze studie dat verschillen in CSD gevoeligheid aan het licht gebracht of verborgen kunnen worden, afhankelijk van het experimentele paradigma. Hoewel het controleren van de fysiologische toestand van een dier de voorkeur heeft, brengt het als risico mee dat bepaalde kenmerken van CSD gevoeligheid in mutante muizen worden gemist, wanneer deze kenmerken afhankelijk zijn van verschillen in fysiologische toestand tussen R192Q en WT muizen tijdens de operatie.

Een manier om de afhankelijkheid van de anesthesie bij CSD gevoeligheidsmetingen in dieren te overkomen is om de hersenactiviteit te meten in wakkere dieren. Daarom onderzochten we in

hoofdstuk 3 de mechanismen die ten grondslag liggen aan CSD gevoeligheid in wakkere FHM1 R192Q en WT muizen. Langdurig corticale DC-EEG-opnames onthulden een toename in de intensiteit van EEG gamma-band activiteit in zowel de visuele als de motorische cortex van R192Q muizen ten opzichte van WT muizen, wat suggereert dat de FHM1 mutatie een versterkte corticale prikkelbaarheid veroorzaakt. Ook werden er spontane gevallen van CSD gevonden in R192Q muizen, gekenmerkt door veranderingen in de patronen van corticale elektrische activiteit, zulke aanvallen werden nooit waargenomen in WT muizen. Helaas zijn er tot nu toe nog onvoldoende spontane CSD gebeurtenissen gemeten om aan te tonen of deze gebeurtenissen bij voorkeur op een bepaalde tijd van de dag gebeuren, zoals verwacht wordt gezien verslagen van patiënten die wijzen op een circadiane component in het optreden van aanvallen. Uit CSD frequentie opnames in dieren onder anesthesie met fysiologische controle bleek dat de verhoogde CSD gevoeligheid van FHM1 R192Q muizen niet verschillend was tussen het begin van de dag en het begin van de nacht. Onze waarnemingen leveren bewijs dat corticale hyperexcitabiliteit bijdraagt aan de verhoogde gevoeligheid voor experimenteel geïnduceerde en spontane CSD in FHM1 muizen.

Veel migraine patiënten melden stress als een prominente factor die leidt tot hun migraineaanvallen. In **hoofdstuk 4** onderzochten we het verband tussen stress en CSD gevoeligheid, als surrogaat voor een migraineaanval. In FHM1 R192Q en WT muizen werden twee methoden gebruikt: ‘restraint stress’, wat inhoudt dat de muis opgesloten wordt in een kleine ruimte waar hij niet kan bewegen, of een injectie met het stress hormoon corticosteron. ‘Restraint stress’ gedurende 20 min of zelfs gedurende 3 uur veranderde de CSD gevoeligheid niet, terwijl de toediening van één enkele injectie van corticosteron de CSD gevoeligheid in R192Q muizen, maar niet in WT muizen, liet toenemen. Onze bevinding suggereert dat een plotselinge stijging van stress hormonen kan leiden tot een migraine aanval, wanneer dit gebeurt bij hersenen die gevoelig zijn voor verhoogde excitatoire neurotransmissie, bijvoorbeeld als er specifieke genetische mutaties aanwezig zijn. Het blijft een raadsel waarom natuurlijke stress - zoals bij de ‘restraint stress’ methode, waarbij corticosteron niveaus ook stijgen, niet een verandering in de CSD gevoeligheid veroorzaakt. Het kan zijn dat in reactie op natuurlijke stress een spatiotemporeel complexere biologische respons met meerdere modulatoren nodig is voordat er een effect op CSD gevoeligheid kan worden gedetecteerd. Ook kan het zijn dat een dergelijke reactie langer duurt dan het 3 uur stress paradigma dat werd gebruikt in dit experiment.

In de **hoofdstukken 5 en 6** onderzochten we de effecten van CSD op biomoleculaire profielen in de hersenen met behulp van verschillende massaspectrometrie (MS) technologieën. MS imaging (MSI) werd gecombineerd met matrix-geassisteerde laser desorptie/ionisatie (MALDI) voor het analyseren van hersencoupees om de moleculaire gevolgen van CSD in de hersenen van muizen te ontrafelen met een hoge spatiale resolutie.

Hoofdstuk 5 beschrijft de toepassing van MALDI MSI bij het identificeren van moleculaire veranderingen in de hersenen van WT muizen die werden onderworpen aan CSD. CSD-gerelateerde verschillen in metabolieten- en peptidensamenstelling werden waargenomen in de hersenhelft waarin

7 CSD voorvallen waren geïnduceerd door lokale toediening van KCl op de dura mater. Er werden geen veranderingen waargenomen in eiwitsamenstelling. Dit kan worden verklaard door het feit dat veranderingen in eiwitexpressie later zichtbaar zijn dan de duur van dit experiment. De gevonden veranderingen in metabolieten en peptiden waren gerelateerd aan de CSD, omdat zij afwezig waren in de controles waar KCl vervangen werd door NaCl, wat geen CSD induceert.

In **hoofdstuk 6** hebben we de toepassing van MALDI MSI uit **hoofdstuk 5** om te onderzoeken of migraine-gerelateerde moleculaire veranderingen in de hersenen van FHM1 R192Q optreden na experimenteel geïnduceerde CSD. CSD voorvallen leidden tot diverse veranderingen in de inhoud van drie moleculaire groepen (d.w.z. metabolieten, peptiden en proteïnen) in zowel de cortex als subcorticale gebieden. Zodra toekomstig onderzoek de identiteit van de moleculaire veranderingen onthult, kunnen deze veranderingen nieuwe neurobiologische routes tonen die betrokken zijn bij de pathofysiologie van migraine. Op dit moment tonen de gevonden bevindingen aan dat CSD voorvallen in R192Q en WT muizen gerelateerd zijn aan verschillende moleculaire profielen, weergegeven als verschillen in m/z waarden.

In **hoofdstuk 7** werd de MS technologie gecombineerd met capillaire elektroforese om zo de veranderingen in plasmametabolietcompositie in FHM1 R192Q en WT muizen na experimenteel geïnduceerde CSD te beoordelen. We konden specifieke veranderingen in metabolieten in perifere lichaamsvloeistof aantonen. In vergelijking met WT muizen werden in R192Q muizen geïnduceerde CSD voorvallen geassocieerd met een lager niveau van lysine en een hoger niveau van pipercolinezuur, een bijproduct van lysine katabolisme. De studie suggereert dat metabolische veranderingen die optreden in de hersenen van migrainepatiënten kunnen worden gemeten in plasma, wat deze veranderingen toegankelijk maakt voor onderzoekers. Als dit inderdaad zo is, kunnen metabolische veranderingen in plasma van migrainepatiënten dienen als potentiële biomarkers.

Hoofdstuk 8 geeft een algemene discussie van de belangrijkste bevindingen in dit proefschrift.

ACKNOWLEDGEMENTS

I can say it now at the end of this journey that indeed it has been a unique and wonderful journey.

First, I would like to express my gratitude to my promotor Arn van den Maagdenberg. Arn, your dedication to science, hard-working spirit and attention to detail have made me both a better scientist and a better person.

Next, I would like to thank my co-promotor and everyday supervisor Else Tolner. Thank you for your patience during the difficult moments of the project and your immense help with my thesis.

My other promotor Michel Ferrari. Michel, I always left your office with an important message that I will always remember.

Curtis, thank you for everything you taught me and your support during the first steps in my thesis.

Zonder goede analist ben je nergens. Sandra, these words best summarize your contribution to my thesis. It was really a privilege to work and learn from you.

Roselin and Else E, you were really my PhD "buddies". In addition, I would like to thank all the other members of van den Maagdenberg group for their help and support during the PhD years.

To my roomies. Lianne, Mathijs and Sam and all the other group Frants members.

I could not forget also all the people from mass spectrometry unit. Ricardo, Isabelle, Benjamin, Liam and Oleg, thank you for the very fruitful collaboration that we had.

Erilda dhe Brunilda nuk mund te harroj kurajon dhe mbështetjen që ju me dhatë ne momente shumë të vështira gjatë kohës të doktoraturës.

Të dashur prinder. Faleminderit për të gjitha sakrificat që keni bërë për të realizuar ëndërrat e mia. Gjithashtu dhe për mbështetjen dhe dashurinë që më keni dhënë.

Sandri. Faleminderit që ke qëndruar gjithmonë pranë meje. Je vëllai më i mirë në botë.

I dashur gjyshi, faleminderit për frymëzimin që më dhe për të studiuar dhe të jem i dobishëm për njerëzit. Shpresoj që të kem arritur atje ku ti do të doje për mua.

Φυσικά θα ήθελα να ευχαριστήσω και όλους τους φίλους μου που στάθηκαν και στέκονται δίπλα μου με τον ένα ή τον άλλο τρόπο. Ιδιαίτερα την Χρυσάνθη για την υπέροχη δουλειά της με το layout και το εξώφυλλο αυτού του βιβλίου.

Finally, I would like to thank my life companion and best friend Marta. Your love and support allows me to believe that everything is possible.

LIST OF PUBLICATIONS

Reinald Shyti, Boukje de Vries, Arn M.J.M. van den Maagdenberg. Migraine genes and the relation to gender. *Headache* 2011;51:880-90

Boyan Todorov, Lieke Kros, Reinald Shyti, Petra Plak, Elize D. Haasdijk, Robert S. Raike, Rune R. Frants, Ellen J. Hess, Freek E. Hoebeek, Chris I. De Zeeuw, Arn M. J. M. van den Maagdenberg. Purkinje cell-specific ablation of Ca_v2.1 channels is sufficient to cause cerebellar ataxia in mice. *Cerebellum* 2012;11:246-58

Emrys Jones, Reinald Shyti, Rene van Zeijl, Sandra H. van Heiningen, Michel D. Ferrari, Andre Deelder, Else A. Tolner, Arn M.J.M. van den Maagdenberg, Liam A. McDonnell. Imaging mass spectrometry to visualize biomolecule distributions in mouse brain tissue following hemispheric cortical spreading depression. *Journal of Proteomics* 2012;75:5027-35

Rawi Ramautar, Reinald Shyti, Bart Schoenmaker, Lotte de Groote, Rico J. E. Derks, Michel D. Ferrari, Arn M. J. M. van den Maagdenberg, André M. Deelder, Oleg A. Mayboroda. Metabolic profiling of mouse cerebrospinal fluid by sheathless CE-MS. *Analytical and Bioanalytical Chemistry* 2012;404:2895-900

Walid M. Abdelmoula, Ricardo J. Carreira, Reinald Shyti, Benjamin Balluff, René J. M. van Zeijl, Else A. Tolner, Boudewijn F.P. Lelieveldt, Arn M.J.M. van den Maagdenberg, Liam A. McDonnell, Jouke Dijkstra. Automatic Registration of Mass Spectrometry Imaging data sets to the Allen Brain Atlas. *Analytical Chemistry* 2014;86:3947-54

Reinald Shyti, Katharina Eikermann-Haerter, Sandra H. van Heiningen, Onno C. Meijer, Cenk Ayata, Joels M, Michel D. Ferrari, Arn M.J.M. van den Maagdenberg, Else A. Tolner. Stress hormone corticosterone enhances susceptibility to cortical spreading depression in familial hemiplegic migraine type-1 mutant mice. *Experimental Neurology* 2015;263:214-20

Reinald Shyti, Isabelle Kohler, Bart Schoemaker, Rico Derks, Michel D. Ferrari, Else A. Tolner, Oleg A. Mayboroda, Arn M.J.M. van den Maagdenberg. Plasma metabolic profiling after cortical spreading depression in a transgenic mouse model of hemiplegic migraine by capillary electrophoresis - mass spectrometry. *Molecular Biosystems* 2015;11:1462-71

Ricardo J. Carreira, Reinald Shyti, Walid Abdelmoula, Benjamin Balluff, Rene van Zeijl, Ludo Broos, Jouke Dijkstra, Michel D. Ferrari, Else A. Tolner, Liam A. McDonnell, Arn M.J.M. van den Maagdenberg. Large-Scale Mass Spectrometry Imaging Investigation of Consequences of Cortical

Spreading Depression in a Transgenic Mouse Model of Migraine. *Journal of the American Society for Mass Spectrometry* 2015;26:853-61

CURRICULUM VITAE

Reinald Shyti was born on 24th September 1981, in Berat, Albania. In May 1992 he moved to Athens, Greece where in 2000 he graduated from the 3rd High School (3^ο Λυκειο) of Argypolis, Athens. In 2001, Reinald started his studies at the American College of Greece where he graduated in 2005 with a Bachelor's degree in Psychology.

In 2006, Reinald went on to complete his Master's studies in Cognitive Neuroscience at the Radboud University Nijmegen in the Netherlands. During the 2nd year of his studies he conducted basic research at the Department of Cellular Animal Physiology, Donders Institute for Brain, Cognition and Behavior, Radboud University Nijmegen. Under the supervision of Prof. Dr. Tamas Kozicz and Prof. Dr. Eric Roubos.

In August 2008, Reinald started his graduate (PhD) studies at the Department of Human Genetics of Leiden University Medical Centre. Reinald investigated the causes and consequences of cortical spreading depression in migraine mouse models under the supervision of Prof. Arn van den Maagdenberg, Prof. Michel Ferrari and Dr. Else Tolner. The findings of this research project are presented in the current thesis. Since August 2015 Reinald is a postdoc researcher in the Department of Experimental Oncology of European Institute of Oncology, Milan, Italy. Reinald is investigating epigenetic mechanisms in induced pluripotent stem cells as a model for neurodevelopmental disorders.

